

Durham E-Theses

Design, synthesis and application of silica-grafted bis(diphenylphosphino)amines and related compounds in heterogenised hydroformylation catalysis

BACKHOUSE, JAKE

How to cite:

BACKHOUSE, JAKE (2024) *Design, synthesis and application of silica-grafted bis(diphenylphosphino)amines and related compounds in heterogenised hydroformylation catalysis*, Durham theses, Durham University. Available at Durham E-Theses Online: <http://etheses.dur.ac.uk/15799/>

Use policy

The full-text may be used and/or reproduced, and given to third parties in any format or medium, without prior permission or charge, for personal research or study, educational, or not-for-profit purposes provided that:

- a full bibliographic reference is made to the original source
- a [link](#) is made to the metadata record in Durham E-Theses
- the full-text is not changed in any way

The full-text must not be sold in any format or medium without the formal permission of the copyright holders.

Please consult the [full Durham E-Theses policy](#) for further details.



Design, synthesis and application of silica-grafted bis(diphenylphosphino)amines and related compounds in heterogenised hydroformylation catalysis

Thesis submitted for the degree of Doctor
of Philosophy

By

Jake Backhouse

Department of Chemistry, Durham
University 2020 – 2024

Declaration

This thesis is based on work carried out by the author in the Department of Chemistry at Durham University, during the period October 2020 – March 2024. All of the work detailed in this thesis is original, unless specifically acknowledged in the text or references. None of this work has been submitted for another degree in this or any other university.

The copyright of this thesis rests with the author. No quotation from it should be published without the author's prior written consent and information derived from it should be acknowledged.

Signed:_____

Date:_____

Abstract

This project develops a range of heterogeneous hydroformylation catalysts by immobilisation of discrete rhodium complexes onto a silica support *via* a bidentate phosphine or phosphine sulfide ligand bearing a pendant silica-tethering functionality.

Bidentate phosphine ligands capable of silica binding were prepared with various silica-tethering groups (alkoxysilane, silatrane and cyclic azasilane). A range of ligands with different phosphine steric and electronic properties were synthesised to enable investigation into the effect of ligand structure on immobilised hydroformylation catalysis.

The synthesis of homogeneous hydroformylation catalyst precursors was achieved by reaction of the aforementioned diphosphine ligands with $[\text{Rh}(\text{COD})_2]\text{BF}_4$, resulting in a $[\text{Rh}(\text{P}^\wedge\text{P})_2]\text{BF}_4$ or $[\text{Rh}(\text{L}^\wedge\text{L})(\text{COD})]\text{BF}_4$ complex (P^\wedgeP = bidentate phosphine ligand, L^\wedgeL = bidentate ligand), depending on the ligand used.

Immobilisation of the prepared rhodium complexes $[\text{Rh}(\text{P}^\wedge\text{P})_2]\text{BF}_4$ or $[\text{Rh}(\text{L}^\wedge\text{L})(\text{COD})]\text{BF}_4$ was achieved by their reaction with AEROPERL 300/30 silica (calcined at 200 °C), and confirmed by solid-state ^{31}P and ^{29}Si NMR spectroscopic and ICP-OES elemental analyses. However, reaction of the parent phosphines with silica results in significant side reactions between the phosphine moieties and silica surface, leading to the formation of unidentified P^V species.

The prepared homogeneous and heterogeneous pre-catalysts were investigated for the hydroformylation of 1-octene (conditions: 90 °C, 20 bar (1:1 H_2 :CO), [1-octene]/[Rh] = 1000, toluene solvent). Silica-immobilised $[\text{Rh}((\text{Ph}_2\text{PCH}_2)_2\text{N}(\text{CH}_2)_3\text{Si}(\text{OCH}_2\text{CH}_2)_3\text{N})_2]\text{BF}_4$ was found to provide the best catalyst performance of the heterogeneous catalysts investigated, giving a TOF of $682 \pm 48 \text{ h}^{-1}$ and an aldehyde *i:b* ratio of 2.6, catalytic performance exactly mirroring that of its soluble analogue in solution. Leaching studies of silica-immobilised $[\text{Rh}((\text{Ph}_2\text{PCH}_2)_2\text{N}(\text{CH}_2)_3\text{Si}(\text{OCH}_2\text{CH}_2)_3\text{N})_2]\text{BF}_4$ found a 1.4% loss of rhodium from the catalyst after a one hour hydroformylation experiment. However, recycling studies showed no loss in activity after one recycle, followed by a subsequent large decrease in catalytic activity down to 25% of initial activity after five runs.

Acknowledgements

First of all, I thank my supervisor Prof. Phil Dyer for his unwavering support and kindness over the course of my PhD. His generosity and enthusiasm helping with anything chemistry (or not) related over the course of the project have been immensely appreciated. I couldn't have asked for a better supervisor.

I would also like to thank my co-supervisors from Johnson Matthey Drs Stephen Bennett Stephen Poulston, as well as Drs Michael Betham and Steve Pollington, for all their encouragement and interesting discussions. Thank you also for allowing me to use JM's ICP analysis service.

Johnson Matthey are gratefully acknowledged for the financial support of this work.

I also thank Durham University and all the Chemistry Department staff for their services and advice. In particular, Drs Toby Blundell, Dmitry Yufit and Andrei Batsanov for their excellent crystallographic work, Drs David Apperley and Samuel Page for their assistance with solid-state NMR and Dr Emily Unsworth for performing CHN and ICP elemental analysis.

Of course, I need to thank the whole Dyer group for their friendship and for making CG100 a wonderful place to work. Special thanks go to Alana for all the assistance with air-sensitive chemistry when I was starting out, Sherry for helping me with all things autoclaves and gas chromatography and Adam for always being there to cheer me up if the chemistry gods were getting me down.

Finally, thanks to my Mum, Dad and the rest of my family for everything that they do.

Contents

Abstract	ii
Acknowledgements	iii
Abbreviations.....	ix
List of compounds	xi

Chapter 1: Introduction

1.0 literature review	1
1.1 Introduction to hydroformylation	1
1.2 Mechanism and kinetics of first generation hydroformylation catalysis	2
1.3 Competing hydroformylation reactions and side products	4
1.4 Second generation phosphine-modified hydroformylation catalysts.....	6
1.5 Third generation rhodium hydroformylation catalysts	8
1.6 Phosphine ligand-metal coordination: steric and electronic effects	12
1.6.1 Determining the electronic contribution of phosphines in metal complexes.....	12
1.6.2 Quantifying the steric demand of phosphines in metal complexes.....	14
1.7 The effect of phosphine ligand structure on hydroformylation catalysis	15
1.8 Diphosphine ligands in hydroformylation catalysis.....	16
1.9 Phosphite ligands in hydroformylation catalysis.....	19
1.10 Bidentate phosphite ligands in hydroformylation catalysis	20
1.11 Small bite angle ligands for rhodium-catalysed hydroformylation	22
1.12 Separation of hydroformylation catalyst and products	26
1.13 Homogeneous vs heterogeneous catalysis - advantages and disadvantages.....	28
1.14 Introduction to heterogeneous hydroformylation catalysis	29
1.15 Mesoporous silicas – oxide supports for hydroformylation.....	30
1.16 Immobilised phosphines for heterogeneous hydroformylation	33
1.17 Recent applications of rhodium hydroformylation catalysts immobilised onto solid supports <i>via</i> tetherable ligands	39
1.18 Chapter 1 summary	44
1.19 Project aims and objectives.....	46
1.20 Chapter 1 references	47

Chapter 2: Design and synthesis of tether-functionalised diphosphine compounds

2.1 Ligand design considerations	53
2.2 PNP ligand design and synthesis	54
2.2.1 PNP ligand synthesis – varying the silica-tethering backbone	56

2.2.2 Synthesis of PNP ligands – varying the phosphine ‘R’ group	60
2.2.3 Attempted synthesis of compound L6 : (ⁱ Pr ₂ P) ₂ N(CH ₂) ₃ Si(OMe) ₃ – synthesis of compound L6X : ⁱ Pr ₂ PNH(CH ₂) ₃ Si(OMe) ₃	61
2.2.4 Attempted synthesis of aminophosphine PNP compounds L7 : (P(N ⁱ Pr) ₂) ₂ N(CH ₂) ₃ Si(OMe) ₃ and L8 : (P(NEt) ₂) ₂ N(CH ₂) ₃ Si(OMe) ₃	63
2.2.5 Synthesis of phosphoramidites PNPs L9 : (P(C ₁₂ H ₈ O ₂) ₂ N(CH ₂) ₃ Si(OMe) ₃ , L10 : (P(C ₁₂ H ₈ O ₂) ₂ N(CH ₂) ₂ (NSi(Me) ₂ CH ₂ CH(CH ₃)CH ₂), L11 : P(C ₁₂ H ₈ O ₂) ₂ N(CH ₂) ₃ Si(OCH ₂ CH ₂) ₃ N and L12 : P(C ₂₀ H ₁₂ O ₂) ₂ N(CH ₂) ₃ Si(OCH ₂ CH ₂) ₃ N	64
2.3 PCNCP ligand design	70
2.4 PCNCP ligand synthesis strategy	71
2.4.1 Synthesis of compound L13 : (Ph ₂ PCH ₂) ₂ N(CH ₂) ₃ Si(OMe) ₃	72
2.4.2 Attempted synthesis of compound L14 : (^t Bu ₂ PCH ₂) ₂ N(CH ₂) ₃ Si(OMe) ₃	73
2.4.3 Attempted synthesis of PCNCP compounds <i>via</i> dialkylbis(hydroxymethyl)phosphonium chloride salts	73
2.4.4 Synthesis of PCNCP compounds L17 : (Ph ₂ PCH ₂) ₂ N(CH ₂) ₃ Si(OCH ₂ CH ₂) ₃ N, L18 : (^t Bu ₂ PCH ₂) ₂ N(CH ₂) ₃ Si(OCH ₂ CH ₂) ₃ N and L19 : (Cy ₂ PCH ₂) ₂ N(CH ₂) ₃ Si(OCH ₂ CH ₂) ₃ N	75
2.5 PCCNCCP ligand design and synthesis	76
2.6 POCCNCCOP ligand design	78
2.6.1 Synthesis of L21 : ((C ₁₂ H ₈ O ₂)POCH ₂ CH ₂) ₂ N(CH ₂) ₃ Si(OMe) ₃	79
2.6.2 Attempted synthesis of L22 : (Ph ₂ POCH ₂ CH ₂) ₂ N(CH ₂) ₃ Si(OMe) ₃	80
2.7 Synthesis of L5S₂ : (P(S)Ph) ₂ N(CH ₂) ₃ Si(OCH ₂ CH ₂) ₃ N	80
2.8 Chapter 2 summary	81
2.9 Chapter 2 references	83

Chapter 3: Understanding ligand coordination behaviour in the development of oxide-supported hydroformylation pre-catalysts

3.1 Chapter 3 Aims/introduction	87
3.2 Characterisation of ligand steric and electronic donor characteristics	87
3.2.1 Assessing phosphine donor properties: phosphine basicity studies	87
3.2.2 Quantifying the steric bulk of tetherable phosphine compounds	91
3.2.3 Plot of phosphine %V _{bur} against ¹ J _{SeP} coupling constants	96
3.3 Coordination studies of (PPh ₂) ₂ N(CH ₂) ₃ Si(OMe) ₃ , (PPh ₂) ₂ N(CH ₂) ₃ Si(OCH ₂ CH ₂) ₃ N, ((C ₁₂ H ₈ O ₂)P) ₂ N(CH ₂) ₃ Si(OMe) ₃ , ((C ₁₂ H ₈ O ₂)P) ₂ N(CH ₂) ₃ Si(OCH ₂ CH ₂) ₃ N, ((C ₂₀ H ₁₂ O ₂)P) ₂ N(CH ₂) ₃ Si(OCH ₂ CH ₂) ₃ N, (Ph ₂ PCH ₂) ₂ N(CH ₂) ₃ Si(OMe) ₃ , (Ph ₂ PCH ₂) ₂ N(CH ₂) ₃ Si(OCH ₂ CH ₂) ₃ N, (^t Bu ₂ PCH ₂) ₂ N(CH ₂) ₃ Si(OCH ₂ CH ₂) ₃ N, (Cy ₂ PCH ₂) ₂ N(CH ₂) ₃ Si(OCH ₂ CH ₂) ₃ N, ((C ₁₂ H ₈ O ₂)POCH ₂ CH ₂) ₂ N(CH ₂) ₃ Si(OMe) ₃ , (PPh ₂) ₂ NCH ₂ CH ₂ CH ₂ CH ₃ and (P(S)Ph) ₂ N(CH ₂) ₃ Si(OCH ₂ CH ₂) ₃ N with rhodium(I)	97
3.3.1 Literature Rh(acac)(P [^] P) complex syntheses	98
3.3.2 Reactions of (Ph ₂ P) ₂ NCH ₂ CH ₂ CH ₂ CH ₃ : L23 , with Rh(acac)(CO) ₂	99

3.3.3 Rh(acac)(L23) synthesis optimisation	100
3.3.4 Coordination studies of (PPh ₂) ₂ N(CH ₂) ₃ Si(OMe) ₃ , (PPh ₂) ₂ N(CH ₂) ₃ Si(OCH ₂ CH ₂) ₃ N, (P(C ₁₂ H ₈ O ₂)) ₂ N(CH ₂) ₃ Si(OMe) ₃ , (Ph ₂ PCH ₂) ₂ N(CH ₂) ₃ Si(OMe) ₃ and ((C ₁₂ H ₈ O ₂)POCH ₂ CH ₂) ₂ N(CH ₂) ₃ Si(OMe) ₃ , with rhodium(acac)(COD)	103
3.3.5 Synthesis of Rh(acac)(L19)	104
3.3.6 Attempted synthesis of Rh(acac)(BISBI)	105
3.3.7 [Rh(P [^] P) ₂]acac complex syntheses	106
3.3.8 Syntheses of [Rh(P [^] P) ₂]BF ₄ complexes	108
3.3.9 Synthesis of [Rh(L19)(COD)]BF ₄	110
3.3.10 Synthesis of [Rh(L5S2)(COD)]BF ₄	111
3.4 Investigation into the coordination chemistry of tetherable phosphines with cobalt(II) and palladium(II)	112
3.4.1 Literature phosphine-containing palladium hydroformylation catalysts	112
3.4.2 Synthesis of PdI ₂ (P [^] P) complexes	115
3.4.3 CoBr ₂ reactivity study with PNP ligands	121
3.5 Chapter 3 summary	124
3.6 Chapter 3 references	125

Chapter 4: Reactivity studies of tetherable phosphines with silica, and synthesis of immobilised phosphine rhodium complexes for applications in hydroformylation

4.1 Introduction to phosphine ligand silica-immobilisation	129
4.2 Silica immobilisation of (3-aminopropyl)trimethoxysilane	134
4.3 Silica immobilisation of L1 : (Ph ₂ P) ₂ N(CH ₂) ₃ Si(OMe) ₃	137
4.4 Investigation the effect of the tethering functionality on side product formation during the silica-immobilisation of dppa-type phosphines	138
4.5 A two-step synthesis of silica-immobilised L1 : (Ph ₂ P) ₂ N(CH ₂) ₃ Si(OMe) ₃ , <i>via</i> silica- immobilised (3-aminopropyl)trimethoxysilane	143
4.6 Reactivity of tetherable phosphites L9 : (P(C ₁₂ H ₈ O ₂)) ₂ N(CH ₂) ₃ Si(OMe) ₃ and L21 : ((C ₁₂ H ₈ O ₂)POCH ₂ CH ₂) ₂ N(CH ₂) ₃ Si(OMe) ₃ with silica	145
4.7 Synthesis and reactivity of L24 : 2,2'-bis(dibenzo[d,f][1,3,2]dioxaphosphepin-6-yloxy)- 1,1'-biphenyl with silica	146
4.8 Possible phosphorus oxidation pathways for phosphites on silica	148
4.9 Introducing the silatrane functionality as a convenient silica tethering group	149
4.10 3-Chloropropylsilatrane synthesis and immobilisation on silica	150
4.11 Investigations into utilising phosphine-borane protecting groups in the synthesis of silica-immobilised phosphines	152
4.11.1 Attempted synthesis of L5 (BH ₃) ₂ : ((BH ₃)PPh ₂) ₂ N(CH ₂) ₃ Si(OCH ₂ CH ₂) ₃ N	153
4.11.2 Synthesis of L17 (BH ₃) ₂ (Ph ₂ P(BH ₃)CH ₂) ₂ N(CH ₂) ₃ Si(OCH ₂ CH ₂) ₃ N	157

4.12. Synthesis of silica-immobilised rhodium(I) complexes	158
4.12.1 Silica immobilisation of [Rh(L5S ₂)(COD)]BF ₄	159
4.12.2 Silica immobilisation of [Rh(L19)(COD)]BF ₄	161
4.12.3 Silica immobilisation of [Rh(L5) ₂]BF ₄	162
4.12.4 Silica immobilisation of [Rh(L17) ₂]BF ₄	164
4.13 Investigating the reaction of Ph ₂ PCI with silica	165
4.14 Rh(acac)(CO) ₂ complexation with silica-PPh ₂	169
4.15 Synthesis of a Fibrecat™ supported rhodium complex	169
4.16 Determination of heterogeneous catalyst rhodium loadings	170
4.17 Chapter 4 summary	171
4.18 Chapter 4 references	173
 Chapter 5: 1-Octene hydroformylation using homogeneous and silica-immobilised rhodium and palladium complex catalysts	
5.1 Aims of hydroformylation catalyst testing	177
5.2 Homogeneous hydroformylation catalysis results and discussion	177
5.2.1 Rh-catalysed homogeneous hydroformylation reaction conditions	177
5.2.2 Comparison of catalyst performance in homogeneous hydroformylation	178
5.2.3 Sulfur donor ligands in homogeneous hydroformylation catalysis results and discussion	185
5.2.4 [Rh(P [^] P) ₂]BF ₄ catalyst induction periods	187
5.2.5 Hydroformylation activity comparison of PNP- and PCNCP-containing catalysts ...	189
5.3 Heterogeneous hydroformylation catalysis results and discussion	191
5.3.1 Rhodium-catalysed heterogeneous hydroformylation reaction conditions	191
5.3.2 Heterogeneous hydroformylation catalyst activity comparison	192
5.3.3 Homogeneous vs heterogeneous [Rh(P [^] P) ₂]BF ₄ catalyst induction period comparison	194
5.3.4 Investigating rhodium loss from heterogeneous catalysts during hydroformylation reactions	200
5.3.5 Sil-[Rh(L17) ₂]BF ₄ catalyst recycling study	204
5.4 Hydroformylation activity comparison between homogeneous and analogous silica-immobilised catalysts	207
5.5 Palladium-catalysed hydroformylation preliminary investigation	210
5.6 Chapter 5 summary	212
5.7 Chapter 5 references	214
Future work	217

Chapter 6: Experimental

6.1 General considerations.....	220
6.2 Chapter 2 experimental.....	223
6.2.1 Synthesis of PNP-type ligands	223
6.2.2 Synthesis of PCNCP-type compounds	233
6.2.3 Synthesis of wide bite angle tetherable phosphines.....	239
6.2.4 Synthesis of tetherable sulfur ligands	241
6.3 Chapter 3 experimental.....	242
6.3.1 General procedure for preparation of diphosphinediselenides.....	242
6.3.2 Synthesis of rhodium(I) complexes	243
6.3.3 Synthesis of Palladium(II) complexes	252
6.3.4 Synthesis of cobalt(II) complexes	258
6.4 Chapter 4 experimental.....	259
6.4.1 Synthesis and stability testing of silica-immobilised (3-aminopropyl)trimethoxysilane	259
6.4.2 Silica-immobilisation of phosphine compounds	260
6.4.3 Investigating phosphine protection as BH_3 adducts.....	266
6.4.4 Synthesis of silica-immobilised rhodium hydroformylation catalysts.....	269
6.4.5 Investigating the reactivity of chlorophosphines with silica and alumina	271
6.4.6 Synthesis of a Fibrecat TM -supported rhodium hydroformylation catalyst	273
6.5 Chapter 5 experimental.....	274
6.5.1 Hydroformylation reactor setup.....	274
6.5.2 Homogeneous hydroformylation catalysis.....	274
6.5.3 Heterogeneous hydroformylation catalysis	275
6.5.4 Autoclave cleaning.....	275
6.6 Chapter 6 references	275
Appendix A: Synthesis of multidentate tetherable phosphine ligands	277
Appendix B: Crystallographic data	281
Appendix C: GC calibration curves for 1-octene and nonanal in the hydroformylation of 1-octene	288

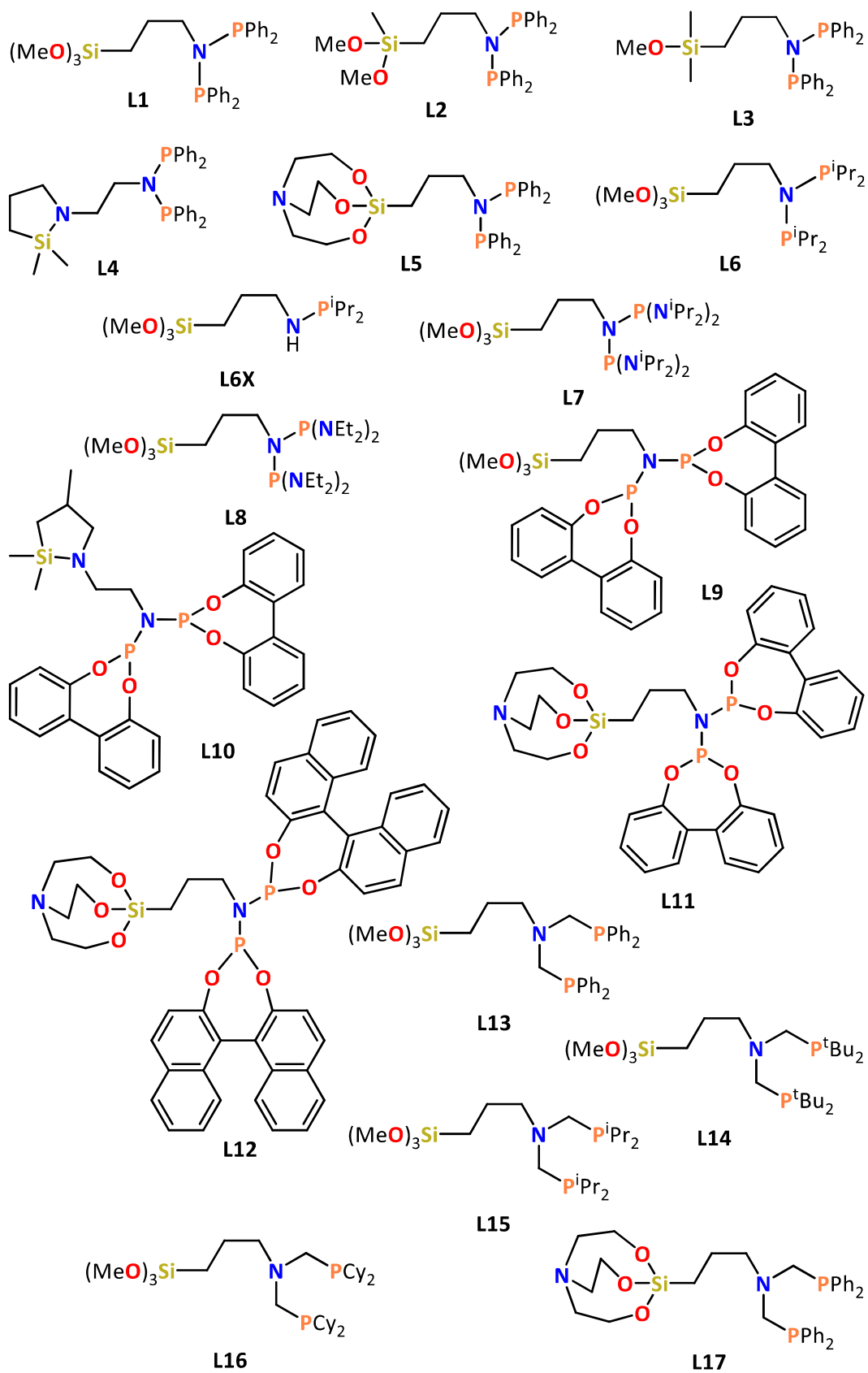
Abbreviations

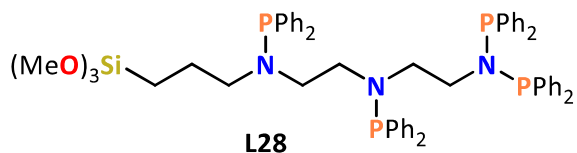
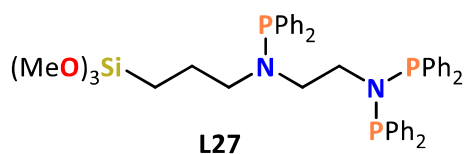
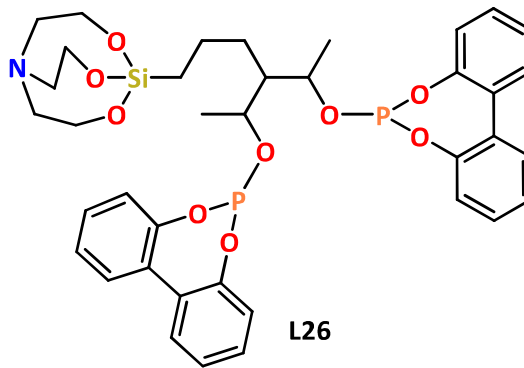
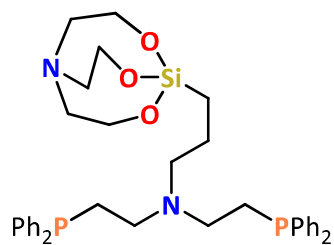
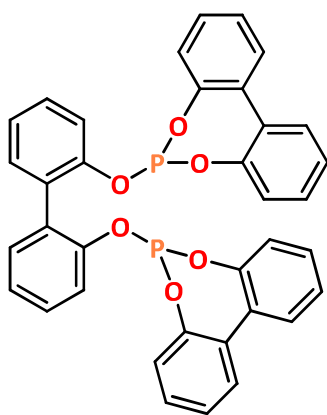
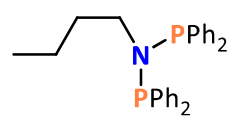
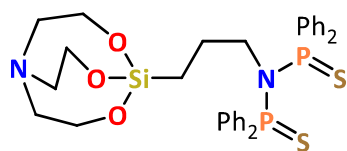
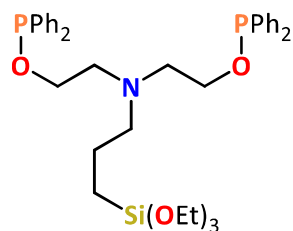
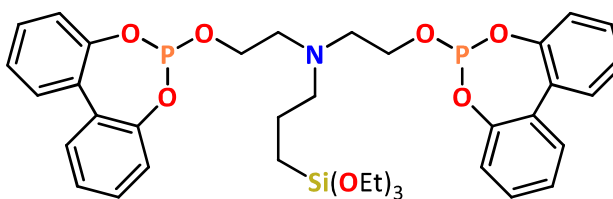
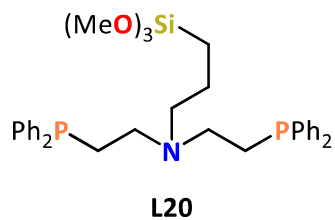
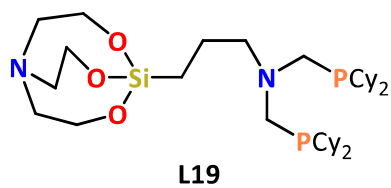
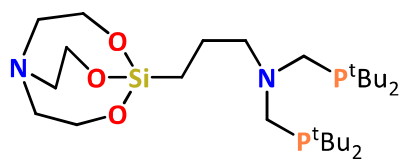
Ac	acetyl	k	kelvin
Ar	aromatic group	<i>l:b</i>	<i>linear:branched (ratio)</i>
ATR	attenuated total reflectance	m	metre
Bn	benzyl (-CH ₂ C ₆ H ₅)	m	multiplet
CHN	Carbon Hydrogen Nitrogen	MAS	magic angle spinning
cm	centimetre	Me	methyl (-CH ₃)
CP	cross-polarisation	ⁿBu	<i>n</i> -butyl (-CH ₂) ₃ CH ₃)
Cp	cyclopentadienyl (C ₅ H ₅)	NMR	nuclear magnetic resonance
Cy	cyclohexyl (-C ₆ H ₁₁)	p^p	bidentate phosphine
d	doublet	Ph	phenyl (-C ₆ H ₅)
DFT	density functional theory	PONA	paraffins, olefins, naphthenes and aromatics
Et	ethyl (-CH ₂ CH ₃)	ppm	parts per million
FT-IR	Fourier transform infrared	Py	pyridyl (-C ₄ H ₄ N)
g	gram(s)	RPM	revolutions per minute
GC-FID	gas chromatography - flame ionisation detector	RT	room temperature
h	hour	s	singlet
HPDEC	high-power decoupling	SS	Solid-state
HR	high-resolution	t	triplet
Hz	Hertz	^tBu	<i>tert</i> -butyl (-C(CH ₃) ₃)
IAR	inverse aqua regia	TOF	turn over frequency
ICP-OES	inductively coupled plasma-optical emission spectroscopy	TON	turn over number
ⁱPr	<i>iso</i> -propyl (-CH(CH ₃) ₂)	tt	triplet of triplets
		UHP	ultra-high purity
		XRD	X-ray diffraction
		Å	Angström (10 ⁻¹⁰ m)
		°C	degrees Celsius
		%V_{bur}	percent buried volume

Chemical compound abbreviations:

acac	acetylacetonate anion
BAr^F₄	tetrakis(3,5-bis(trifluoromethyl)phenyl)borate anion
BINAP	2,2'-bis(diphenylphosphino)-1,1'-binaphthyl
BISBI	2,2'-bis(diphenylphosphino-methyl)-1,1'-biphenyl
COD	cyclooctadiene
Cyp	cyclopropane
<i>dbtpp</i>	di-tertbutyl-1,3-bisphosphinopropane
DCM	dichloromethane
dppa	diphenylphosphinoamine
dppe	diphenylphosphinoethane
dppf	1,1'-ferrocenediyl-bis(diphenylphosphine)
dppm	diphenylphosphinomethane
DsBPP	di-secbutyl-1,3-bisphosphinopropane
LDA	lithium diisopropylamide
NMP	<i>N</i> -methyl-2-pyrrolidone
TEA	triethanolamine
TFA	trifluoroacetic acid
THF	tetrahydrofuran
TMOS	tetramethyl orthosilicate
TPPTS	triphenylphosphine trisodium sulfonate
VMD	2-vinyl-5-methyl-1,3-dioxane

List of compounds





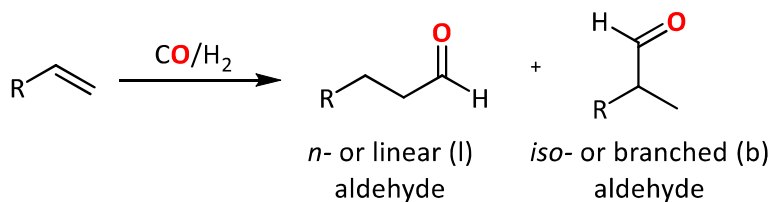
Chapter 1: Introduction

1.0 literature review

This literature review presents a short introduction to aspects of hydroformylation chemistry relevant to the work presented in the following chapters of this thesis. Of particular focus are the development and challenges faced in industrial hydroformylation processes. Additionally, the approaches used to immobilise homogeneous catalysts onto solid oxide supports, alongside their application in immobilised hydroformylation catalysis will be discussed. This literature review was performed up to February 2024.

1.1 Introduction to hydroformylation

Hydroformylation, also known as the Oxo process, has become one of the largest and most important homogeneously-catalysed processes since its discovery by Otto Roelen in 1938.¹ In the reaction, an alkene is combined with CO and hydrogen (synthesis gas) to produce an aldehyde, extending the carbon chain by one atom (Scheme 1.1).



Scheme 1.1. General hydroformylation reaction.

The industrial importance of the hydroformylation reaction primarily derives from the value of the aldehyde products as intermediates for the manufacture of a wide variety of commercially important chemicals.^{2,3} Indeed, hydroformylation is used to produce over 10 million metric tonnes of so-called oxo chemicals per year worldwide.⁴ These chemicals find application in a range of roles such as solvents, detergent alcohols, plasticisers and surfactants *via* various subsequent chemical processes (Figure 1.1). Typically, linear aldehydes are desired for these commercial applications although there is also demand for branched aldehydes, such as isobutanal. One industrially attractive benefit of hydroformylation is its theoretical 100% atom economy that, combined with

the use of a metal complex catalyst, makes the reaction attractive from a sustainable, green chemistry point of view.^{5,6}

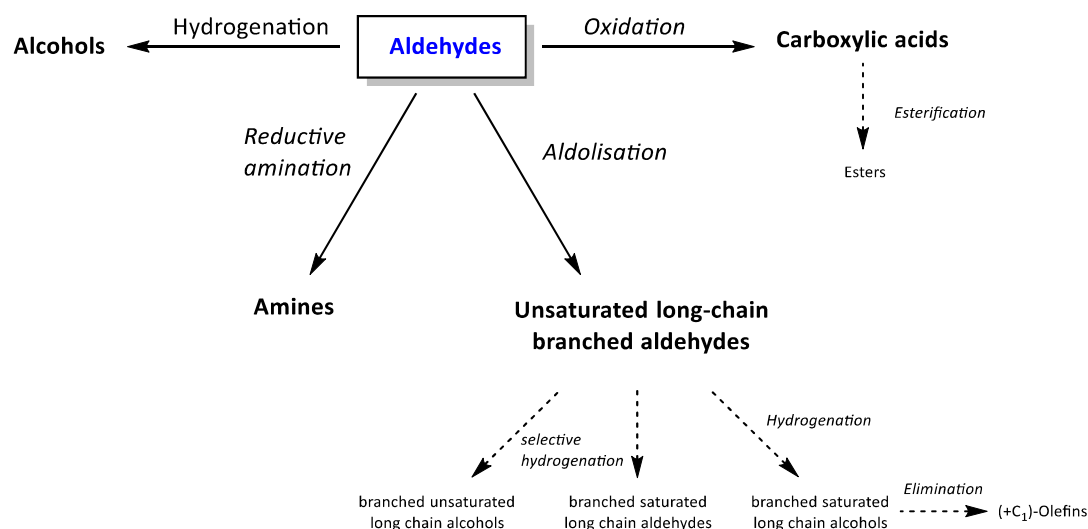
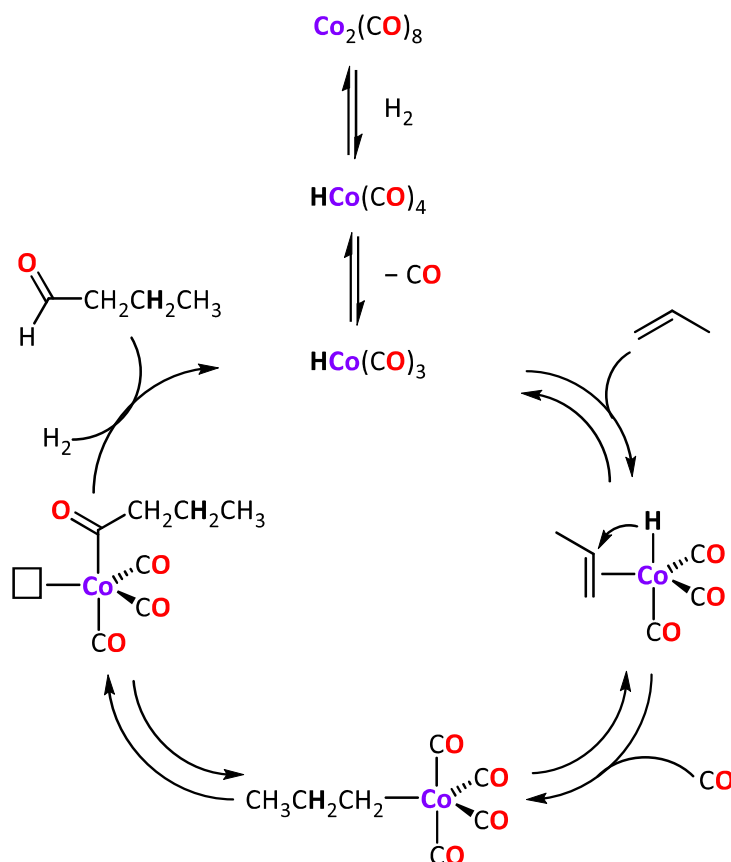


Figure 1.1. Products derived from aldehydes produced by hydroformylation. Modified from Franke et al.⁴

1.2 Mechanism and kinetics of first generation hydroformylation catalysis

The active catalytic species used by Otto Roelen in hydroformylation was determined to be the hydride-containing cobalt carbonyl species $\text{HCo}(\text{CO})_3$, generated from $\text{Co}_2(\text{CO})_8$ under a pressure of hydrogen, *via* a $\text{HCo}(\text{CO})_4$ resting state (Scheme 1.2).^{7–10} Much work has gone into determining the kinetics and rate determining step for the hydroformylation reaction, which are highly variable depending on the conditions used.^{11–13} Under most conditions, the derived kinetics of the reaction show that rate is proportional to the concentration of alkene substrate, cobalt catalyst and H_2 concentration, but inversely proportional to CO concentration (Equation 1.1).^{8,9} This rate equation corresponds to coordination of the alkene substrate to the metal as the rate determining step. The inverse proportionality with respect to CO concentration is explained as CO dissociation from the complex is required to produce a vacant coordination site for alkene complexation.



Scheme 1.2. Catalytic cycle for the HCo(CO)_3 -catalysed hydroformylation of propene to give the linear aldehyde, excluding side reactions.⁹

$$\frac{d(\text{aldehyde})}{dt} = \frac{k[\text{alkene}][\text{Co}][\text{H}_2]}{[\text{CO}]}$$

Equation 1.1. General rate equation for the cobalt-catalysed hydroformylation of alkenes.¹¹

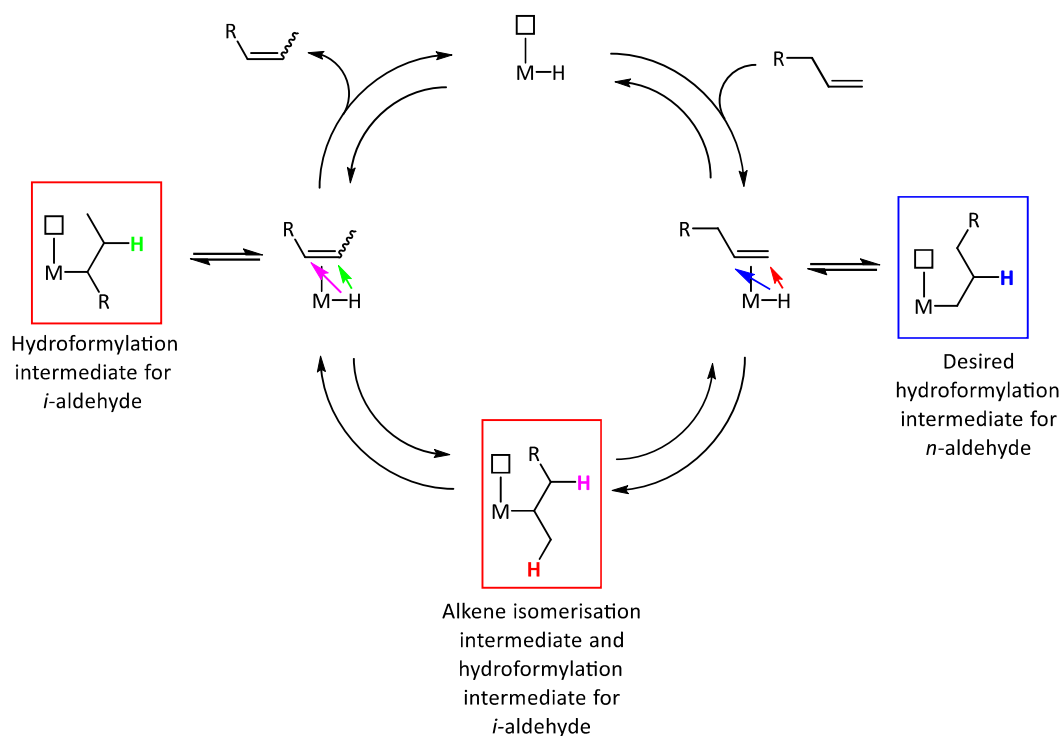
Although alkene coordination to the metal centre is the most commonly identified rate determining step in hydroformylation, other steps, such as the oxidative addition of H_2 , have been observed to be rate determining under differing reaction conditions.¹⁴ Such conditions can occur when under sufficiently low pressures of CO and H_2 , which results in facile alkene complexation alongside slow oxidative addition of H_2 . Indeed, the hydroformylation reaction conditions (temperature and pressure), catalyst precursor,

alkene substrate and the ratio of metal to substrate can all affect the exact species present in the reaction and the rate determining step.

Hydroformylation using $\text{HCo}(\text{CO})_4$ is usually performed using high pressures of syngas of at least 200 bar of H_2 and CO, conditions used to maximise catalyst stability.⁴ A minimum CO partial pressure is needed to balance the high reaction temperatures required to ensure a viable reaction rate (typically 110 - 180 °C), against the thermal instability of $\text{HCo}(\text{CO})_4$, which decomposes to metallic cobalt if the CO partial pressure is too low. Despite the suppressive effect of CO on reaction kinetics, higher CO partial pressures have the additional advantage of decreasing the amount of alkene isomerisation side reactions, while increasing the aldehyde linear to branched product ratio.

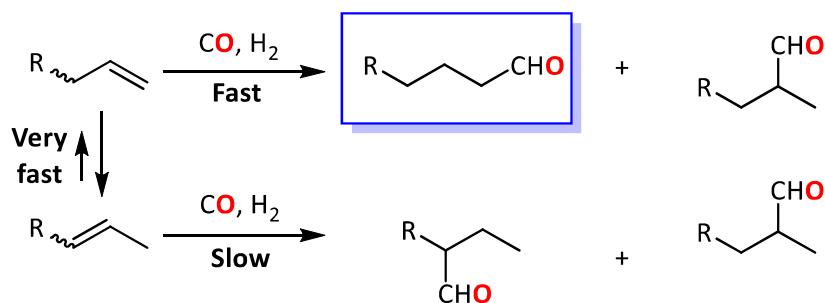
1.3 Competing hydroformylation reactions and side products

Understanding of the hydroformylation reaction becomes significantly more complicated when the regiochemistry of the reaction is considered, since hydride transfer to the double bond during catalysis can occur at either carbon, giving rise to the possibility of branched isomers being produced (Scheme 1.3).¹⁵ In addition, isomerisation of the substrate double bond, which can also be transition metal-catalysed, can further complicate the reaction and lead to the formation of other branched species. Together, these competing reactions result in a typical selectivity for the linear aldehyde of around 66% for $\text{HCo}(\text{CO})_4$ catalyst systems.⁴ The high syngas pressures employed during the reaction can help to further suppress side reactions, resulting in *l:b* ratios of up to 3:1 being achieved using $\text{HCo}(\text{CO})_4$ -based systems.⁸ Indeed, it is often assumed that competition between isomerisation and hydroformylation is primarily a function of CO partial pressure (especially for cobalt-based systems).



Scheme 1.3. Metal-catalysed isomerisation of alkenes, showing possible hydroformylation intermediates that can be formed to give linear or branched isomers.¹⁵

Since internal alkenes are more thermodynamically stable than the terminal alkenes, good kinetic control is required during hydroformylation to produce a linear aldehyde, as this requires reaction of the terminal alkene.¹⁵ During hydroformylation, CO migratory insertion has been shown to be faster for terminal alkenes than internal alkenes, due to predominantly steric effects.¹⁶ When combined with very fast double bond isomerisation, the linear aldehyde is found to be the favoured product (Scheme 1.4). However, as described above, the exact ratio of products is very dependent on the reaction conditions and therefore producing a system that gives the best possible control over selectivity is one of the greatest ongoing challenges in hydroformylation chemistry.¹⁶



Scheme 1.4. Possible aldehyde products from hydroformylation when considering alkene isomerisation and hydride insertion at either C=C carbon.

Alkene branching has a large effect on isomerisation and hydroformylation when non-linear alkene substrates are employed. In a study of various methylheptenes, Haymore found that there was very little hydroformylation at the carbon center with the branch, even if it was part of the double bond.¹⁷ Additionally, it was observed that isomerisation past the branching carbon is not a dominant reaction.

Yet a further complication in olefin hydroformylation using $\text{HCo}(\text{CO})_4$ catalyst systems is commonly observed aldehyde hydrogenation to alcohols, typically 5-12%.¹⁸ However, aldehyde hydrogenation is not always considered to be a negative side reaction, since depending on the target market, the aldehyde products are often hydrogenated to alcohols in a later reaction step. Aldehyde hydrogenation, however, consumes additional H_2 , so H_2/CO ratios greater than 1:1 are used (1-1.5:1 are common).¹⁸ Other possible side products observed during $\text{HCo}(\text{CO})_4$ -catalysed hydroformylation are alkanes resulting from alkene hydrogenation, but their formation is usually quite low (~1%), particularly under higher CO partial pressures.¹⁹

1.4 Second generation phosphine-modified hydroformylation catalysts

In order to improve the selectivity for linear aldehydes, Slaugh and Mullineaux from the Shell Development Company developed an alternative catalytic system using $\text{Co}_2(\text{CO})_8$ / PBu_3 as a catalyst precursor. This gives what is now known to be the catalytically active *trans*- $\text{CoH}(\text{CO})_3(\text{PR}_3)$ species under reaction conditions.^{20,21} By replacing labile CO with phosphine ligands, a more stable catalyst is produced, enabling lower reaction pressures

by circumventing the issues of $\text{HCo}(\text{CO})_{3/4}$ stability. Indeed, the incorporation of a phosphine ligand enables a dramatic reduction in the CO partial pressures required to stabilise the catalyst and prevent formation of cobalt metal. Instead of 200-300 bar of H_2/CO pressure needed for $\text{HCo}(\text{CO})_4$, the monophosphine-substituted $\text{HCo}(\text{CO})_3(\text{PR}_3)$ requires 50-100 bar of pressure, and can be run at higher temperatures without any decomposition of catalyst to cobalt metal. An obvious additional benefit of phosphine-modified systems comes from the steric constraints imposed by the incorporation of a bulkier phosphine ligand compared to CO, with the additional steric bulk favouring formation of linear products. While linear to branched ratios of only 2-3:1 are found typically for $\text{HCo}(\text{CO})_4$, higher regioselectivities of 7-8:1 can be achieved with $\text{HCo}(\text{CO})_3(\text{PR}_3)$.²¹ Despite it being possible to incorporate additional steric bulk (greater cone angle) through choice of different phosphines, it has been demonstrated that there is a phosphine cone angle cutoff at about 132° , above which increasing the phosphine ligand's steric demands do not increase further the product linear regioselectivity.²²

Despite the apparent benefits achieved through addition of phosphine ligands, several downsides are also encountered compared with the un-modified catalyst systems.⁴ Firstly, a vastly reduced rate is observed (typically 5-10 times slower than with $\text{HCo}(\text{CO})_4$). By replacing the strongly π back-bonding CO ligands with σ -electron donating, very poorly π -accepting phosphines, the cobalt complex is made much more electron rich. This increases the interaction between the remaining CO ligands and the cobalt, disfavoring CO ligand dissociation required for alkene substrate binding. To combat this, higher reaction temperatures of 120-190 $^\circ\text{C}$ are used to maintain an acceptable rate of the $\text{HCo}(\text{CO})_3(\text{PR}_3)$ systems.²¹ Another consequence of the more electron-rich metal center resulting from phosphine coordination is that the Co-H bond is more hydridic in character. This results in the catalyst being highly active for hydrogenation, which has a large effect on the composition of the resulting organic products, as the aldehydes produced are reduced to alcohols *in situ*. The increased hydridic character of the Co-H bond also contributes to the enhanced *l/b* selectivity, as the more hydridic H is even more favoured to react with the most electrophilic carbon of the bound alkene substrate, increasing selectivity for the linear product.^{22,23} The better hydrogenation ability, however, also results in increased alkene hydrogenation

side-reactions producing alkanes, that can range from 10-20% of the product distribution (depending on the phosphine and reaction conditions). Combined hydroformylation/hydrogenation processes can be advantageous and are used industrially to produce alcohols directly in one step. As a result of the occurrence of aldehyde hydrogenation, more H₂ is consumed, so H₂/CO ratios of 2:1 (or slightly higher) are typically used.²¹

1.5 Third generation rhodium hydroformylation catalysts

As a result of the problems encountered with cobalt hydroformylation catalysts, attention turned to investigating other transition metals for activity in hydroformylation catalysis.²⁴ The result of these investigations using unmodified metal carbonyl catalysts showed that rhodium has the highest activity and selectivity for aldehyde formation, followed by cobalt, with a large drop in performance for all other metals tested (Figure 1.2). However, more recently, modification of the metal catalyst, *e.g.*, by addition of phosphine ligands, has been shown to provide significant enhancement in catalyst performance for some of the traditionally poor performing metals, especially Pd, which will be discussed in chapter 3.3.

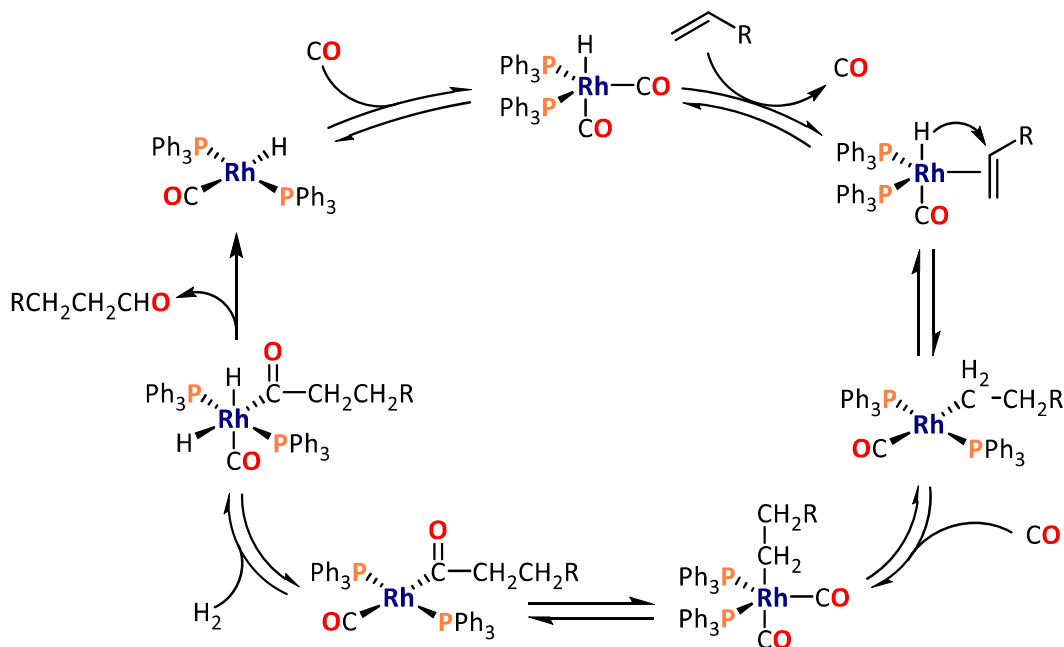


Figure 1.2. Trend of hydroformylation catalytic activity for some transition metals.

Due to the high catalytic performance of rhodium in hydroformylation, development of so-called “second generation hydroformylation processes” has taken place, using firstly unmodified rhodium catalysts, followed by phosphine ligand modified catalysts.^{25–27} The high activity and selectivity of rhodium has enabled industrial processes to be developed using significantly lower reaction temperatures and pressures. Additionally, the greater stability of the rhodium complexes used also allows distillation of the product without the costly separation steps required for cobalt (See section 1.12). The significant developments associated around rhodium-based hydroformylation led to 80% of the world’s hydroformylation processes exploiting rhodium catalysts by 1995.²⁸ However, cobalt catalysts are still often used for the hydroformylation of long chain alkenes

derived from the Shell Higher Olefin Process (SHOP) or Fischer–Tropsch synthesis, as they are better suited to the conversion of the mixtures of linear and branched alkenes present in these feedstocks.⁴

The mechanism of rhodium-catalysed hydroformylation has been shown to be similar to that of the cobalt-catalysed process. The rhodium catalyst is most selective for the linear aldehyde when coordinated by two phosphine ligands.²⁹ The catalytic cycle starts from a trigonal bipyramidal $\text{HRh}(\text{CO})_2(\text{PPh}_3)_2$ species, analogous to $\text{HCo}(\text{CO})_4$, that loses a CO ligand, enabling alkene substrate coordination (Scheme 1.5).²⁹



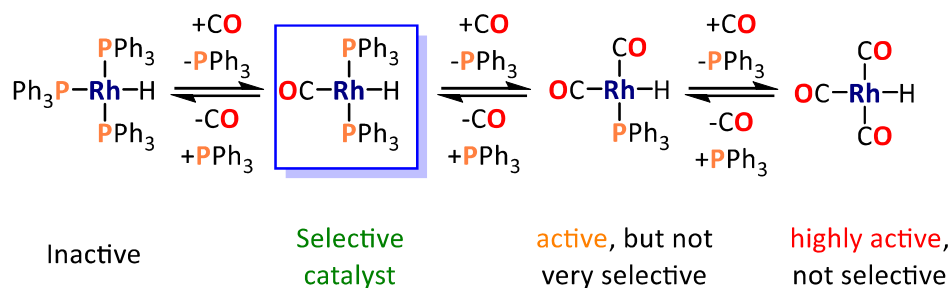
Scheme 1.5. Rhodium-catalysed hydroformylation catalytic cycle.^{8,29}

The first rhodium-based hydroformylation catalyst system was derived from Wilkinson's catalyst, $\text{RhCl}(\text{PPh}_3)_3$, but it was rapidly discovered that halides were inhibitors for hydroformylation.^{30,31} Thus, it is therefore often preferable to employ halide-free rhodium starting complexes; for example, $\text{HRh}(\text{CO})(\text{PPh}_3)_3$ and $\text{Rh}(\text{acac})(\text{CO})_2$ (acac = acetyl acetonate) are two commonly used starting materials. Pruett (Union Carbide) and Booth (Union Oil) both separately demonstrated that use of a catalyst system based on $\text{HRh}(\text{CO})(\text{PPh}_3)_2$, allowed commercialisation of the hydroformylation technology for propylene conversion to butyraldehyde (Table 1.1).³² They found that the use of rhodium with excess phosphine ligand created an active, selective, and stable catalyst

system, which could operate at just 5-7 bar syngas pressure and 90 °C. Union Carbide, in conjunction with Davy Powergas and Johnson Matthey, subsequently developed the first commercial hydroformylation process using rhodium and excess PPh_3 in the early 1970s.³⁰ The need for excess phosphine arises as a consequence of the facile Rh-PPh_3 dissociation equilibrium (Scheme 1.6). Loss of PPh_3 from $\text{HRh(CO)(PPh}_3)_2$ generates considerably more active, but less regioselective hydroformylation catalysts.³⁰ The addition of excess phosphine ligand shifts the phosphine dissociation equilibrium towards the more selective $\text{HRh(CO)(PPh}_3)_2$ species. This explains why higher CO partial pressures lower the product regioselectivity, in marked contrast to what is observed for HCo(CO)_3 -catalysed hydroformylation.

Table 1.1. Summary – Comparison of Industrial Hydroformylation Processes.^{4,23,30,32}

	Co		Rh		
	<i>Unmodified</i>	<i>Modified</i>	<i>Unmodified</i>	<i>Modified</i>	
Active species	HCo(CO)_4	$\text{HCo(CO)}_3\text{L}$	HRh(CO)_4	HRh(CO)L_3	HRh(CO)L_3
T / °C	150-180	160-200	100-140	60-120	110-130
P / bar	200-300	50-150	200-300	10-50	40-60
Cat: olefin (%)	0.1-1	0.5-0.8	0.0001-0.01	0.01-0.1	0.001-1
Products	Aldehydes	Alcohols	Aldehydes	Aldehydes	Aldehydes
By-products	High	High	Low	Low	Low
Typical <i>n/i</i>	60:40	85:15	50:50	92:8	95:5
Sensitivity to poisons	low	low	low	high	low
Operator	BASF/ Ruhrchemie	Shell	Ruhrchemie	Union Carbide	Rhône-Poulenc

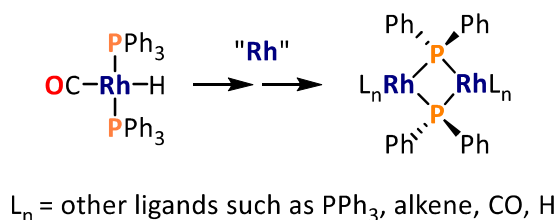


Scheme 1.6. Equilibria associated with rhodium- PPh_3 hydroformylation catalysts.^{29,30}

Remarkably, the rate determining step in Rh/ PPh_3 -catalysed hydroformylation remains poorly understood even today. It was assumed initially, by analogy with the $\text{HCo}(\text{CO})_4$ catalyst system, that oxidative addition of H_2 to the Rh^{I} -acyl species (Scheme 1.5) would be rate-determining due to the low syngas pressures employed. However, Kastrup and coworkers concluded from ^{31}P NMR spectroscopic studies that the rate determining step could be the initial coordination of alkene to the $\text{HRh}(\text{CO})(\text{PPh}_3)_2$ catalyst species.³³ In a similar fashion, Moser and colleagues proposed that the rate determining step is CO dissociation from $\text{HRh}(\text{CO})_2(\text{PPh}_3)_2$ to once again generate the 16e^- species $\text{HRh}(\text{CO})(\text{PPh}_3)_2$ required for alkene coordination (Scheme 1.5).³⁴ Indeed, more recent combined experimental and computational approaches have suggested that the kinetics of rhodium-catalysed hydroformylation are more complicated than expected, as a single rate determining steps does not control the overall reaction rate, as would be predicted from classical kinetics.^{35,36} Instead several similar-energy transition states contribute to the overall energy barrier and reaction rate.

The high product regioselectivity achieved using $\text{HRh}(\text{CO})(\text{PPh}_3)_2$ is strongly related to the concentration of PPh_3 in solution (up to a certain point) and the H_2/CO ratio used.³⁰ Commercial hydroformylation reactions are run using solutions that have PPh_3 concentrations of 0.3 M or higher (typical Rh concentration around 1 mM). This corresponds to PPh_3 weight percentages of 8-50% of the total solution in commercial reactors (Table 1.1). Lower CO partial pressures would also be expected to favour higher regioselectivities, and this is indeed the case. Rh/ PPh_3 reactions are often run with an excess of hydrogen (1.2:1 $\text{H}_2:\text{CO}$ ratios are common). However, if the hydrogen partial pressure is too high, or the CO partial pressure too low, this increases the alkene hydrogenation and isomerisation side reactions to an unacceptable level.³⁰ The other

principle, important reason for adding excess phosphine ligand is to minimize ligand fragmentation reactions that lead to catalyst deactivation. At the typical operating conditions for hydroformylation, especially the higher temperatures employed with cobalt systems, arylphosphines can undergo P–C bond cleavage (a process that is rapid at $\geq 190^\circ\text{C}$) generating arenes and a variety of metal phosphide-type complexes.^{37–39} For example, highly unsaturated and electrophilic species such as $\text{HRh}(\text{CO})(\text{PPh}_3)$ present in the reaction can attack the PPh_3 ligand (either through an *intra*- or *inter*-molecular pathway), resulting in oxidative addition of the P–Ph bond to an unsaturated Rh center. This leads to the formation of either alkyldiphenyl phosphines or, in the worst case, phosphide-bridged dimers, which are inactive for hydroformylation (Scheme 1.7).^{37–39}



*Scheme 1.7. PPh_3 degradation under hydroformylation reaction conditions leading to formation of rhodium phosphide-bridged dimers species.*³⁸

In order to further improve the efficiency of the hydroformylation reaction, many detailed investigations into the effect of different phosphine ligands on catalysis have been performed.^{40–44} A comprehensive understanding of the behaviour and reactivity of phosphines is required to accomplish this, so that catalysts can be designed to maximise activity and selectivity. Therefore, a brief overview of phosphine coordination to metals will be presented in Section 1.6.

1.6 Phosphine ligand-metal coordination: steric and electronic effects

1.6.1 Determining the electronic contribution of phosphines in metal complexes

The electronic bonding contribution of phosphines to metals consists of σ -bond lone pair donation from the phosphine to metal and π -back bonding from filled metal orbitals to phosphine P–R σ^* orbitals (Figure 1.3).⁴⁵ Note, the extent of metal-to-phosphorus

retrodonation is extremely dependent on the nature of the substituents at phosphorus, with alkyl phosphines generally regarded as having little/no π -acceptor character, while amido- and alkoxide-substituted derivatives are more complicated because of competing π -donation from the OR and NR₂ motifs, despite these substituents lowering the energy of the σ^* MO acceptor orbitals. To facilitate comparisons, Tolman defined an electronic parameter, ν , which categorises the overall electronic contribution of phosphines to metal complexes by examining the carbonyl stretching frequencies of sterically unhindered [Ni(CO)₃(PR₃)] complexes.⁴⁶

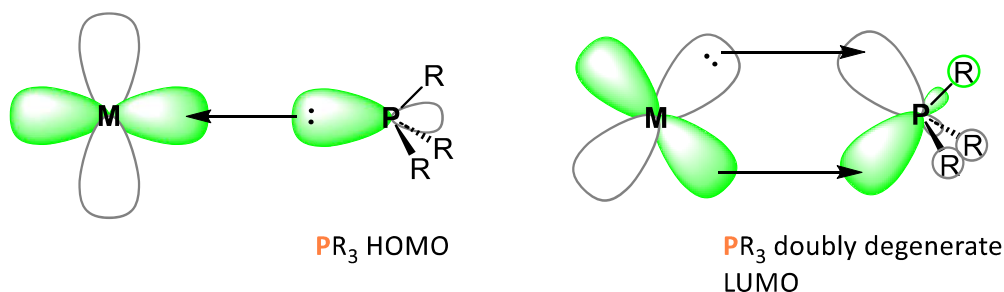


Figure 1.3. σ -Bonding and π -back bonding orbital interactions of a metal-phosphine bond.⁴⁵

The general trend in the change of ν as a function of R, outlined in Table 1.2, shows that as the phosphine R group becomes more electronegative, the value of ν increases, *e.g.*, $\text{P}(\text{CH}_3)_3 < \text{P}(\text{OCH}_3)_3 < \text{PF}_3$. More electron donating R groups increase electron density on the phosphorus, enabling greater sigma donation from P to Ni.⁴⁷ The resulting more electron rich metal centre increases back-bonding into CO π^* orbitals, weakening the CO bonds and reducing ν . Electron withdrawing phosphines have weaker sigma donation from P to Ni and therefore less electron density on the metal that can be donated into CO π^* orbitals, resulting in a larger value of ν . In the context of hydroformylation a larger value of ν results in a weaker M-CO bond that enables faster CO ligand dissociation, resulting in higher rates of catalysis.

Table 1.2. Examples of phosphine electronic parameters for the $[\text{Ni}(\text{CO})_3(\text{PR}_3)] A_1$ band.⁴⁶

Phosphine	ν / cm^{-1}	Phosphine	ν / cm^{-1}
PF_3	2111	PPh_2NMe_2	2067
P(OMe)_3	2080	$\text{P(NMe}_2)_3$	2062
PPh_3	2069	P^tBu_3	2056

Several other methods used to probe the electronic character of phosphines have been developed, such as through analysis of $|^1J_{\text{SeP}}|$ coupling constants values obtained by ^{31}P NMR spectroscopic analysis of the corresponding phosphine selenides, R_3PSe .⁴⁸ A large $|^1J_{\text{SeP}}|$ corresponds with a low basicity phosphine, which thus equates to the ligand being a poor σ donor.⁴⁹ Typically, electron withdrawing groups bound to the phosphorus result in larger $|^1J_{\text{SeP}}|$, suggesting that they are poorer σ donors. ^{31}P NMR spectroscopic analysis can also be used to probe the bonding of phosphines to metals more directly by analysis of $|^1J_{\text{PPt}}|$ coupling constants of platinum(II) or platinum(0) complexes, for example.⁵⁰ For platinum(II) complexes, $|^1J_{\text{PPt}}|$ was shown to linearly decrease as more electron-withdrawing phosphine substituents were used (characterised by their Hammett substituent constant, a well-known metric for assessing a substituent's electronic effect in organic chemistry).^{50,51} Conversely, for platinum(0) complexes the opposite trend was observed.

1.6.2 Quantifying the steric demand of phosphines in metal complexes

Steric effects of ligands can also play a large role in the chemistry at the metal centre to which they are bound, including influencing the structure and spectroscopic properties of the complex formed.⁴⁶ Therefore a quantitative method to describe phosphine steric demands, the Tolman cone angle, θ , was devised. The defined cone comprises all of the space that a phosphine bonded at a fixed phosphorus–metal bond length of 2.28 Å would fill as it is rotated around the phosphorus–metal axis (Figure 1.4).

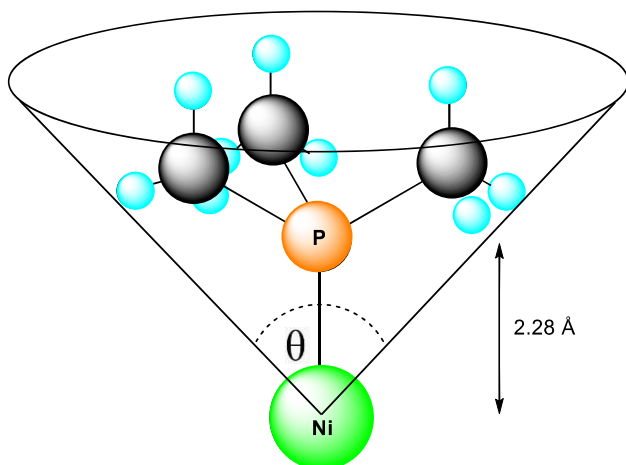


Figure 1.4. Defining a phosphine cone angle; circles representing van der Waals radii of the substituents.⁴⁶

Known values of phosphine cone angles start from 87° for PH_3 and can exceed 200° for bulky phosphines such as $\text{P}(\text{mesityl})_3$, with a value of 212° . Triphenylphosphine has a cone angle of 145° , in between these extremes, contributing to a ligand that can perform well in a range of metal complex-catalysed reactions, including hydroformylation.⁴ For bidentate and asymmetric ligands the Tolman cone angle becomes less useful, which has resulted in the development of several other methods for assessing ligand steric bulk such as the “Percent Buried Volume” ($\%V_{\text{bur}}$) approach (see Section 3.2.2).⁵²

1.7 The effect of phosphine ligand structure on hydroformylation catalysis

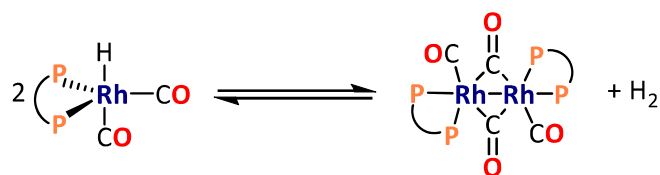
For rhodium-catalysed hydroformylation, experiments have shown that of all the group 15 elements, potential ligands based on phosphines were most successful, as they gave rise to catalysts with the greatest activity and selectivity (Figure 1.5).^{53–55}



Figure 1.5. Trend in rhodium-catalysed hydroformylation activity using different group 15 ligands.^{53–55}

Many possible phosphines can be used as ligands in hydroformylation catalysis. The catalytic results obtained when using each different phosphine will be a result of their unique combination of steric and electronic effects. For example, increasing the steric

bulk of the phosphine has been shown to favour production of the linear aldehydes, although bulky ligands can also result in the reversible formation of binuclear rhodium complexes that are catalytically inactive (Scheme 1.8).⁵⁶ Meanwhile, more basic phosphines generally provide greater selectivity for the linear isomer, but a decreased reaction rate is observed due to the suppression of CO dissociation associated with a more electron rich metal centre (see Section 1.4). In order to maximise the activity and selectivity of the hydroformylation reaction a balance has to be struck between these factors, along with other influences such as reaction temperature and pressure, to give a process that provides the best possible performance.



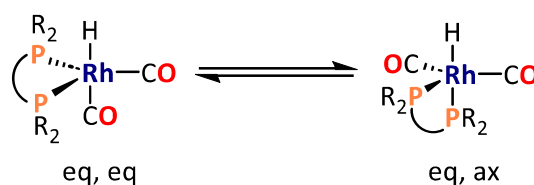
*Scheme 1.8. Reversible dimer formation of rhodium hydroformylation catalysts; the equilibrium is controlled by the nature of the bidentate phosphine ligand.*⁵⁶

Another factor to consider when choosing a ligand to use in an industrial process is its cost and stability. This has led to triphenylphosphine, PPh_3 , becoming the phosphine of choice in several industrial processes.⁵⁷ Due to its low preparation cost and stability in air, a large excess of PPh_3 can be used in reactions to suppress catalyst decomposition. PPh_3 -modified rhodium catalysts can also achieve $l:b$ ratios of ~ 11 , which are good compared to those achieved for phosphine-modified cobalt systems previously described (see section 1.4).⁵⁷

1.8 Diphosphine ligands in hydroformylation catalysis

Another way to improve the efficiency of hydroformylation catalysis that has been investigated, is use of diphosphine ligands. These ligands offer the benefit of the chelate effect, and hence give higher catalyst stability because of larger equilibrium constants of phosphine binding than when using monodentate phosphines.⁵⁸ The entropic advantage of using a diphosphine also provides a useful way to ensure two phosphine donors are coordinated to the metal centre, maximising the performance of the catalyst.

Considering diphosphine-modified rhodium hydroformylation catalysts, there are two possible isomers of the trigonal bipyramidal rhodium catalyst when a bidentate phosphine is coordinated (Scheme 1.9), one with both phosphines in the equatorial position and one with a phosphine in an equatorial and axial position. It has been found that selective formation of the di-equatorial isomer favours the production of the linear aldehyde and gives much higher *l:b* ratios than the eq-ax confirmation, due to a combination of steric and electronic effects.⁵⁷



*Scheme 1.9 Isomerisation of rhodium hydroformylation catalysts containing a bidentate phosphine ligand.*⁵⁷

Initial investigations using diphosphine ligands for hydroformylation explored common, readily available diphosphines that had been previously applied in other catalytic processes. For example, experiments using traditional diphosphines containing two PPh₂ moieties connected *via* an alkyl chain, such as dppp, initially gave uninspiring results, with poor selectivity for the linear aldehyde (Table 1.3).⁵⁹ However, by using more elaborate, synthesis-intensive diphosphines, which have a large bite angle, improved catalyst selectivity can be observed. The ligand *trans*-dppm-cyp (Figure 1.6) was found to give better selectivity for the linear aldehyde product than that achieved using dppp.⁶⁰ Similar product selectivity was achieved using ferrocene-based diphosphines, which have variable bite angles as a result of rotation of their Cp groups.⁶¹ The selectivity for linear aldehyde products can be improved further by the use of even wider bite angle phosphines, such as BISBI (Figure 1.7).⁶² Other large bite angle diphosphines, such as the Xantphos series of ligands, typically provide the best *l:b* selectivity currently available.⁴⁰ The reason for the increased selectivity arising from application of wider bite angle ligands is due to the increased likelihood that the ligand will bind to metals in the di-equatorial conformation. To identify ligands with wide bite angles, the “natural bite angle” concept was developed using molecular mechanics.⁶³

This calculation takes into account the ligand backbone constraints, but disregards electronics effects of ligand metal interactions.

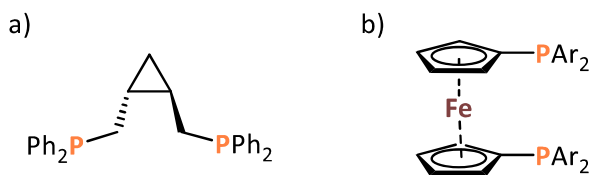


Figure 1.6. Structures of a) *trans*-dppm-cyp and b) ferrocene diphénylphosphine, dppf.

Table 1.3. Natural bite angle (β) and resulting *l:b* ratio of some bidentate phosphines.^{57,64}

Ligand	Bite angle $\beta_n / ^\circ$	<i>l:b</i> ratio
dppp	91	0.8
<i>trans</i> -dppm-cyp	99	3.6
dppf	107	4.4
BISBI	122	25.1
Xantphos ^a	111	52.2
PPh ₃	-	2.4

Conditions: syn gas pressure 16 bar, [Rh] = 1.5 mM, ligand/Rh = 2.4, 95 - 125 °C, solvent 2,2,4-trimethyl pentane-1,3-diolmonoisoisobutyrate (Texanol), p(propene) 5 bar. ^asyn gas pressure 20 bar, [Rh] = 1.0 mM ligand/Rh = 5, substrate/Rh = 637.

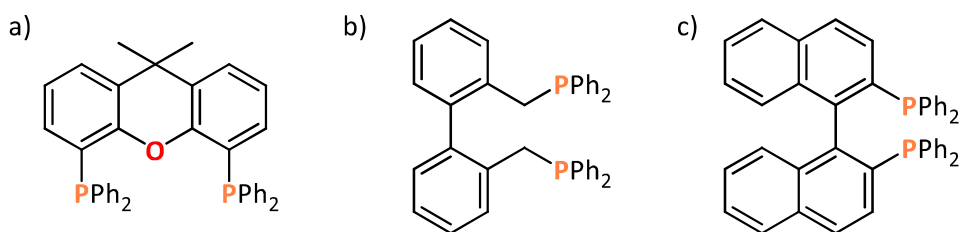


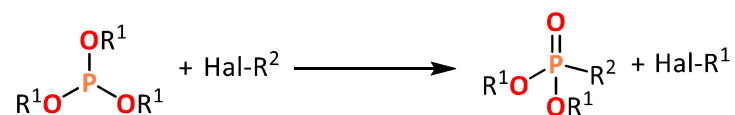
Figure 1.7. Structure of a) Xantphos, b) BISBI and c) BINAP.

Despite the improved hydroformylation selectivity provided by these wide bite angle ligands, their industrial application can be challenging due to the cost associated with their synthesis on the desired scale. Additionally, their generally lower stability than air-

stable PPh_3 means that PPh_3 often remains the industrial ligand of choice for single phase hydroformylation catalysis.⁵⁷

1.9 Phosphite ligands in hydroformylation catalysis

Phosphites, $\text{P}(\text{OR}_3)$, have also been applied as ligands in hydroformylation catalysis.^{43,57} The rationale behind their use comes from the fact that facile CO dissociation is required for high reaction rates. Phosphites are more electron deficient than phosphines, resulting in a stronger metal to ligand π -backbonding component upon metal coordination.⁵⁷ This lowers the electron density on the metal and promotes CO dissociation, therefore increasing hydroformylation reaction rates. Phosphites have an additional advantage in that they can be easily prepared and are less sensitive to sulfur impurities and oxidising agents than phosphines. However, they are more susceptible to side reaction such as hydrolysis, alcoholysis and the Arbuzov reaction (Scheme 1.10).⁶⁵ Aryl phosphites do not typically undergo the Arbuzov rearrangement and are therefore the most attractive option for catalytic applications.⁶⁵ Many similar concepts to those established for phosphine ligand-containing catalysts still apply with phosphite systems, such as the increased linearity of the aldehyde when using bulky ligands. This led to the development of bulky aryl phosphites, which have been subsequently used industrially by Shell and UCC (Figure 1.8).^{63,64}



*Scheme 1.10. Arbuzov rearrangement.*⁶⁵

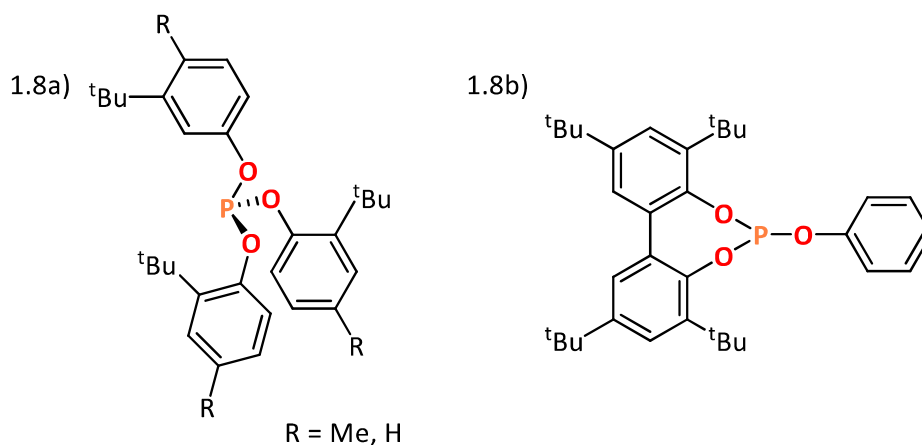
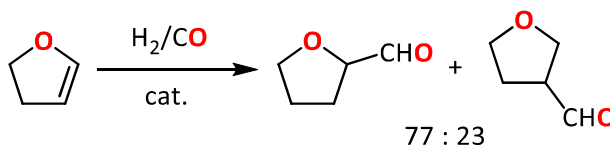


Figure 1.8. Structure of a) tris(ortho tert-butyl)phosphite (Shell) and b) (3,3',5,5'-tetra-tert-butyl-2,2'-biphenyl)phenylphosphite (UCC).^{66,67}

The high activity of phosphite-ligated rhodium catalysts has several beneficial applications; firstly, milder reaction conditions can be employed to give desired reaction rates, reducing costs, but also allowing functionalisation of substrates that would not survive regular hydroformylation conditions. An example of this is the hydroformylation of 2,3-dihydrofuran (Scheme 1.11).^{57,68} The high activity of phosphite-containing catalysts can also allow the hydroformylation of less reactive substrates, such as internal alkenes, with reasonable rates. Indeed, when isomerisation of internal alkenes is also very fast, linear aldehydes can still be produced with reasonable yields.⁵⁷



Scheme 1.11. Hydroformylation of 2,3-dihydrofuran using a Rh-tris(ortho tert-butylphenyl)phosphite catalyst (shown in Figure 1.8a).⁶⁸

1.10 Bidentate phosphite ligands in hydroformylation catalysis

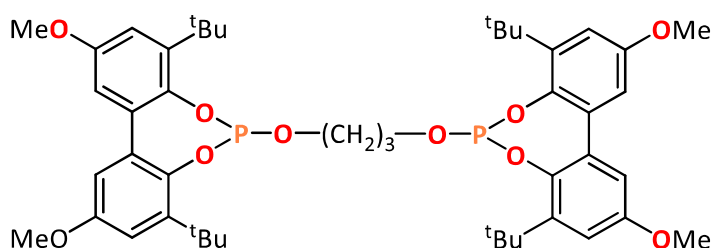
Diphosphites were first explored as ligands for rhodium-catalysed hydroformylation of alkenes by Bryant and co-workers of UCC in 1987.⁶⁹ They showed that by using a bisphenol linker they could produce diphosphite ligands that give significantly higher selectivity for linear aldehydes than the previously used monophosphite systems.

Table 1.4. Hydroformylation using bulky mono- and di-phosphite catalysts.⁵⁷

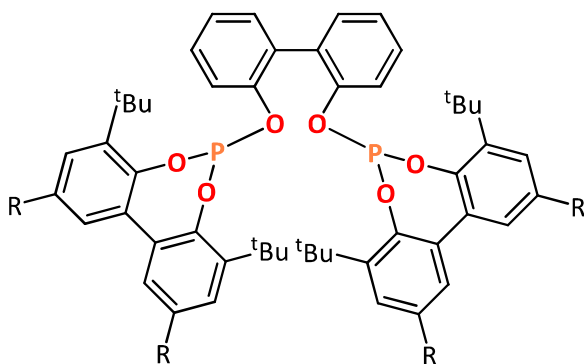
Ligand	T / °C	p CO/H ₂ bar	Ratio CO/H ₂	alkene	Initial rate / mol. (mol Rh ⁻¹) h ⁻¹	<i>l:b</i>
PPh ₃	80	10	1:1	1-octene	2200	2.8
1.8a	80	10	1:1	1-octene	40,000	1.9
1.9a	90	7.1	1:1	1-butene	1320	3.8
1.9b	70	7	1:2	1-butene	1480	3.2
1.9c	74	4.5	1:1	propene	402	53

Conditions: 0.1 – 1 mM Rh, L/Rh = 10 – 20, [alkene] = 0.5 – 1 M in toluene.

1.9a)



1.9b)



1.9c)

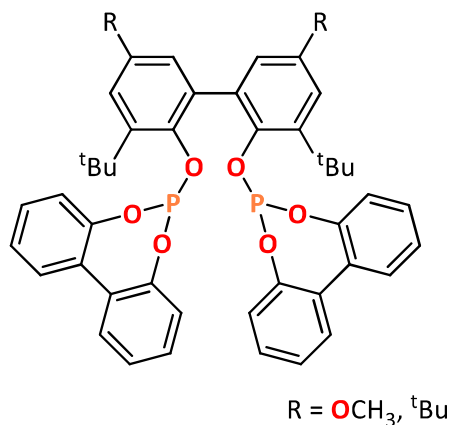


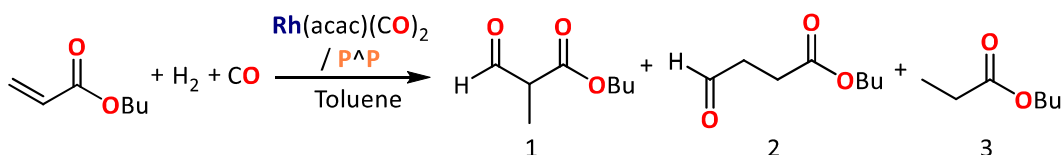
Figure 1.9. Structures of the bulky diphosphite ligands developed by Bryant at UCC corresponding to the data in Table 1.5.⁶⁹

The data summarised in Table 1.4 show that significant steric bulk at the bridging bisphenol (Figure 1.9c) is necessary to impart the desired high selectivity for the linear aldehyde. These results also show that diphosphite systems exhibit lower rates of

reaction in hydroformylation than their monophosphite analogues, but still provide acceptable reaction rates compared to standard PPh_3 systems.⁵⁶

1.11 Small bite angle ligands for rhodium-catalysed hydroformylation

Due to the general trend of large bite angle ligands giving high performance in rhodium-catalysed hydroformylation, usually in the form of high linear to branched ratios and reasonable reaction rates, small bite angle ligands have remained largely unexplored.⁵⁰ Despite this, simple, small bite angle ligands are interesting from an industrial point of view due to their high tunability, simple synthesis and low cost compared to more complex wide bite angle ligands. Small bite angle ligands may be able to bridge the gap between high performance wide bite angle ligands, which are too expensive for industrial application and PPh_3 , which is cheap and allows hydroformylation systems employing large excesses of ligand to be commercially viable. One example of a small bite angle ligand that has been investigated in hydroformylation catalysis is dppe, employed in a rhodium-based system with butyl acrylate as the substrate (Scheme 1.12).⁷⁰



Scheme 1.12. Rhodium-catalysed hydroformylation of butyl acrylate, where $\text{P}^{\wedge}\text{P}$ is a bidentate phosphine ligand (see Table 1.6).⁷⁰

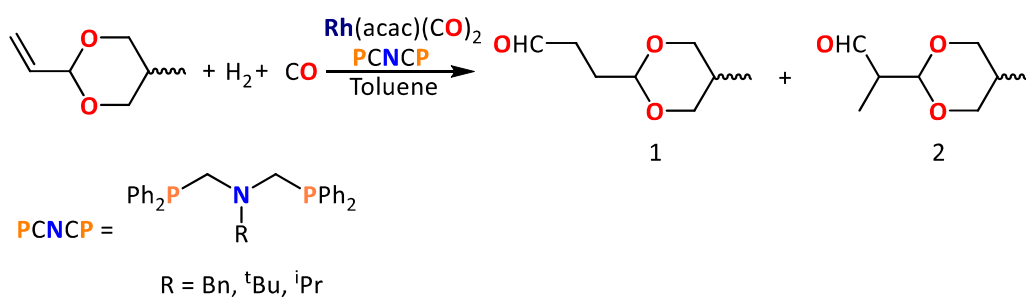
As can be seen from the data in Table 1.5, dppe provides better selectivity for the hydroformylation of butyl acrylate than the wider bite angled BINAP ligand, a common asymmetric bidentate phosphine, and Xantphos (Figure 1.7).⁷⁰ However, catalysis employing dppe ligands proceeded with a much lower TOF than that achieved with Xantphos. This result shows that bite angle is not always the primary factor affecting hydroformylation selectivity.

Table 1.5. Hydroformylation of butyl acrylate using a $Rh(acac)(CO)_2$ / $P^{\wedge}P$ catalyst system.⁷⁰

Ligand ($P^{\wedge}P$)	Bite angle / °	Selectivity / %			TOF / h ⁻¹
		1	2	3	
dppe	85	100	0	0	118
binap	92	90	0	10	177
xantphos	107	88	5	7	3052

Conditions: [alkene] = 1.69 M, S/Rh = 1314 (mol/mol), L/Rh = 7, 80 °C, 20 bar syngas pressure, 20 minutes in toluene (3 ml).

Another example of the use of small bite angle ligands in hydroformylation catalysis is the hydroformylation of 2-vinyl-5-methyl-1,3-dioxane (VMD) (Scheme 1.13). This process was investigated using small bite angle ($\sim 92^\circ$) so called κ^2 - P,P -PCNCP ligands, resulting in complete selectivity for aldehyde products.⁷¹



Scheme 1.13. Rhodium-catalysed hydroformylation of VMD, using a $Rh(acac)(CO)_2$ / PCNCP catalyst.⁷¹

As shown by the data in Table 1.6, the various PCNCP ligands give approximately 75% selectivity for the branched aldehyde, with the functionalisation of the amine having only a very small effect on the catalyst performance.⁷¹ This is to be expected, as the amine functionalisations used are unlikely to have large differences in their steric or electronic effect contribution at the metal centre, which is usually required to effect catalyst performance. This could be investigated further by also changing the functionalisation at the phosphine. As the phosphine moieties are directly bound to the metal centre, they are likely to have a much larger effect on the sterics and electronics of the complex formed, and hence the catalysis. No TOFs were reported in this work,

instead the conversion at 4 h was compared to that of Xantphos under the same conditions. Xantphos was shown to give a 90% conversion, compared to 90 – 96% for the PCNCP systems, suggesting that PCNCP ligands provide high activity alongside moderate selectivity in hydroformylation catalysis.⁷¹

Table 1.6. Hydroformylation of VMD using a $Rh(acac)(CO)_2$ / PCNCP catalyst system.⁷¹

Ligand	Selectivity / %		Conversion / %
	1	2	
PCNCP ^{Bn}	28	72	96
PCNCP ^{tbu}	27	73	90
PCNCP ^{iPr}	23	77	92

Conditions: [VMD] = 5.0 mmol, [VMD]/[Rh] = 5000, L/Rh = 5, 120 °C, 20 bar syngas pressure, 4 h in toluene (10 ml).

It is possible to further decrease the bite angle of the ligands used by moving to systems employing κ^2 -*P,P*-PNP ligands, which form strained 4-membered chelate rings with metals, giving rise to typical P-P bite angles of approximately 70°. ⁷² The PNP ligand *N,N*-bis(diphenylphosphanyl)-*n*-propylamine (Figure 1.10) was investigated in the hydroformylation of 1-octene using a $Rh(acac)(\kappa^2$ -*P,P*-PNP) catalyst precursor. The investigation found that the complex was highly active for 1-octene hydroformylation and isomerisation, which led to a mixture of isomerisation and aldehyde products, with no reduction products, *e.g.*, alcohols or alkanes, detected (Table 1.7).⁷³

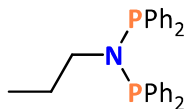


Figure 1.10. PNP ligand used in rhodium-catalysed hydroformylation of 1-octene.⁷³

No tuning of the ligand design was attempted during the investigation, so it remains unknown how the substituents on the phosphorus or nitrogen atoms of the ligand will affect catalyst performance. This remains an interesting area for future research as these catalytic testing results show that small bite angle ligand containing rhodium(I) complexes have potential to act as highly active and selective hydroformylation catalysts, despite the lack of literature in this area.

Table 1.7. Hydroformylation of 1-octene using a $Rh(acac)(\kappa^2\text{-P,P-PNP})$ catalyst precursor.⁷³

Ligand	TOF ₅₀ / h ⁻¹			Selectivity / %			
	total	Hydro- formylation	Isom- erisation	nonanal	2- methyl octanal	2- octene	3- octene
PrN(PPh ₂) ₂	57,000	36,300	20,600	45.1	18.6	35.2	0.8

Conditions: substrate to metal ratio = 122,700, [Rh] = 0.0405, L/Rh = 1, 100 °C, 125 bar syngas pressure, THF solvent. All data collected at 50% conversion, hydro = hydroformylation product, iso = isomerisation product.

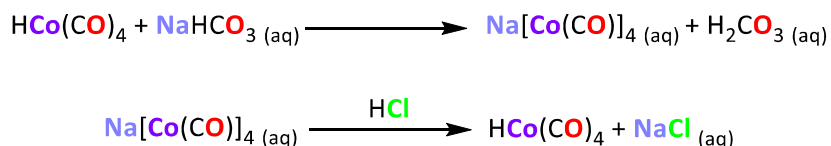
Another often overlooked consideration of ligand bite angle on hydroformylation is the effect that the ligand bite angle has on metal hydride character. As discussed in Section 1.5, increasing the hydride character of hydroformylation catalysts has a positive impact on the attainable aldehyde *l:b* ratios produced and is therefore generally desirable. It was shown by Dubois that as the P-M-P angle of bidentate phosphines decreases, the resulting enforced change in geometry around the metal centre increases the electron density on the hydride ligand of $[PdH(PH_3)_3]^+$, making it less acidic and more hydridic in nature.⁷⁴ This was achieved using extended Hückel calculations to qualitatively calculate molecular orbitals for $[Pd(PH_3)_3]^{2+}$ and $[PdH(PH_3)_3]^+$ complexes under a range of enforced P-M-P angles.

Later, the effect of varying diphosphine bite angle on the hydricity of a series of $[HPd(diphosphine)_2]^+$ cations was investigated experimentally by Dubois.⁷⁵ The heterolytic bond-dissociation free energies, $\Delta G^\circ_{H^-}$, of $[HPd(diphosphine)_2]^+$ to $[Pd(diphosphine)_2]^{2+} + H^-$, were calculated from thermochemical cycles, half-wave potentials, and measured pKa values for a series of 7 complexes in which the diphosphine ligand natural bite angle varied from 78° to 111°. The diphosphine ligands investigated included dppe (78°) and xantphos (111°), with the subsequent results showing that the hydricities of the complexes investigated containing these two ligands vary by 27 kcal/mol. By systematically changing the structures of the phosphine ligands investigated, it was shown that ligand bite angle was the dominant factor influencing $[HPd(diphosphine)_2]^+$ hydricity, with smaller bite angle phosphines resulting in a more

hydridic complex, although the identity of the substituents on the phosphine also played a role.⁷⁵ More recent efforts have combined experimental and computational techniques to investigate an increasing library of metal hydrides containing different ligands and metal centres, including Rh, Co and Ni, for different applications, showing similar trends in the effect of ligand bite angle on metal hydride complex hydricity to those seen by Dubois.^{76–78} Despite these findings, the effect of ligand bite angle on hydroformylation regioselectivity is often discussed purely in terms of favouring *eq,eq* or *ax,eq* phosphine conformations, whereas a complex combinations of steric and electronic effects are likely also involved.⁴⁰

1.12 Separation of hydroformylation catalyst and products

A key challenge in the development of sustainable and economical industrial hydroformylation processes is separation of the products and catalyst recycling.⁴ In early industrial processes employing $\text{HCo}(\text{CO})_4$ catalysts, removal of the catalyst before isolation of the products was required due to the poor stability of the catalyst under the high temperatures and low pressures of CO required for product distillation. To achieve this, a two-step approach has been employed by Produits Chimiques Ugine Kuhlmann (now Exxon). In this process the catalyst is treated with an aqueous solution of NaHCO_3 followed by use of a phase separation to extract the cobalt as $\text{Na}[\text{Co}(\text{CO})_4]_{\text{aq}}$ (Scheme 1.14).⁷⁹ The catalyst can then be recovered by reaction with an acid under a pressure of syngas to regenerate the $\text{HCo}(\text{CO})_4$ catalyst.



*Scheme 1.14. Method of $\text{HCo}(\text{CO})_4$ removal and recovery from the reaction mixture.*⁷⁹

Another approach, developed by BASF, removes the cobalt from the crude mixture by reaction with formic or acetic acid under oxygen to produce aqueous soluble cobalt(II) carboxylate. After phase separation the catalyst is regenerated under high pressure of syngas.⁸⁰ These methods both suffer the downside that catalyst separation involves

multiple steps, requiring chemical reactions first to remove, then to re-form the catalyst. As a result, catalyst separation is time consuming, waste producing and expensive, leading to the research of more facile catalyst separation methods (see section 1.14).

Rhodium hydroformylation catalysts were found to be more stable to high temperatures and low pressures relative to their cobalt analogues. As a result, distillation of the aldehyde hydroformylation products directly from the catalysis reaction mixture without additional separation steps is possible when employing rhodium catalysts.³ Despite this, methods for the easier, and less energy intensive, separation of rhodium-based hydroformylation catalyst from products were later developed. This included employing phosphine ligands containing a sulfonate group, TTPPTS (Figure 1.11), that renders the catalyst water soluble.^{81,82} The Ruhrchemie/Rhône-Poulenc process for hydroformylation of propene employs a two-phase system, with the catalyst in the aqueous phase while the products and reactants are in the organic phase.^{81,82} TPPTS has a solubility in water of ~ 1.1 kg / L, while remaining insoluble in most common organic solvents used in hydroformylation, which together allows for effective catalyst/product separation.⁵⁷ The hydroformylation reaction proceeds at the aqueous-organic phase boundary and in the aqueous phase where the substrate is sparingly soluble, before a phase separation is performed to separate the catalyst and product. As well as the improved separation, high selectivity is maintained in the reaction with high *I:b* ratios achievable. Unfortunately, this approach can only be utilised with short chain alkenes, *e.g.*, C₃ and C₄, as longer chain alkenes lead to low reaction rates due to their insolubility in the aqueous phase.^{81,82} Attempts to adjust the polarity of the phases to increase the reaction rate run into issues, such as leaching of the catalyst into the organic phase, which is unviable due to the high cost of rhodium metal.⁵⁷

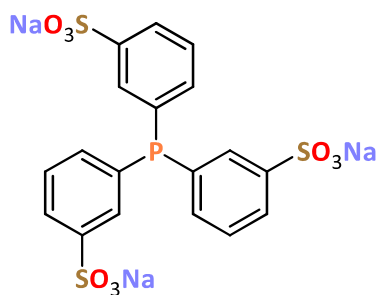


Figure 1.11. Structure of meta-triphenylphosphine trisodium sulfonate, TPPTS, a water-soluble phosphine.⁸²

It is also possible to employ a “one-phase catalysis, two-phase separation process” approach involving a homogeneously-catalysed reaction followed by a liquid-liquid extraction purification step.^{83,84} One such example of this approach has been developed by Union Carbide. The reaction takes place in an apolar phase consisting of the alkene substrate 58%, N-Methyl-2-pyrrolidone (NMP) 40% and water 2%. The catalyst contains mono-sulfonated phosphine ligands, allowing solubility in polar and non-polar solvents. Once the reaction is complete, water is added to give a 1:1 polar:apolar phase ratio, and the catalyst is extracted into the polar water/NMP phase, enabling facile catalyst-product separation. This approach enables a much wider substrate scope than the two-phase catalysis method, up to C₁₄ alkenes, albeit at the cost of lower activities due to the required changes in ligand design.⁵⁷

1.13 Homogeneous vs heterogenous catalysis - advantages and disadvantages

Many successful hydroformylation systems have been developed with homogeneous catalysts, where the catalyst is in the same phase as the reactants, including all the examples included so far in this report. These reactions benefit from the typical advantages of homogeneous catalysts, including high reaction rates and selectivities, in addition to well defined catalytic species and relatively easy catalyst characterisation.⁸⁵ However, there are also several possible downsides of using homogeneous catalysts, such as difficult separation of catalyst and products, reactor corrosion and low stability of the catalyst. An alternative to homogeneous catalysis is heterogeneous catalysis, where the catalyst is in a different phase to the reactants. This is usually achieved using

a solid catalyst with liquid or gaseous reactants. By employing heterogeneous catalysis, several advantages are gained over homogeneous catalyst, such as increased ease of separation of catalyst and products, the ability to use fixed bed catalysts in continuous processes, and better catalyst stability. However, these advantages often come at the cost of lower activity and selectivity, as well as less well-defined catalysts, that make mechanistic studies more challenging.⁸⁰

1.14 Introduction to heterogeneous hydroformylation catalysis

In the context of Rh-catalysed hydroformylation there is a desire to develop heterogeneous catalysts for industrial application, in order to remove the costly distillation step required to separate the catalyst from reaction products. Removal of this process step also provides the added benefit that the employed catalyst does not need to withstand harsh distillation conditions, making catalyst recycling easier. This is especially important due to the high cost of rhodium, which reached prices above 28,000 \$ Oz⁻¹ in 2021 during the course of this project (Figure 1.12).

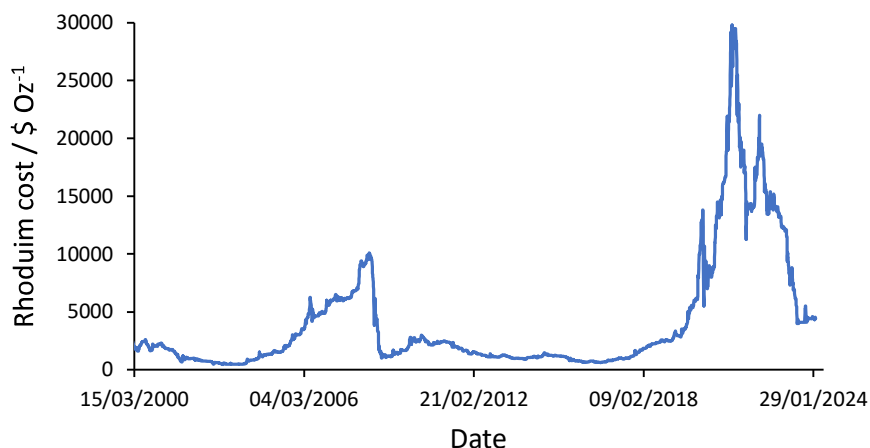
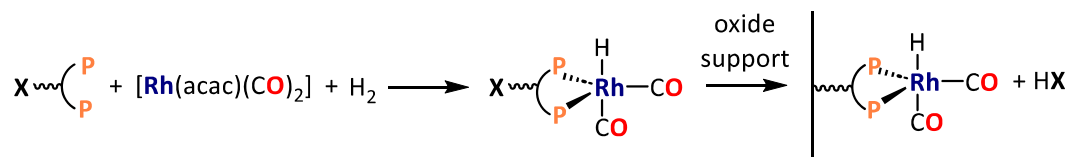


Figure 1.12. Rhodium price per month from March 2000 – February 2024 in \$ Oz⁻¹.⁸⁶

Many different methods of producing heterogeneous hydroformylation catalysts have been employed to develop systems that benefits from the easier separation of a heterogeneous system, while trying to maintain activities and selectivities that are comparable to the homogeneous catalysis currently used in industry. These methods include silica-supported rhodium nanoparticles, polymer-supported rhodium complexes

(*via* polymerised phosphine ligands), supported rhodium single atom catalysts, rhodium catalysts in supported ionic liquids and rhodium complexation to trialkylphosphine ligands anchored onto carbosilane dendrimers.^{87–91} Unfortunately, however, these systems generally suffer from several issues, such as low reaction rates, loss of selectivity, and/or leaching of the metal from the solid support. Together, these issues mean that such heterogeneous systems are not currently commercially viable solutions and will not be discussed further in this review in order to keep this literature review brief, as they are not strictly relevant to the work described in chapters 2–6 of this report.

Another possible approach for the “heterogenization” of rhodium hydroformylation catalysts is by using phosphine ligands modified with an extra functionality (remote from the metal binding site) that can be used to tether a complex containing the ligand to an insoluble support, such as a solid oxide (Scheme 1.15).⁹² This allows the tethering of the rhodium catalyst to the support *via* an inert spacer-tether, whilst essentially maintaining a coordination environment around the rhodium centre that is comparable to that in solution for completely soluble (homogeneous) catalyst systems. The aim of this is to mirror the high rates and high selectivities of the reaction typically obtained in solution. For discussion on the performance of a range of phosphine-immobilised hydroformylation catalysts see section 1.16.



Scheme 1.15. Synthesis of heterogeneous hydroformylation catalysts via an immobilised phosphine ligand containing a tethering functionality (X).⁹²

1.15 Mesoporous silicas – oxide supports for hydroformylation

Oxide supports, specifically mesoporous silicas, are the ideal choice of support for immobilisation of transition metal complex catalysts for several reasons. Firstly, their high mechanical and thermal stability means that the structural integrity of the support

is assured under the reaction conditions, which usually involves high temperatures and pressures for hydroformylation.⁹³ In addition to this, large pore size and surface area allow for adequate diffusion of reactants and suitable sites for catalyst immobilisation. Also, the well-defined nature of the silica allows greater confidence in the identity of the catalytically active species, than with less well-defined supports, *e.g.*, amorphous materials and polymers.⁹⁴ Finally, adjusting the synthesis conditions of oxide supports allows for tuning of pore size and surface sites, providing extra control over the catalyst system.

The surface chemistry of mesoporous silica is dominated predominantly by silanol groups, Si–OH (Figure 1.13), which offer reactive sites at which appropriately functionalised ligands may be immobilised.⁹⁵ Isolated silanols are preferred for catalyst immobilisation as they provide well-defined, discrete binding sites for metal complex tethering. The distribution of silica surface sites can be controlled by post-synthesis heat treatment. For example, vicinal silanols can be converted to isolated silanols by heat treatment (calcination). In addition, the overall hydroxyl density can be controlled by calcination at different temperatures, allowing control over the number of available binding sites, allowing optimisation of the silica for use as a catalyst support.

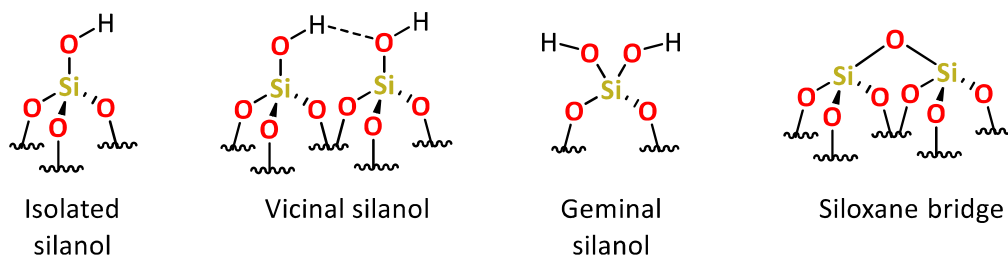


Figure 1.13. Surface sites present in silica.⁹⁵

Further opportunities for the modification of the support system are also available during synthesis depending on the reaction conditions and templating agent used when preparing porous materials, resulting in silicas with different properties (Table 1.8). This allows the production of silicas with differing pore sizes and channel structures, allowing for further tuning of the support system. Commonly used, well-defined silicas include MCM-41, SBA-15 and KIT-6.^{96–98} MCM-41 and SBA-15 possess hexagonal 1-dimensional channels, whereas KIT-6 has a 3-dimensional structure of interconnected cylindrical

channels (Figure 1.14).⁹⁹ As already stated, the structure of the silica is determined by the templating agent used during synthesis: alkyltrimethylammonium or alkyltriethylammonium surfactants of alkyl chain lengths 12 to 22 for MCM-41; triblock copolymer Pluronic 123 ($\text{EO}_{20}\text{PO}_{70}\text{EO}_{20}$) for SBA-15; and ($\text{EO}_{20}\text{PO}_{70}\text{EO}_{20}$)-butanol for KIT-6. During synthesis, tetraethoxysilane (TEOS) condenses around the templating agent, with the templating agent then being removed by calcination at a later stage.¹⁰⁰

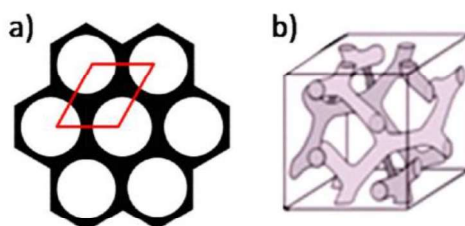


Figure 1.14. Representations of the unit cells of a) MCM-41 and SBA-15 and b) KIT-6.

Reprinted (adapted) with permission from Wilson et al. Copyright 2024 American Chemical Society.⁹⁹

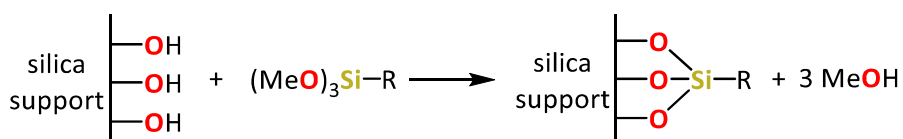
Table 1.8. Typical properties of some mesoporous silicas.^{96–98}

	MCM-41	SBA-15	KIT-6
Pore diameter / nm	3 – 5.5	5 – 11	4 – 12
BET surface area / $\text{m}^2 \text{g}^{-1}$	1000	800	800
Channel structure	1-D	1-D	3-D

Large channel diameters along with channel structure are important factors to consider for “heterogenised” catalysis, as diffusion of the reactants or products can be rate-limiting and have a significant impact on the activity of the catalysts. It has been shown that the 3-dimensional network of channels in KIT-6 can allow for much higher activities than the 1-dimensional channels in SBA-15 for heterogeneously-catalysed fatty acid esterification, as diffusion is no longer the rate limiting step compared to 1-dimensional systems.⁹⁹ A high surface area is also desired to increase the chance of collisions between surface-bound catalyst and reactants in solution/slurry.

1.16 Immobilised phosphines for heterogeneous hydroformylation

In order to tether phosphine ligands onto silica, the most common method employed is the condensation of an alkoxy silane moiety with silica surface silanols (Scheme 1.16).¹⁰¹ This has the advantage of a facile synthesis, while only producing volatile alcohols as a by-product that can be easily removed under vacuum. As alcohols are also possible reaction by-products of hydroformylation, trace amounts remaining in the catalyst are unlikely to cause problems with subsequent catalysis. By employing a trialkoxysilane tethering group, up to three bonds can be made between the ligand and the silica surface, improving the robustness of the tether and reducing the chance of hydrolysis separating the ligand from the silica surface.



*Scheme 1.16. Condensation of a trimethoxysilane with silica surface silanols.*¹⁰¹

A simple catalyst system prepared by silica-immobilisation of a phosphine ligand using a pendant alkoxy silane functionality investigated for hydroformylation was a modified Wilkinson's catalyst with one of the phosphine ligands tethered to MCM-41 silica (Figure 1.15).¹⁰² Results showed the phosphine tether provided significantly higher initial turnover rates than a separately investigated tethered thiol (Table 1.9), but leaching of rhodium out of the reaction resulted in large decreases in activity over time when using the phosphine tether. Leaching was also observed for the thiol tether, although to a much lesser extent, which levelled off over time. These findings were attributed to the fact that SH is a much stronger π -acceptor ligand than PPh₂, which could disfavour displacement of the dative coordination of the thiol SH moiety by CO during the reaction. It is noted here however that metal to ligand π -back bonding is likely to account for only a small part of the full metal-ligand interaction, with ligand to metal σ -donation dominating in these systems.

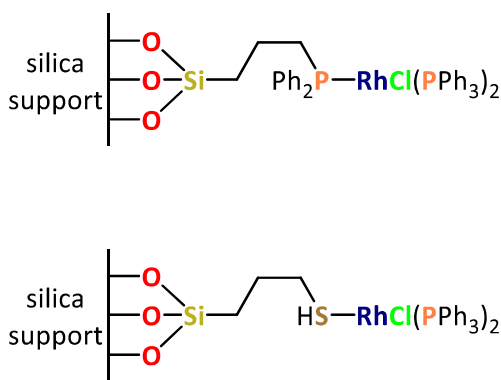


Figure 1.15. Immobilised Wilkinson's catalyst analogues for hydroformylation of cyclohexene using modified phosphine and thiol donor motifs.¹⁰²

The performance of the catalysts depicted in Figure 1.15 were also compared to that of Wilkinson's catalyst operating in solution, which was found to have a much higher activity, likely due to the mass transport limitations inherent in heterogeneous catalysis.¹⁰² However, the activity of the solution phase catalyst was also shown to decrease over time, attributed to deactivation of the catalyst by side reactions such as dimerisation, which appear to be suppressed for these immobilised catalysts. This suggests that if rhodium leaching can be prevented, the immobilised catalysts could perform at peak performance with much longer lifetimes than their homogeneous analogues. The catalyst selectivity was shown to be maintained between the homogeneous and heterogeneous catalysts.¹⁰²

Table 1.9. Hydroformylation of cyclohexene with immobilised Wilkinson's catalyst.¹⁰²

Catalyst precursor	Cyclohexene conversion / %	Turnover frequency / mol h ⁻¹	Selectivity / %	
			Cyclohexene carboxaldehyde	cyclohexane
RhCl(PPh ₃) ₃	89.4	1915	99.2	0.5
RhCl(PPh ₃) ₃ / SiO ₂ (PPh ₂)	30.3	649	99.5	0.5
RhCl(PPh ₃) ₃ / SiO ₂ (SH)	17.5	429	98.2	1.2

Conditions: Rh loading = 2.0%, L/Rh = 1, 100 °C, H₂:CO = 1:1, 28 bar syngas pressure, 20 h in toluene (12 ml).

Another investigation was performed to determine the effect of the tether alkyl spacer length on immobilised hydroformylation performance, while tethered to SBA-15. To do this, a PPh_2 moiety was tethered to silica *via* various different length alkyl chains ranging from C_1 to C_{11} (Figure 1.16).¹⁰³ Investigation into the effect of tether length on catalyst selectivity showed no visible trend, with a range of $I:b$ ratios between 1.4 – 1.9 observed during 1-octene hydroformylation regardless of the alkyl spacer used.¹⁰³ These results were highly variable between each catalyst cycle for a specific spacer length. In contrast to the previous work, rhodium leaching was shown to be small, decreasing from 0.37 – 0.13% per cycle from a C_1 to C_{11} spacer. This suggests that alongside the ligand used, other factors may influence rhodium leaching, such as support effects, catalyst synthesis conditions and catalysis reaction conditions.

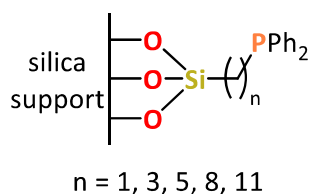


Figure 1.16. Silica-immobilised phosphine ligands with varying tether lengths.

Major differences in catalytic activity were observed when using the systems with the differing spacer chain lengths, with a steady increase in activity as chain length increases (Figure 1.17).¹⁰³ When chain length was increased to C_{11} , activity increased to almost equal that of Wilkinson's catalyst run under standard homogeneous conditions. It was hypothesised that this increase in activity for the system with the longer tether is a result of the catalyst being much further away from the solid surface, providing greater freedom of movement and orientation of the catalyst, allowing catalysis to occur more effectively.¹⁰³

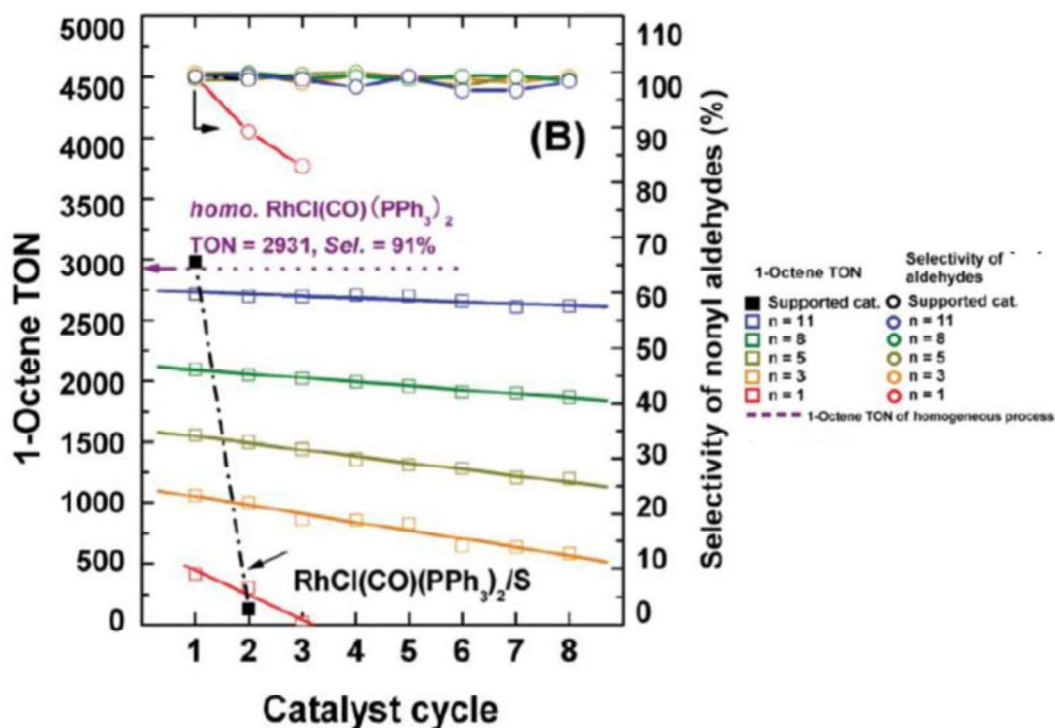


Figure 1.17. Graph showing 1-octene hydroformylation selectivity and TON using a tethered Wilkinson's catalyst, with alkyl chain spacer varying from C_1 to C_{11} (reproduced from Ref. 98 with permission from the Royal Society of Chemistry).¹⁰³ Conditions: 393 K, initial syngas pressure 5.0 MPa, reaction time 2.5 h. Initial Rh/1-octene ratio (10^{-4}): 1.2 ($S-C_1-PPh_2-Rh$), 1.9 ($S-C_3-PPh_2-Rh$), 1.7 ($S-C_5-PPh_2-Rh$), 1.6 ($S-C_8-PPh_2-Rh$), 1.5 ($S-C_{11}-PPh_2-Rh$), 2.6 (homogeneous $\text{RhCl(CO)(PPh}_3)_2$).

In an alternative approach, rhodium is bonded directly to silica and further anchored through coordination to surface tethered phosphine ligands (Figure 1.18).¹⁰⁴ The rhodium was supported on silica as Rh^0 nanoparticles and subsequently oxidised to Rh^+ under air, before syngas addition and *in situ* phosphine coordination to form the active catalyst.

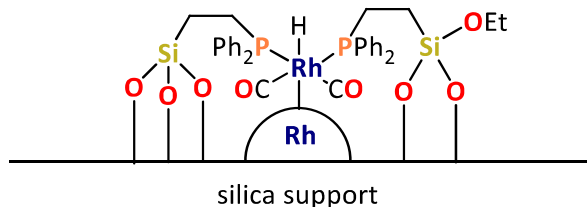
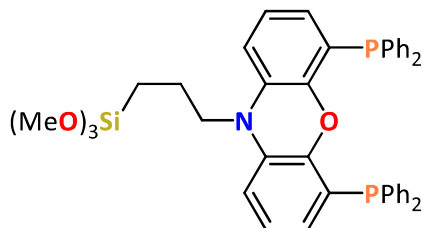


Figure 1.18. Rhodium hydroformylation catalyst with metal and ligand both bonded to silica.¹⁰⁴

Results of catalyst testing for the hydroformylation of ethene by the catalyst described in Figure 1.18 showed an initial TOF of 18 h^{-1} rising to a modest 48 h^{-1} after 150 hours.¹⁰⁴ The catalyst was tested for a total of 1000 h on stream, after which time the TOF remained at 48 h^{-1} , with no detectable leaching of rhodium from the system, as determined by ICP analysis. Reaction conditions used were: 1.0 MPa, 393 K; space velocity of mixed gas ($\text{C}_2\text{H}_4:\text{CO}:\text{H}_2 = 1:1:1$) 2000 h^{-1} . Rhodium nanoparticles used without any tethered ligands were found to have a much lower activity of 2.7 h^{-1} (c.f. 48 h^{-1}) highlighting the importance of the ligands in promoting catalytic activity. Despite the relatively low activities achieved using this system, the absence of rhodium leaching from the support provides a step forward towards a commercially viable heterogeneous hydroformylation processes.¹⁰⁵

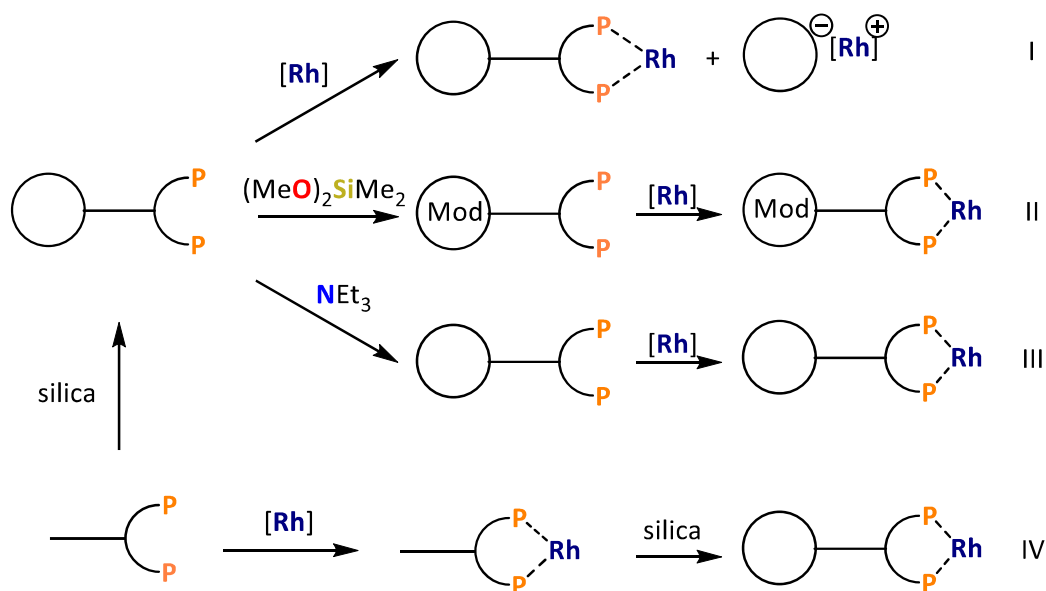
Another approach to developing highly active heterogeneous catalysts for hydroformylation, whilst reducing metal leaching, employed the use of tetherable bidentate phosphine ligands (Figure 1.19). In these systems continuous coordination of the ligands to metal is favoured by the chelate effect, which should therefore reduce rhodium leaching from the system.¹⁰⁶



*Figure 1.19. Xantphos-derived ligand for immobilised bidentate coordination to rhodium.*¹⁰⁶

Interestingly, in this research different strategies for ligand immobilisation to commercial silica and rhodium complexation were investigated (Scheme 1.17). In the first instance, ligand immobilisation was performed, followed by rhodium complexation. However, it was found that interaction between acidic silanol sites and the rhodium precursor had a large impact on catalytic performance (Table 1.10). Following this, two methods were employed to reduce the acidity of surface silanols, firstly by modifying the surface silanol sites using dimethoxydimethylsilane, secondly, *via* the addition of NEt_3 as base to reduce the silica acidity before rhodium complexation. Finally, a rhodium

complex containing the tetherable ligand was pre-made before immobilisation, to negate the interactions between rhodium and the surface.¹⁰⁶



*Scheme 1.17. Four approaches for immobilisation of a $\text{Rh}(\text{acac})(\text{CO})_2$ complex onto commercial silica using a Xantphos-derived bidentate phosphine.*¹⁰⁶

*Table 1.10. Hydroformylation of 1-octene using Xantphos-derived phosphine I-IV (Scheme 17) tethered to silica / $\text{Rh}(\text{acac})(\text{CO})_2$.*¹⁰⁶

Catalyst	Time / h	TOF / h ⁻¹	I:b ratio	Selectivity / %			
				I- aldehyde	b- aldehyde	I- alcohol	Octene isomers/ octane
I	0.5	n.d	2	40.1	22.0	0	37.9
II	23	8.0	19	85.5	4.5	0	9.9
III	22	8.7	37	96.2	2.6	1.0	0.2
IV	22	13.2	37	90.7	2.6	5.1	1.6
homo	2	283	32	93.3	2.9	0	3.7

Conditions: $\text{H}_2:\text{CO} = 1:1$, 50 bar syngas pressure, 80 °C, ligand:Rh = 10:1, substrate:Rh = 637:1, Rh = 10 μmol .

Contrary to the other immobilised catalysts previously discussed in this report, *l:b* ratios of the resulting aldehydes were determined for the systems described in Scheme 1.17.¹⁰⁶ Catalysts **II**, **III** and **IV** gave very good *l:b* ratios, with **III** giving better selectivity for 1-nonanal than the homogeneously catalysed reaction. As mentioned, the poor selectivity of catalyst **I** is likely a result of rhodium ionically bonded to the silica surface, showing that the method of immobilisation can significantly affect catalysis. Catalysts **III** and **IV** are shown to be the most favourable for highly selective heterogeneous catalysis with **III** being slightly more selective, while **IV** was more active. Repeated testing of the catalysts showed that the rates and selectivities were maintained, suggesting that any leaching of rhodium is negligible (but no analysis was performed to quantify this) and that employing bidentate tethered phosphines could be an effective way to reduce leaching and vastly improve catalyst selectivity.

1.17 Recent applications of rhodium hydroformylation catalysts immobilised onto solid supports *via* tetherable ligands

One recent example of a heterogeneous hydroformylation catalyst in which rhodium was immobilised through tetherable ligands, involved the production of a rhodium complex anchored to the surface of a silica/polyamine composite.¹⁰⁷ To achieve this, poly(allylamine) was covalently grafted onto the surface of amorphous silica gel to provide a hybrid organic-inorganic surface. The resulting modified surface was then further functionalised with 4-diphenylphosphinobenzoic acid in an amide bond-forming reaction, providing phosphine ligand donor sites for rhodium complexation. Subsequent reaction with $\text{Rh}(\text{acac})(\text{CO})_2$ provided a heterogeneous rhodium hydroformylation catalyst (Figure 1.20).

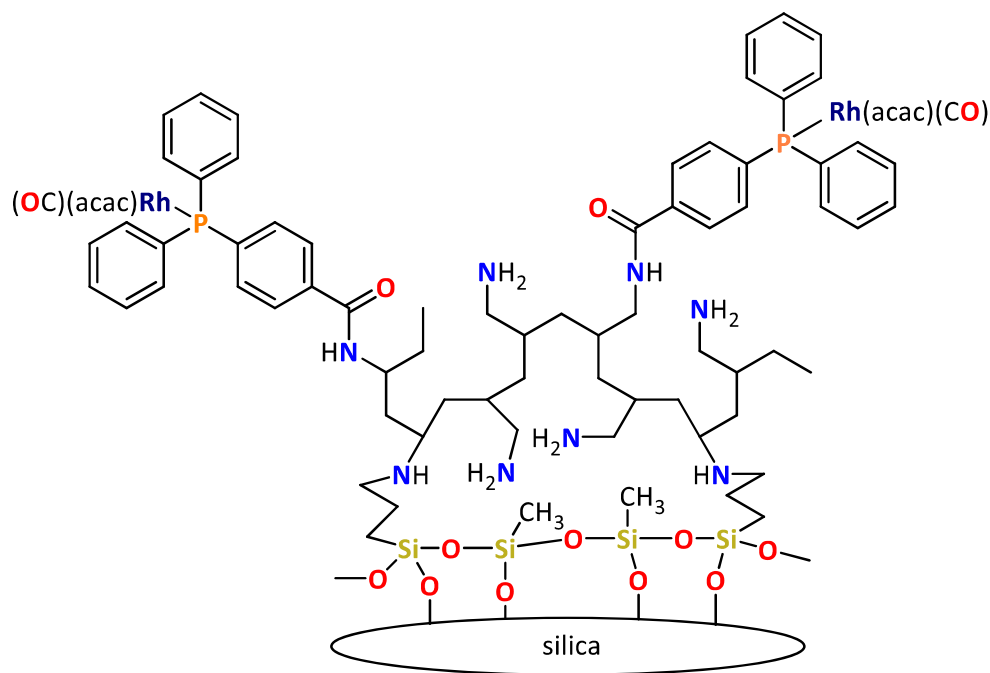


Figure 1.20. Structure of the heterogeneous rhodium hydroformylation catalyst produced from amorphous silica modified with poly(allylamine) followed by 4-diphenylphosphinobenzoic acid and $\text{Rh}(\text{acac})(\text{CO})_2$.¹⁰⁷

Catalyst testing for 1-octene hydroformylation was then performed using this immobilised catalyst system (Table 1.11), showing an initial TOF of 150 h^{-1} for the first run.¹⁰⁷ Upon reuse, the catalyst activity was found to be much lower, $80 - 100 \text{ h}^{-1}$ for runs 2 – 4, followed by a large decrease in activity after 5 runs. The decrease in activity after the first run is explained due to the rhodium initially being present as a surface bound species alongside a weakly bound physically adsorbed species that was not successfully bound to the surface during catalyst synthesis. Upon catalyst testing the physically adsorbed species can leach into solution and act as a homogenous catalyst, improving activity during the first run before it is lost from the system. Subsequent runs 2-4 showed better catalyst stability with little change in catalyst performance, before a significant loss in catalyst activity during run 5. These results show that rhodium leaching is an on-going issue with these systems that requires further investigation.

Table 1.11. 1-Octene hydroformylation performance of a silica/polyamine composite
Rh-anchored catalyst.¹⁰⁷

run	Octene conversion	Reaction mixture composition / %				<i>n</i> : <i>l</i> of aldehydes
		1-octene	<i>iso</i> -octenes	octane	aldehydes	
1	99	1	4	1	93	1.6
2	99	1	33	1	64	1.7
3	98	1	45	1	60	1.7
4	98	1	46	1	60	1.7
5	22	2	42	2	12	1.7
6	15	7	40	2	8	1.7

Conditions: 30 mg catalyst, 5 h, T = 80 °C, $p(\text{CO}/\text{H}_2 \text{ 1:1}) = 4 \text{ mPa}$, 3.5 mmol 1-octene in toluene (2 ml).

Further work has also recently been published investigating supported NiXantphos ligands (Figure 1.21).^{108,109} In this work the ligands were supported on hyperbranched poly(arylene oxindole) polymers (HBPAO) and investigated for the microwave-assisted hydroformylation of 1-octene (Table 1.12). The active rhodium catalyst species was produced *in situ* by reaction of the supported ligand with $\text{RhH}(\text{CO})(\text{PPh}_3)_3$ in toluene before addition of the alkene substrate.

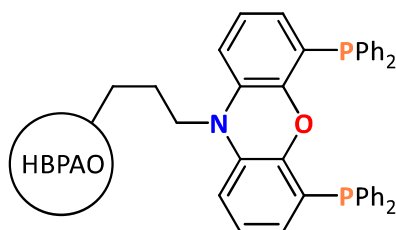


Figure 1.21. Structure of NiXanthphos supported on a hyperbranched poly(arylene oxindole) polymer.¹⁰⁸

Table 1.12. Microwave-assisted hydroformylation of 1-octene by HBPAO-supported NiXantphos / RhH(CO)(PPh₃)₃.¹⁰⁸

Run	Conv / %	<i>l:b</i>	Leached Rh / ppm
1	95	15:1	2.81
2	93	15:1	0.25
3	94	15:1	0.22
4	92	15:1	0.19
5	92	15:1	0.17

Conditions: 1-octene (0.035 mmol), ligand: Rh = 8:1, 20 min microwave, T = 75 °C, *p*(CO/H₂ 1:1) = 4.8 bar, in toluene (0.3 ml), initial rhodium loading = 11.2 mg.

Inductively coupled plasma (ICP) analysis was used to determine any leaching of rhodium from the system after recovery and reuse of the catalyst. The results showed a small amount of leaching during the first cycle, which drastically reduced after the first cycle and continued to gradually decrease on each subsequent cycle.¹⁰⁸ During repeated catalyst tests the *l:b* ratio of 15:1 was maintained along with high substrate conversion. These results provide additional evidence that application of a bidentate phosphine ligand can be an effective way to reduce leaching from heterogenised hydroformylation catalyst systems.

The HBPAO-supported NiXantphos / RhH(CO)(PPh₃)₃ catalyst system was then tested for a range of other alkene substrates. Pent-4-ene, allylbenzene, *N*-allylphthalimide, and allyltrimethylsilane were all successfully converted to the linear aldehyde in good yields, 66 – 99%, showing the tolerance of this catalyst system to various substrate functional groups. Unusually, the hydroformylation of styrene was shown to favour the linear aldehyde (*l:b* = 2:1), whereas the branched product is usually strongly favoured due to the formation of a η^3 -benzylic complex under homogeneous reaction conditions.¹¹⁰ This reversed regioselectivity observed may result from the dendritic nature of the support, which provides a unique microenvironment in which reactions take place.¹⁰⁸

Rhodium hydroformylation catalysts immobilised onto multiwalled carbon nanotubes (MWCNT) have recently been achieved using diphosphite ligands functionalised with a pyrene moiety (Figure 1.22).¹¹¹ During ligand synthesis a modified furanose backbone was reacted with (bromomethyl)pyrene, followed by two equivalents of a phosphochloridite to give the desired diphosphite that can be immobilised by π - π

stacking between the pyrene moiety and a suitable solid support, such as MWCNTs, reduced graphene oxide or carbon beads.

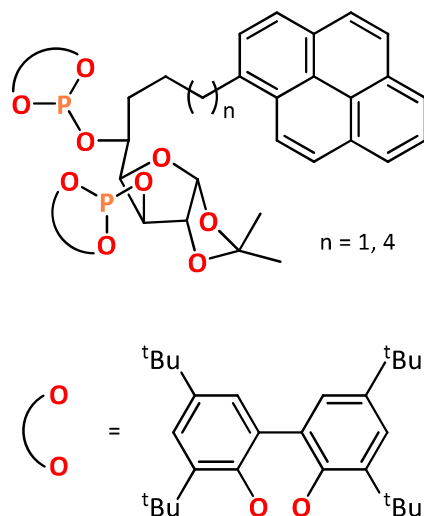
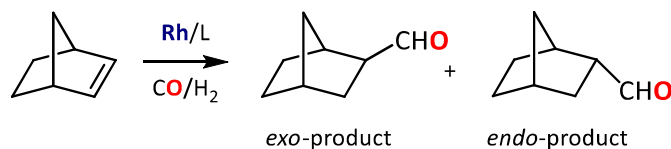


Figure 1.22. Structure of diphosphite ligand with tetherable pyrene moiety.¹¹¹

Upon rhodium complexation the resulting catalyst was investigated for the asymmetric hydroformylation of norbornene (Scheme 1.18).¹¹¹ Catalyst testing showed that *exo*-product was produced with >99% selectivity. The *ee* achieved varied from 30 – 72% depending on the exact reaction conditions used. Unfortunately, ICP analysis showed 78% loss of rhodium after one batch catalyst test cycle, and no detectable rhodium remaining on the support after 3 cycles. This is likely due to the weak, non-covalent interaction between the pyrene moiety and the support, resulting in a large degree of leaching from the system. The catalyst performed better in a continuous flow reactor, but, after maximising performance by optimising the reaction conditions and changing to a carbon bead support, 31% of rhodium was lost from the system after running in continuous flow for 190 minutes.¹¹¹ This suggests that a more robust tethering method is required to make use of the high activities offered by phosphite ligands in immobilised hydroformylation catalysis.



Scheme 1.18. Rhodium-catalysed hydroformylation of norbornene.¹¹¹

1.18 Chapter 1 summary

The development of hydroformylation catalyst technologies has been an ongoing endeavour since its initial discovery by Otto Roelen in 1938. This brief literature review has aimed to illustrate some of the key challenges and corresponding solutions that have driven research in this area. In particular, the appropriate design and application of phosphine ligands has proved vital in obtaining high catalyst activities and selectivities, with a wide variety of different phosphine ligands with differing steric and electronic properties (and P[∧]P bite angles for bidentate ligands) being utilised to suit particular hydroformylation applications. Another key challenge in hydroformylation is the separation of the transition metal catalyst from the reaction products, something that is currently predominantly performed by distillation for Rh-catalysed systems. Development of heterogeneous hydroformylation catalysts that can be separated and recycled by filtration would provide a great economic and environmental boost to current industrial hydroformylation processes. Despite significant research into this area, heterogeneous hydroformylation catalysts are yet to see industrial application due to ongoing issues with catalyst leaching and reducing activity compared to homogeneous processes that have yet to be fully addressed. It is our belief that by careful tuning of an immobilised phosphine ligand combined with appropriate catalyst support, a heterogeneous hydroformylation catalyst suitable for industrial application is achievable and will feature as the goal of this work.

Table 1.13. Summary of some hydroformylation Processes.^{4,23,30,32,103,106}

	Co		Rh				
	homogeneous		homogeneous			heterogeneous	
(phosphine) Ligand	none HCo(CO) ₄	PBu ₃	PPh ₃	TPPTS	Phosphite / bisphosphite	Silica-immobilised PPh ₂	Silica- immobilised xantphos
Typical substrate/s	C ₃	C ₉₋₁₅	<C10 Usually C ₃	<C ₅	Various including internal alkenes	C ₈	C ₈
T / °C	150-180	160-200	60-120	110-130	60-120	100-120	80
P / bar	200-300	50-150	10-50	40-60	10-50	30-50	50
Products	Aldehydes	Alcohols	Aldehydes	Aldehydes	Aldehydes	Aldehydes	Aldehydes
Typical n/i	60:40	85:15	92:8	95:5	97:3	65:35	97:3
Separation method	Chemical Co extraction (decobalting)	Distillation	Gas stripping / distillation	Aqueous extraction of Rh	Distillation	Filtration	Filtration
example Operator	BASF/ Ruhrchemie	Shell	Union Carbide	Rhône- Poulenc	Johnson Matthey	None / academia	None / academia

1.19 Project aims and objectives

The overall aim of this project is the development, understanding and refinement of tuneable oxide-supported bidentate phosphines for applications in rhodium-catalysed hydroformylation. To successfully achieve these aims, several key targets need to be met:

Initially, a range of potential bidentate ligands must be designed and synthesised. Ligand design will focus on exploring the effect of phosphine sterics, electronics and bite angle on hydroformylation catalysis by adjusting the ligand backbone and phosphine 'R' groups (Chapter 2).

The steric and electronic characteristics of the produced ligands phosphine donors will be investigated *via* use of the %V_{bur} and R₃PSe |¹J_{SeP}| coupling constant methods in order to allow more effective comparison of the role phosphine steric and electronic factors play during immobilised catalysis. The coordination chemistry of the ligands with catalytically active metals Rh, Pd and Co will then be investigated to produce catalyst precursors for hydroformylation (Chapter 3).

The immobilisation of the produced phosphine ligands and subsequent complexes onto solid oxide supports *via* various silane derived tethering groups to silica will be investigated *via* ²⁹Si and ³¹P MAS NMR spectroscopic analysis to understand the reactivity and stability of immobilised phosphines and produce pre-catalysts suitable for hydroformylation applications (Chapter 4).

The ultimate goal of this work is 1-octene hydroformylation catalyst testing of the pre-catalysts developed over the course of this project. Catalyst performance will be assessed by measuring catalyst activity and selectivity for (linear) aldehydes, with comparison between the homogenous and heterogeneous systems developed of great interest. The long-term stability of the immobilised catalyst systems will also be investigated *via* catalyst leaching and recycling experiments (Chapter 5).

1.20 Chapter 1 references

1. (a) O. Roelen, DE Patent, 849 548, 1938. (b) O. Roelen, US Patent, 2 327 066, 1943.
2. D. N. Gorbunov, M. V. Terenina, Y. S. Kardasheva, A. L. Maksimov and E. A. Karakhanov, *Pet. Chem.*, 2017, **57**, 1137–1140, DOI: 10.1134/S0965544117060159.
3. H. Bahrmann, H. Bach and G. D. Frey, *Ullmann's Encyclopedia of Industrial Chemistry*, Wiley-VCH Verlag GmbH & Co. KGaA, 2013, DOI: 10.1002/14356007.a18_321.pub2.
4. R. Franke, D. Selent and A. Börner, *Chem. Rev.*, 2012, **112**, 5675–5732, DOI: 10.1021/cr3001803.
5. P. Anastas and N. Eghbali, *Chem. Soc. Rev.*, 2010, **39**, 301–312, DOI: 10.1039/b918763b.
6. B. M. Trost, *Science*, 1991, **254**, 1471–1477, DOI: 10.1126/science.1962206.
7. R. F. Heck and D. S. Breslow, *J. Am. Chem. Soc.*, 1961, **19**, 4023–4027, DOI: 10.1021/ja01480a017.
8. F. Hebrard and P. Kalck, *Chem. Rev.*, 2009, **109**, 4272–4282, DOI: 10.1021/cr8002533.
9. P. Pino, A. Major, F. Spindler, R. Tannenbaum, G. Bor and I. T. Horváth, *J. Organomet. Chem.*, 1991, **417**, 65–76, DOI: 10.1016/0022-328X(91)80161-C.
10. I. Wender, H. Greenfield and M. Orchin, *J. Am. Chem. Soc.*, 1953, **75**, 3041–3042, DOI: 10.1021/ja01108a528.
11. G. Natta, R. Ercoli, S. Castellano and F. H. Barbieri, *J. Am. Chem. Soc.*, 1954, **76**, 4049–4050, DOI: 10.1021/ja01644a071.
12. I. Wender, S. Metlin, S. Ergun, H. W. Sternberg and H. Greenfield, *J. Am. Chem. Soc.*, 1956, **78**, 5401–5405, DOI: 10.1021/ja01601a064.
13. E. Zuidema, L. Escorihuela, T. Eichelsheim, J. J. Carbó, C. Bo, P. C. J. Kamer and P. W. N. M. Van Leeuwen, *Chem. Eur. J.*, 2008, **14**, 1843–1853, DOI: 10.1002/chem.200700727.
14. J. A. Fuentes, P. Wawrzyniak, G. J. Roff, M. Bühl and M. L. Clarke, *Catal. Sci. Technol.*, 2011, **1**, 431–436, DOI: 10.1039/c1cy00026h.
15. M. Vilches-Herrera, L. Domke and A. Börner, *ACS Catal.*, 2014, **4**, 1706–1724, DOI: 10.1021/cs500273d.
16. P. Dingwall, J. A. Fuentes, L. E. Crawford, A. M. Z. Slawin, M. Bühl and M. L. Clarke, *J. Am. Chem. Soc.*, 2017, **139**, 15921–15932, DOI: 10.1021/jacs.7b09164.
17. B. L. Haymore, A. van Asselt and G. R. Beck, *Ann. N. Y. Acad. Sci.*, 1983, **415**, 159–175, DOI: 10.1111/j.1749-6632.1983.tb47357.x.
18. G. G. Stanley, *Kirk-Othmer Encyclopedia of Chemical Technology*, 2017, 1–26, DOI: 10.1002/0471238961.1524150209121.a01.pub2.
19. G. M. Torres, R. Frauenlob, R. Franke and A. Börner, *Catal. Sci. Technol.*, 2015, **5**, 34–54, DOI: 10.1039/c4cy01131g.

20. L. G. Canell, L. H. Slaugh and R. D. Mullineaux (to Shell Internationale Research Maatschappij B. V.), DE Patent 1 186 455, 1965.
21. L. H. Slaugh and R. D. Mullineaux, *J. Organomet. Chem.*, 1968, **13**, 469–477, DOI: 10.1016/S0022-328X(00)82775-8.
22. P. N. Bungu and S. Otto, *Dalton Trans.*, 2011, **40**, 9238–9249, DOI: 10.1039/c1dt10581g.
23. H. van Rensburg, W. Janse van Rensburg, R. P. Tooze and D. F. Foster, in Proceedings of the DGMK/SCI-Conference "Synthesis Gas Chemistry" 2006; Dresden, ed S. Ernst, DGMK, Hamburg, 2006, p. 247–254.
24. F. P. Pruchnik, *Organometallic Chemistry of Transition Elements*, Plenum Press, New York, 1990.
25. J. F. Young, J. A. Osborn, F. H. Jardine and G. Wilkinson, *Chem. Commun.*, 1965, 131–132, DOI: 10.1039/C19650000131.
26. D. Evans, J. A. Osborn and G. Wilkinson, *J. Chem. Soc. A*, 1968, 3133–3142, DOI: 10.1039/J19680003133.
27. F. H. Jardine, *Polyhedron*, 1982, **1**, 569–605, DOI: 10.1016/S0277-5387(00)80853-0.
28. M. Beller, B. Cornils, C. D. Frohning and C. W. Kohlpaintner, *J. Mol. Catal. A: Chem.*, 1995, **104**, 17–85, DOI: 10.1016/1381-1169(95)00130-1.
29. C. K. Brown and G. Wilkinson, *J. Chem. Soc. A*, 1970, 2753–2764, DOI: 10.1039/J19700002753.
30. R. Tudor and M. Ashley, *Platinum Metals Rev.*, 2007, **51**, 116–126, DOI: 10.1595/147106707X216855.
31. D. Evans, G. Yagupsky and G. Wilkinson, *J. Chem. Soc. A*, 1968, 2660–2665, DOI: 10.1039/J19680002660.
32. R. L. Pruett and J. A. Smith, *J. Org. Chem.*, 1969, **34**, 327–330, DOI: 10.1021/jo01254a015.
33. R. V. Kastrup, J. S. Merola and A. A. Oswald, in 'ACS Advances in Chemistry Series', eds. E. L. Alyea and D. W. Meek, ACS, Washington, D.C., 1982, Vol. 196, Ch. 3, p. 43.
34. W. R. Moser, C. J. Papile, D. A. Brannon, R. A. Duwell, and S. J. Weininger, *J. Mol. Catal.*, 1987, **41**, 271, DOI: 10.1016/0304-5102(87)80106-2.
35. U. Gellrich, T. Koslowski and B. Breit, *Catal. Sci. Technol.*, 2015, **5**, 129–133, DOI: 10.1039/c4cy01209g.
36. E. Zuidema, L. Escorihuela, T. Eichelsheim, J. J. Carbó, C. Bo, P. C. J. Kamer and P. W. N. M. Van Leeuwen, *Chem. Eur. J.*, 2008, **14**, 1843–1853, DOI: 10.1002/chem.200700727.
37. M. Lewin, Z. Aizenshtat and J. Blum, *J. Organomet. Chem.*, 1980, **184**, 255–261, DOI: 10.1016/S0022-328X(00)83492-0.
38. A. G. Abatjoglou, E. Billig and D. R. Bryant, *Organometallics*, 1984, **3**, 923–926, DOI: 10.1021/om00084a017.
39. A. Bara-Estaún, C. L. Lyall, J. P. Lowe, P. G. Pringle, P. C. J. Kamer, R. Franke and U. Hintermair, *Catal. Sci. Technol.*, 2022, **12**, 5501–5516, DOI: 10.1039/d2cy00312k.

40. P. Dierkes and P. W. N. M. Van Leeuwen, *J. Chem. Soc., Dalton Trans.*, 1999, 1519–1530, DOI: 10.1039/A807799A.
41. Y. Jiao, M. S. Torne, J. Gracia, J. W. Niemantsverdriet and P. W. N. M. Van Leeuwen, *Catal. Sci. Technol.*, 2017, **7**, 1404–1414, DOI: 10.1039/c6cy01990k.
42. Y. Feng, J. Qi, M. Li, J. Wei, Q. Yang, J. Ding, M. Wang and X. Ma, *J. Catal.*, 2023, **427**, 115093, DOI: 10.1016/j.jcat.2023.08.009.
43. A. Bara-Estaún, C. L. Lyall, J. P. Lowe, P. G. Pringle, P. C. J. Kamer, R. Franke and U. Hintermair, *ChemCatChem*, 2023, **15**, e2022012, DOI: 10.1002/cctc.202201204.
44. E. Zuidema, E. Daura-Oller, J. J. Carbó, C. Bo and P. W. N. M. Van Leeuwen, *Organometallics*, 2007, **26**, 2234–2243, DOI: 10.1021/om060981.
45. A. G. Orpen and N. G. Connelly, *Organometallics*, 1990, **9**, 1206–1210, DOI: 10.1021/om00118a048.
46. C. A. Tolman, *Chem. Rev.*, 1977, **77**, 313–348, DOI: 10.1021/cr60307a002.
47. G. Pacchioni and P. S. Bagus, *Inorg. Chem.*, 1992, **31**, 4391–4398, DOI: 10.1021/ic00047a029.
48. D. W. Allen and B. F. Taylor, *J. Chem. Soc., Dalton Trans.*, 1982, 51–54, DOI: 10.1039/DT9820000051.
49. J. C. S. Dalton, W. Mcfarlane and D. S. Rycroft, *J. Chem. Soc., Dalton Trans.*, 1973, 2162–2166, DOI: 10.1039/DT9730002162.
50. C. J. Cobley and P. G. Pringle, *inorganica Chim. Acta*, 1997, **265**, 107–115, DOI: 10.1016/S0020-1693(97)05638-7.
51. C. Hansch, A. Leo and R. W. Taft, *Chem. Rev.*, 1991, **91**, 165–195, DOI: 10.1021/cr00002a004.
52. L. Falivene, Z. Cao, A. Petta, L. Serra, A. Poater, R. Oliva, V. Scarano and L. Cavallo, *Nat. Chem.*, 2019, **11**, 872–879, DOI: 10.1038/s41557-019-0319-5.
53. J. T. Carlock, *Tetrahedron*, 1984, **40**, 185–187, DOI: 10.1016/0040-4020(84)85118-2.
54. L. A. van der Veen, P. K. Keeven, P. C. J. Kamer and P. W. M. N. van Leeuwen, *J. Chem. Soc., Dalton Trans.*, 2000, 2105–2112, DOI: 10.1039/B002126L.
55. T. Mizoroki, M. Kioka, M. Suzuki, S. Sakatani, A. Okumura and K. Maruya, *Bull. Chem. Soc. Jpn.*, 1984, **57**, 577–578, DOI: 10.1246/bcsj.57.577.
56. P. W. N. M. Van Leeuwen, *Appl. Catal. A-Gen.*, 2001, **212**, 61–81, DOI: 10.1016/S0926-860X(00)00844-9.
57. P. W. N. M. van Leeuwen and C. Claver, *Rhodium Catalysed Hydroformylation*, Kluwer Academic Publishers, Dordrecht, 2000.
58. V. Vallet, U. Wahlgren and I. Grenthe, *J. Am. Chem. Soc.*, 2003, **125**, 14941–14950, DOI: 10.1021/ja036646j.
59. C. U. Pittman Jr. and A. Hirao, *J. Org. Chem.*, 1978, **43**, 640–646, DOI: 10.1021/jo00398a026.
60. O. R. Hughes and J. D. Unruh, *J. Mol. Catal.*, 1981, **12**, 71–83, DOI: 10.1016/0304-5102(81)80020-X.

61. J. D. Unruh and J. R. Christenson, *J. Mol. Catal.*, 1982, **14**, 19–34, DOI: 10.1016/0304-5102(82)80046-1.
62. T. J. Devon, G. W. Phillips, T. A. Puckette, J. L. Stavinoha and J. J. Vanderbilt (to Texas Eastman), US Patent 4 694 109, 1987.
63. C. P. Casey and G. T. Whiteker, *Isr. J. Chem.*, 1990, **30**, 299–304, DOI: 10.1002/ijch.199000031.
64. M. N. Birkholz, Z. Freixa and P. Van Leeuwen, *Chem. Soc. Rev.*, 2009, **38**, 1099–1118, DOI: 10.1039/b806211k.
65. A. K. Bhattacharya and G. Thyagarajan, *Chem. Rev.*, 1981, **81**, 415–430, DOI: 10.1021/cr00044a004.
66. P. W. N. M. Van Leeuwen and C. F. Roobeek, *J. Organomet. Chem.*, 1983, **258**, 343–350, DOI: 10.1016/S0022-328X(00)99279-9.
67. D. R. Bryant and T. K. Leung (to Union Carbide Chemicals & Plastics Technology Corporation), US Patent 5 741 943, 1998.
68. A. Polo, C. Claver, S. Castellón and J. C. Bayon, *J. Chem. Soc. Chem. Commun.*, 1990, 600–601, DOI: 10.1039/C39900000600.
69. E. Billig, A. G. Abatjoglou and D. R. Bryant (to Union Carbide Corporation), EP Patent 0 213 639 B1, 1991.
70. O. Saidi, S. Liu and J. Xiao, *J. Mol. Catal. A: Chem.*, 2009, **305**, 130–134, DOI: 10.1016/j.molcata.2008.10.034.
71. J. Ternel, J. L. Dubois, J. L. Couturier, E. Monflier and J. F. Carpentier, *ChemCatChem*, 2013, **5**, 1562–1569, DOI: 10.1002/cctc.201200630.
72. C. Fliedel, A. Ghisolfi and P. Braunstein, *Chem. Rev.*, 2016, **116**, 9237–9304, DOI: 10.1021/acs.chemrev.6b00153.
73. E. Piras, B. Powietzka, F. Wurst, D. Neumann-Walter, H. J. Grützmacher, T. Otto, T. Zevaco and O. Walter, *Catal. Lett.*, 2013, **143**, 673–680, DOI: 10.1007/s10562-013-1010-x.
74. S. A. Wander, A. Miedaner, B. C. Noll, R. M. Barkley and D. L. Dubois, *Organometallics*, 1996, **15**, 3360–3373, DOI: 10.1021/om960072s.
75. J. W. Raebiger, A. Miedaner, C. J. Curtis, S. M. Miller, O. P. Anderson and D. L. DuBois, *J. Am. Chem. Soc.*, 2004, **126**, 5502–5514, DOI: 10.1021/ja0395240.
76. K. M. Waldie, A. L. Ostericher, M. H. Reineke, A. F. Sasayama and C. P. Kubiak, *ACS Catal.*, 2018, **8**, 1313–1324, DOI: 10.1021/acscatal.7b03396.
77. V. A. Glezakou, R. Rousseau, S. T. Elbert and J. A. Franz, *J. Phys. Chem. A*, 2017, **121**, 1993–2000, DOI: 10.1021/acs.jpca.6b11655.
78. E. S. Wiedner, M. B. Chambers, C. L. Pitman, R. M. Bullock, A. J. M. Miller and A. M. Appel, *Chem. Rev.*, 2016, **116**, 8655–8692.
79. H. Lemke, FR Patent 1 089 983, 1953.

80. H. J. Nienburg, R. Kummer, H. Hohenschutz, M. Strohmeyer and P. Tavs, DE Patent 2 206 252, 1973.
81. L. Gärtner, B. Cornils and P. Lappe (to Ruhrchemie AG), EP Patent 0 107 006, 1983.
82. B. Cornils and E. G. Kuntz, *J. Organomet. Chem.*, 1995, **502**, 177–186, DOI: 10.1016/0022-328X(95)05820-F.
83. M. J. Betts, M. E. Dry, A. Geertsma and G. J. H. Hall (to Sasol Chemicals Europe), WO Patent 9 701 521, 1997.
84. G. Abatjoglou, D. R. Bryant and R. R. Peterson (to Union Carbide), US Patent 5 180 854, 1993.
85. M. E. Ali, M. M. Rahman, S. M. Sarkar and S. B. A. Hamid, *J. Nanomater.*, 2014, **2014**, 192038, DOI: 10.1155/2014/192038.
86. Johnson Matthey PGM prices, <http://www.platinum.matthey.com/prices/price-charts#>, (accessed February 2024).
87. S. C. Chuang and S. I. Pien, *J. Catal.*, 1992, **135**, 618–634, DOI: 10.1016/0021-9517(92)90058-P.
88. Q. Sun, M. Jiang, Z. Shen, Y. Jin, S. Pan, L. Wang, X. Meng, W. Chen, Y. Ding, J. Li and F. S. Xiao, *Chem. Commun.*, 2014, **50**, 11844–11847, DOI: 10.1039/c4cc03884c.
89. R. Lang, T. Li, D. Matsumura, S. Miao, Y. Ren, Y. Cui, Y. Tan, B. Qiao, L. Li, A. Wang, X. Wang and T. Zhang, *Angew. Chem. Int. Ed.*, 2016, **44**, 16054–16058, DOI: 10.1002/anie.201607885.
90. H. P. Steinrück, J. Libuda, P. Wasserscheid, T. Cremer, C. Kolbeck, M. Laurin, F. Maier, M. Sobota, P. S. Schulz and M. Stark, *Adv. Mater.*, 2011, **23**, 2571–2587, DOI: 10.1002/adma.201100211.
91. L. Ropartz, R. E. Morris, D. F. Foster and D. J. Cole-Hamilton, *J. Mol. Catal. A: Chem.*, 2002, **182**, 99–105, DOI: 10.1016/S1381-1169(01)00502-7.
92. S. Hanf, L. A. Rupflin, R. Gläser and S. A. Schunk, *Catalysts*, 2020, **10**, 510–586, DOI: 10.3390/catal10050510.
93. A. Galarneau, H. Cambon, F. Di Renzo and F. Fajula, *Langmuir*, 2001, **17**, 8328–8335, DOI: 10.1021/la0105477.
94. R. Kishor and A. K. Ghoshal, *Microporous Mater.*, 2017, **242**, 127–135, DOI: 10.1016/j.micromeso.2017.01.020.
95. L. T. Zhuravlev, *Colloids Surf. A: Physicochem. Eng. Asp.*, 2000, **173**, 1–38, DOI: 10.1016/S0927-7757(00)00556-2.
96. L. Y. Chen, S. Jaenicke and G. K. Chuah, *Microporous Mater.*, 1997, **12**, 323–330, DOI: 10.1016/S0927-6513(97)00079-5.
97. P. Yang, D. Zhao, D. I. Margolese, B. F. Chmelka, and G. D. Stucky, *Nature*, 1998, **396**, 152–155, DOI: 10.1038/24132.
98. F. Kleitz, S. H. Choi and R. Ryoo, *Chem. Commun.*, 2003, **3**, 2136–2137, DOI: 10.1039/b306504a.

99. C. Pirez, J. M. Caderon, J. P. Dacquin, A. F. Lee and K. Wilson, *ACS Catal.*, 2012, **2**, 1607–1614, DOI: 10.1021/cs300161a.
100. M. Kruk, M. Jaroniec, Y. Sakamoto, O. Terasaki, R. Ryoo and C. H. Ko, *J. Phys. Chem. B*, 2000, **104**, 292–301, DOI: 10.1021/jp992718a.
101. C. Li, W. Wang, L. Yan and Y. Ding, *Front. Chem. Eng.*, 2018, **12**, 113–123, DOI: 10.1007/s11705-017-1672-9.
102. L. Huang and S. Kawi, *Catal. Lett.*, 2004, **92**, 57–62, DOI: 10.1023/B:CATL.0000011087.58049.32.
103. W. Zhou and D. He, *Green Chem.*, 2009, **11**, 1146–1154, DOI: 10.1039/b900591a.
104. X. Li, Y. Ding, G. Jiao, J. Li, R. Lin, L. Gong, L. Yan and H. Zhu, *Appl Catal A Gen*, 2009, **353**, 266–270, DOI: 10.1016/j.apcata.2008.10.052.
105. Â. C. B. Neves, M. J. F. Calvete, T. M. V. D. Pinho E Melo and M. M. Pereira, *Eur. J. Org. Chem.*, 2012, **2012**, 6309–6320, DOI: 10.1002/ejoc.201200709.
106. A. J. Sandee, J. N. H. Reek, P. C. J. Kamer and P. W. N. M. Van Leeuwen, *J. Am. Chem. Soc.*, 2001, **123**, 8468–8476, DOI: 10.1021/ja010150p.
107. D. Gorbunov, D. Safronova, Y. Kardasheva, A. Maximov, E. Rosenberg and E. Karakhanov, *ACS Appl. Mater. Interfaces*, 2018, **10**, 26566–26575, DOI: 10.1021/acsami.8b02797.
108. T. Verheyen, N. Santillo, D. Marinelli, E. Petricci, W. M. De Borggraeve, L. Vaccaro and M. Smet, *ACS Appl. Polym. Mater.*, 2019, **1**, 1496–1504, DOI: 10.1021/acsapm.9b00240.
109. F. M. S. Rodrigues, R. M. B. Carrilho and M. M. Pereira, *Eur. J. Inorg. Chem.*, 2021, **2021**, 2294–2324, DOI: 10.1002/ejic.202100032.
110. E. Boymans, M. Janssen, C. Müller, M. Lutz and D. Vogt, *Dalton Trans.*, 2013, **42**, 137–142, DOI: 10.1039/c2dt31738a.
111. A. Cunillera, C. Blanco, A. Gual, J. M. Marinkovic, E. J. Garcia-Suarez, A. Riisager, C. Claver, A. Ruiz and C. Godard, *ChemCatChem*, 2019, **11**, 2195–2205, DOI: 10.1002/cctc.201900211.

Chapter 2: Design and synthesis of tether- functionalised diphosphine compounds

2.1 Ligand design considerations

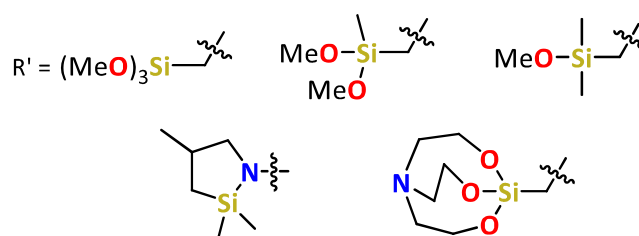
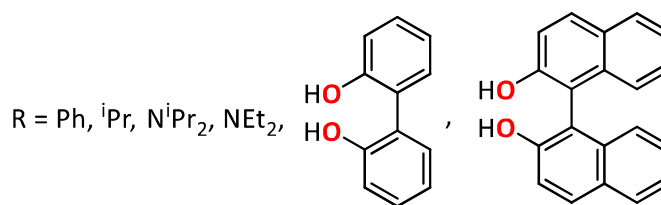
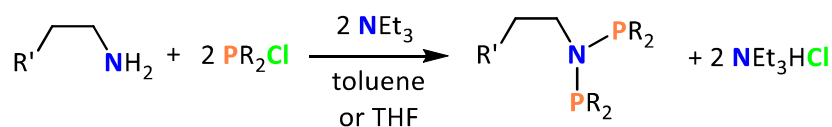
In the development of heterogenised catalyst systems using organic linker ligands to immobilise discrete metal centres onto a solid support, it is well-established that the structure of the organic linker ligand employed profoundly effects many aspects of catalyst performance. For example, the correct choice of ligand is vital for achieving good catalyst activity and selectivity, as is also observed for homogeneous catalysis (see sections 1.8, 1.10 and 1.11).¹ In addition to this, the linker ligand also controls the stability of the catalyst, specifically the propensity for the metal to remain anchored to the support and hence avoid leaching of the metal into solution. This is a key consideration in heterogenised catalysis, since separation of the immobilised catalyst from the reaction mixture by filtration is the main advantage of this chemistry and is fully dependant on the metal remaining firmly attached to the insoluble support. In this regard, the linker ligand has two main roles: firstly, it must coordinate the metal strongly enough that metal dissociation from the ligand is not a major issue, and secondly the linker itself must be robustly attached to the solid support so that the metal-linker ligand complex does not detach from the support into solution.

Taking into consideration these factors, three key aspects/factors of ligand design were initially considered. Firstly, phosphine ligands are desired for metal complexation, as phosphines are ubiquitous in hydroformylation catalysis due to the high catalyst activity they impart. In particular, bidentate phosphines will be employed as they have been shown to enable higher product selectivities relative to monodentate phosphines (see sections 1.10 and 1.11), especially in terms of achieving high aldehyde *I:b* ratios in Rh-catalysed hydroformylation.² In addition, exploiting the chelate effect of bidentate ligands can improve catalyst stability and resistance to metal leaching due to metal dissociation or ligand exchange.³ Secondly, a functional group that can irreversibly bind to a solid support (*e.g.* silica) in a facile reaction is required that is also stable to hydroformylation reaction conditions and practical to incorporate into ligand synthesis. Finally, it is desired to explore a broad range of ligand characteristics that have been shown to affect hydroformylation catalyst performance, such as phosphine sterics, electronics and bite angle, as there has so far been only limited exploration of these factors in immobilised hydroformylation catalysis. Therefore, a flexible ligand synthesis

strategy that allows facile modification of these properties by simple, modular changes to the ligand structure will be of great advantage (see Sections 2.2-2.4). Other aspects of ligand design to consider include the cost and number of synthetic transformations required for synthesis. As the aim of this project is the development of an industrially viable heterogenised hydroformylation catalyst, the production cost of the catalyst needs to be as low as possible. Heterogenised catalysts fundamentally consist of more constituent parts than the currently operated homogenous catalysts, due to the presence of the inorganic support. Although the financial cost of the support is likely to be low relative to the cost of the precious metal salts required for catalyst synthesis, the time and financial cost of the extra synthetic steps required to immobilise the metal catalyst onto the support also need to be considered. As such, the use of catalyst components that are cheap and readily available, and the design of linker ligands that are simple and require as few synthetic steps as possible while still maintaining catalyst performance, are desired to minimise the overall cost of the catalyst.

2.2 PNP ligand design and synthesis

An initial target for ligand investigation was a family of bis(diphenyl)phosphinoamine (dppa-type) compounds that can act as small bite angle bidentate ligands, forming 4-membered chelate rings when coordinated to metals. They are attractive targets as there has been little research on their application in hydroformylation catalysis, although they have been shown to be highly active (1-octene, $\text{Rh}(\text{acac})((\text{Ph}_2\text{P})_2\text{NCH}_2\text{CH}_2\text{CH}_3)$).⁴ Indeed, the narrow bite angle of these ligands is likely to have some interesting and underexploited effects in hydroformylation catalysis. This is due to the strengthening effect of decreasing P-M-P bond angles on metal-hydride character, which can be beneficial for increasing linear aldehyde selectivity in hydroformylation, in contrast to the general favouring of wide bite angle ligands in hydroformylation (see Chapter 1.13).⁵



Scheme 2.1. Synthesis of various tetherable PNP compounds.

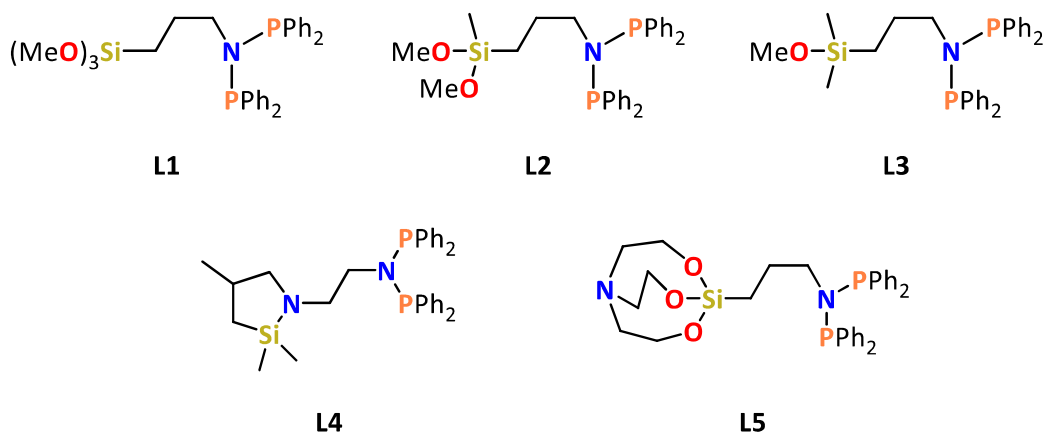
Synthesis of these ‘PNP’ compounds is generally readily achieved in one synthetic step by reaction of a primary amine with two equivalents of a chlorophosphine, providing an attractive synthesis strategy, which affords a symmetric diphosphine (Scheme 2.1). This modular synthesis enables flexible control of several key ligand properties; by varying the chlorophosphine used during synthesis, a range of compounds with different phosphine steric and electronic characteristics can be produced, which are likely to result in differing catalyst performance. For example, electron donating alkyl phosphine groups can be incorporated to produce more electron-rich phosphines, whereas incorporation of electron withdrawing alkylamino and phosphite moieties would result in electron-poor phosphines. Phosphine electronic character is well established as an important factor in controlling hydroformylation rates and selectivities in solution (see sections 1.10 and 1.11) and is therefore of great interest to explore for heterogenised catalysts.

Another key aspect of ligand design is incorporation of a tethering group that can covalently anchor the ligand to a solid oxide support. For the production of tetherable PNP ligands this can be readily achieved by application of a primary amine that has an

appropriate additional functionality capable of covalently bonding to oxide supports by reaction with surface silanols. It is of interest to investigate the use of a wide variety of tethering groups for phosphine immobilisation, with the most desirable being a tether that can be immobilised under mild conditions, while also being stable to the hydroformylation catalyst testing conditions that will later be employed (*e.g.* Rh cat., 90 °C, 20 bar 1:1 H₂:CO, toluene). The tethering group should also not interact with the coordination sphere of the metal centre employed during catalysis, in order to retain the ‘solution like’ metal environment that typically provides high catalyst performance in homogeneous hydroformylation processes. It was possible to identify several commercially available amines containing relevant tethering groups that could be investigated in the first instance. Combining these amines with various commercially available (or readily accessible from simple starting materials) chlorophosphines means that a large library of tetherable phosphine ligands can be produced to be investigated in hydroformylation catalysis.

2.2.1 PNP ligand synthesis – varying the silica-tethering backbone

In order to investigate the effect of the tethering groups on solid-oxide-immobilisation of PNP compounds, five related PNP compounds were designed and prepared with varying tethering groups, **L1-5** (Figure 2.1). Each compound features the same bis(diphenyl)phosphinoamine moiety for metal complexation. Phenyl groups were selected as phosphine ‘R’ groups, as they are the most commonly observed groups for PNP compounds in the literature, allowing comparisons between this work and other work in the literature, as well as sharing similarities to other established arylphosphine ligands widely used in hydroformylation. The phenyl groups should result in aminophosphines with moderate steric and electronic properties, that will be useful for initial investigations. Each compound features a three-atom spacer between its aminophosphine nitrogen atom and tethering group silicon atom, as these were the most readily synthetically accessible from commercially available start materials. Also, this three-atom spacer motif has been widely explored for various applications where organic compounds are immobilised onto oxide supports in the literature.^{6,7}



*Figure 2.1. Structures of PNP compounds **L1-5**.*

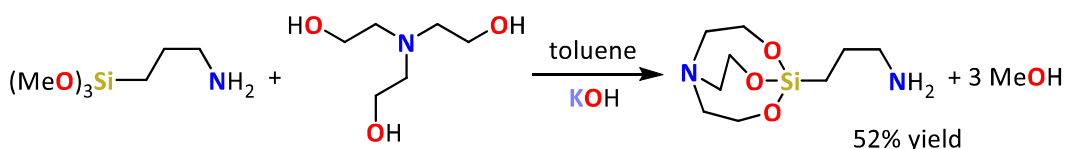
All compounds **L1-5** are capable of covalently bonding to oxide supports by nucleophilic attack of oxide-support surface silanols to the electrophilic silicon atom of the various silane-type tethering groups, the details of which will be discussed in Chapter 4 (see section 4.2).

The trialkoxysilane **L1**, $(\text{PPh}_2)_2\text{N}(\text{CH}_2)_3\text{Si}(\text{OMe})_3$, has been previously investigated for the immobilisation of palladium complexes onto silica, providing a useful literature comparison for our initial immobilisation attempts (see section 4.2), while remaining completely unexplored in regard to hydroformylation catalysis or rhodium coordination more generally.⁸ Novel compounds **L2**, $(\text{PPh}_2)_2\text{N}(\text{CH}_2)_3\text{Si}(\text{OMe})_2\text{Me}$, and **L3**, $(\text{PPh}_2)_2\text{N}(\text{CH}_2)_3\text{Si}(\text{OMe})\text{Me}_2$ feature reduced numbers of OMe groups relative to **L1** (two and one respectively). This change will affect the tethering group's reactivity with oxide supports and allow us to probe the effect that the number of bonds between the ligand and surface has on the robustness of immobilisation. The compound **L4**, $(\text{PPh}_2)_2\text{N}(\text{CH}_2)_2(\text{NSi}(\text{Me})_2\text{CH}_2\text{CH}(\text{CH}_3)\text{CH}_2)$, features a cyclic azasilane group that can undergo a ring opening "click" reaction with silanols, resulting in an immobilisation process that is extremely facile and 100% atom efficient, making for a very attractive target. The disadvantage of this approach is the high cost of the azasilane starting material relative to the alkoxyasilanes previously discussed. Another important consideration for compounds **L1-4** is that the tethering functionalities are very water sensitive due to being designed to be reactive with silanols. This can make handling of the compounds difficult as they are very susceptible to hydrolysis and therefore need to

be carefully handled and stored under inert conditions to prevent decomposition. As a result of this, an air-stable alternative to these compounds was desired for investigation, for which compound **L5**, $(\text{PPh}_2)_2\text{N}(\text{CH}_2)_3\text{Si}(\text{OCH}_2\text{CH}_2)_3\text{N}$, featuring a silatrane tethering functionality, was designed and synthesised.

The silatrane functional group exhibits greatly improved stability to water and other nucleophiles over alkoxysilanes due to the macrocyclic nature of the triethoxyamine moiety bound to the silicon atom.⁹ Furthermore, the nitrogen lone pair is donated into an empty Si-C σ^* orbital, providing further increased stability. As a result, in contrast to the decomposition of alkoxysilanes induced by water, which takes minutes, silatranes only fully decompose in water over a period of days.⁹ Additionally, silatranes are commonly crystalline solids, which makes handling and purification of their compounds significantly easier than their alkoxysilane analogues. However, the increased stability of the silatrane group relative to alkoxysilanes does have the drawback of reducing its rate of reaction with oxide supports. Nevertheless, this reaction has still been successfully achieved using a number of different oxides in the literature (including SiO_2 , TiO_2 , SnO_2), although harsher conditions are often required for immobilisation relative to alkoxysilanes, something that will be explored later (see section 4.10).¹⁰

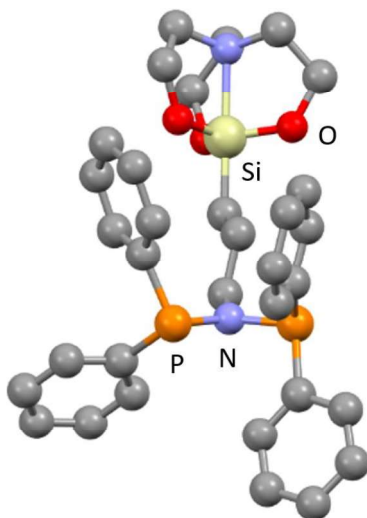
The required amine for the synthesis of **L5** was not commercially available and was therefore synthesised according to an adapted literature procedure by reaction of (3-aminopropyl)trimethoxysilane with triethanolamine in the presence of catalytic KOH (Scheme 2.2).¹¹



Scheme 2.2. Synthesis of (3-aminopropyl)silatrane.

The synthesis of the compounds described in Figure 2.1 was performed *via* an adaption of a literature procedure reported by Braunstein *et al.* (Scheme 2.1).⁸ Several solvent options for this reaction were investigated such as, DCM, THF and toluene, with THF or toluene being preferred as they do not dissolve the resulting NEt_3HCl , facilitating a more straightforward reaction work-up. No effect on reaction selectivity was observed when

these different solvents were employed. Compounds **L1-4** were all isolated as viscous colourless/pale yellow oils that required no further purification in moderate yields (43 – 69%). Compound **L5** was isolated as a white solid (64% yield) that was recrystallised from DCM/hexane to give single crystals suitable for X-ray crystallography, which was performed at Durham University by Dr D. Yufit. ^{31}P NMR spectroscopic analysis of these compounds all showed the presence of a characteristic singlet at ~ 61 ppm, diagnostic for $\text{RN}(\text{PPh}_2)_2$ compounds.¹²



*Figure 2.2. Molecular structure of **L5**. Hydrogens and DCM solvent molecule omitted for clarity. Selected bond angles / $^\circ$: P-N-P 120.08(8); P-N-C 115.1(1), 122.7(1). Selected bond distances / \AA : P-N 1.715(1), 1.718(1); C-N 1.485(2); Si-O 1.668(1), 1.663(1), 1.666(1); Si-N 2.171(1); Si-C 1.880(2).*

The molecular structure of **L5** (Figure 2.2) shows a P-N-P bond angle of 120.08(8) $^\circ$, corresponding to a trigonal planar nitrogen atom typical for bis(diphenylphosphino)amine ligands.¹² The two tetrahedral phosphorus atoms adopt the commonly observed staggered conformation relative to each other, with the two P lone pairs pointing in opposite directions.¹² Also of note is the pentacoordinate silicon atom, which adopts a distorted trigonal bipyramidal geometry typical of silatranes.⁹ The Si-N bond distance of 2.171(1) \AA also agrees with typical literature values for silatranes. It is significantly longer than a regular Si-N bond distance of ~ 1.8 \AA .¹³ This is due to the three-centre four-electron bonding present in silatranes, with Si-N bond distance shown to decrease as the Si-C bond opposite increases in length.¹⁴

After recrystallization of **L5**, the filtrate was left to stand, resulting in formation of further colourless crystals suitable for XRD analysis, which was performed in Durham by Dr D. Yufit. These were identified as the previously reported compound $O(Ph_2PO)_2$, although the molecular structure of this compound had not previously been determined (Figure 2.3).¹⁵ The compound presumably formed as a side reaction of **L5** with trace water and oxygen present in solution. This compound is of interest as the un-oxidised species $O(PPh_2)_2$ has been previously reported as a ligand for hydroformylation after its accidental formation by P-N bond hydrolysis of an aminophosphine ligand, while its direct synthesis proves difficult.⁴

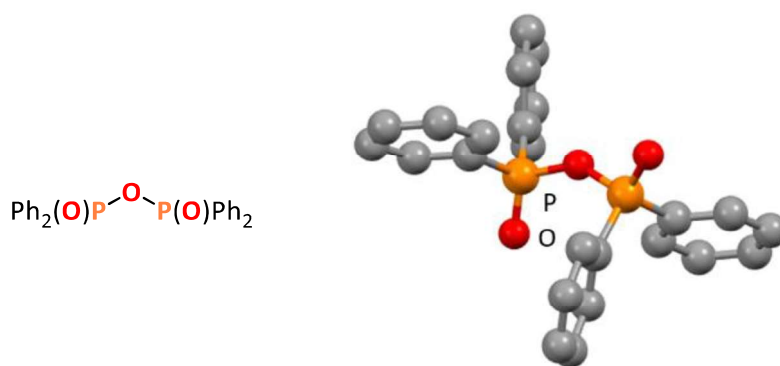


Figure 2.3. Molecular structure of $O(Ph_2PO)_2$. Hydrogens omitted for clarity. Selected bond angles / °: P-O-P 142.18(8). Selected bond distances / Å: P-O 1.606(1), 1.610(1); P=O 1.473(1), 1.470(1).

2.2.2 Synthesis of PNP ligands – varying the phosphine ‘R’ group

Alongside PNP compounds containing various silica-tethering groups, synthesis of PNP compounds with different phosphine moieties were required. By changing the phosphine ‘R’ group, potential PNP ligands with varying steric and electronic phosphine properties could be produced. By systematically changing these properties, their effect on hydroformylation catalysis following rhodium complexation can be determined, allowing the catalyst system to be optimised to provide the best combination of catalyst activity, selectivity and stability. Thus, a series of target PNP compounds with varying

electronic properties moving from electron-rich dialkyl phosphines to more electron deficient amino-phosphines and phosphoramidites was devised (Figure 2.4).

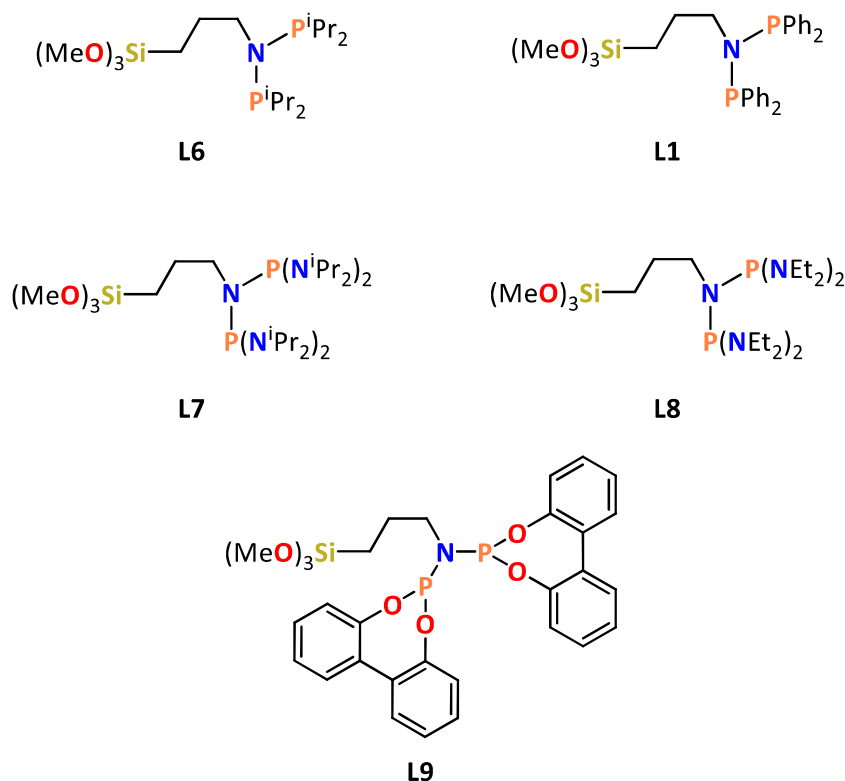
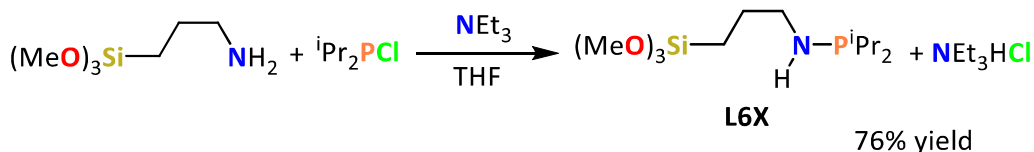


Figure 2.4. Structures of target PNP ligands with varying phosphine electronic characters.

2.2.3 Attempted synthesis of compound L6: $(^i\text{Pr}_2\text{P})_2\text{N}(\text{CH}_2)_3\text{Si}(\text{OMe})_3$ – synthesis of compound L6X: $^i\text{Pr}_2\text{PNH}(\text{CH}_2)_3\text{Si}(\text{OMe})_3$

Attempted synthesis of compound L6, $(^i\text{Pr}_2\text{P})_2\text{N}(\text{CH}_2)_3\text{Si}(\text{OMe})_3$ was performed according to the methodology described in Scheme 2.1. However, when analysed by ^1H , ^{13}C and ^{31}P NMR spectroscopies, the product was found to be the 1:1 reaction product of $^i\text{Pr}_2\text{PCl}$ and (3-aminopropyl)trimethoxysilane, **L6X**, $^i\text{Pr}_2\text{PNH}(\text{CH}_2)_3\text{Si}(\text{OMe})_3$, rather than the fully substituted target compound L6 (Scheme 2.3).



*Scheme 2.3. Synthesis of **L6X**.*

It is likely that the attempted synthesis of **L6** giving rise instead to the formation of **L6X**, is due to the steric hinderance of the ⁱPr groups disfavouring a 2:1 reaction stoichiometry. Despite this, the reaction to form **L6X** proceeded cleanly, with **L6X** being isolated in 76% yield. In order to try and favour the formation of **L6** rather than **L6X**, an alternate procedure was performed using DCM solvent rather than THF. It was rationalised that the more polar solvent may enhance the favourability of the S_N2 nucleophilic attack of the amine to the chlorophosphine, encouraging formation of the disubstituted product **L6**. Using DCM as the solvent also had literature precedent for the synthesis of sterically encumbered PNP compounds, where it was suggested that the partial solubility of NEt₃HCl in DCM may favour the desired PNP-forming reaction.¹⁶ Unfortunately, this revised method again resulted in the formation of compound **L6X**, alongside an iminobisphosphine product (Figure 2.5), confirmed by two characteristic doublets in the ³¹P NMR spectrum at -7 and -21 ppm. These iminobisphosphine compounds are commonly formed side products during the synthesis of PNP compounds, particularly when more sterically demanding substituents are applied on the phosphine and/or amine.¹⁷ Other alternative methods to achieve the synthesis of compound **L6** were considered, such as using higher reaction temperatures or stronger bases, such as LDA or ⁿBuLi, that have been widely applied in the literature for various P-N bond forming reactions.¹⁸ However, these strategies were disregarded due to the sensitive nature of the trialkoxysilane tethering functionality that cannot withstand these more forcing conditions.¹⁹

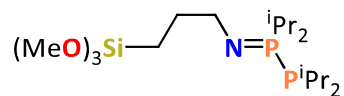


Figure 2.5. Structure of iminobisphosphine side product.

2.2.4 Attempted synthesis of aminophosphine PNP compounds **L7**:

(P(NⁱPr₂)₂)₂N(CH₂)₃Si(OMe)₃ and **L8: (P(NEt₂)₂)₂N(CH₂)₃Si(OMe)₃**

In order to synthesise compound **L7**, (P(NⁱPr₂)₂)₂N(CH₂)₃Si(OMe)₃ the required chlorophosphine reagent was first prepared according to a literature preparation (Scheme 2.4).²⁰



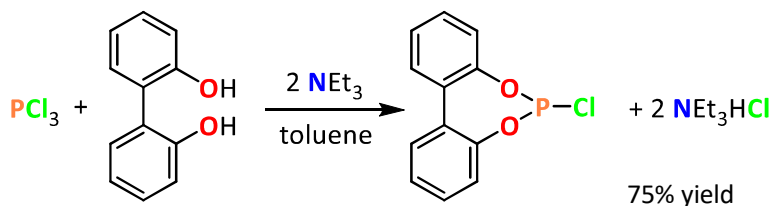
*Scheme 2.4. Synthesis of bis(diisopropylamino)chlorophosphine.*²⁰

Attempted synthesis of compound **L7** was then performed by reaction of (3-aminopropyl)trimethoxysilane with bis(diisopropylamino)chlorophosphine in toluene according to the methodology shown in Scheme 2.1. No reaction was detected by ³¹P NMR spectroscopic analysis of an aliquot of the reaction mixture despite prolonged reactions times and heating the reaction to reflux, so the reaction was abandoned. The lack of reaction is likely due to the large steric bulk of the NⁱPr₂ groups on the phosphine. However, unlike the attempted synthesis of **L6**, none of the mono reaction product was observed.

In order to reduce the steric bulk of the chlorophosphine used in the reaction, ClP(NⁱPr₂)₂ was replaced with ClP(NEt₂)₂, resulting in the design of compound **L8**, (P(NEt₂)₂)₂N(CH₂)₃Si(OMe)₃. This allowed for a reduction in phosphine sterics relative to **L7** without drastically changing the electronic character of the phosphine. ClP(NEt₂)₂ was reacted with (3-aminopropyl)trimethoxysilane in DCM according to the methodology described in Scheme 2.1. After stirring at room temperature for 18 hours no reaction was detected by ³¹P NMR spectroscopic analysis of an aliquot of the reaction mixture. The reaction mixture was subsequently brought to reflux; however, after 2 hours of heating, ³¹P NMR spectroscopic analysis showed complete decomposition of the reactant phosphine into multiple unidentified phosphine-containing species. This result shows that by reducing the steric strain around the phosphine, its reactivity was increased as desired, but this was not selective for the desired product and so the reaction was abandoned.

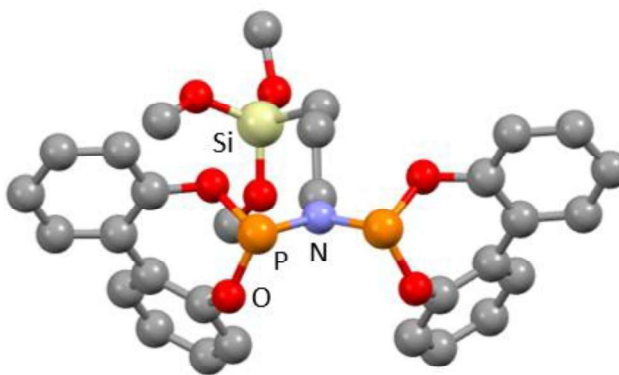
2.2.5 Synthesis of phosphoramidites PNPs L9: $(P(C_{12}H_8O_2)_2N(CH_2)_3Si(OMe)_3)$, L10: $(P(C_{12}H_8O_2)_2N(CH_2)_2(NSi(Me)_2CH_2CH(CH_3)CH_2))$, L11: $P(C_{12}H_8O_2)_2N(CH_2)_3Si(OCH_2CH_2)_3N$ and L12: $P(C_{20}H_{12}O_2)_2N(CH_2)_3Si(OCH_2CH_2)_3N$

The phosphoramidite **L9**, $(P(C_{12}H_8O_2)_2N(CH_2)_3Si(OMe)_3)$, was an important target PNP compound that could potentially act as an electron-deficient diphosphine ligand due to its electron-withdrawing biphenol groups. Comparison of the catalytic performance of **L1** and **L9** in rhodium-catalysed hydroformylation allows the effect of phosphine electronics on the process to be investigated for small bite angle ligands (see Section 5.3.1). Due to the high sensitivity of phosphites to alcohols and other nucleophiles, an aromatic, chelating, 2,2'-biphenol moiety was incorporated into the design to provide as much stability as possible. In order to synthesise **L9**, the required chlorophosphite reagent, 2,2'-biphenol phosphochloridite, was first synthesised according to an adapted literature procedure (Scheme 2.5).²¹



Scheme 2.5. Synthesis of 2,2'-biphenol phosphochloridite.²¹

Subsequently, compound **L9** was synthesised through reaction of the 2,2'-biphenol phosphochloridite with the appropriate amine according to the methodology described in Scheme 2.1. Unusually for typically oily alkoxy silane-type compounds, **L9** was successfully recrystallised from a DCM:hexane solution to give a white crystalline solid suitable for single crystal XRD analysis, which was performed in Durham by Dr A. Batsanov (Figure 2.6). The ^{31}P NMR spectrum of **L9** shows a single resonance at +152 ppm, in good agreement with similar compounds in the literature.²² The phosphorus electron character of **L9** was investigated *via* measurement of the $|^1J_{SeP}|$ coupling constant of the corresponding selenide derivative, **L9Se₂**, as will be discussed in the next Chapter (see Section 3.2). Compound **L9** is of specific interest, as phosphite/phosphoramidite ligands have yet to be employed in heterogenized hydroformylation catalysis to the best of the author's knowledge.



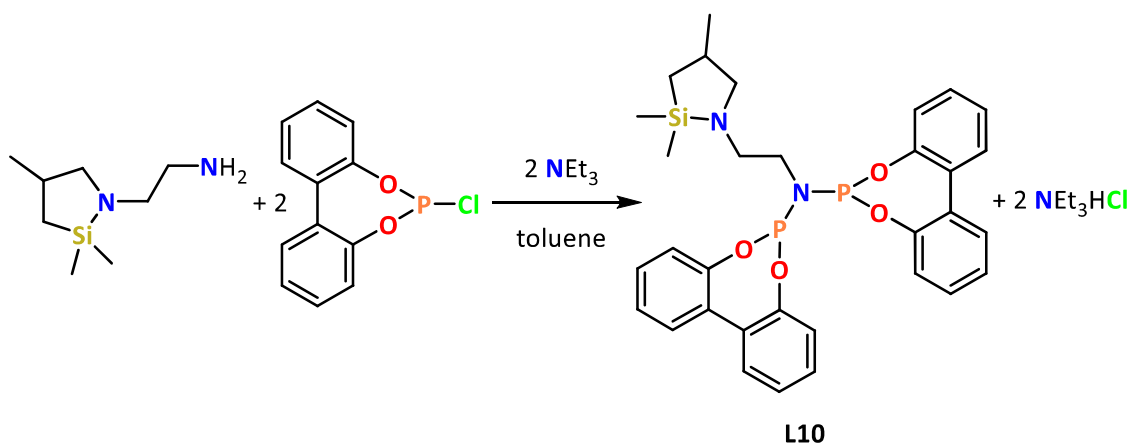
*Figure 2.6. Molecular structure of **L9**. Hydrogens and alkyl chain disorder have been omitted for clarity. Selected bond angles / °: P-N-P 110.62(6); P-N-C 124.86(8), 124.43(8). Selected bond distances / Å: P-N 1.693(1), 1.694(1); C-N 1.501(1); P-O 1.6454(9), 1.6368(9), 1.6459(9), 1.6351(9).*

The molecular structure determination of **L9** gives bond distances and angles that are comparable to those for related compounds reported previously in the literature.^{22,23} In contrast to typical examples of PNP compounds, where the phosphine lone pairs are staggered in order to reduce electron–electron repulsion, the phosphorus lone pairs in **L9** are parallel to each other, with the phosphite moieties bent backwards.²³ This conformation suggests that **L9** should readily coordinate to metal fragments, as the phosphorus lone pairs are already in the necessary conformation. It is therefore of interest whether this has any effect on the coordination chemistry of **L9**, which can be assessed by producing rhodium and cobalt complexes of the ligand and also performing hydroformylation testing on **L9**-containing complexes and comparing the results to the other PNP compounds produced.

Unfortunately, the repeated synthesis of compound **L9** proved to be unreliable, resulting in a mixture of products that could not be separated, including the mono-phosphoramidite-containing product. Due to the highly air sensitive nature of both the phosphorus-containing moiety and the trialkoxysilane group, purification of these compounds is very challenging. Additionally, the reactivity of the alkoxy silane functionality with silica means that standard silica-column chromatography purification techniques are also not possible. It was initially hypothesised that the reason for lower selectivity of the reaction when repeated maybe due to the poor long-term stability of

the chlorophosphite starting material, despite it being stored in a glovebox. However, re-purification of the compound before use did not significantly improve selectivity to the desired compound **L9**, which may be very sensitive to the exact reaction conditions employed that are not possible to fully replicate between syntheses.

Due to the difficulties encountered in developing a reliable synthesis for **L9**, attention turned to the development of a new phosphoramidite PNP compound featuring an azasilane tethering group rather than the alkoxy silane previously investigated. By incorporating a different tethering group into the design, it would be possible to determine whether the tethering functionality was impacting the effectiveness of the attempted synthesis of these types of compound.



*Scheme 2.6. Synthesis of **L10**.*

Attempted synthesis of **L10**, $((C_{12}H_8O_2)P)_2N(CH_2)_2(NSi(Me)_2CH_2CH(CH_3)CH_2)$ was performed according to the methodology described in Scheme 2.6. The formation of **L10** proceeds cleanly in toluene, as evidenced by the singlet at +150 ppm in the $^{31}P\{^1H\}$ NMR spectrum of an aliquot of crude reaction mixture (Figure 2.7), in good agreement with the +152 ppm ^{31}P NMR shift of **L9**. Indeed, integration of the signals show 96% conversion to **L10** after 12 hours, with 4% 2,2'-biphenol phosphochloridite starting material remaining ($^{31}P\{^1H\}$ NMR = +179 ppm), which did not change after a further 12 hours. However, during removal of NEt_3HCl by filtration and concentration of **L10** by removal of all volatile components from the reaction mixture *in vacuo*, decomposition of **L10** readily begins to occur. The green spectra in Figure 2.7 corresponds to partial decomposition of **L10** after these simple work up procedures were performed. It is not

clear why **L10** is unstable when concentrated, but this suggests that it is some form of intermolecular self-reaction that only occurs at high local concentrations. Despite this, **L10** was found to be stable in the crude reaction mixture for several days. Since the phosphoramidite containing compound **L9** and azasilane PNP compound **L4** were both found to be stable as neat oils, this suggests that some form of interaction between the azasilane and phosphoramidite functionalities may be the origin of the observed instability. The two largest peaks in the resulting ^{31}P NMR spectrum reside at +150 and +148 ppm, respectively, and occur in equal intensities. No coupling is observed between these peaks and hence one possible explanation of this NMR data is P-N bond cleavage to give two phosphorus-containing compounds. Additionally, there are multiple other smaller resonances corresponding to other unidentified degradation products at +136, +138, +144, +146, +148, +149 and +150 ppm. **L10** was also shown to be highly sensitive to halogenated compounds such as DCM and CDCl_3 resulting in complete decomposition of **L10** in the time taken to perform an ^{31}P NMR experiment. Due to multiple overlapping signals in the resulting ^{31}P NMR spectra (Figure 2.7, red) it was not possible to attribute these to any specific degradation pathways however many of the signals appear to be the same as observed after degradation of neat **L10**. Since isolation of **L10** was not possible, further investigation into this compound was abandoned.

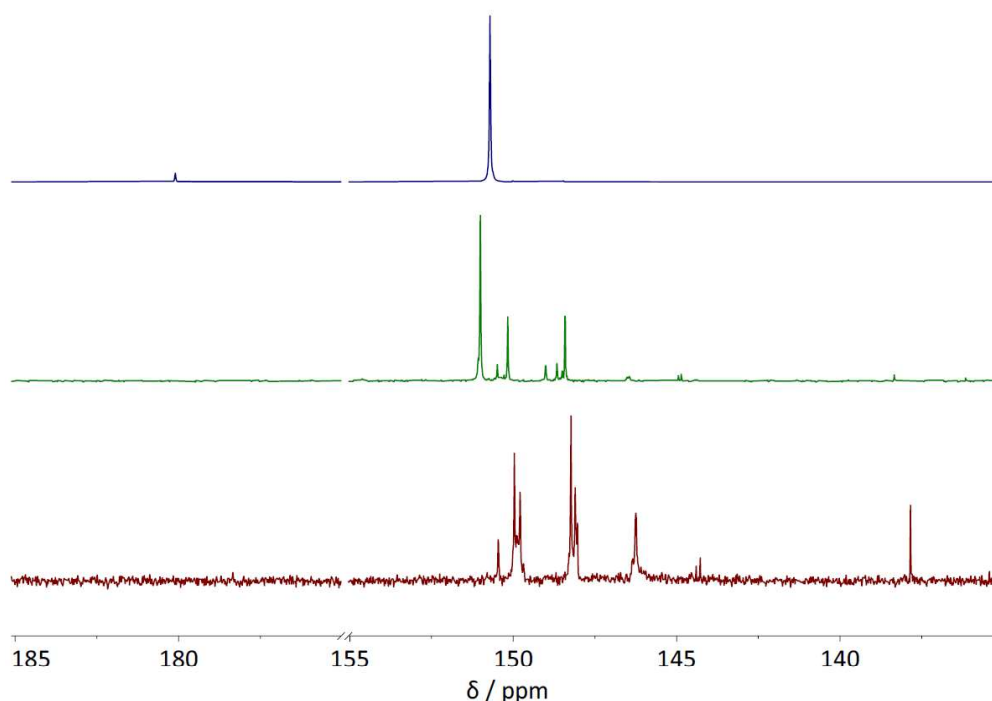
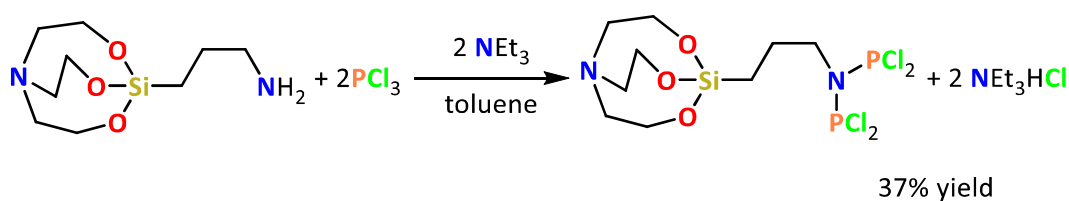


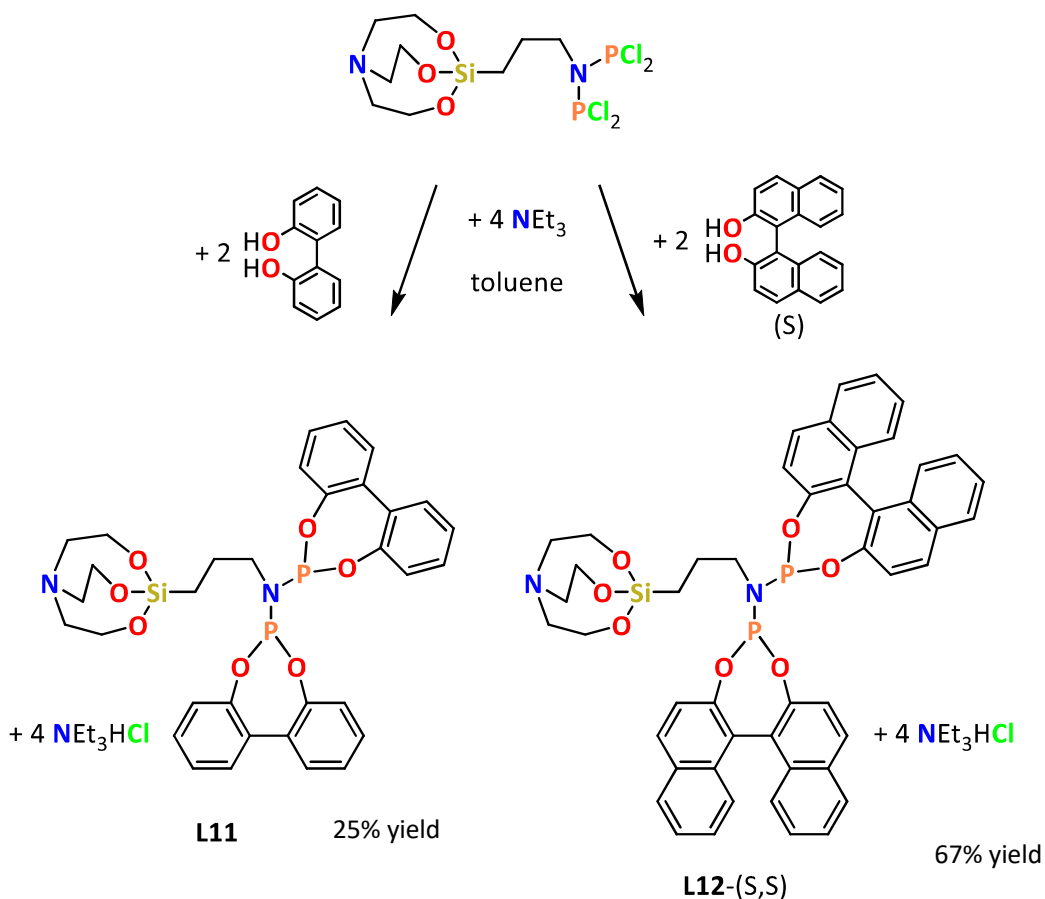
Figure 2.7. $^{31}\text{P}\{^1\text{H}\}$ NMR spectroscopic analysis (162 MHz, 295 K) of **L10**: *blue*; crude reaction mixture in toluene ($^{31}\text{P}\{^1\text{H}\}$ unlocked experiment), *green*; in C_6D_6 after filtration and removal of all volatile components in vacuo, *red*; in CDCl_3 .

In order to develop a phosphoramidite PNP compound that could be reliably accessed, a different synthesis strategy was employed. This required incorporation of a silatrane tethering functionality due to its enhanced stability to air and moisture. A two-step procedure was then performed whereby (3-aminopropyl)silatrane was initially reacted with two equivalents of PCl_3 to produce a PNP compound with 4 P-Cl bonds (Scheme 2.7). This compound was then reacted with two equivalents of the desired biphenol to produce the target compound **L11**, $((\text{C}_{12}\text{H}_8\text{O}_2)\text{P})_2\text{N}(\text{CH}_2)_3\text{Si}(\text{OCH}_2\text{CH}_2)_3\text{N}$ (Scheme 2.8). This two-step procedure has been successfully employed for similar compounds in the literature and boasted several benefits over the previous synthesis of **L9**, including facile repeatable synthesis of the target compound.²⁴ Additionally, the unstable and challenging to make phosphochloridite intermediates employed in the synthesis of **L9** could be avoided, providing an overall more facile synthesis route. As well as this, isolation of the bis(dichlorophosphino)amine intermediate facilitates access to a variety of phosphoramidites ligand targets by reaction of the bis(dichlorophosphino)amine intermediate with different alcohols. In this fashion, alongside the compound **L11**,

analogous to the previously synthesised **L9**, another potential ligand, **L12**, $((\text{C}_{12}\text{H}_8\text{O}_2)\text{P})_2\text{N}(\text{CH}_2)_3\text{Si}(\text{OCH}_2\text{CH}_2)_3\text{N}$ was produced by using (s)-BINOL as the alcohol (Scheme 2.8). Incorporation of a chiral alcohol into compound design results in an overall chiral potential-ligand. This enables the possibility of investigating **L12** in enantioselective hydroformylation catalysis, which is a topic of considerable interest.²⁵ However, analysis of the steric properties of **L12**, using the SambVca 2.1 web tool to calculate a “Percent Buried Volume” and steric map, suggested this chirality is too far removed from a metal centre upon coordination of **L12** to impart any chiral selectivity in reactions at a metal centre (see Section 3.2.2).



Scheme 2.7. Synthesis of bis(dichlorophosphino)amine intermediate.



Scheme 2.8. Synthesis of compounds **L11** and **L12**.

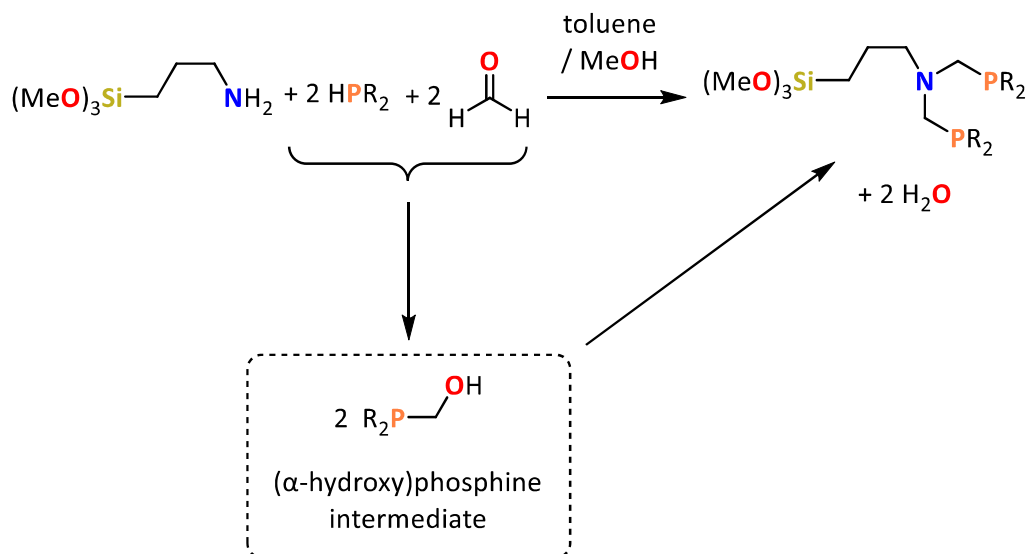
2.3 PCNCP ligand design

To complement the small bite angle PNP compounds produced, potential ligands with a wider bite angle were desired to allow a comparison of bite angle effects on heterogeneous hydroformylation catalysis. To accomplish this, a simple change in design to the PNP compounds was devised by “inserting” CH_2 spacers between the P and N atoms. This would have the effect of increasing the bite angle from $\sim 70^\circ$ to $\sim 90^\circ$ upon coordination to a metal, producing a so-called medium-sized bite angle ligand scaffold.²⁶ By employing only a small change in ligand design, changes to the phosphine electronics and sterics between the PNP and PCNCP compounds could be minimised to focus on bite angle effects during catalyst testing.



2.4 PCNCP ligand synthesis strategy

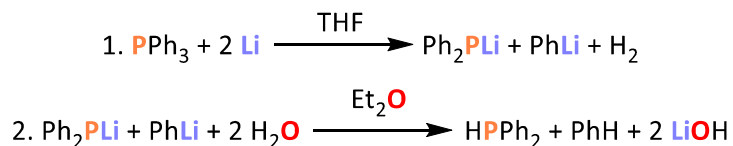
71



Scheme 2.9. General synthesis strategy for preparation of PCNCP compounds.²⁶

2.4.1 Synthesis of compound **L13**: $(\text{Ph}_2\text{PCH}_2)_2\text{N}(\text{CH}_2)_3\text{Si}(\text{OMe})_3$

In order to synthesise compound **L13**, $(\text{Ph}_2\text{PCH}_2)_2\text{N}(\text{CH}_2)_3\text{Si}(\text{OMe})_3$, it was first necessary to prepare the required diphenylphosphine precursor. This was achieved following a literature procedure involving the lithiation of triphenylphosphine with elemental lithium in THF at 0 °C (Scheme 2.10).²⁷



Scheme 2.10. Synthesis of Ph_2PH .²⁷

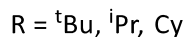
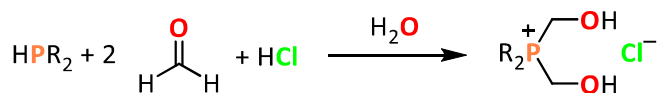
The synthesis of **L13** was then performed according to the methodology described in Scheme 2.9 by reaction of (3-aminopropyl)trimethoxysilane with diphenylphosphine and paraformaldehyde in toluene/methanol, affording the target compound in 64% yield as a yellow viscous oil upon workup. ^{31}P NMR spectroscopic analysis of the compound showed a lone resonance singlet at -29 ppm, in good agreement with related literature compounds.²⁶

2.4.2 Attempted synthesis of compound **L14**: (^tBu₂PCH₂)₂N(CH₂)₃Si(OMe)₃

Attempted synthesis of compound **L14**, (^tBu₂PCH₂)₂N(CH₂)₃Si(OMe)₃, was performed according to the methodology described in Scheme 2.9 by reaction of (3-aminopropyl)trimethoxysilane with di-*tert*-butylphosphine and paraformaldehyde in toluene/methanol. The product was isolated in low yield (10%) and ¹H and ³¹P NMR spectroscopic analyses showed the sample to contain several impurities. One possible explanation for this is that the water produced as a by-product during the reaction could react with the trimethoxysilane group to form silanols. This could result in oligomerisation of the silane moiety, which would cause the reaction to fail. It is known that water/methanol mixtures exacerbate this effect of alkoxysilane hydrolysis.²⁸ When this synthesis of **L13** was repeated, similar impurities were also observed, suggesting this synthesis strategy is not very reliable when alkoxysilane functionalities are present.

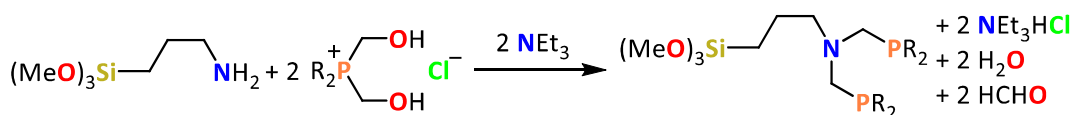
2.4.3 Attempted synthesis of PCNCP compounds *via* dialkylbis(hydroxymethyl)phosphonium chloride salts

In order to gain better control and understanding of the chemistry occurring during the attempted synthesis of compound **L14**, a two-step synthesis was performed, whereby the methylhydroxyphosphine intermediate (R₂PCH₂OH), shown in Scheme 2.9, is first isolated as a phosphonium salt by reaction with HCl (Scheme 2.11).²⁹ Following this, in a second reaction the phosphonium salt is combined with NEt₃ and (3-aminopropyl)trimethoxysilane to afford the target PCNCP compound (Scheme 2.12), as has been performed for similar compounds in the literature.²⁹ This alternative reaction pathway had two proposed benefits. Firstly, by isolating and purifying the crystalline salt intermediate, any impurities produced during the formation of the intermediate could be removed, with the aim of simplifying the system before the water-sensitive alkoxysilane-functionalised amine is added. Secondly, as the phosphonium salts produced are readily soluble in MeOH, unlike paraformaldehyde, which is very slow to dissolve, only a short one-hour reaction time is required. This shorter reaction time may minimise trimethoxysilane oligomerisation due to the presence of water.



Scheme 2.11. Synthesis of dialkylbis(hydroxymethyl)phosphonium chloride salts.²⁹

Synthesis of dialkylbis(hydroxymethyl)phosphonium chloride salts featuring different alkyl phosphine functionalities was performed according to the methodology described in Scheme 2.11, with the products isolated as white solids in good yields (63 – 80%).



Scheme 2.12. Attempted synthesis of PCNCP compounds from dialkylbis(hydroxymethyl)phosphonium chloride salts.²⁹

The attempted synthesis of compound **L14** was then repeated following the methodology described in Scheme 2.12, where $\text{R} = \text{}^t\text{Bu}$. After heating at reflux in methanol for 1 hour, ^{31}P NMR spectroscopic analysis of an aliquot of the reaction mixture showed the primary product to be **L14** ($\delta^{31}\text{P} = +13$ ppm) alongside an unknown impurity ($\delta^{31}\text{P} = +41$ ppm, singlet) in a ratio of 1:0.6 by integration of the ^1H -coupled ^{31}P NMR spectrum. Consequently, the reaction was again heated at reflux for another hour. However, a second ^{31}P NMR spectrum of an aliquot of the reaction mixture showed the concentration of the impurity had not changed significantly relative to the target product. To try and identify the reason for by-product formation (and to identify this impurity), the reaction was repeated in stages. Initially di-*iso*-propylbis(hydroxymethyl)phosphonium chloride was reacted with two equivalents of NEt_3 without (3-aminopropyl)trimethoxysilane present. ^{31}P NMR spectroscopic analysis of an aliquot of the reaction mixture showed formation of the $\text{R}_2\text{PCH}_2\text{OH}$ intermediate ($\delta^{31}\text{P} = +20$ ppm) along with the unknown impurity ($\delta^{31}\text{P} = +41$ ppm, singlet) in similar ratios to those observed between the impurity and product in the previous reaction.

Due to the water-sensitive and difficult to purify nature of the alkoxy silane group present the reaction was abandoned and a different synthesis strategy considered.

2.4.4 Synthesis of PCNCP compounds L17: $(\text{Ph}_2\text{PCH}_2)_2\text{N}(\text{CH}_2)_3\text{Si}(\text{OCH}_2\text{CH}_2)_3\text{N}$, L18: $(^t\text{Bu}_2\text{PCH}_2)_2\text{N}(\text{CH}_2)_3\text{Si}(\text{OCH}_2\text{CH}_2)_3\text{N}$ and L19: $(\text{Cy}_2\text{PCH}_2)_2\text{N}(\text{CH}_2)_3\text{Si}(\text{OCH}_2\text{CH}_2)_3\text{N}$

In order to avoid the issues caused by the combined presence of water and alkoxy silanes in the attempted synthesis of silica-tetherable PCNCP compounds, ligand designs incorporating silatrane tethering groups were devised (Figure 2.9).

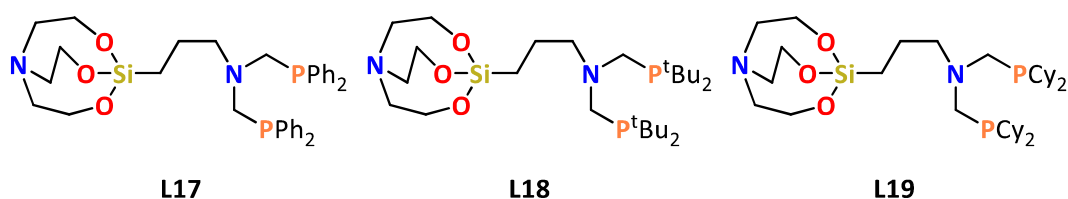
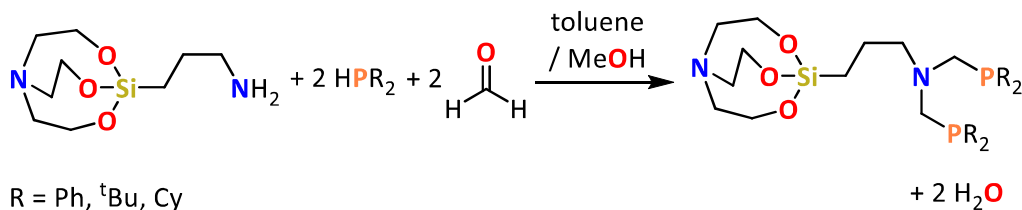


Figure 2.9. Structure of silatrane functionalised PCNCP compounds.

The synthesis of silatrane-functionalised PCNCP compounds, **L17** – **L19**, were performed according to the methodology described in Scheme 2.13. ^{31}P NMR spectroscopic analysis of aliquots of each crude reaction mixture showed that much smaller quantities ($\sim 10\%$) of the same phosphorus-containing impurities were produced relative to when synthesis of their alkoxy silane analogues were attempted ($\sim 40\%$). Additionally, due to the increased stability of the silatrane-functionalised compounds, **L17** – **L19**, and their superior physical properties relative to alkoxy silane analogues, they could be effectively purified by recrystallisation, allowing clean isolation of the compounds as white solids in moderate yields (52–66%).



Scheme 2.13. Synthesis of silatrane-functionalised PCNCP compounds.

Single crystals of **L17** suitable for XRD analysis, which was performed in Durham by Dr T. Blundell, were obtained from a solution of DCM/hexane (Figure 2.10). The unit cell of

the crystal was large, containing 8 molecules of **L17**, resulting in long refinement cycle times and therefore the resulting data was not refined to a publishable quality (although this would be possible with enough computation time). Despite this, the current data is good enough to show clear connectivity of the compound and calculate angles and distances albeit with a higher than usual associated error. The structure shows that the two phosphine fragments sit in a staggered conformation with their lone pairs pointing in opposite directions. Additionally, the central nitrogen is shown to be in a distorted tetrahedral geometry with approximate 109.5° bond angles, as is commonly expected for tertiary amines. This is in contrast to the planar nitrogen geometry observed in PNP compounds due to P-N multiple bond character, which is obviously removed when a CH_2 spacer separates the phosphorus and nitrogen atoms.

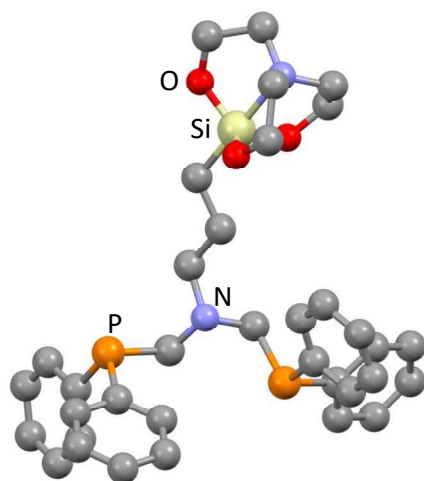


Figure 2.10. Molecular structure of **L17**.

Hydrogens have been omitted for clarity. Selected bond angles / $^\circ$: N-C 110.9(3), P-N-C 109.6(3), 110.2(3). Selected bond distances / \AA : P- CH_2 1.861(4), 1.859(5); Si-N 2.170(4).

2.5 PCCNCCP ligand design and synthesis

To further increase the chelation bite angle, while maintaining several other structural features present in the PNP and PCNCP compounds previously detailed in this chapter, a PCCNCCP backbone ligand target was devised (Figure 2.11). The design maintains the silica-tethering group and three-carbon alkyl spacer between the chelate ring and tethering group incorporated into the PNP and PCNCP compounds prepared.

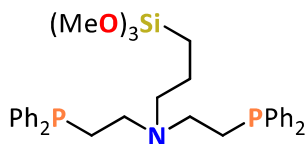
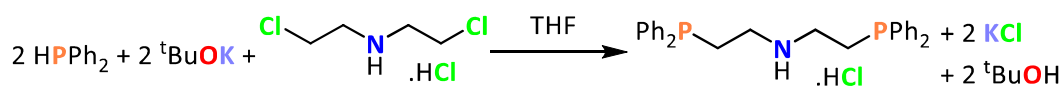


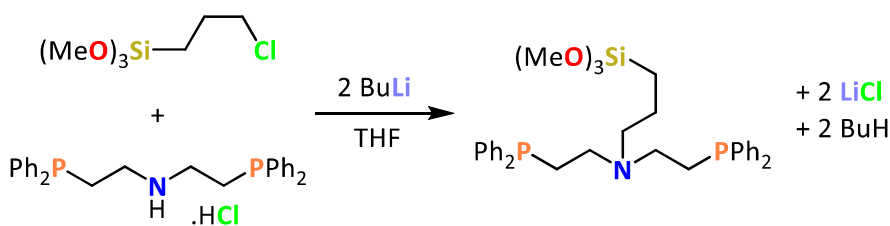
Figure 2.11. Structure of PCCNCCP compound **L20**.

The synthesis of target compound **L20**, $(\text{Ph}_2\text{PCH}_2\text{CH}_2)_2\text{N}(\text{CH}_2)_3\text{Si}(\text{OMe})_3$ (Figure 2.11) was attempted using a two-step method. In the first step bis(2-chloroethyl)amine hydrochloride was reacted with two equivalents of diphenylphosphine in the presence of two equivalents of potassium *tert*-butoxide, to form bis(2-(diphenylphosphino)ethyl)amine hydrochloride according to a literature procedure (Scheme 2.14).³⁰ After an acid workup the product was isolated as a crystalline white solid (35% yield).



Scheme 2.14. Synthesis of bis(2-(diphenylphosphino)ethyl)amine hydrochloride.³⁰

Subsequently, bis(2-(diphenylphosphino)ethyl)amine hydrochloride was reacted with a stoichiometric quantity of the commercially available (3-chloropropyl)trimethoxysilane. A base is required to form the amine from the amine salt, which can then react in an $\text{S}_{\text{N}}2$ reaction with the alkyl halide. In this particular system, competing reactions may be expected, as the phosphine groups present can be quaternised by reaction with alkyl halides.³¹ In order to negate this issue, the use of two equivalents of the strong base $^n\text{BuLi}$ was used to generate the amide anion (Scheme 2.15). It was envisioned that reaction of this highly reactive amide would out compete reaction of the phosphines present.

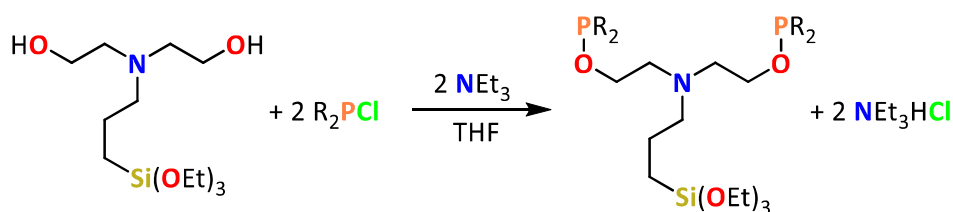


Scheme 2.15. Synthesis of **L20**.

On a small scale (100 mg) test reaction, a solution of bis(2-(diphenylphosphino)ethyl)amine hydrochloride in THF was treated with 2 equivalents of $n\text{BuLi}$. After stirring for 30 minutes at room temperature the resulting yellow solution was treated with (3-chloropropyl)trimethoxysilane. After 6 hours, ^{31}P NMR spectroscopy of an aliquot of the reaction mixture showed no visible change from the bis(2-(diphenylphosphino)ethyl)amine hydrochloride starting material. This was to be expected as the desired reaction takes place several atoms away from the phosphorus nuclei. However, this did confirm that no phosphonium salt impurities were being formed during the reaction. ^1H NMR spectroscopy showed complete consumption of the starting materials and formation of the product along with an unknown impurity. Due to the difficulty purifying the air-sensitive viscous oil produced and concerns over the strong base employed in the reaction being unsuitable for use in the presence of alkoxy silanes, the reaction was abandoned. One potential method to enable the synthesis of silica-tetherable PCCNCCP compounds could be to incorporate a silatrane tethering functionality into the ligand design rather than an alkoxy silane (see Chapter 5 Future work).

2.6 POCCNCCOP ligand design

A method devised for the synthesis of wide bite angle, tetherable phosphites and phosphinites that has been investigated, is the reaction of commercially available bis(2-hydroxyethyl)-3-aminopropyltriethoxysilane with two equivalents of a chloro-phosphine/phosphite in the presence of a base (Scheme 2.16).



Scheme 2.16. General synthesis of POCCNCCOP compounds.

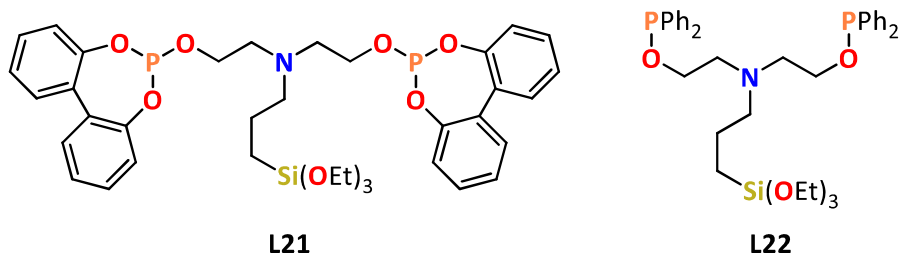


Figure 2.12. Structure of POCCNCCOP target compounds **L20** and **L21**.

Compound **L21**, $((C_{12}H_8O_2)PCH_2CH_2)_2N(CH_2)_3Si(OMe)_3$, (Figure 2.12) was designed as a tetherable phosphite ligand, to enable investigations into the effect of wide bite angle ligands with electron-poor donor atoms on rhodium-catalysed heterogenised hydroformylation. In comparison, compound **L22**, $(Ph_2PCH_2CH_2)_2N(CH_2)_3Si(OMe)_3$ will likely share a similar bite angle, to **L22** while featuring more electron-rich phosphine fragments.

2.6.1 Synthesis of **L21**: $((C_{12}H_8O_2)POCH_2CH_2)_2N(CH_2)_3Si(OMe)_3$

Synthesis of compound **L21**, $((C_{12}H_8O_2)POCH_2CH_2)_2N(CH_2)_3Si(OMe)_3$, was performed according to the methodology described in Scheme 2.16 by reaction of bis(2-hydroxyethyl)-3-aminopropyltriethoxysilane with 2,2'-biphenol phosphochloridite and triethylamine in acetonitrile solution. After stirring the mixture overnight, the product was isolated as a pale-yellow viscous oil (28% yield) upon workup and characterised by 1H , ^{13}C and ^{31}P NMR spectroscopies. Unfortunately, **L21** was found to slowly degrade over the course of weeks when stored under inert conditions in the glovebox due to oligomerisation of the compound's alkoxy silane moieties.

For **L21**, protection of the alkoxy silane moiety as a silatrane to increase the long-term stability of the compound would not be possible. This is because neither the bis(2-hydroxyethyl)-3-aminopropyltriethoxysilane nor **L21** are likely to be stable to the basic conditions required for reaction between alkoxy silanes and triethanolamine.

2.6.2 Attempted synthesis of **L22**: $(\text{Ph}_2\text{POCH}_2\text{CH}_2)_2\text{N}(\text{CH}_2)_3\text{Si}(\text{OMe})_3$

Synthesis of compound **L22**, $(\text{Ph}_2\text{POCH}_2\text{CH}_2)_2\text{N}(\text{CH}_2)_3\text{Si}(\text{OMe})_3$, was attempted according to the methodology described in Scheme 2.16 by reaction of bis(2-hydroxyethyl)-3-aminopropyltriethoxysilane with chlorodiphenylphosphine and triethylamine in acetonitrile. After stirring the mixture overnight at RT, ^{31}P NMR spectroscopic analysis of an aliquot of the reaction mixture showed that no reaction had occurred. Subsequently, the reaction was brought to reflux for one hour. However, this resulted in decomposition of the PPh_2Cl starting material according to ^{31}P NMR spectroscopic analysis of an aliquot of the reaction mixture. The difference in reactivity observed between the attempted synthesis of **L22** and **L21** can be explained by the difference in electrophilicities between the chlorodiphenylphosphine and 2,2'-biphenol phosphochloridite start materials. Chlorodiphenylphosphine is much less electrophilic than 2,2'-biphenol phosphochloridite, which disfavours the reaction with nucleophilic alcohol groups of bis(2-hydroxyethyl)-3-aminopropyltriethoxysilane. To try and compensate for this difference in reactivity, the reaction was repeated using LDA as a stronger base, instead of triethylamine. ^{31}P NMR spectroscopic analysis of the crude reaction mixture again showed decomposition of the starting materials and so the reaction was abandoned.

2.7 Synthesis of **L5S₂**: $(\text{P}(\text{S})\text{Ph}_2)_2\text{N}(\text{CH}_2)_3\text{Si}(\text{OCH}_2\text{CH}_2)_3\text{N}$

Phosphine ligands are by far the most investigated and commercialised ligands in hydroformylation, but ligands featuring different donor atoms have also been investigated.³² One example of this are sulfur ligands. As discussed in Section 1.7, monodentate sulfur ligands have been shown offer greater resistance to rhodium leaching in immobilised hydroformylation relative to analogous phosphine ligands, albeit at the expense of poorer activity and selectivity.³³ Few examples of bidentate sulfur ligands, especially with neutral sulfur donors, have been explored in hydroformylation. One such example is the chiral sulfur containing BINOL derivative Me_2BINAS (Figure 2.13), which has been shown to provide good activity in the hydroformylation of styrene.³⁴

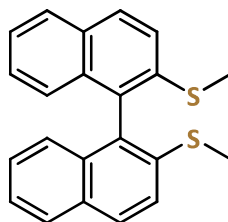
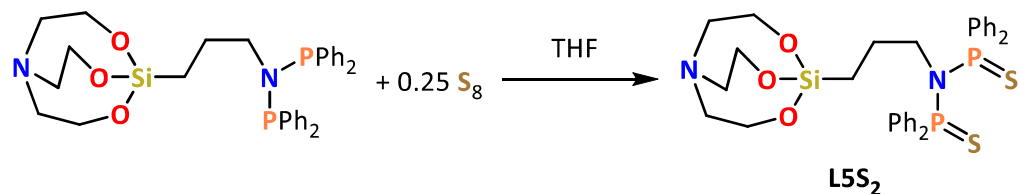


Figure 2.13. Structure of Me_2BiNAS .

As minimising the catalyst leaching of immobilised hydroformylation processes is one of the key targets of this project, the synthesis of a novel bidentate sulfur ligand capable of silica immobilisation was desired. It was envisioned that by employing a bidentate ligand compared to the immobilised monodentate sulfur ligand investigated in the literature, the resistance to rhodium leaching of the system could be improved further. To this end, a bidentate sulfur ligand was readily produced by the reaction of **L5** with elemental sulfur to give the compound **L5S₂** (scheme 2.17), following an adapted literature procedure.³⁵ Modification of the PNP ligand in this way changes the potential ligand chelate ring size from 4 atoms for PNP-metal coordination to 6 atoms for SPNPS-metal coordination, increasing the predicted S[^]S bite angle to be comparable to that of the PCNCP compounds detailed in Section 2.4. **L5S₂** was isolated as an air-stable white solid (79% yield) allowing for easier handling than the air-sensitive phosphine compounds that comprise the rest of this chapter.



Scheme 2.17. Synthesis of **L5S₂**.

2.8 Chapter 2 summary

In this chapter a variety of compounds that have been designed and synthesised for application as ligands in immobilised hydroformylation catalysis were discussed. Of great importance are several fundamental design criteria that were identified and incorporated into each ligand design. Firstly, each compound was required to be a diphosphine/diphosphorus sulfide capable of coordinating rhodium(I) in a bidentate

fashion. In order to undertake a thorough investigation into the effect of the linker ligand employed in ligand immobilised hydroformylation, systematic tuning of several parameters, such as phosphine steric and electronic character, P[^]P bite angle and tethering group identity was performed. A focus on small bite angle hydroformylation ligand design was utilised due to the lack of literature exploration in this area combined with easier access to target compounds through simple synthetic transformations.

Small bite angle PNP compounds **L1-5** were produced with different tethering groups to explore the effect of different silica-immobilisation modes on immobilised hydroformylation catalysis. **L1-3** contain different commonly employed alkoxysilane linkers, while **L4** contains a strained azasilane tethering group and **L5** contains a more chemically robust silatrane functionality for silica immobilisation.

Alongside this, the development of PNP compounds with different phosphine electronic characteristics was explored. The attempted synthesis of the more electron-rich alkyl phosphine target **L6** resulted instead in the mono-substituted derivative **L6X**. Meanwhile, the synthesis of the aminophosphines **L7** and **L8** was not possible due to phosphine decomposition during the reaction. The electron-deficient phosphoramidite **L9** was synthesised to allow comparison to the more electron-rich derivative **L1**. The phosphoramidite PNP with an alternative azasilane tethering functionality, **L10**, could not be isolated due to instability with respect to itself when concentrated to a neat oil. Due to the unreliable synthesis of **L9** and **L10**, an alternate method for accessing PNP phosphoramidites was employed, leading to the synthesis of **L11**, alongside chiral derivative **L12**. These compounds both featured the air-stable silatrane tethering functionality that proved to be an important factor in accessing several of our target ligand structures once it was identified as a suitable silica-tethering functionality for phosphine compounds part-way through much of the attempted synthesis in this chapter.

In order to produce potential ligands with larger bite angles than the PNP compounds produced, PCNCP targets were explored. The reliability of the synthesis of the alkoxysilane functionalised PCNCP, such as **L13**, was again improved by moving to a silatrane functionalised system, giving rise to compounds **L17**, **L18** and **L19**. The design of these three compounds will allow the effect of phosphine sterics on immobilised

hydroformylation catalysis to be probed when moving from Ph-, ^tBu- and Cy-functionalised phosphine compounds.

A PCCNCCP scaffold was also targeted resulting in the design of compound **L20**. However this compound could not be purified, and its attempted synthesis was abandoned. In order to further increase the potential ligand bite angle relative to PCCNCCPs a POCCNCCOP scaffold was devised that resulted in the design of compounds **L21** and **L22**. The commercially available bis(2-hydroxyethyl)-3-aminopropyltriethoxysilane was found to react with the electrophilic 2,2'-biphenol phosphochloridite to produce compound **L21**, however was not nucleophilic enough to react with PPh₂Cl during the attempted synthesis of **L22**. Unfortunately, **L21** was found to be unstable with respect to self-condensation of its alkoxysilane functionality over several months despite being stored under inert conditions in a glovebox.

Finally, compound **L5** was reacted with two equivalents of elemental sulfur to produce the compound **L5S₂** to act as a potential bidentate sulfur donor ligand. This will allow comparison in performance between phosphine and sulfur donor ligands in immobilised hydroformylation catalysis, especially in regard to catalyst leaching.

2.9 Chapter 2 references

1. F. Frank, D. Selent and A. Börner, *Chem. Rev.*, 2012, **112**, 5675–5732, DOI: 10.1021/cr3001803.
2. P. W. N. M. van Leeuwen and C. Claver, *Rhodium Catalysed Hydroformylation*, Kluwer Academic Publishers, Dordrecht, 2000.
3. A. J. Sandee, J. N. H. Reek, P. C. J. Kamer and P. W. N. M. van Leeuwen, *J. Am. Chem. Soc.*, 2001, **123**, 8468–8476, DOI: 10.1021/ja010150p.
4. E. Piras, B. Powietzka, F. Wurst, D. Neumann-Walter, H. Grützmacher, T. Otto, T. Zevaco and O. Walter, *Catal. Lett.*, 2013, **143**, 673–680, DOI: 10.1007/s10562-013-1010-x.
5. S. A. Wander, A. Miedaner, B. C. Noll, R. M. Barkley, and D. L. DuBois, *Organometallics*, 1996, **15**, 3360–3373, DOI: 10.1021/om960072s.

6. C. Merckle, S. Haubrich and J. Blümel, *J. Organomet. Chem.*, 2001, **627**, 44–54, DOI: 10.1016/S0022-328X(01)00696-9.
7. L. Tensi, A. V. Yakimov, C. Trotta, C. Domestici, J. De Jesus Silva, S. R. Docherty, C. Zuccaccia, C. Copéret and Alceo Macchioni, *Inorg. Chem.*, 2022, **61**, 10575–10586, DOI: 10.1021/acs.inorgchem.2c01640.
8. P. Braunstein, H. Kormann, W. Meyer-Zaika, R. Pugin and G. Schmid, *Chem. Eur. J.*, 2000, **6**, 4637–4646, DOI: 10.1002/1521-3765(20001215)6:24<4637::AID-CHEM4637>3.0.CO;2-A.
9. (a) J. K. Puri, R. Singha and V. K. Chahala, *Chem. Soc. Rev.*, 2011, **40**, 1791–1840, DOI: 10.1039/B925899J. (b) V. K. Pestunovich and M. G. Voronkov, in *The Chemistry of Organic Silicon Compounds*, eds. Z. Rappoport and Y. Apeloig, Wiley, Chichester, UK, 1998, vol. 3, pp. 1447–1537.
10. (a) T. Lee, L. Chau, and C. Huang, *Langmuir*, 2020, **36**, 5935–5943, DOI: 10.1021/acs.langmuir.0c00745. (b) C. Huang and Y. Zheng, *Langmuir*, 2019, **35**, 1662–1671, DOI: 10.1021/acs.langmuir.8b01981. (c) C. Geibel, J. Theiner, M. Wolter, M. Kramer, W. Lindner and M. Lämmerhofer, *J. Chromatogr. A*, 2021, **1653**, 462418, DOI: 10.1016/j.chroma.2021.462418.
11. (a) G. Singh, Sushma, Priyank, Suman, Diksha, J. D. Kaur, A. Saini, A. Devi and P. Satija, *Inorganica Chim. Acta*, 2021, **525**, 120465, DOI: 10.1016/j.ica.2021.120465. (b) K. Szpakolski, K. Latham, C. Rix, R. A. Rani and K. Kalantar-Zadeh, *Polyhedron*, 2013, **52**, 719–732, DOI: 10.1016/j.poly.2012.07.078.
12. C. Fliedel, A. Ghisolfi, and P. Braunstein, *Chem. Rev.*, 2016, **116**, 9237–9304, DOI: 10.1021/acs.chemrev.6b00153.
13. M. S. Gordon, M. T. Carroll and J. H. Jensen, *Organometallics*, 1991, **10**, 2657–2660, DOI: 10.1021/om00054a028.
14. R. D. Harcourt, *J. Phys. Chem. A*, 1999, **103**, 4293–4297, DOI: 10.1021/jp9900988.
15. S. Fang, J. Tan, J. Pan, H. Zhang, Y. Chen, X. Ren and T. Wang, *Angew. Chem.*, 2021, **60**, 14921–14930, 10.1002/anie.202102352.
16. M. C. Maumela, K. Blann, H. de Bod, J. T. Dixon, W. F. Gabrielli, and D. B. G. Williams, *Synthesis*, 2007, **24**, 3863–3867, DOI: 10.1055/s-2007-990868.
17. Z. Fei, R. Scopelliti and P. J. Dyson, *Dalton Trans.*, 2003, 2772–2779, DOI: 10.1039/B303645F.

18. (a) K. Blann, A. Bollmann, G. M. Brown, John T. Dixon, M. R. J. Elsegood, C. R. Raw, M. B. Smith, K. Tenza, J. A. Willemse and P. Zweni, *Dalton Trans.*, 2021, **50**, 4345–4354, DOI: 10.1039/D1DT00287B. (b) C. E. Anderson, A. S. Batsanov, P. W. Dyer, J. Fawcett and J. A. K. Howard, *Dalton Trans.*, 2006, 5362–5378, DOI: 10.1039/B611652C. (c) L. Baiget, A. S. Batsanov, P. W. Dyer, M. A. Fox, M. J. Hanton, J. A. K. Howard, P. K. Lane and S. A. Solomon, *Dalton Trans.*, 2008, 1043–1054, DOI: 10.1039/B715736C.
19. D. Derouet, S. Forgeard and J. Brosse, *Macromol. Chem. Phys.*, 1999, **200**, 10–24, DOI: 10.1002/(SICI)1521-3935(19990101)200:1<10::AID-MACP10>3.0.CO;2-V.
20. R. B. King and N. D. Sadanani, *Synth. React. Org. Met.-Org. Chem.*, 1985, **15**, 149–153, DOI: 10.1080/00945718508059375.
21. J. Li, M. Lutz, A. L. Spek, G. P. M. van Klink, G. van Koten, R. J. M. K. Gebbink, *J. Organomet. Chem.*, 2010, **695**, 2618–2628, DOI: 10.1016/j.jorganchem.2010.08.026.
22. G. Prabusankar, N. Palanisami, R. Murugavel and R. J. Butcher, *Dalton Trans.*, 2006, 2140–2146, DOI: 10.1039/B516316A.
23. T. Posset, F. Rominger, and J. Blümel, *Chem. Mater.*, 2005, **17**, 586–595, DOI: 10.1021/cm048236f.
24. M. S. Balakrishna, S. Naik and S. M. Mobin, *Inorganica. Chim. Acta*, 2010, **363**, 3010–3016, DOI: 10.1016/j.ica.2010.03.030.
25. S. Chakraborty, A. A. Almasalma and J. G. de Vries, *Catal. Sci. Technol.*, 2021, **11**, 5388–5411, DOI: 10.1039/D1CY00737H.
26. A. Del Zotto, C. Greco, W. Baratta, K. Siega, P. Rigo, *Eur. J. Inorg. Chem.*, 2007, **18**, 2909–2916, DOI: 10.1002/ejic.200700044.
27. H. Gulyás, J. Benet-Buchholz, E. C. Escudero-Adan, Z. Freixa, and P. W. N. M. van Leeuwen, *Chem. Eur. J.*, 2007, **13**, 3424–3430, DOI: 10.1002/chem.200601640.
28. O. Paquet, M. B. Salon, E. Zeno and M. N. Belgacem, *Mater. Sci. Eng. C.*, 2012, **32**, 487–493, DOI: 10.1016/j.msec.2011.11.022.
29. (a) J. Fawcett, P. A. T. Hoye, R. D. W. Kemmitt, D. J. Lawa and D. R. Russell, *J. Chem. Soc., Dalton Trans.*, 1993, 2563–2568, DOI: 10.1039/DT9930002563. b) K. Heuzý, D. Mýry, D. Gauss, J. Blais and D. Astruc, *Chem. Eur. J.*, 2004, **10**, 3936–3944, DOI: 10.1002/chem.200400150.
30. R. G. Nuzzo, S. L. Haynie, M. E. Wilson, and G. M. Whitesides, *J. Org. Chem.*, 1981, **46**, 2861–2867, DOI: 10.1021/jo00327a005.

31. X. Zhang and F. G. Bordwell, *J. Am. Chem. Soc.*, 1994, **116**, 968–972, DOI: 10.1021/ja00082a018.
32. L. A. van der Veen, P. K. Keeven, P. C. J. Kamer and P. W. N. M. van Leeuwen, *Chem. Commun.*, 2000, 333–334, DOI: 10.1039/A906903H.
33. L. Huang and S. Kawi, *Catalysis Letters*, 2004, **92**, 57–62, DOI: 10.1023/B:CATL.0000011087.58049.32.
34. C. Claver, S. Castellón, N. Ruiz, G. Delogu, D. Fabbri and S. Gladiali, *J. Chem. Soc., Chem. Commun.*, 1993, 1833–1834, DOI: 10.1039/C39930001833.
35. E. Simón-Manso, M. Valderrama, Peter Gantzel and C. P. Kubiak, *J. Organomet. Chem.*, 2002, **651**, 90–97, DOI: 10.1016/S0022-328X(02)01317-7.

Chapter 3: Understanding ligand coordination behaviour in the development of oxide- supported hydroformylation pre- catalysts

3.1 Chapter 3 Aims/introduction

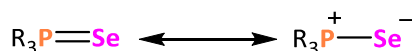
In Chapter 2 syntheses of novel compounds targeted as potential ligands for immobilised hydroformylation were described. Before these potential ligands were investigated in catalysis, the coordination behaviour and donor characteristics of these compounds was probed, so that insightful conclusions can be made about their resulting performance during catalysis. Consequently, in this chapter, assessment of the electronic character and basicity of the phosphine compounds reported in Chapter 2 *via* analysis of $|^1J_{\text{SeP}}|$ coupling constants of their corresponding phosphorus selenides is reported (see Section 3.2). These phosphine basicity studies are complemented by investigations into phosphine steric demands using $\%V_{\text{bur}}$ values calculated from crystallographic data of relevant phosphine complexes (see Section 3.3). Together these studies will allow for greater understanding of the combined steric and electronic character of the phosphine compounds reported in Chapter 2. Additionally, the coordination chemistry of the potential ligands is explored with the hydroformylation-active metals rhodium, cobalt and palladium, in order to develop pre-catalysts suitable for use in homogeneous hydroformylation catalysis (or heterogeneous hydroformylation catalysis after immobilisation of the complexes onto a solid oxide support; see Chapter 4 for details).

3.2 Characterisation of ligand steric and electronic donor characteristics

3.2.1 Assessing phosphine donor properties: phosphine basicity studies

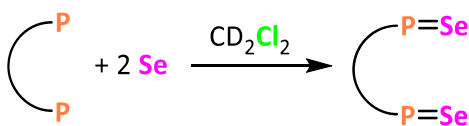
The electronic character of phosphines is well known to play an important role in the coordination chemistry of phosphine ligands and subsequent catalyst performance of phosphine-ligated metal complexes. Therefore, phosphine electronic character is an important parameter to understand for the novel phosphine compounds discussed in Chapter 2. Synthesis and characterisation, *via* ^{31}P NMR spectroscopy, of phosphine selenides is widely used as a convenient diagnostic tool for assessing the basicity of corresponding parent phosphines, strongly correlating to phosphine electronic character (see Section 1.7.1).¹ This is because the phosphorus selenium bond, which has

two possible resonance forms (Scheme 3.1), mostly exhibits s character with little π -contribution. This allows the relative magnitude of s character in the P-Se bond to be investigated by ^{31}P NMR spectroscopy. As the nuclear spin $\frac{1}{2}$ ^{77}Se isotope is 7.5% abundant, satellite peaks are readily observed in the ^{31}P NMR spectrum of phosphorus selenides, allowing a $|^1J_{\text{SeP}}|$ coupling constant to be measured. Large $|^1J_{\text{SeP}}|$ coupling constants are associated with a large degree of s character in the P-Se bond and hence a weakly Lewis basic phosphine, with non-directional electron density held close to the nucleus, denoting a poor phosphine σ donor.²



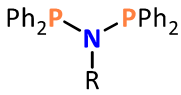
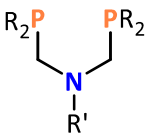
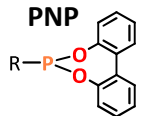
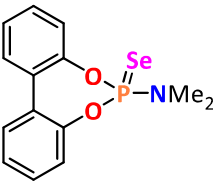
*Scheme 3.1. Resonance canonical forms of phosphine selenides.*¹

Phosphorus selenides of all the potential phosphine ligands prepared in the previous Chapter were synthesised from their parent phosphorus(III) compounds by reaction with an excess of elemental selenium (grey) in CD_2Cl_2 , (Scheme 3.2). The resulting mixtures were sonicated until complete conversion to the selenide derivatives was observed by ^{31}P NMR spectroscopic analysis. In each case, a large excess ~ 10 equivalents of selenium was used. The compounds were not isolated as only their $|^1J_{\text{SeP}}|$ coupling constants were of interest (Table 3.1).



Scheme 3.2. Synthesis of diphosphinediselenides.

Table 3.1. $|^1J_{\text{SeP}}|$ coupling constants of phosphine selenides in CD_2Cl_2 at 162 MHz.

Compound type	Compound	Diselenide δ / ppm	$ ^1J_{\text{SeP}} $ / Hz
dppa-type PNP 	L1(Se)₂	+67	786
	L2(Se)₂	+67	785
	L3(Se)₂	+67	786
	L4(Se)₂	+68	787
	L5(Se)₂	+67	786
PCNCP 	L13(Se)₂	+24	732
	L17(Se)₂	+26	729
	L18(Se)₂	+67	688
	L19(Se)₂	+46	684
Biphenol phosphite moiety-containing 	L9(Se)₂	+77	1012
	L11(Se)₂	+78	1010
	L12(Se)₂	+80	1010
	L21(Se)₂	+77	1031
Mono phosphine	L6X(Se)	+87	752
Literature examples	$\text{PPh}_3(\text{Se})$	+35	732*
	$\text{BISBI}(\text{Se})_2$	+34	738
		+91	1037*

* CDCl_3 solvent used.^{3,4}

The data in Table 3.1 shows a wide range in the $|^1J_{\text{SeP}}|$ coupling constants of the phosphine selenides prepared, which depend on the precise phosphorus environment of each individual compound. These data have been divided into relevant groups to simplify discussion (orange lines in table). The magnitude of the $|^1J_{\text{SeP}}|$ coupling

constants measured were compared to the measured literature value for SePPh_3 , so that the basicity of the new phosphines could be assessed relative to that of PPh_3 , an extensively used ligand in hydroformylation chemistry (along with a representative literature phosphoramidite).^{3,4} Taking $\text{PPh}_3(\text{Se})$ and $\text{BISBI}(\text{Se})_2$ as hydroformylation relevant benchmarks, where $|^1J_{\text{SeP}}|$ is 732 Hz and 738 Hz, respectively, the $(\text{Ph}_2\text{P})_2\text{N}$ -containing, dppa-type PNP compounds **L1-5**, have much larger $|^1J_{\text{SeP}}|$ coupling constants ranging from 785 – 787 Hz. These larger $|^1J_{\text{SeP}}|$ coupling constants relative to PPh_3 are to be expected due to the electron withdrawing nitrogen in the PNP fragment reducing electron density on the phosphorus and hence resulting in a weaker lone pair donor. The exact values of **L1-5** are all very similar suggesting that the structure of the different tethering groups employed in each compound are too far away from the phosphorus atoms to influence the electronic character of the phosphine. These values agree with other $|^1J_{\text{SeP}}|$ coupling constants for $(\text{Ph}_2\text{P}\{\text{Se}\})_2\text{N}$ - compounds in the literature.^{5,6}

As expected, the PCNCP diselenides are more basic than their PNP analogues due to the electron donating CH_2 fragment directly attached to the phosphorus atom that separates the phosphorus from the electron-withdrawing nitrogen atom. Compounds **L13** and **L17** have $|^1J_{\text{SeP}}|$ coupling constants of 732 and 729 Hz, respectively, values comparable to that of SePPh_3 , suggesting that the $-\text{CH}_2\text{N}-$ fragment has a similar effect as a phenyl group on phosphine electronic character. Compounds **L18** and **L19** proved to be the most Lewis basic phosphines investigated and hence the strongest σ -donors, with $|^1J_{\text{SeP}}|$ coupling constants of 688 and 684 Hz, respectively, for the corresponding diselenides. These small $|^1J_{\text{SeP}}|$ coupling constants are due to the compounds containing electron-donating alkyl fragments directly bound to the phosphorus atom, increasing phosphine basicity. The $|^1J_{\text{SeP}}|$ coupling constants of the PCNCP compounds show good agreement with those of similar compounds reported in the literature.^{7,8}

The phosphite and phosphoramidite compounds, containing biphenolphosphite moieties, show large $|^1J_{\text{SeP}}|$ coupling constants of over 1000 Hz for their corresponding diselenides due to the electron withdrawing nature of the oxygen substituents directly bonded to the phosphorus atoms, resulting in weak σ -donor character. Finally, the $|^1J_{\text{SeP}}|$ coupling constant of the mono-phosphine selenide **L6X(Se)** was measured to be 752 Hz, suggesting the electron withdrawing P-N bond counteracts the electron

donating $i\text{Pr}_2$ - fragments, resulting in a slightly weaker σ -donating parent phosphine than PPh_3 .

In the context of immobilised hydroformylation catalysis, which constitutes the overarching goal of this project, the wide variety in Lewis basicity of the phosphines produced will allow for important insights during catalysis to be made. As discussed in Section 1.6, in traditional homogeneous hydroformylation processes, poor σ -donor phosphite-containing complexes often give rise to highly active catalysts due to the faster CO dissociation associated with electron-poor metal centres.⁹ Meanwhile, more electron-rich catalysts containing strongly σ -donating alkyl phosphines are generally less active, but display enhanced stability relative to more electron-poor catalysts. Catalyst activity and stability are two of the major challenges that need to be overcome to allow for financially viable immobilised catalyst heterogeneous hydroformylation processes.¹⁰ As such, determining whether these issues can be addressed by tuning the phosphine electronic character of immobilised hydroformylation catalysts is of great interest.

3.2.2 Quantifying the steric bulk of tetherable phosphine compounds

Alongside phosphine electronic character, the steric bulk of phosphine ligands has a significant effect on hydroformylation catalyst performance, often playing a particularly important role in catalyst selectivity for linear/branched aldehydes. As discussed in Section 1.7.2, the Tolman cone angle, θ , is an important parameter for assessing the steric bulk of monodentate phosphine ligands.¹¹ However, application of this model becomes challenging for bidentate and asymmetric ligands, which has resulted in the development of several other methods for assessing ligand steric bulk.¹² One example of an alternative approach for assessing the steric demand of multidentate systems is the “Percent Buried Volume” ($\%V_{\text{bur}}$) approach (Figure 3.1).¹³ $\%V_{\text{bur}}$ values can be calculated using the freely available SambVca 2.1 web tool that has been successfully applied to mono- and bi-dentate phosphines, as well as asymmetrical ligands, such as *N*-heterocyclic carbenes, which it was originally designed for.^{13,14} The value $\%V_{\text{bur}}$ is defined as “the percentage of the total volume of a sphere occupied by a ligand at a fixed metal-ligand bond distance” and can be calculated from crystallographic or computational data containing the relevant ligand. A greater value of $\%V_{\text{bur}}$ corresponds

to additional space around a metal centre being occupied, as a result of increased ligand steric bulk. Values of %V_{bur} have been shown by Nolan *et al.* to correlate well with the Tolman cone angle calculated for a series of AuCl(PR₃) complexes at a fixed M-P distance of 2.0 Å, suggesting that %V_{bur} is a practical and reliable method of quantifying the steric bulk of phosphines.¹⁴ In addition to the %V_{bur} calculations, the SambVca 2.1 software can be used to produce “steric maps” of a ligand coordinated to a metal, providing a visual method for considering the available space around a metal centre, which may have important connotations for coordination chemistry and behaviour of the metal complex.

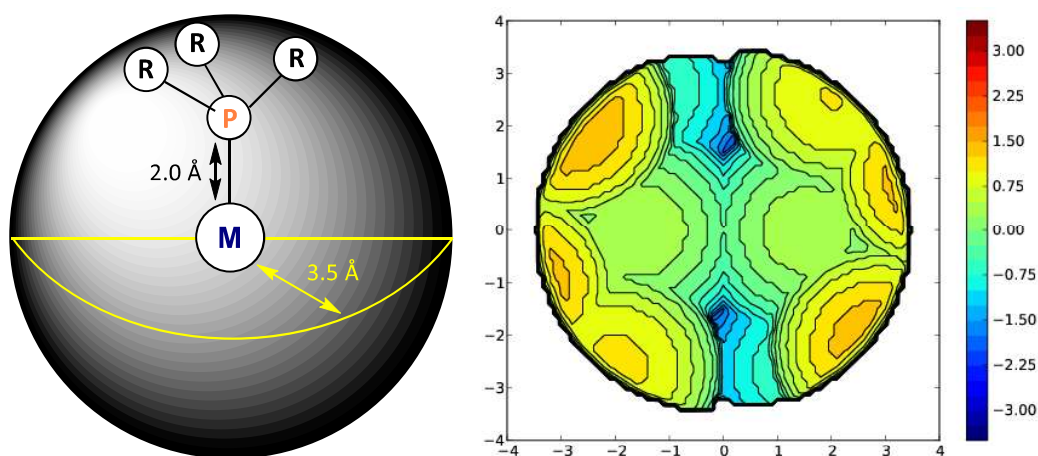


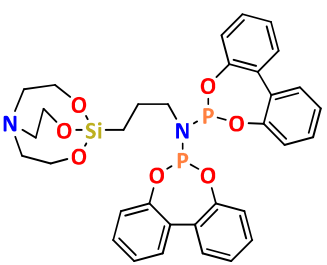
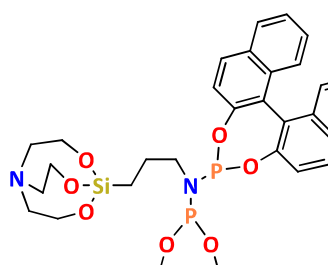
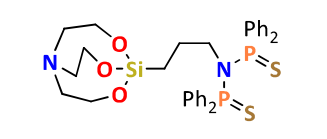
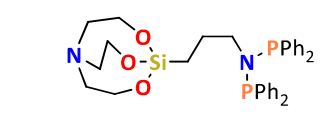
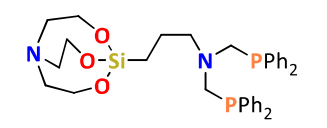
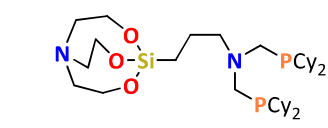
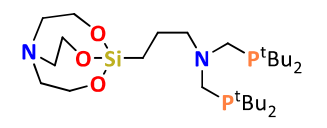
Figure 3.1. Left: Tertiary phosphine Percentage Buried Volume determination, assuming a fixed M-P distance of 2.0 Å and sphere radius of 3.5 Å.¹² Right: example steric map produced using SambVca 2.1 software of a bidentate phosphine.¹²

The SambVca 2.1 web tool was used to calculate %V_{bur} values for a selection of the phosphine compounds synthesised in this work, with the relevant data reported in Table 3.2 in ascending order of magnitude of %V_{bur}. The values for each ligand displayed in Table 3.2 were calculated from crystallographic data of [PdI₂(P[^]P)] compounds containing the relevant ligand, apart from **L5S₂**, where crystallographic data of [Rh(COD)(κ²-S,S-**L5S₂**)]BF₄ was used. The similar ionic radii of Rh⁺ and Pd²⁺ and the same square planar geometry in the PdI₂(P[^]P) and [Rh(COD)(κ²-S,S-**L5S₂**)]BF₄ complexes means that the %V_{bur} of the ligands in these complexes can be compared.¹⁵ To assess the validity of this comparison, the value of %V_{bur} for **L5** was also calculated using crystallographic data of a square planar rhodium complex, [Rh(κ²-P,P-**L5**)₂](BF₄) (%V_{bur} = 44%), which showed good agreement with the value calculated for PdI₂(**L5**)

(%V_{bur} = 45%). Determination of %V_{bur} for a literature example of a commonly used ligand in industrial homogeneous hydroformylation applications was also desired to enable comparison of our ligands to a standard benchmark. To this end, PPh₃ was selected and analysed, using the crystallographic data for PdI₂(PPh₃)₂ taken from the CCDC (refcode: GODGIP) to generate the steric map and value of %V_{bur}.¹⁶

All the novel ligands featured in Table 2 contain the silatrane tethering functionality. The identity of the tethering functionality is likely to have no effect on the values of %V_{bur} calculated since they are far removed from the metal centre, certainly at a greater distance than the 3.5 Å radius sphere considered in the calculation.

Table 3.2. %V_{bur} values of bidentate tetherable phosphines coordinated to PdI₂.

Ligand	%V _{bur}	Ligand	%V _{bur}
L11 	38	L12 	38
L5S₂ 	39*	L5 	45 (44*)
L17 	54	L19 	57
L18 	60	2 × PPh₃	57 ¹⁶

* values calculated from crystallographic data of [Rh(COD)(κ²-S,S-L5S₂)]BF₄ and [Rh(κ²-P,P-L5)]BF₄.

The results of the %V_{bur} calculations listed in Table 3.2 show that the phosphoramidite ligands **L12** and **L11**, alongside the sulfur ligand **L5S₂**, have the smallest buried %V_{bur} values of 38 – 39%. This is due to the steric bulk of the aryl groups of these ligands residing far away from the metal centre and thus having a relatively small effect on the magnitude of the %V_{bur}.

As expected, increasing the ligand bite angle from 70 to 90° from **L5** to **L17** results in an increase to the %V_{bur}, with the %V_{bur} value rising from 45 to 54%. Additionally, changing the R groups on the phosphine has an effect on the %V_{bur} value of the ligand, with the sterically hindered *di-tert*butyl phosphine, **L18**, showing the largest %V_{bur} of the ligands investigated in this study, with a value of 60%.

Alongside the %V_{bur} calculations, steric maps were produced for each of the ligands featured in Table 3.2 (Figure 3.2). For the various ligands studied, the steric maps show a general increase in proximity of the ligand to the metal centre as %V_{bur} increases. However, despite **L18** having just a three percent greater %V_{bur} than the dicyclohexyl analogue, **L19**, the steric map shows a large increase in proximity of the ligand to the metal centre. Together this shows that both the %V_{bur} and steric map are important to consider when analysing the steric contribution of a ligand around a metal centre, as the %V_{bur} gives an overall proportion of the metal centre enclosed by a ligand, whereas the steric map gives topological insight into steric environment of the metal centre.

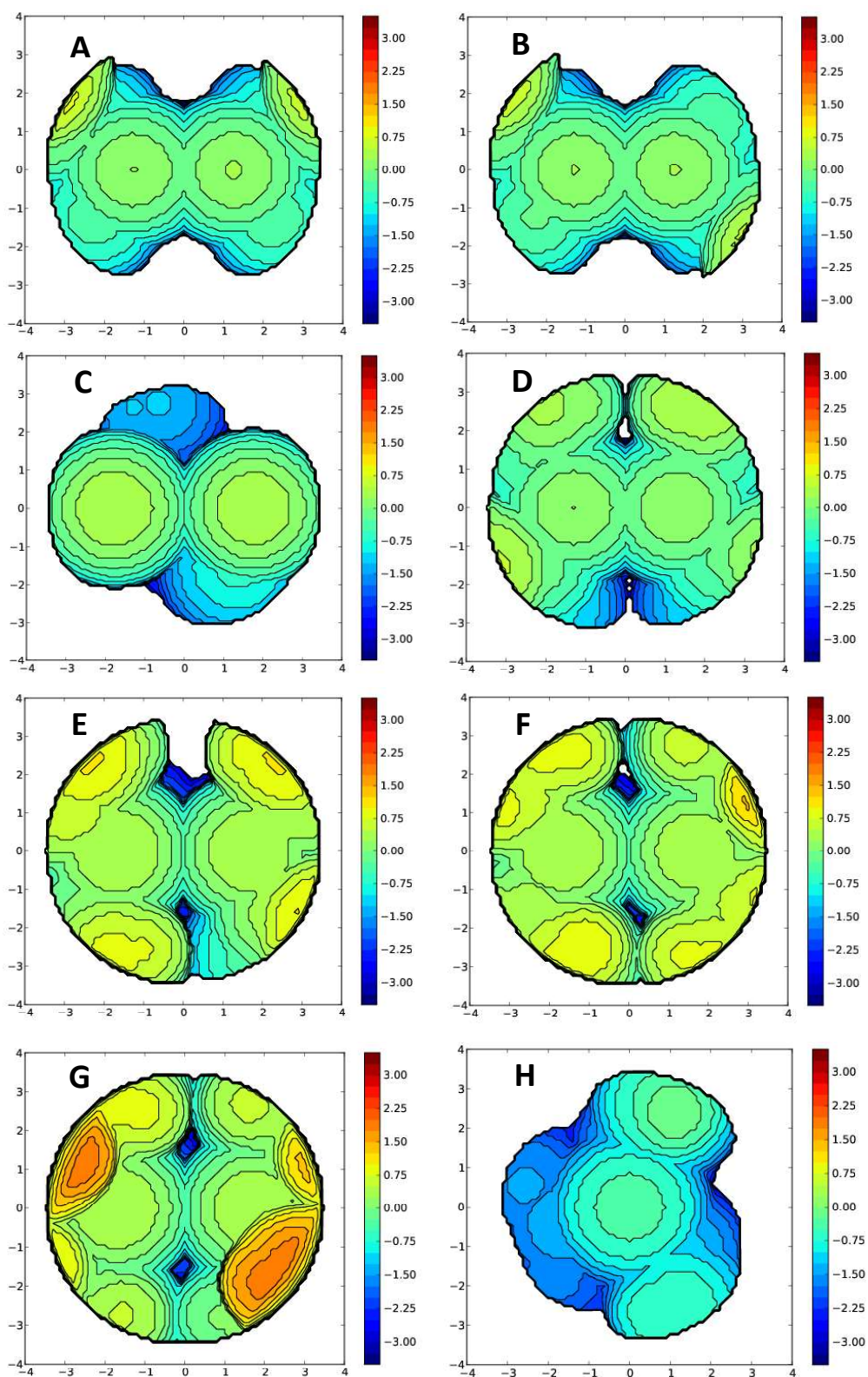


Figure 3.2. Steric maps obtained for diphosphine ligands when coordinated to PdI_2 where $(P^{\wedge}P) =$ A: **L12**, B: **L11**, C: **L5S₂** ($[\text{Rh}(\text{COD})(\kappa^2\text{-S,S-L5S}_2)]\text{BF}_4$), D: **L5**, E: **L17**, F: **L19**, G: **L18**, H: **PPh₃**.

3.2.3 Plot of phosphine %V_{bur} against $|^1J_{\text{SeP}}|$ coupling constants

When assessing the performance of phosphine ligands in homogenous catalysis, a complex combination of steric and electronic factors are often required to rationalise the performance of a specific phosphine-containing catalyst.¹⁷ As a result, 2D and 3D maps combining various calculated ligand parameters have become useful tools for analysing homogeneous catalysts, aiding in catalyst optimisation, screening and exploration.¹⁸ This approach has been successfully employed for hydroformylation catalysis, leading to the design of a new class of stable, electron-deficient fluorophosphine ligands, for example.¹⁹

Although computational methods are currently the major focus of the literature in this area to produce more sophisticated ‘maps’ of chemical space combining multiple different chemical parameters, in this work a simple two-parameter study was performed.²⁰ To this end, the values of the $|^1J_{\text{SeP}}|$ coupling constants determined for the phosphine selenides (a proxy for the electronic character of the phosphine) were plotted against the corresponding %V_{bur} values determined for the parent phosphines (phosphine steric character) to produce a ‘map’ of combined phosphine steric-electronic character to enable facile comparison of the ligands produced (Figure 3.3). The plot shows that the PCNCP ligands synthesised are generally more sterically bulky and electron rich relative to $2 \times \text{PPh}_3$, while the PNP ligands are less sterically bulky and electron rich, particularly the phosphoramidite PNPs **L11** and **L12**. This map also clearly shows phosphine steric-electronic ‘space’ that has not been investigated in this work, for example large $|^1J_{\text{SeP}}|$, large %V_{bur} (see future work). However, this is largely due to the difficulties encountered when trying to prepare more sterically hindered PNP ligands, as discussed in Chapter 2. From Figure 3.3 it can be predicted that the industrially relevant PPh_3 is likely to behave most similarly to **L17** due to their similar steric and electronic characters, which will be useful to verify during subsequent catalyst testing (see Section 5.3).

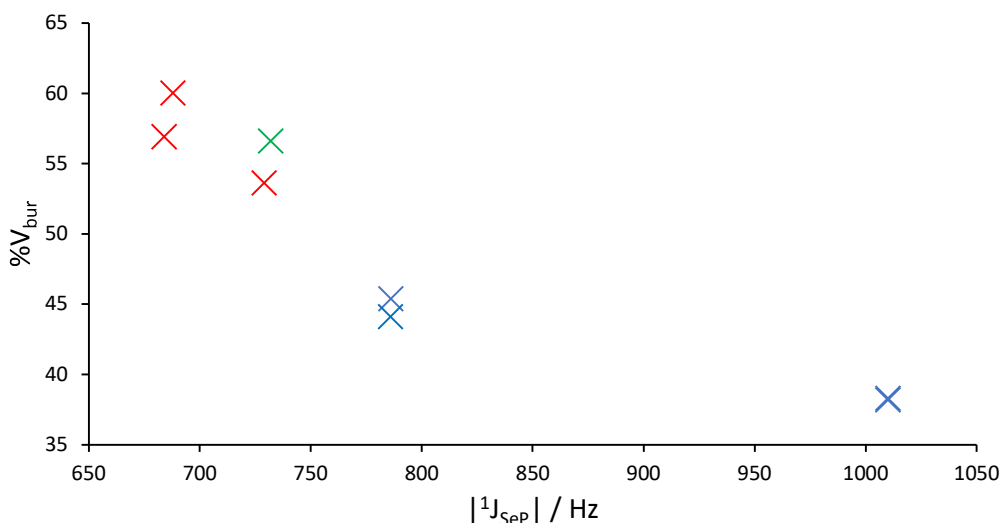


Figure 3.3. Plot contrasting steric and electronic characteristics of the various $P^{\wedge}P$ ligands prepared as a part of this thesis, as assessed from determination of $|^1J_{SeP}|$ coupling constants for their corresponding selenides and of $\%V_{bur}$ values. Red crosses denote PCNCP, blue crosses denote PNP ligand backbones and the green cross represents $2 \times PPh_3$.

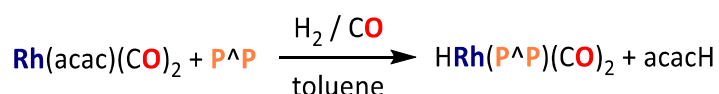
3.3 Coordination studies of $(PPh_2)_2N(CH_2)_3Si(OMe)_3$, $(PPh_2)_2N(CH_2)_3Si(OCH_2CH_2)_3N$, $((C_{12}H_8O_2)P)_2N(CH_2)_3Si(OMe)_3$, $((C_{12}H_8O_2)P)_2N(CH_2)_3Si(OCH_2CH_2)_3N$, $((C_{20}H_{12}O_2)P)_2N(CH_2)_3Si(OCH_2CH_2)_3N$, $(Ph_2PCH_2)_2N(CH_2)_3Si(OMe)_3$, $(Ph_2PCH_2)_2N(CH_2)_3Si(OCH_2CH_2)_3N$, $(tBu_2PCH_2)_2N(CH_2)_3Si(OCH_2CH_2)_3N$, $(Cy_2PCH_2)_2N(CH_2)_3Si(OCH_2CH_2)_3N$, $((C_{12}H_8O_2)POCH_2CH_2)_2N(CH_2)_3Si(OMe)_3$, $(PPh_2)_2NCH_2CH_2CH_2CH_3$ and $(P(S)Ph_2)_2N(CH_2)_3Si(OCH_2CH_2)_3N$ with rhodium(I)

Following on from the design, synthesis and subsequent characterisation of the developed tetherable phosphines, the coordination chemistry of these potential ligands with hydroformylation-active metals was explored, with the aim of producing suitable hydroformylation pre-catalysts. As the intended final application of this work is in immobilised hydroformylation catalysis, which brings additional challenges in terms of catalyst synthesis and characterisation, a thorough understanding the solution-state chemistry of these complexes before immobilisation was required. This would ensure greater confidence in the identity of the likely active catalyst species generated under hydroformylation reaction conditions (namely a pressure of syngas) for homogeneous and heterogeneous catalysis. As rhodium is widely accepted as the most effective metal

for the vast majority of hydroformylation applications, rhodium complexes formed the primary focus for the coordination chemistry detailed in this Chapter, in conjunction with supplementary work on cobalt and palladium.²¹

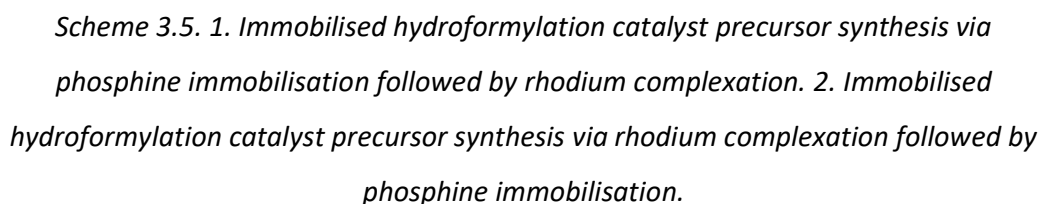
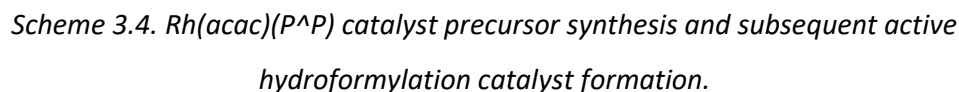
3.3.1 Literature Rh(acac)(P^P) complex syntheses

The vast majority of literature pertaining to rhodium-catalysed hydroformylation with bidentate phosphine ligands focuses on formation of the catalytically-active rhodium species *in situ* in the vessel in which catalysis is undertaken. A general example is given in Scheme 3.3.²²

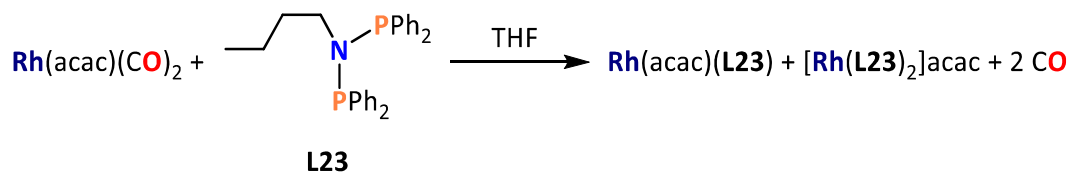


Scheme 3.3. Generic example of in situ formation of active rhodium hydroformylation catalysts.

However, this “*in situ*” approach has disadvantages for the synthesis of immobilised hydroformylation catalysts *via* tetherable ligands, as the catalyst immobilisation step also has to be considered during catalyst formation, providing additional uncertainty into the exact catalyst species generated in the reaction. Therefore, initial isolation and characterisation of well-defined d⁸ square planar Rh(acac)(P^P) catalyst precursors prior to immobilisation and subsequent catalyst testing was desired for this work (Scheme 3.4). Isolation of such a rhodium phosphine catalyst precursor has several benefits. Firstly, this catalyst precursor can be fully characterised in solution (and purified if necessary). This is important for immobilised catalysts, as once they are attached to a solid support characterisation (and purification) becomes much more difficult. Secondly, immobilisation of the pre-formed rhodium complex can then be investigated alongside immobilisation of free ligand followed by complexation, to assess the most effective overall immobilisation method for heterogenised catalyst synthesis, Scheme 3.5 (See Chapter 4 for more details).

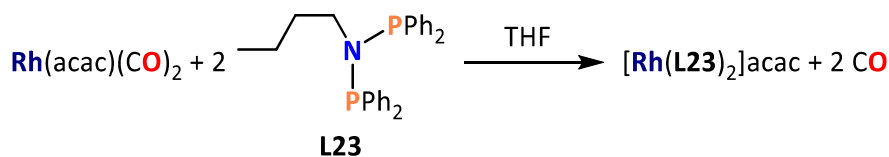


The few examples of Rh(acac)(P^P) synthesis and isolation that appear in the literature employ a variety of different reaction conditions to produce the desired complexes. These include different reaction temperatures ranging from -78 to 110 °C, various solvents, different addition methods of the reactants (*e.g.*, fast or dropwise addition of ligand to metal or metal to ligand), and different rhodium sources.^{23–25} In order to probe the reactivity of a small bite angle phosphine ligand with Rh(acac)(CO)₂, a simple dppa-type ligand (Ph₂P)₂NCH₂CH₂CH₂CH₃, **L23**, was selected. Following an adapted literature procedure, **L23** was reacted one equivalent of Rh(acac)(CO)₂ in THF at room temperature (Scheme 3.6).



Scheme 3.6. Reaction of Rh(acac)(CO)₂ with L23.

Unexpectedly, ^{31}P NMR spectroscopic analysis of an aliquot of reaction mixture indicated that a mixture of two rhodium-containing products had formed in an approximately 2:1 ratio, corresponding to the desired product; $\text{Rh}(\text{acac})(\text{L23})$, and $[\text{Rh}(\text{L23})_2]\text{acac}$, respectively. The identity of the side product as $[\text{Rh}(\text{L23})_2]\text{acac}$ was confirmed by a second reaction where two equivalents of **L23** were reacted with $\text{Rh}(\text{acac})(\text{CO})_2$ under the same reaction conditions as the analogous stoichiometric reaction (Scheme 3.7).

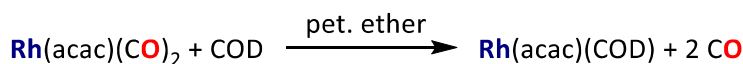


Scheme 3.7. Synthesis of $[\text{Rh}(\text{L23})_2]\text{acac}$.

^{31}P NMR spectroscopic analysis of the reaction mixture showed a single doublet in the NMR spectrum at +67 ppm ($^1J_{\text{RhP}} = 120$ Hz), in agreement with the side product in the NMR spectrum of the 1:1 reaction. This NMR splitting pattern suggests that all four phosphorus atoms are equivalent and coupling to the ^{103}Rh nuclei. This is consistent with this product being the salt $[\text{Rh}(\text{L23})_2]\text{acac}$. This assignment is further supported by the 120 Hz $^1J_{\text{RhP}}$ coupling constant, which is diagnostic of bis(bidentate) chelating phosphine coordination at a Rh^{I} centre.^{26,27} The ^1H and ^{13}C NMR spectra obtained were also consistent with the proposed composition of $[\text{Rh}(\text{L23})_2]\text{acac}$.

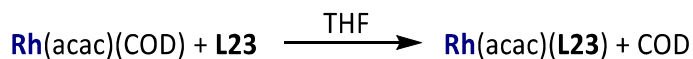
3.3.3 $\text{Rh}(\text{acac})(\text{L23})$ synthesis optimisation

In order to develop a synthesis strategy to selectively produce $\text{Rh}(\text{acac})(\text{L23})$, a series of reactions were undertaken in which $\text{Rh}(\text{acac})(\text{CO})_2$ starting material was replaced by $\text{Rh}(\text{acac})(\text{COD})$. This latter COD complex was synthesised following a literature procedure (Scheme 3.8).²⁸ It was of interest to explore whether changing the rhodium precursor would change the selectivity towards $\text{Rh}(\text{acac})(\text{L23})$, whilst also allowing this phosphine coordination study to be performed using a more convenient rhodium precursor that does not liberate toxic CO gas upon reaction.



Scheme 3.8. Synthesis of Rh(acac)(COD).²⁸

Further attempted syntheses of Rh(acac)(**L23**) using Rh(acac)(COD) as the starting material (Scheme 3.9) showed a small increase in selectivity for Rh(acac)(**L23**), of <10% relative to when Rh(acac)(CO)₂ was used as the rhodium precursor. However, this observation cannot be fully attributed to the change in rhodium precursor, as several other variables, such as the volume of solvent and the rate of addition of **L23** to the rhodium precursor were not controlled during these reactions. Meanwhile, an investigation into the effect of the reaction solvent on the selectivity of Rh(acac)(**L23**) formation showed no observable change when THF, toluene or DCM were employed.



Scheme 3.9. Attempted synthesis of Rh(acac)(L23) from Rh(acac)(COD).

A ³¹P NMR study into the effect of temperature on the reaction of **L23** with Rh(acac)(COD) was conducted (Figure 3.4, Table 3.3). The results of this study showed that a large increase in selectivity for Rh(acac)(**L23**) was observed when addition of ligand to metal was performed in a dropwise manner at –78 °C, before slowly allowing the reaction mixture to warm up to room temperature. Conversely, attempts to perform the reaction at elevated temperatures resulted in ³¹P NMR spectra that were too complicated to be interpreted, indicating complete decomposition of the phosphine-containing components. These results show that reduced temperatures and low local concentrations of **L23** relative to Rh(acac)(COD) during complexation improve selectivity towards Rh(acac)(**L23**), up to a maximum observed selectivity of 92%. Unfortunately, a method to further improve the selectivity of Rh(acac)(**L23**) formation up to 100% could not be identified. Additionally, attempts to purify the Rh(acac)(**L23**) produced by washing or recrystallisation were unsuccessful.

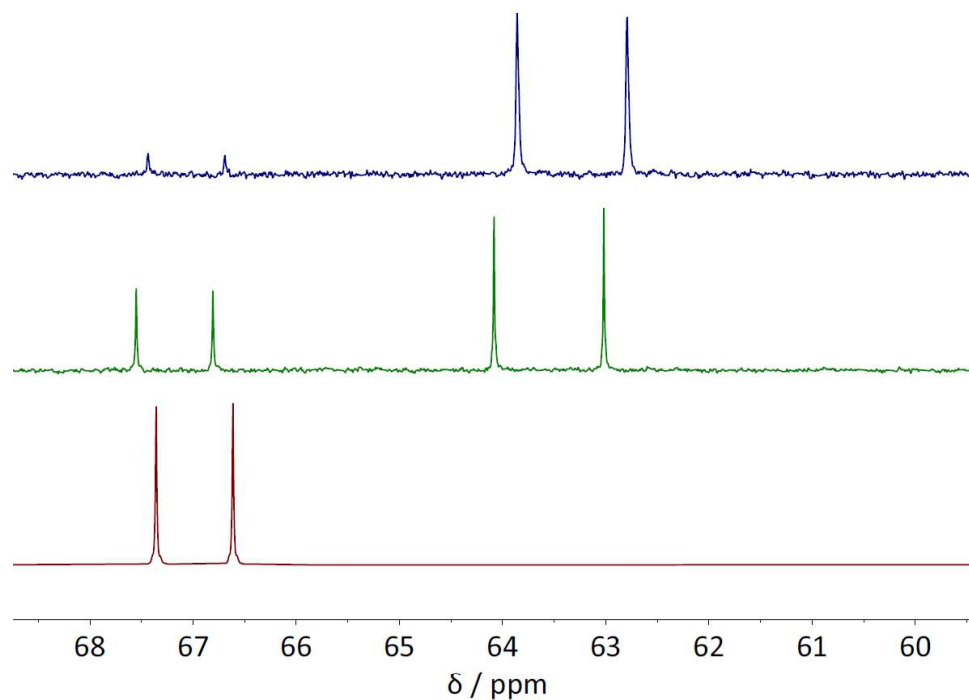


Figure 3.4. $^{31}\text{P}\{^1\text{H}\}$ NMR spectroscopic analysis (162 MHz, 295 K) of **red**: $[\text{Rh}(\text{L23})_2]\text{acac}$ (in CDCl_3), **green**: $\text{Rh}(\text{acac})(\text{L23})$ produced at r.t. (in THF-d_8) and **blue**: $\text{Rh}(\text{acac})(\text{L23})$ produced at -78°C with dropwise addition of ligand **L23** to $\text{Rh}(\text{acac})(\text{COD})$ (in THF, $^{31}\text{P}\{^1\text{H}\}$ unlocked experiment).

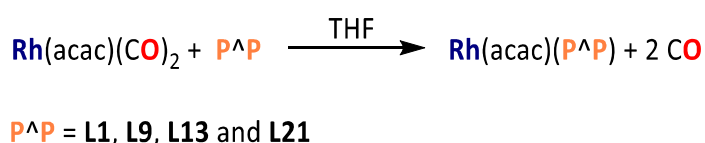
Table 3.3. The effect of reaction temperature on the product distribution of the reaction of $\text{Rh}(\text{acac})(\text{COD})$ with **L23** in THF determined by ^{31}P NMR spectroscopic analysis.

Reaction temperature / $^\circ\text{C}$	$\text{Rh}(\text{acac})(\text{L23})$ selectivity / %	$[\text{Rh}(\text{L23})_2]\text{acac}$ selectivity / %
20	66	33
-78°C	92	8
45	0	0
20*	0	100

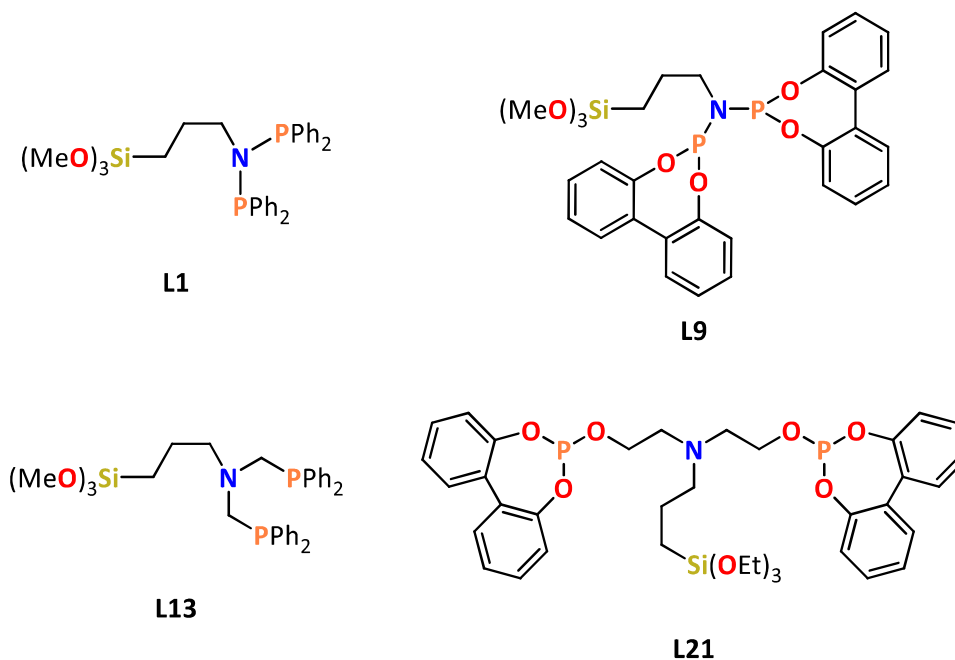
*two equivalents of **L23**.

3.3.4 Coordination studies of $(PPh_2)_2N(CH_2)_3Si(OMe)_3$, $(PPh_2)_2N(CH_2)_3Si(OCH_2CH_2)_3N$, $(P(C_{12}H_8O_2))_2N(CH_2)_3Si(OMe)_3$, $(Ph_2PCH_2)_2N(CH_2)_3Si(OMe)_3$ and $((C_{12}H_8O_2)POCH_2CH_2)_2N(CH_2)_3Si(OMe)_3$, with rhodium(acac)(COD)

In order to assess the effect of ligand structure on the synthesis of $Rh(acac)(P^AP)$ complexes, a selection of tetherable bidentate phosphines were reacted with $Rh(acac)(COD)$ and $Rh(acac)(CO)_2$ (Scheme 3.10). Ligands **L1**, **L9**, **L13**, **L21** (Figure 3.5) were chosen for these reactions due to their differing phosphine electronic characters and bite angles, which could affect their coordination chemistry with rhodium(I) precursors.



Scheme 3.10. Attempted synthesis of some silica-tetherable $Rh(acac)(P^AP)$ complexes.

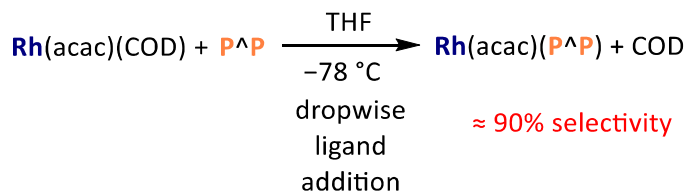


*Figure 3.5. Structures of tether-modified P^AP ligands **L1**, **L9**, **L13** and **L21**.*

When **L1**, **L9**, **L13** and **L21** were reacted with $Rh(acac)(COD)$ or $Rh(acac)(CO)_2$ at room temperature, a mixture of $Rh(acac)(P^AP)$ and $[Rh(P^AP)_2]acac$ complexes were formed in

an approximately 2:1 ratio. This showed good agreement with the reactivity observed when **L23** was employed as the bidentate phosphine ligand (See section 3.3.2)

The reactions of **L1**, **L9**, **L13** and **L21** with Rh(acac)(COD) were repeated using the optimised reaction conditions devised for **L23** (see Section 3.3.3), namely THF solvent and dropwise addition of ligand to metal $-78\text{ }^{\circ}\text{C}$ before slowly warming to room temperature (Scheme 3.11). Using this approach led to increased selectivities to the desired Rh(acac)(P[^]P) complexes of $\approx 90\%$, as determined by ^{31}P NMR spectroscopic analysis in each case. Attempts to further improve selectivity were unsuccessful, however. An additional difficulty observed with these rhodium complexes was their low stability. Despite handling the complexes under an inert nitrogen atmosphere in rigorously dried and degassed solvents, oxidised phosphines were repeatedly observed in ^{31}P NMR spectra recorded after an hour, making work up and purification of these compounds challenging. As these Rh(acac)(P[^]P) complexes, where P[^]P = **L1**, **L9**, **L13** or **L21** could not be obtained pure, they are not suitable for use as catalysts, especially when another reaction would be required to immobilise them onto a silica support to produce a heterogenous catalyst.

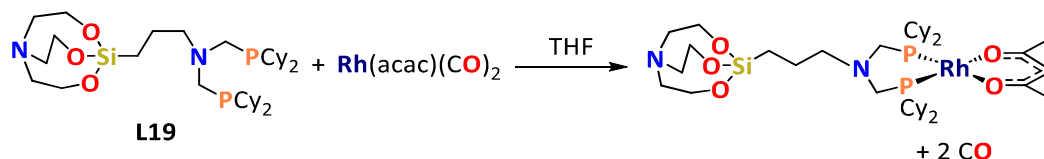


Scheme 3.11. Optimised synthesis conditions of Rh(acac)(P[^]P).

3.3.5 Synthesis of Rh(acac)(L19)

In contrast to the observed reactivity of **L1**, **L9**, **L13**, **L21** and **L23** with Rh(acac)(CO)₂, the reaction between **L19** and Rh(acac)(CO)₂, proceeded cleanly at room temperature to produce the target complex Rh(acac)(**L19**) (Scheme 3.12). **L19** is more sterically bulky and electron-rich than the other ligands **L1**, **L9**, **L13**, **L21** and **L23** that were reacted with Rh(acac)(CO)₂ in this work, which could affect its coordination chemistry with rhodium(I). However, dppa-type and other less electron rich and less sterically hindered

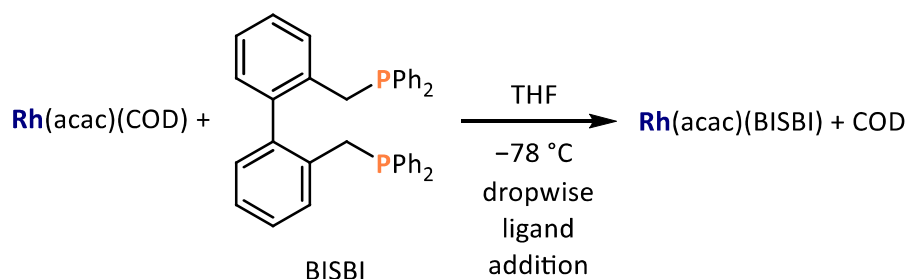
ligands have been shown to selectively produce $\text{Rh}(\text{acac})(\text{P}^{\wedge}\text{P})$ complexes in the literature, so the reason for this differing reactivity remains unclear.²⁴



Scheme 3.12. Synthesis of $\text{Rh}(\text{acac})(\text{L19})$.

3.3.6 Attempted synthesis of $\text{Rh}(\text{acac})(\text{BISBI})$

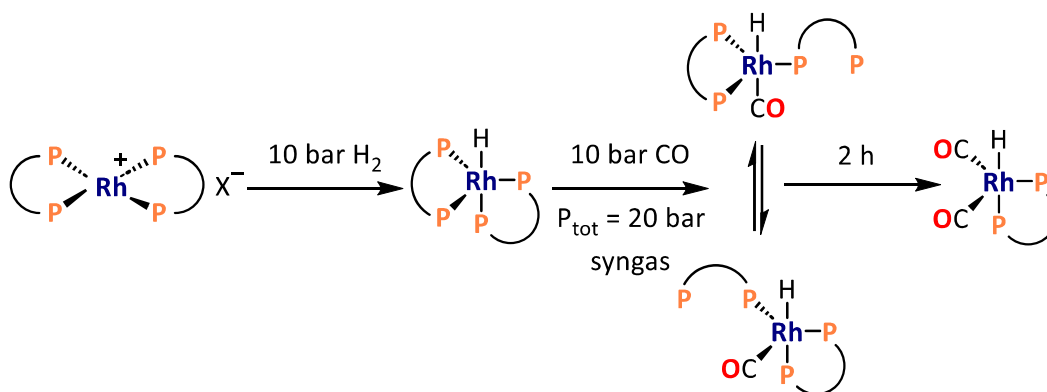
In order to contextualise the difficulties found with the preparation of well-defined rhodium hydroformylation catalyst precursors containing **L1**, **L9**, **L13** and **L21**, the synthesis of $\text{Rh}(\text{acac})(\text{BISBI})$ was investigated (Scheme 3.13). As discussed in Section 1.10, the diphosphine BISBI, 2,2'-bis(diphenylphosphinomethyl)-1,1'-biphenyl, has been successfully used as a ligand in industrial rhodium-catalysed hydroformylation processes, which show high activity and selectivity.^{29,30} However, in these industrial processes, the proposed active rhodium/BISBI complex, $\text{HRh}(\text{BISBI})(\text{CO})_2$, is formed *in situ* under operating conditions (*i.e.* in presence of syn gas) without isolation of a rhodium-BISBI complex being performed.^{29,31} The identity of the active catalyst species as $\text{HRh}(\text{BISBI})(\text{CO})_2$ has recently been validated computationally.³¹



Scheme 3.13. Attempted synthesis of $\text{Rh}(\text{acac})(\text{BISBI})$.

Attempted synthesis of $\text{Rh}(\text{acac})(\text{BISBI})$ from the reaction of $\text{Rh}(\text{acac})(\text{COD})$ and BISBI (dropwise addition of ligand to metal at $-78\text{ }^{\circ}\text{C}$ in THF before slowly warming to room temperature) resulted in a similar product distribution to that found when the ligands **L1**, **L9**, **L13** and **L21** were used under identical reactions conditions. This suggests that

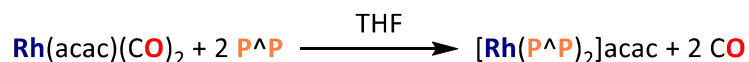
both $\text{Rh}(\text{acac})(\text{BISBI})$ and $[\text{Rh}(\text{BISBI})_2]\text{acac}$, may be able to be converted to the active catalyst $\text{HRh}(\text{BISBI})(\text{CO})_2$ under hydroformylation reaction conditions. This agrees with the work of van Leeuwen, who showed that $[\text{Rh}(\text{P}^\wedge\text{P})_2]^+$ cations, where P^\wedgeP is (*S,S*)-2,4-bis(diphenylphosphino)pentane, can be converted to $\text{HRh}(\text{P}^\wedge\text{P})(\text{CO})_2$ species that are active hydroformylation catalysts when pressurised under an atmosphere of syngas (Scheme 3.14).³² Additionally, active hydroformylation catalysts have previously been reported to form under syngas from both $\text{Rh}(\text{acac})(\text{dppe})$ and $[\text{Rh}(\text{dppe})_2]\text{acac}$, suggesting that different phosphine ligand stoichiometries in the catalyst precursor are tolerated, although the nature of the resulting hydroformylation-active species may be different.³³



Scheme 3.14. Conversion of $[\text{Rh}(\text{P}^\wedge\text{P})_2]\text{X}$ to $\text{HRh}(\text{P}^\wedge\text{P})(\text{CO})_2$ under syngas, where X^- is MeO^- and P^\wedgeP is (*S,S*)-2,4-bis(diphenylphosphino)pentane, adapted from van Leeuwen *et al.*³²

3.3.7 $[\text{Rh}(\text{P}^\wedge\text{P})_2]\text{acac}$ complex syntheses

Synthesis of $[\text{Rh}(\text{P}^\wedge\text{P})_2]\text{acac}$ complexes for use as hydroformylation catalyst precursors was investigated by the reaction of $\text{Rh}(\text{acac})(\text{CO})_2$ with two equivalents of the desired diphosphines in THF at room temperature (Scheme 3.15).



Scheme 3.15. General synthesis of $[\text{Rh}(\text{P}^\wedge\text{P})_2]\text{acac}$ complexes.

The reaction of **L5** with Rh(acac)(CO)₂ following the methodology described in Scheme 3.15 resulted in the successful synthesis of [Rh(**L5**)₂]acac. ³¹P{¹H} NMR spectroscopic analysis of the isolated complex showed a single doublet at 66 ppm (¹J_{RhP} = 119 Hz), in good agreement with the data obtained for [Rh(**L23**)₂]acac and that of other square planar bis(bidentate) phosphine coordination of Rh^I in the literature.^{26,27} Following attempted recrystallisation of a sample of [Rh(**L5**)₂]acac from DCM/hexane, crystals of [Rh(**L5**)₂]Cl were instead isolated. These crystals were suitable for XRD analysis, which was performed in Durham by Dr T. Blundell, confirming the identity of the cation (Figure 3.6). The Cl[−] in the crystals is likely to have originated from the DCM solvent used for the recrystallisation, as this was the only source of chlorine that came into contact with the sample of [Rh(**L5**)₂]acac.

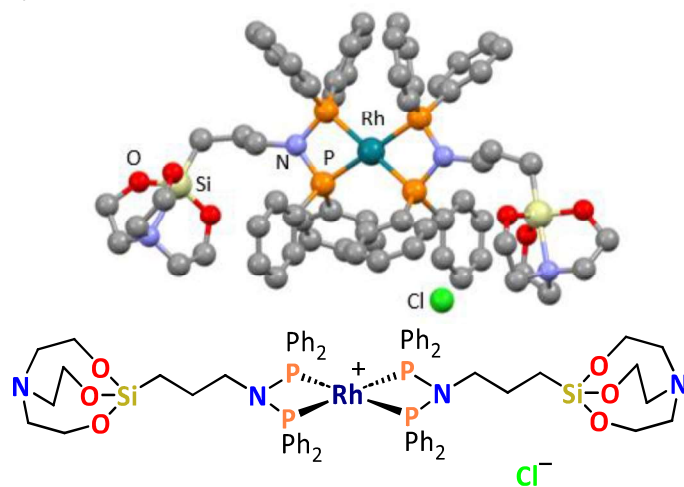
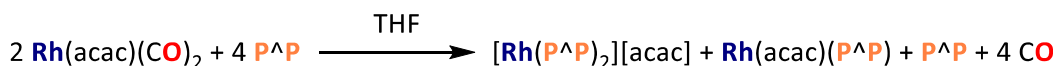


Figure 3.6. Molecular structure of [Rh(**L5**)₂]Cl. Hydrogens omitted for clarity. Selected bond lengths / Å: Rh-P 2.275(2), 2.278(2), 2.274(2), 2.271(2); P-N 1.700(5), 1.703(5), 1.700(7), 1.709(6); Selected bond angles / °: P-Rh-P 70.10(6), 70.10(6); P-N-P 100.4(3), 99.9(3).

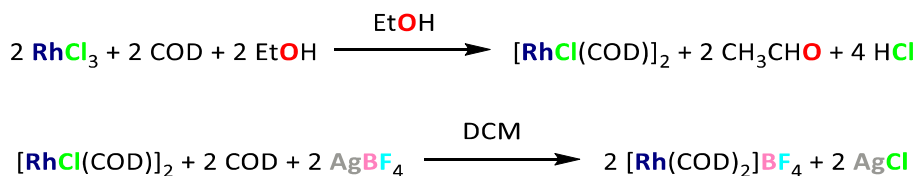
Attempted synthesis of the corresponding [Rh(P[^]P)₂]acac complexes with PCNCP ligands **L17** and **L18**, using the methodology shown in Scheme 3.15 resulted in a mixture of products, including the mono-substituted Rh(P[^]P)(acac) complexes (as evidenced by ³¹P NMR spectroscopy). As complete conversion to the [Rh(P[^]P)₂]acac complexes was not achieved, unreacted phosphine remained in the reaction mixture despite prolonged reaction times of up to 72 hours (Scheme 3.16).



Scheme 3.16. Attempted synthesis of $[\text{Rh}(\text{P}^{\wedge}\text{P})_2]\text{acac}$ complexes with PCNCP ligands **L17** and **L18**.

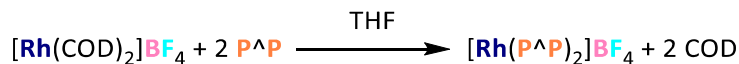
3.3.8 Syntheses of $[\text{Rh}(\text{P}^{\wedge}\text{P})_2]\text{BF}_4$ complexes

$[\text{Rh}(\text{COD})_2]\text{BF}_4$ was investigated as an alternative rhodium source to $\text{Rh}(\text{acac})(\text{CO})_2$ for the synthesis of $[\text{Rh}(\text{P}^{\wedge}\text{P})]^{+}$ -containing hydroformylation catalyst precursors. This has the advantage of utilising BF_4^{-} as a well-established non-coordinating counter ion that is unlikely to interfere with any ligand exchange reactions taking place at the metal centre, unlike acac^{-} , which can also act as a coordinating ligand.²⁷ Synthesis of $[\text{Rh}(\text{COD})_2]\text{BF}_4$ was performed in two steps from RhCl_3 via $[\text{RhCl}(\text{COD})]_2$ following literature procedures (Scheme 3.17).^{27,34}



Scheme 3.17. Synthesis of $[\text{Rh}(\text{COD})_2]\text{BF}_4$ from RhCl_3 .^{27,34}

Preliminary studies suggested that the reaction of $[\text{Rh}(\text{COD})_2]\text{BF}_4$ with PNP and PCNCP diphosphines proceeded selectively towards $[\text{Rh}(\text{P}^{\wedge}\text{P})_2]\text{BF}_4$ complexes regardless of whether one or two equivalents of diphosphine was added. Therefore, the synthesis of catalyst precursor $[\text{Rh}(\text{P}^{\wedge}\text{P})_2]\text{BF}_4$ complexes was performed by reacting two equivalents of diphosphines **L5**, **L11**, **L12** and **L17** with $[\text{Rh}(\text{COD})_2]\text{BF}_4$ in THF at room temperature (Scheme 3.18).



Scheme 3.18. Synthesis of $[\text{Rh}(\text{P}^{\wedge}\text{P})_2]\text{BF}_4$, where $\text{P}^{\wedge}\text{P}$ is **L5**, **L11**, **L12**, and **L17**.

Recrystallisation of $[\text{Rh}(\text{L5})_2]\text{BF}_4$ from $\text{CDCl}_3/\text{hexane}$ produced single crystals suitable for XRD analysis, which was performed in Durham by Dr T. Blundell. The molecular structure

obtained was heavily disordered, including partial oxidation ($\sim 10\%$) of the Rh^{I} centre to Rh^{III} as $[\text{RhCl}_2(\text{L5})_2]^+$ (Figure 3.7). The chloride present in the molecular structure is likely to have come from the CDCl_3 solvent during crystallisation. ^{31}P NMR spectroscopic analysis showed $[\text{Rh}(\text{L5})_2]\text{BF}_4$ as the only phosphorus-containing species, suggesting that incorporation of chloride into $[\text{Rh}(\text{L5})_2]\text{BF}_4$ incorporation may be limited to individual crystals rather than a bulk reaction. For phosphoramidite-containing complexes $[\text{Rh}(\text{L11})_2]\text{BF}_4$ and $[\text{Rh}(\text{L12})_2]\text{BF}_4$ however, complete decomposition of the compounds in CDCl_3 was observed in the time taken to run a ^{31}P NMR experiment. This suggests that the electron-withdrawing nature of the phosphoramidite ligands **L11** and **L12** relative to that of the phosphine derivatives **L5** and **L17**, increases susceptibility of $[\text{Rh}(\text{P}^\wedge\text{P})_2]\text{BF}_4$ complexes to side reaction with chlorinated solvents. Attempts to grow crystals of $[\text{Rh}(\text{P}^\wedge\text{P})_2]\text{BF}_4$ complexes from non-chlorinated solvents proved unsuccessful.

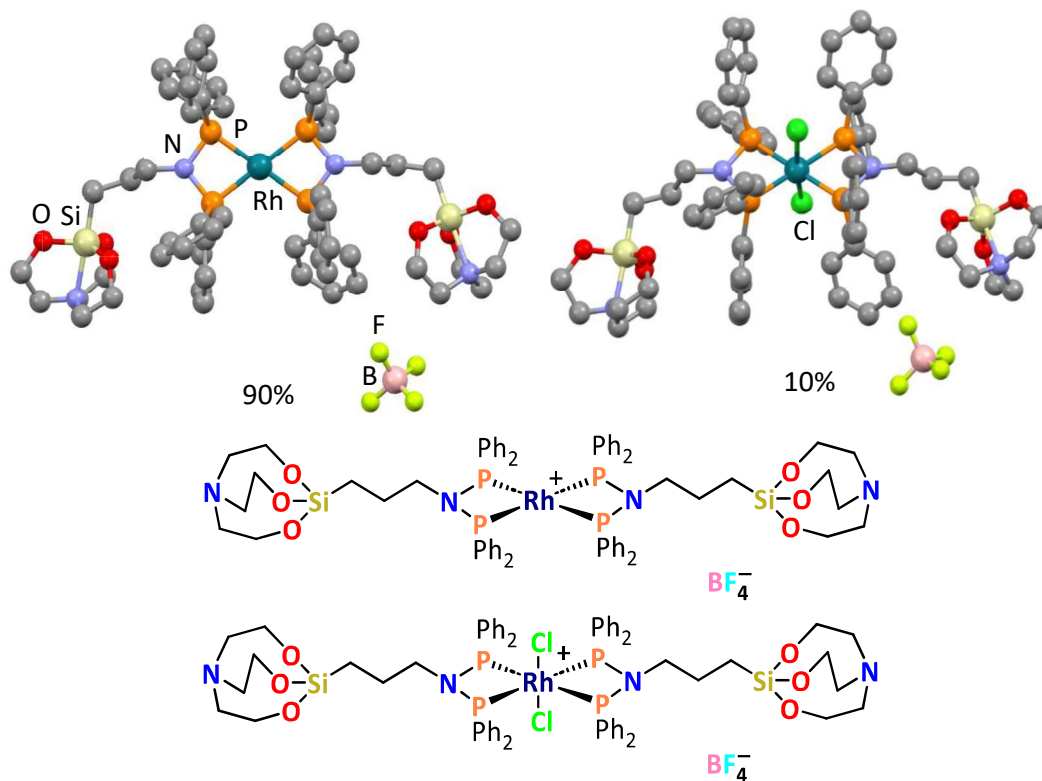
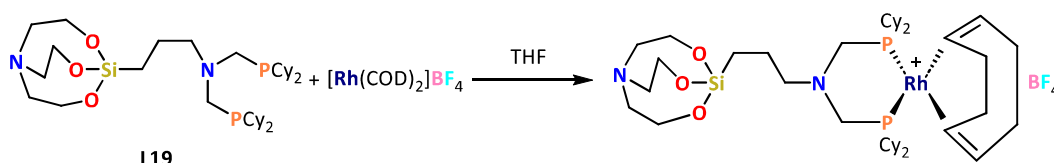


Figure 3.7. Molecular structure of $[\text{Rh}(\text{L5})_2]\text{BF}_4$ showing partial occupancy of Cl. Hydrogen atoms, 3 CDCl_3 solvent molecules and alkyl chain disorder omitted for clarity. Selected bond lengths / Å: Rh-P 2.283(1), 2.287(1), 2.276(1), 2.279(1); P-N 1.694(4), 1.699(3), 1.692(3), 1.702(4); Selected bond angles / °: P-Rh-P 70.23(4), 70.06(4); P-N-P 100.4(2), 101.5(2).

3.3.9 Synthesis of $[\text{Rh}(\text{L19})(\text{COD})]\text{BF}_4$

Contrary to the reactivity of diphosphine ligands with $[\text{Rh}(\text{COD})_2]\text{BF}_4$ described in Section 3.3.8, ligand **L19** reacts with $[\text{Rh}(\text{cod})_2]\text{BF}_4$ to selectively produce $[\text{Rh}(\text{L19})(\text{COD})]\text{BF}_4$, even when multiple equivalents of ligand **L19** are employed (Scheme 3.19). This reactivity is consistent with that observed for **L19** with $\text{Rh}(\text{acac})(\text{CO})_2$, where $\text{Rh}(\text{L19})(\text{acac})$ selectively formed and no bis(diphosphine) species were observed. The origin of the different reactivity of **L19** with rhodium(I) complexes relative to that of **L5**, **L11**, **L12**, and **L17** is not well understood, but possibly due to the unique phosphine steric and electronic character of **L19**, as discussed in Section 3.3.2.



Scheme 3.19. Synthesis of $[\text{Rh}(\text{L19})(\text{COD})]\text{BF}_4$.

Recrystallisation of $[\text{Rh}(\text{L19})(\text{COD})]\text{BF}_4$ from PhCl /petroleum ether resulted in crystals suitable for XRD analysis, which was performed in Durham by Dr T. Blundell (Figure 3.8). The molecular structure of $[\text{Rh}(\text{L19})(\text{COD})]\text{BF}_4$ shows a P-Rh-P bite angle of $91.56(2)^\circ$ and P-Rh bond length of $2.3115(6) \text{ \AA}$, in good agreement with other PCNCP metal coordination in the literature (for rhodium(I) and palladium(II) complexes).^{35–37} Additionally, the average COD C=C bond length of $1.380(3) \text{ \AA}$ and Rh-C bond length of $2.226(2) \text{ \AA}$ fall within an expected range for COD coordinated to a rhodium(I) centre.³⁸

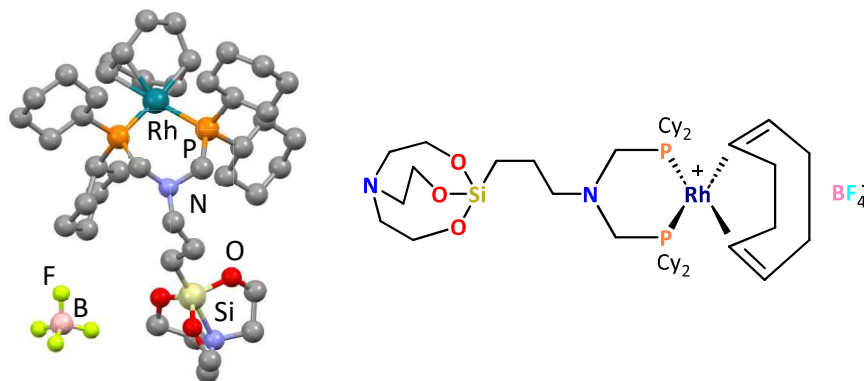


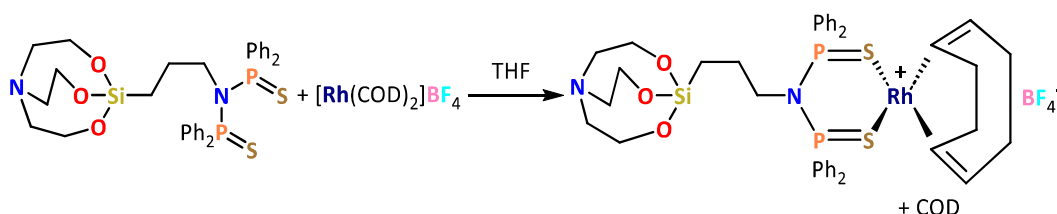
Figure 3.8. Molecular structure of $[\text{Rh}(\text{L19})(\text{COD})]\text{BF}_4$ showing partial occupancy of Cl.

Hydrogens, 3 CDCl_3 solvent molecules and alkyl chain disorder omitted for clarity.

Selected bond lengths / \AA : Rh-P 2.2992(5), 2.3236(6); Rh-C 2.240(2), 2.185(2), 2.204(2), 2.273(2); C=C 1.377(3), 1.382(3); selected bond angles / $^\circ$: P-Rh-P 91.56(2).

3.3.10 Synthesis of $[\text{Rh}(\text{L5S}_2)(\text{COD})]\text{BF}_4$

While parent phosphine, **L5**, reacts with $[\text{Rh}(\text{COD})_2]\text{BF}_4$ displacing both equivalents of COD to produce $[\text{Rh}(\text{L5})_2]\text{BF}_4$ (See Section 3.3.8), diphosphine disulfide, **L5S₂**, was found to react with $[\text{Rh}(\text{COD})_2]\text{BF}_4$, following an adapted literature procedure, to produce selectively $[\text{Rh}(\text{L5S}_2)(\text{COD})]\text{BF}_4$ (Scheme 3.20).³⁹ The $^{31}\text{P}\{^1\text{H}\}$ NMR spectra of $[\text{Rh}(\text{L5S}_2)(\text{COD})]\text{BF}_4$ in solution shows a doublet at +66 ppm ($^2J_{\text{RhP}} = 4.2$ Hz), relative to the free ligand at +69 ppm.



Scheme 3.20. Synthesis of $[\text{Rh}(\text{L5S}_2)(\text{COD})]\text{BF}_4$.

Crystals of $[\text{Rh}(\text{L5S}_2)(\text{COD})]\text{BF}_4$ suitable for XRD analysis were obtained from a solution of CDCl_3 layered with hexane; crystallography was performed by Dr T. Blundell in Durham. The molecular structure of $[\text{Rh}(\text{L5S}_2)(\text{COD})]\text{BF}_4$ (Figure 3.9) shows a S-Rh-S bite angle of $96.14(2)^\circ$, slightly larger than the PCNCP bite angle in $[\text{Rh}(\text{L19})(\text{COD})]\text{BF}_4$ of $91.56(2)^\circ$. The average Rh-S bond length of $2.3718(7)$ Å is in good agreement with those of representative compounds reported in the literature.⁴⁰

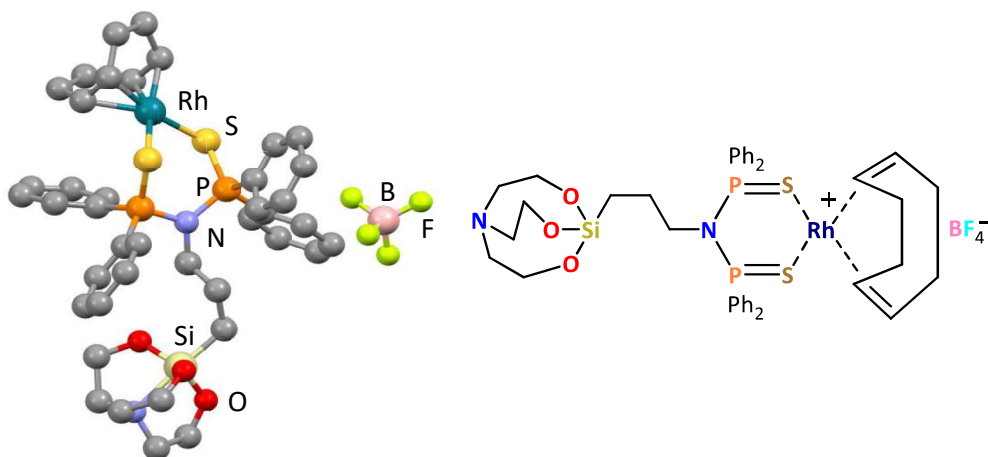


Figure 3.9. Molecular structure of $[\text{Rh}(\text{L5S}_2)(\text{COD})]\text{BF}_4$. Alkyl chain disorder omitted for clarity. Selected bond lengths / Å: Rh-S 2.3775(6), 2.3661(7); Rh-C 2.11(1), 2.12(1), 2.17(1), 2.15(1); C=C 1.40(2), 1.38(2); P-S 2.0006(7), 1.9804(8); P-N 1.694(2), 1.680(2); Selected bond angles / °: S-Rh-S 96.14(2); P-N-P 120.6(1).

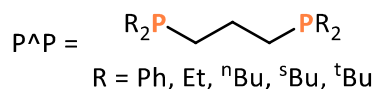
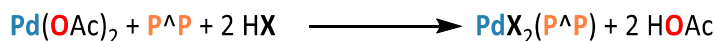
3.4 Investigation into the coordination chemistry of tetherable phosphines with cobalt(II) and palladium(II)

During the course of this PhD project the price of rhodium metal reached an all-time high of \$28,775 per troy ounce on the 30/04/21.⁴¹ The extremely high cost of rhodium was one of the key driving forces behind this project's research and development of immobilised hydroformylation catalysts that may benefit from easier catalyst separation and recycling relative to currently operated homogenous hydroformylation industrial processes. Maximising catalyst lifetime by employing more efficient catalyst recycling processes should result in a more cost-effective catalytic process, that becomes increasingly financially appealing as the price of rhodium increases. Another potential method for reducing the cost of hydroformylation catalysts could be the application of potentially cheaper alternative metals, such as palladium or cobalt. To this end, the coordination chemistry of small bite angle ligands with palladium(II) and cobalt(II) precursors was investigated for potential later application in hydroformylation catalysis.

3.4.1 Literature phosphine-containing palladium hydroformylation catalysts

Despite very early work demonstrating its viability, hydroformylation using palladium catalysts has not been widely investigated.²¹ As the price of palladium is significantly lower than rhodium (Pd = \$967/troy oz and Rh = \$4725/troy oz on 03/05/24), development of a high-performance palladium hydroformylation catalyst could potentially result in a more cost-effective catalyst than is possible with rhodium, if high catalyst activity and selectivity could be achieved.⁴¹ Historically, the activity of palladium complexes in hydroformylation was thought to be low and not industrially relevant due to the poor performance of palladium carbonyl complexes in hydroformylation.²¹ However, more recent work by Drent *et al.* showed that modification of palladium(II) carbonyl complex catalysts with phosphine ligands and non-coordinating anions led to significantly improved catalyst performance in terms of activity and selectivity.⁴² Drent *et al.* prepared a range of palladium hydroformylation catalysts *in situ* by reaction of palladium(II) acetate with different bidentate phosphines and acids (Scheme 3.21). The effect of catalyst structure on hydroformylation catalysis was then investigated for a number of different alkene substrates (results of octene hydroformylation summarised

in Table 3.4). Of specific interest was the role of phosphine ligand steric and electronic character, as well as acid strength and coordination behaviour on hydroformylation catalysis performance.



*Scheme 3.21. In situ synthesis of PdX₂(P[∧]P) hydroformylation catalysts where HX can be CH₃COOH, CF₃COOH, CF₃SO₃H, CH₃SO₃H, (CH₃)₃CSO₃H or *p*-CH₃C₆H₄SO₃H.⁴²*

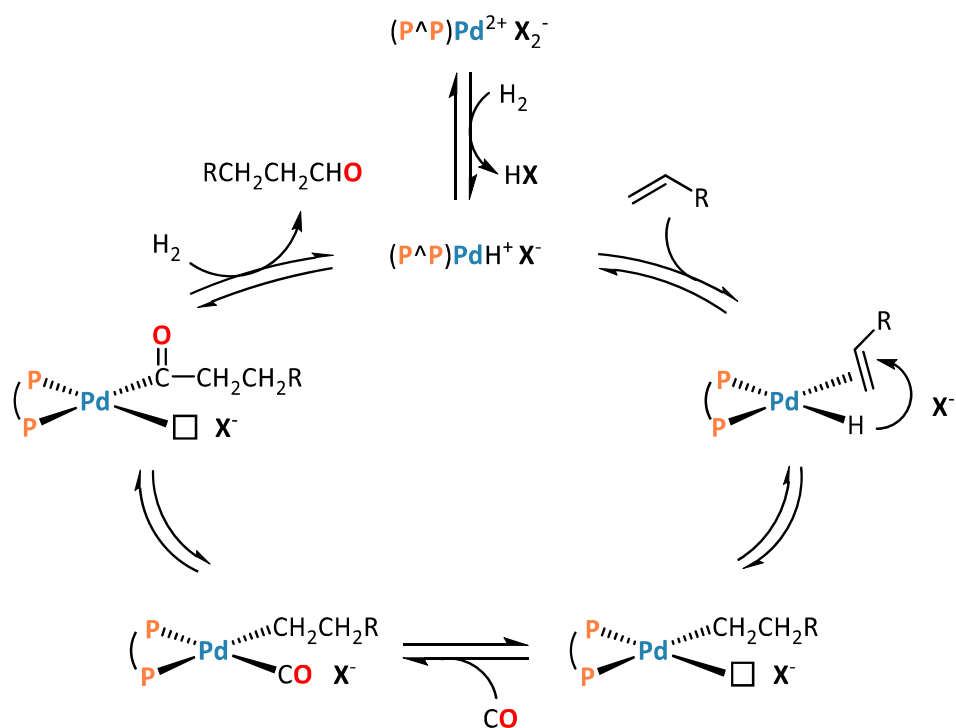
Table 3.4. 1-Octene hydroformylation using PdX₂(P[∧]P) catalysts described by Drent et al. and summarised in Scheme 3.21.⁴²

P [∧] P Ligand	Acid	T (°C)	Rate / mol mol ⁻¹ h ⁻¹	Solvent	Products (%)		
					aldehyde	alcohol	ketone
R = Ph	CF ₃ COOH	125	100	Diglyme	98	0	trace
R = ⁿ Bu	CF ₃ COOH	90	60	Diglyme	96	0	trace
	<i>p</i> -CH ₃ C ₆ H ₄ SO ₃ H	90	100	Diglyme	80	5	10
	<i>p</i> -CH ₃ C ₆ H ₄ SO ₃ H	125	120	Diglyme	3	93	trace
	<i>p</i> -CH ₃ C ₆ H ₄ SO ₃ H	125	100	Methanol	0	0	95
	CF ₃ SO ₃ H	125	80	Diglyme	0	0	98
R = ^s Bu	CF ₃ COOH	115	100	Diglyme	96	2	trace
	<i>p</i> -CH ₃ C ₆ H ₄ SO ₃ H	125	150	Diglyme	3	95	trace
	CF ₃ SO ₃ H	125	40	Diglyme	0	0	98

20 ml octene, 0.25 mmol Pd(OAc)₂, 0.6 mmol ligand, 1 mmol acid. 45 ml solvent, P_{CO} = P_{H₂} = 30 bar (at room temperature). Rates averaged over <30% olefin conversion.

The hydroformylation selectivity data summarised in Table 3.4 show that tuning of the catalyst system can have a large effect on the reaction chemoselectivity. Interestingly, the desired high selectivity for aldehydes is generally favoured with increasing phosphine basicity and utilisation of weaker acids.⁴² However, by changing the catalyst or reaction conditions it was shown that selectivity towards alcohols *via in situ* reduction or ketones *via* hydroacylation could also be achieved. Bidentate phosphines were found

to be essential for these systems, with use of monodentate phosphines resulting in no catalytic activity. The aldehyde regioselectivity was found to be dependent on catalyst composition, with increasing phosphine steric bulk and weaker acids favouring linear aldehyde production. A maximum linear aldehyde selectivity of $n/iso = 5$ was observed using phosphine DsBPP (di-secbutyl-1,3-bisphosphinopropane) and trifluoroacetic acid during the hydroformylation of propene under the same conditions as those described in Table 3.4.⁴²



Scheme 3.22. Proposed mechanism for palladium-catalysed hydroformylation using $PdX_2(P^A P)$ complexes modified from the work of Drent *et al.*⁴²

The active hydroformylation catalyst species studied by Drent *et al.* is thought to be a cationic palladium(II) hydride centre, $[(P^A P)PdH]X$, formed by heterolytic splitting of dihydrogen at the electrophilic palladium centre of the $PdX_2(P^A P)$ precursors.⁴² Catalysis then proceeds by coordination of an alkene substrate followed by hydride transfer to form a palladium-alkyl intermediate (Scheme 3.22). CO ligation followed by migratory insertion then gives a palladium acyl intermediate that reacts with dihydrogen to reform the active $[(P^A P)PdH]X$ species and releasing an equivalent of aldehyde.

Building on the work by Drent *et al.*, recent studies by Dydio *et al.* have shown that PdI_2L_2 complexes, where L is a phosphine ligand, can also be used as effective catalysts precursors for propene hydroformylation.^{43–45} In these experiments two equivalents of monophosphine, or one equivalent of diphosphine, were reacted with PdI_2 *in situ* in aromatic solvents such as anisole or toluene under a pressure of syngas (CO/H_2 :20/80 bar) resulting in the formation of $[\text{PdH}(\text{L}_2)]\text{I}$ active catalyst species, analogous to those used by Drent *et al.*⁴² Under these conditions the presence of iodide was shown to be vital, with other palladium precursors, such as $\text{Pd}(\text{OAc})_2$, $\text{Pd}(\text{BF}_4)_2$, $\text{Pd}(\text{acac})_2$, PdBBr_2 and PdCl_2 giving rise only to trace aldehyde formation. The identity of the phosphine ligand was also shown to play an important role in the catalysis.⁴⁵ Trialkyl monophosphine ligands with a cone angle in the range of $152 - 178^\circ$ resulted in the highest aldehyde TOFs of up to 17 h^{-1} at 100°C . Formation of the branched aldehyde was shown to be favoured with *iso/n* ratios of 1.5 – 3.5 depending on the identity of the ligand, in contrast to rhodium-catalysed hydroformylation where the linear aldehyde is generally favoured. It was shown that the *iso/n* ratio could be further improved by decreasing the reaction temperature to 80°C giving rise to *n/iso* ratios up to 40, albeit at the cost of ten-fold reduction in activity.⁴⁵ The high *iso/n* ratios reported by Dydio *et al.* when using PdI_2L_2 -based hydroformylation catalysts greatly contrast those achieved using Drent's $[(\text{P}^\wedge\text{P})\text{PdH}]\text{X}$ -based systems, where linear aldehydes were favoured. Interestingly, the phosphines required for these two processes also differ, with bulky alkyl monophosphines shown to be the most effective phosphine ligands in Dydio's PdI_2L_2 system, whereas bidentate phosphines are required for Drent's $[(\text{P}^\wedge\text{P})\text{PdH}]\text{X}$ system.

3.4.2 Synthesis of $\text{PdI}_2(\text{P}^\wedge\text{P})$ complexes

The development of $\text{PdI}_2(\text{P}^\wedge\text{P})$ complexes featuring silica-tetherable phosphine ligands for application as immobilised hydroformylation catalysts was identified as a potential method to develop more cost-effective hydroformylation catalysts than the commonly used rhodium systems. The rationale for this being the lower cost of palladium relative to rhodium and the easier recyclability of heterogeneous compared to homogeneous catalysts. $\text{PdI}_2(\text{P}^\wedge\text{P})$ complexes are advantageous for this purpose due to their facile synthesis and good stability, which has been previously exploited in the development of

homogeneous and silica-immobilised catalysts for hydroalkoxycarbonylation and Suzuki–Miyaura C–C cross-coupling reactions (Figure 3.10).^{46–48}

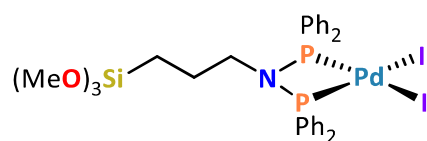
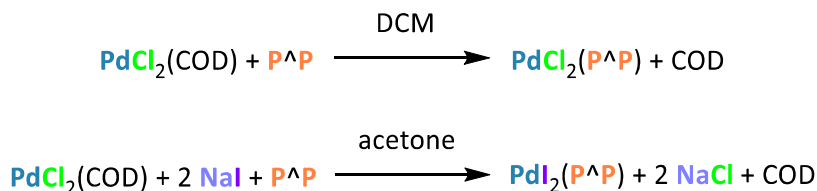


Figure 3.10. $\text{PdI}_2(\text{P}^\wedge\text{P})$ catalyst capable of silica immobilisation, developed for hydroalkoxycarbonylation and Suzuki–Miyaura C–C cross-coupling reactions.⁴⁸

As the work by Dydio *et al.* focused on the investigation of monodentate and wide bite angle bidentate ligands for PdI_2L_2 -catalysed hydroformylation, it was of interest to investigate some of the smaller bite angle ligands developed in this current work for this reaction. Additionally, palladium-catalysed hydroformylation using silica-immobilised molecular catalysts has not been attempted to the best of the author's knowledge and is of interest to this project. To this end a range of silica-tetherable $\text{PdI}_2(\text{P}^\wedge\text{P})$ complexes were prepared according to an adapted literature procedure.⁴⁹

The preparation of $\text{PdCl}_2(\text{P}^\wedge\text{P})$ complexes is simply achieved through ligand exchange starting from $\text{PdCl}_2(\text{MeCN})_2$ or $\text{PdCl}_2(\text{COD})$. Access to the required $\text{PdI}_2(\text{P}^\wedge\text{P})$ complexes was readily achieved through addition of an excess of NaI to $\text{PdCl}_2(\text{COD})$ in the presence of P^\wedgeP (Scheme 3.23).⁴⁹ Using this method $\text{PdI}_2(\text{P}^\wedge\text{P})$ complexes of **L5**, **L11**, **L12**, **L17**, **L18** and **L19** were prepared, reaching complete conversion in each case, as determined by $^{31}\text{P}\{^1\text{H}\}$ NMR spectroscopic analysis of aliquots of reaction mixture. Recrystallisation of the products from a solution of DCM or CHCl_3 layered with hexane resulted in crystals suitable for XRD analysis, which was performed at Durham University by Dr D. S. Yufit ($\text{PdI}_2(\text{L5})$, $\text{PdI}_2(\text{L11})$, $\text{PdI}_2(\text{L17})$ and $\text{PdI}_2(\text{L18})$) or Dr T. Blundell ($\text{PdI}_2(\text{L12})$ and $\text{PdI}_2(\text{L19})$) (Figure 3.11).



Scheme 3.23. Synthesis of $[\text{PdCl}_2(\text{P}^\wedge\text{P})]$ and $[\text{PdI}_2(\text{P}^\wedge\text{P})]$ complexes.

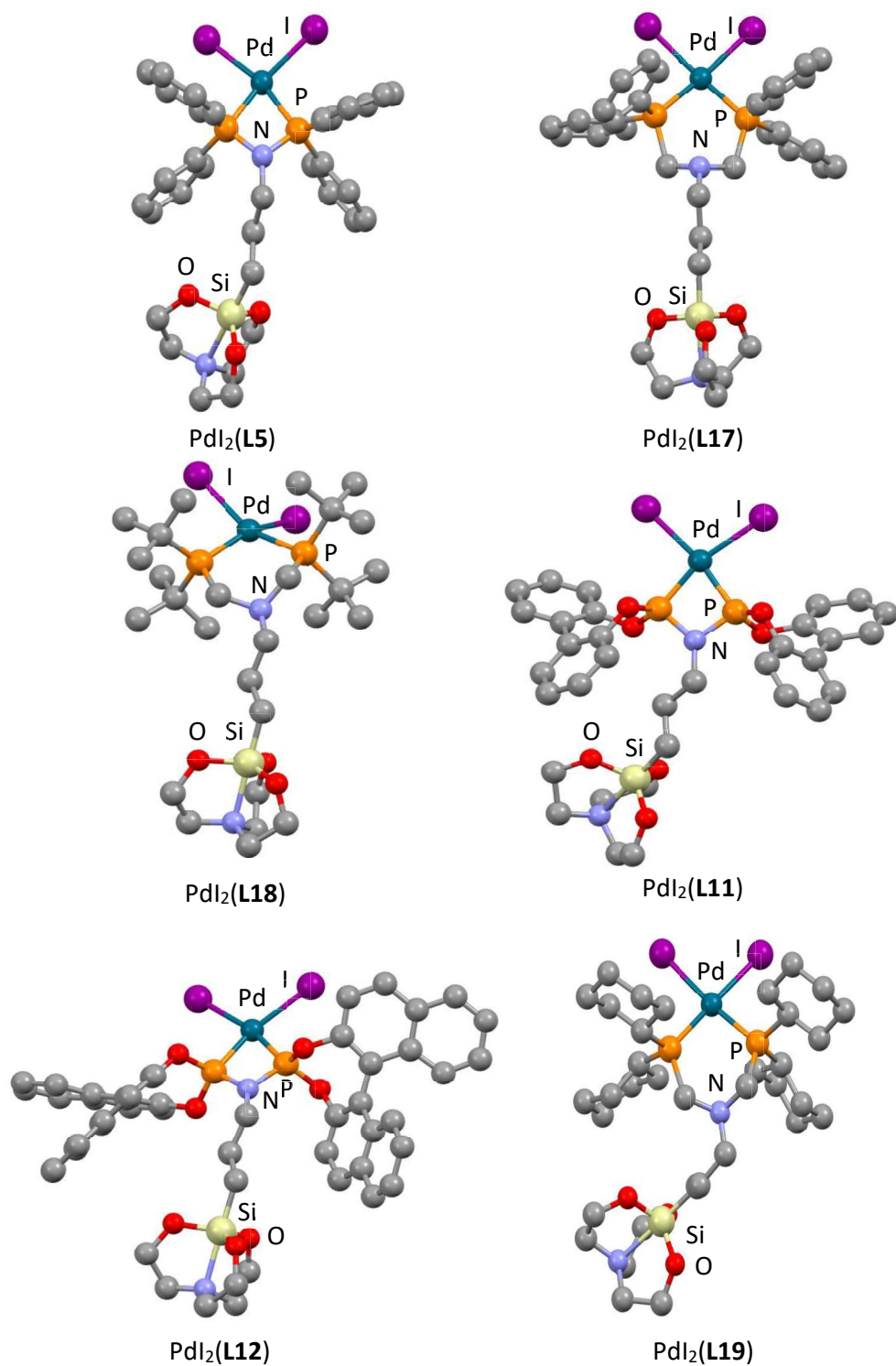


Figure 3.11. Molecular structures of $\text{PdI}_2(\text{L5})$, $\text{PdI}_2(\text{L11})$, $\text{PdI}_2(\text{L12})$, $\text{PdI}_2(\text{L17})$ and $\text{PdI}_2(\text{L18})$ and $\text{PdI}_2(\text{L19})$. Hydrogen atoms, solvent molecules and alkyl chain disorder omitted for clarity.

Table 3.5. Selected average bond lengths and angles of the $\text{PdI}_2(\text{P}^{\wedge}\text{P})$ complexes shown in Figures 3.11 and 3.12.

Complex	Pd-P bond length / Å	Pd-I bond length / Å	P-N bond length / Å	P-Pd-P angle / °	I-Pd-I angle / °	P-N-P angle / °
$\text{PdI}_2(\mathbf{L11})$	2.206(1)	2.6184(6)	1.674(3)	70.28(3)	96.67(2)	98.6(1)
$\text{PdI}_2(\mathbf{L12})$	2.210(4)	2.628(2)	1.68(1)	70.3(1)	99.86(5)	99.1(6)
$\text{PdI}_2(\mathbf{L5})$	2.232(1)	2.6449(6)	1.6905(2)	71.16(2)	96.07(2)	100.37(8)
$\text{PdI}_2(\mathbf{L17})$	2.261(1)	2.6447(3)	-	94.74(3)	92.12(1)	-
$\text{PdI}_2(\mathbf{L19})$	2.277(2)	2.6710(8)	-	93.64(7)	88.31(2)	-
$\text{PdI}_2(\mathbf{L18})$	2.320(1)	2.692(2)	-	95.78(5)	86.95(4)	-
$\mathbf{C1}^{47}$	2.2281(14)	2.6304(5)	1.699(4)	71.73(7)	96.04(2)	100.4(3)
$\mathbf{C2}^{50}$	2.277(3)	2.652(3)	-	94.82(9)	91.50(8)	-

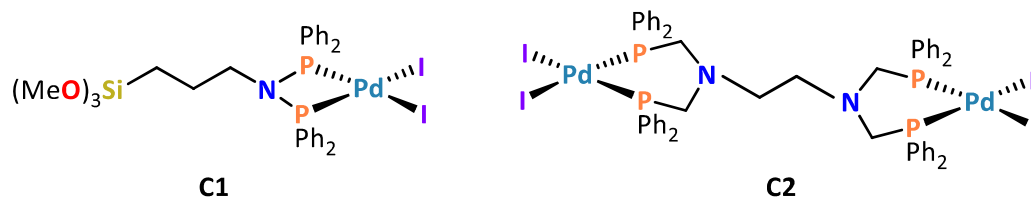


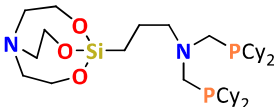
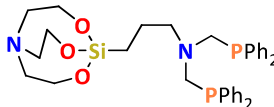
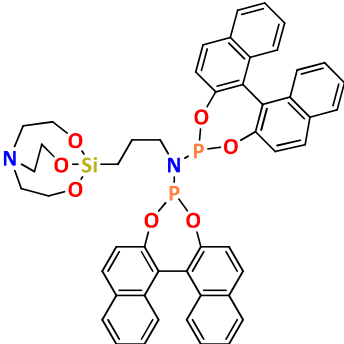
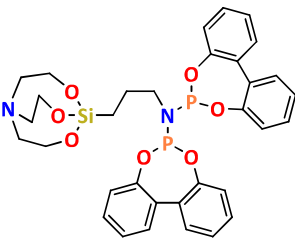
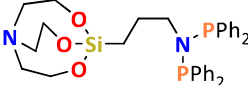
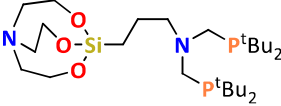
Figure 3.12. Structures of literature $\text{PdI}_2(\text{P}^{\wedge}\text{P})$ complexes **C1** and **C2**.

A comparison of the metric parameters of the various $\text{PdI}_2(\text{P}^{\wedge}\text{P})$ complexes shown in Figure 3.11 reveals that each complex has Pd-P bond length in the range of 2.206(1) to 2.320(1) Å, which is in good agreement with reported literature values (Table 3.5).^{47,50–52} The variation in the Pd-P bond distances correlates well with the values of $|^1J_{\text{SeP}}|$ determined for the diselenide derivatives of the parent diphosphine ligands (see Section 3.2): there is a decrease in Pd-P bond distance as the phosphine becomes more electron-deficient. The only outlier to this trend is $\text{PdI}_2(\mathbf{L18})$, which has a longer Pd-P bond length than $\text{PdI}_2(\mathbf{L19})$ despite the slightly less electron rich nature of the parent phosphine ($|^1J_{\text{SeP}}|$: 688 Hz ($\mathbf{L19}(\text{Se})_2$) vs 684 Hz ($\mathbf{L18}(\text{Se})_2$). This deviation is likely to be due to the increased steric bulk of **L18** relative to **L19** resulting in weaker coordination and hence elongated Pd-P bond distance.

Also of interest are the P-Pd-P bite angles of the $\text{PdI}_2(\text{P}^{\wedge}\text{P})$ complexes. The PNP-ligated palladium centres have bite angles of 70–71° typical for PNP coordination to

palladium.^{47,53} In contrast, the PCNCP ligands have larger P-Pd-P bite angles of 93-95° typical for these types of ligand.³⁶ Contrary to predication, there is no obvious trend in P-Pd-P bite angle for the PCNCP complexes according to phosphine electronic character or steric bulk, although the difference in angle between the three complexes is small when the error of the measurement is taken into account. This suggests that another factor is the cause of the observed differences in P-Pd-P bite angle of the PCNCP complexes; PdI₂(**L17**) (94.74(3)°), PdI₂(**L18**) (95.78(5)°) and PdI₂(**L18**) (93.64(7)°). Indeed, although d⁸ square planar geometry is expected for the palladium(II) metal centre, distortion of the square planar geometry can be seen in some of the structures. This distortion was calculated by measuring the angle between the P-Pd-P and I-Pd-I planes in each structure, as shown for PdI₂(**L18**) in Figure 3.13 (Table 3.6).

Table 3.6. Distortion from ideal square planar geometry of [PdI₂(P[^]P)] complexes.

Complex (Ligand shown)	Square planar distortion / °	Complex (Ligand shown)	Square planar distortion / °
PdI ₂ (L19) 	2.4	PdI ₂ (L17) 	7.5
PdI ₂ (L12) 	5.2	PdI ₂ (L11) 	2.4
PdI ₂ (L5) 	11.0	PdI ₂ (L18) 	35.2
PdBr ₂ (BINAP) ⁵⁴	30.9	PdCl ₂ (dtbpp) ⁵⁵	24.7

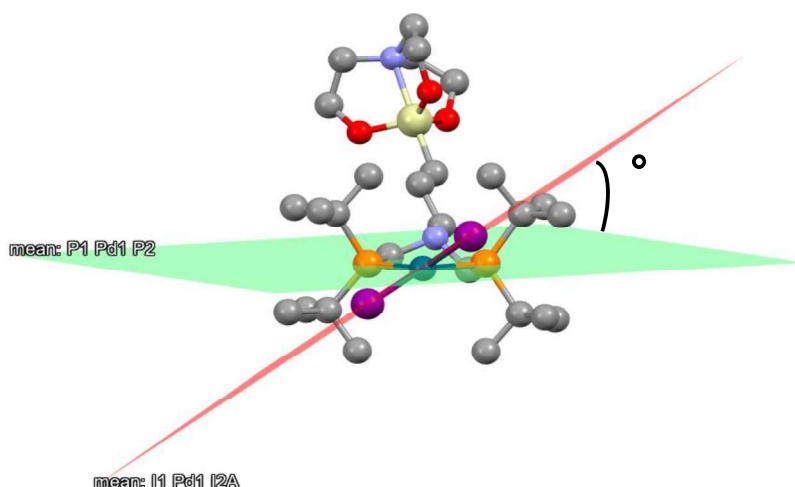


Figure 3.13. Molecular structure of $\text{PdI}_2(\text{L18})$, showing P-Pd-P (green) and I-Pd-I (red) planes used to calculate square planar distortion.

In particular, complex $\text{PdI}_2(\text{L18})$ (Figure 3.13) shows a very large distortion from square planar geometry of 35.2° , the largest of any $[\text{PdI}_2(\text{P}^{\wedge}\text{P})]$ type complexes in the CSD, where the largest value found was 30.9° for the complex $[\text{PdBr}_2(\text{BINAP})]$ (CSD refcode: POPZIE).⁵⁴ Another useful literature comparison is the complex $\text{PdCl}_2(\text{dtbpp})$ (CSD refcode: WUMKAR).⁵⁵ Since dtbpp (Figure 3.14) has a very similar structure to **L18** with respect to phosphorus environment, similar coordination properties of the two ligands would be expected, with $\text{PdCl}_2(\text{dtbpp})$ also producing a large square planar distortion of 24.7° . The $\sim 10^\circ$ difference in square planar distortion for these two complexes is likely therefore due to the identity of the halide substituents. As the iodide ligands in $\text{PdI}_2(\text{L18})$ are much larger than the chloride ligands in $\text{PdCl}_2(\text{dtbpp})$, this could lead to a greater degree of distortion from ideal square planar geometry due to the increased steric demand when these ligands are present (ionic radii $\text{I}^- = 2.2$, $\text{Br}^- = 1.96$, $\text{Cl}^- = 1.81$).¹⁵ Indeed, this is further supported by the fact that $\text{PdBr}_2(\text{BINAP})$ has an intermediate value of square planar distortion at 30.9° (although this a less ideal comparison due to the additional differences in phosphine ligand structure).

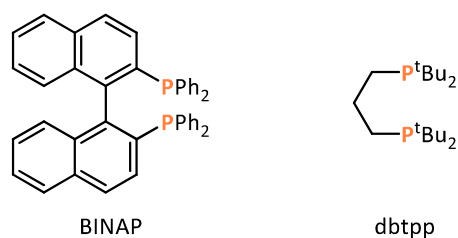


Figure 3.14. Chemical structures of BINAP and dbtpp.

The origin of the square planar distortion is further evidenced from the space filling model of the molecular structure of $\text{PdI}_2(\text{L18})$ (Figure 3.15), which clearly shows methyl fragments of the phosphine ^tBu groups taking up space in the P-Pd-P plane and forcing the iodide ligands to distort away from ideal square planar geometry. This is also supported by the computed steric maps displayed in Section 3.2.2 that corroborate these findings.

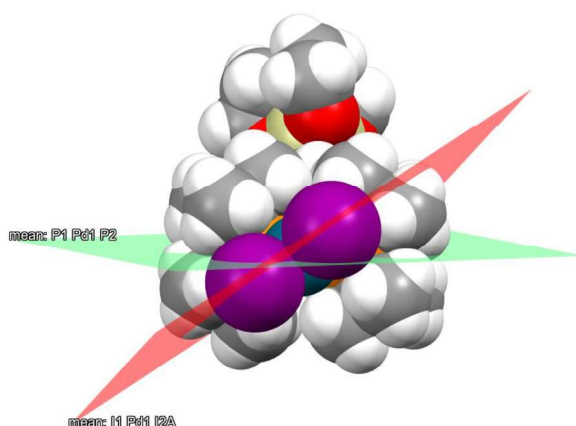


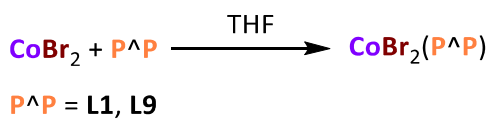
Figure 3.15. Space filling molecular structure model of $\text{PdI}_2(\text{L18})$, showing P-Pd-P (green) and I-Pd-I (red) planes used to calculate square planar distortion.

3.4.3 CoBr_2 reactivity study with PNP ligands

As discussed in Chapter 1, cobalt complexes are frequently used in hydroformylation catalysis for certain applications, particularly when *in situ* reduction of the resultant aldehyde products to alcohols is required.⁵⁶ The coordination chemistry of the small bite angle $\text{P}^{\wedge}\text{P}$ type ligands relevant to this work with cobalt is poorly explored and understood, particularly with PNP ligands, although other small bite angle ligands, such as dpmm, have been used successfully in cobalt-catalysed hydrovinylations reactions, for

example.⁵⁷ Therefore, a small reactivity study of cobalt(II) halides with some of the tetherable PNP ligands produced in this work was performed in line with other ongoing work in the Dyer research group.

PNP ligands **L1** and **L9** were selected for a small reactivity study with CoBr₂ due to their small bite angles and varying phosphine electronic characters. This would facilitate a comparison in reactivity of the more electron rich aminophosphine **L1** and electron poor phosphoramidite **L9**, upon reaction with CoBr₂. Synthesis of complexes CoBr₂(**L1**) and CoBr₂(**L9**), shown in Scheme 3.24, was performed by stirring of a solution of CoBr₂ and **L1** or **L9** overnight in THF at ambient temperature. Upon mixing the solutions, they immediately changed colour from blue to a dark green/brown, suggesting facile coordination of the PNP ligands. Single crystals suitable for XRD were obtained from a solution of CoBr₂(**L1**) in chlorobenzene layered with hexane; structure determination performed by Dr A. Batsanov at Durham University (Figure 3.16).



Scheme 3.24. Synthesis of CoBr₂(**L1**) and CoBr₂(**L9**).

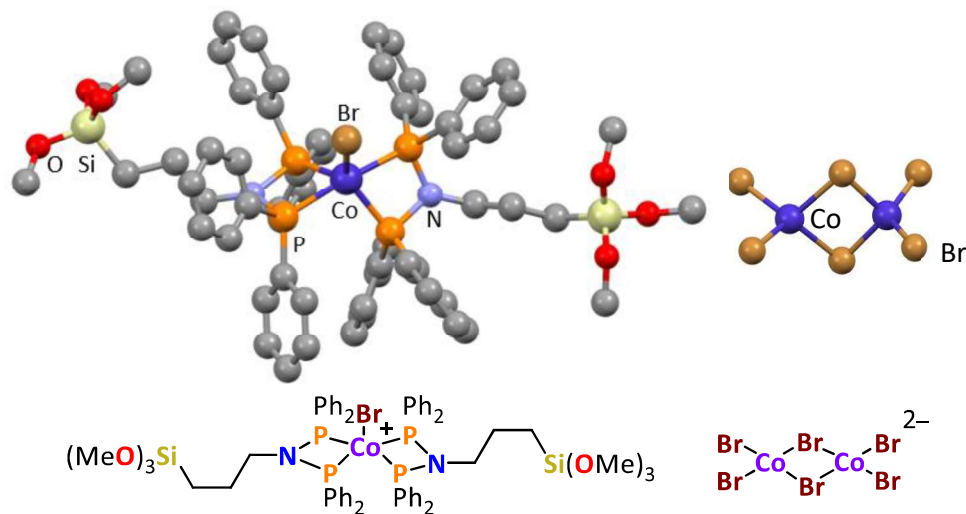


Figure 3.16. Molecular structure of CoBr₂(**L1**). Hydrogens and alkyl chain disorder have been omitted for clarity. Selected bond lengths / Å: Co-Br 2.3600(6); P-Co 2.278(1), 2.244(1), 2.223(1), 2.234(1); P-N 1.804(7), 1.734(6), 1.685(3), 1.700(4); selected bond angles / °: P-Co-P 71.24(4), 71.33(4); P-N-P 96.2(3), 100.3(2).

The molecular structure of $\text{CoBr}_2(\mathbf{L1})$ was determined to be a $\text{Co}^{\text{II}} 1^+$ cation coordinated by two molecules of $\mathbf{L1}$ and Br^- in a distorted trigonal bipyramidal geometry. The anionic charge is balanced by a strained $\text{Co}_2\text{Br}_6^{2-}$ anion in a (cation:anion) 2:1 ratio. Minor disorder was observed in the alkyl chain of one of the cobalt-bound PNP ligands. These types of complex have been verified in other, as yet unpublished, work in the Dyer group for different $\text{CoBr}_2(\text{PNP})$ complexes.⁵⁸ The observed ionic structure of $[\text{CoBr}(\mathbf{L1})_2]_2[\text{Co}_2\text{Br}_6]$ clearly differs from the expected simple molecular structure that would result from 1:1 coordination of a bidentate ligand with a CoBr_2 fragment, which has been reported for other wider bite angle P^P ligands with cobalt halides.^{59–61} The origin of this differing reactivity is likely a function of P^P bite angle, again showing the unique reactivity of small bite angle PNP ligands. In the complex $[\text{CoBr}(\mathbf{L1})_2]_2[\text{Co}_2\text{Br}_6]$, the average PNP bite angle was measured to be $71.29(4)^\circ$, a typical PNP ligand bite angle.⁶² As cobalt(II) is paramagnetic, these complexes cannot be readily characterised by NMR spectroscopy, making characterisation and structure elucidation of these complexes more challenging. Unfortunately, crystals of $\text{CoBr}_2(\mathbf{L2})$ suitable for SXRD analysis could not be obtained, making a comparison of the structure of $[\text{CoBr}(\mathbf{L1})_2]_2[\text{Co}_2\text{Br}_6]$ and $\text{CoBr}_2(\mathbf{L2})$ very difficult from FT-IR spectroscopy and CHN elemental analysis alone.

The two distinct cobalt environments in $[\text{CoBr}(\mathbf{L1})_2]_2[\text{Co}_2\text{Br}_6]$ means that this complex would not be well suited to catalysis. Immobilisation of this complex would also be challenging, since only the cations can be covalently anchored to an oxide support, while $\text{Co}_2\text{Br}_6^{2-}$ anions would be associated by electrostatic forces. However, this does allow the possibility of ion-exchanging the $\text{Co}_2\text{Br}_6^{2-}$ anions with a non metal-containing anion, such as BF_4 so that only one cobalt environment is present in the complex.

The challenges of employing $[\text{CoBr}(\mathbf{L1})_2]_2[\text{Co}_2\text{Br}_6]$ as a catalyst were partially addressed by Adam Carrick working in the Dyer group, who successfully prepared $[\text{Co}(\text{P}^{\wedge}\text{P})_2]\text{BAR}^{\text{F}_4}$ complexes.⁵⁸ As $[\text{Co}(\text{P}^{\wedge}\text{P})_2]\text{BAR}^{\text{F}_4}$ complexes have a cobalt(I) centre analogous to the rhodium(I) centre in the $[\text{Rh}(\text{P}^{\wedge}\text{P})_2]\text{BF}_4$ complexes described in Section 3.3.8, the hydroformylation catalyst performance of these complexes was investigated as part of this work. To this end, a sample of the complex $[\text{Co}((\text{PPh}_2)_2\text{NCH}_2\text{CH}_2\text{Ph})_2]\text{BAR}^{\text{F}_4}$ was acquired and subsequently investigated as a catalyst for 1-octene hydroformylation (for

test conditions see Section 5.2). Unfortunately, no catalytic activity was observed. Subsequent studies performed by Carrick suggest that this is due to the formation of a stable $[\text{Co}(\text{P}^{\wedge}\text{P})_2(\text{CO})]\text{BAr}^{\text{F}}_4$ complex under syngas and test conditions employed.⁵⁸ As a result of these findings further investigations into cobalt oxo chemistry with small bite angle ligands were not performed as part of this work.

3.5 Chapter 3 summary

In this chapter the coordination chemistry of the tether-modified ligands reported in Chapter 2 was investigated with hydroformylation-relevant metals rhodium, cobalt and palladium, in addition to non-metal selenium.

Phosphine selenides of the diphosphine ligands were prepared and their resulting $|^1J_{\text{SeP}}|$ coupling constants used to assess the electronic character of their parent diphosphines. As expected, the diphosphite ligand **L21** is the most electron deficient, while the alkyl diphosphines **L18** and **L19** are the most electron rich. The investigation into ligand electronic character was combined with a study of their steric demands performed using the SambVca 2.1 web tool to calculate percent buried volumes ($\%V_{\text{Bur}}$) and steric maps, from X-ray crystallographic data.

$\text{Rh}(\text{acac})(\text{L19})$ was synthesised as a hydroformylation catalyst precursor by reaction of **L19** with $\text{Rh}(\text{acac})(\text{CO})_2$. In contrast, the reaction of ligands **L1**, **L9**, **L13**, **L21** and **L23** with $\text{Rh}(\text{acac})(\text{CO})_2$ or $\text{Rh}(\text{acac})(\text{COD})$ gave a mixture of products that could not be purified. The selectivity of these reactions could be maximised to $\approx 90\%$ by dropwise addition of the ligand to metal at -78°C in THF. Unlike the synthesis of $\text{Rh}(\text{acac})(\text{P}^{\wedge}\text{P})$ complexes, the synthesis of $[\text{Rh}(\text{P}^{\wedge}\text{P})_2]\text{acac}$ complexes was shown to proceed selectively at room temperature for ligand **L5** when two equivalents of phosphine were added to $\text{Rh}(\text{acac})(\text{CO})_2$. It was found that the stability of the rhodium complexes improved when the acac counter-anion was substituted for BF_4^- and therefore $[\text{Rh}(\text{COD})_2]\text{BF}_4$ was selected as a preferred rhodium salt to generate the diphosphine-modified catalyst precursors for hydroformylation. The $[\text{Rh}(\text{P}^{\wedge}\text{P})_2]\text{BF}_4$ complexes where $\text{P}^{\wedge}\text{P} = \text{L5}, \text{L11}, \text{L12}$ or **L17** were produced from $[\text{Rh}(\text{COD})_2]\text{BF}_4$ and the parent ligand. Again, **L19** showed differing reactivity to the other ligands investigated and selectively formed

[Rh(**L19**)(COD)]BF₄ when reacted with [Rh(COD)₂]BF₄, regardless of the Rh:P stoichiometry. A hydroformylation catalyst precursor featuring a sulfur ligand was also prepared by reaction of [Rh(P[^]P)₂]BF₄ with **L5S₂** to produce [Rh(**L5S₂**)(COD)]BF₄.

With a view to preparing tetherable palladium hydroformylation catalysts, the PdI₂(P[^]P) complexes of **L5**, **L11**, **L12**, **L17**, **L18** and **L19** were also prepared, and their structures analysed by XRD crystallography.

A brief reactivity study of CoBr₂ with **L1** and **L9** was performed to assess the potential to produce tetherable cobalt phosphine complexes for applications in hydroformylation. The reaction of CoBr₂ with **L1** gave the complex [CoBr(**L1**)₂]₂[Co₂Br₆] rather than the expected CoBr₂(**L1**), as determined by XRD analysis. [CoBr(**L1**)₂]₂[Co₂Br₆] was disregarded for future applications in catalysis due to the presence of two cobalt environments in the complex. Meanwhile, the complex [Co(PPh₂)₂NCH₂CH₂Ph]₂BARF₄ was shown to be inactive for the catalysis of 1-octene hydroformylation.

3.6 Chapter 3 references

1. D. W. Allen and B. F. Taylor, *Dalton Trans.*, 1982, 51–54, DOI: 10.1039/DT9820000051.
2. F. Wossidlo, D. S. Frost, J. Lin, N. T. Coles, K. Klimov, M. Weber, T. Böttcher and C. Müller, *Chem. Eur. J.*, 2021, **27**, 12788–12795, DOI: 10.1002/chem.202102390.
3. W. Mcfarlane and D. S. Rycroft, *Dalton Trans.*, 1973, 2162–2166, DOI: 10.1039/DT9730002162.
4. A. Lee, S. Ahn, K. Kang, M. S. Seo, Y. Kim, W. Y. Kim and H. Kim, *Org. Letters*, 2014, **16**, 5490–5493, DOI: 10.1021/ol502772m.
5. T. S. Venkatakrishnan, S. S. Krishnamurthy and M. Nethaji, *J. Organomet. Chem.*, 2005, **690**, 4001–4017, DOI: 10.1016/j.jorganchem.2005.05.041.
6. N. Biricik, F. Durap, C. Kayan, B. Gümgüm, N. Gürbüz, I. Özdemir, W. H. Ang, Z. Fei and R. Scopelliti, *J. Organomet. Chem.*, 2008, **693**, 2693–2699, DOI: 10.1016/j.jorganchem.2008.05.010.
7. Q. Zhang, G. Hua, P. Bhattacharyya, A. M. Z. Slawin and J. D. Woollins, *Eur. J. Inorg. Chem.*, 2003, 2426–2437, DOI: 10.1002/ejic.200300037.
8. A. Phanopoulos, A. J. P. White, N. J. Long and P. W. Miller, *Dalton Trans.*, 2016, **45**, 5536–5548, DOI: 10.1039/c6dt00170j.
9. A. Börner and R. Franke, *Hydroformylation: Fundamentals, Processes, and Applications in Organic Synthesis*, Wiley-VCH Verlag GmbH & Co. KGaA, Weinheim, 2nd Ed., 2016.

10. R. Franke, D. Selent and A. Börner, *Chem. Rev.*, 2012, **112**, 5675–5732, DOI: 10.1021/cr3001803.
11. C. A. Tolman, *Chem. Rev.*, 1977, **77**, 313–348, DOI: 10.1021/cr60307a002.
12. L. Falivene, Z. Cao, A. Petta, L. Serra, A. Poater, R. Oliva, V. Scarano and L. Cavallo, *Nat. Chem.*, 2019, **11**, 872–879, DOI: 10.1038/s41557-019-0319-5.
13. A. Poater, B. Cosenza, A. Correa, S. Giudice, F. Ragone, V. Scarano and L. Cavallo, *Eur. J. Inorg. Chem.*, 2009, **2009**, 1759–1766, DOI: 10.1002/ejic.200801160.
14. H. Clavier and S. P. Nolan, *Chem. Commun.*, 2010, **46**, 841–861, DOI: 10.1039/b922984a.
15. R. D. Shannon, *Acta Cryst.*, 1976, **32**, 751, DOI: 10.1107/S0567739476001551.
16. G. W. V. Cave, W. Errington and J. P. Rourke, *Acta Cryst.*, 1999, **55**, 320–322, DOI: 10.1107/S0108270198015868.
17. Y. Jiao, M. S. Torne, J. Gracia, J. W. Niemantsverdriet and P. W. N. M. Van Leeuwen, *Catal. Sci. Technol.*, 2017, **7**, 1404–1414, DOI: 10.1039/c6cy01990k.
18. N. Fey, *Chem. Cent. J.*, 2015, **9**, 38, DOI: 10.1186/s13065-015-0104-5.
19. N. Fey, M. Garland, J. P. Hopewell, C. L. McMullin, S. Mastroianni, A. G. Orpen and P. G. Pringle, *Angew. Chem. Int. Ed.*, 2012, **51**, 118–122, DOI: 10.1002/anie.201105954.
20. M. Villares, C. M. Saunders and N. Fey, *Artif. Intell. Chem.*, 2024, **2**, 100055, DOI: 10.1016/j.aichem.2024.100055.
21. F. P. Pruchnik, *Organometallic Chemistry of Transition Elements*, Plenum Press, New York, 1990.
22. B. Zhang, D. Peña Fuentes and A. Börner, *ChemTexts*, 2022, **8**, 1–26, DOI: 10.1007/s40828-021-00154-x.
23. I. S. Mikhel, N. V. Dubrovina, I. A. Shuklov, W. Baumann, D. Selent, H. Jiao, A. Christiansen, R. Franke and A. Börner, *J. Organomet. Chem.*, 2011, **696**, 3050–3057, DOI: 10.1016/j.jorganchem.2011.05.004.
24. E. Piras, B. Powietzka, F. Wurst, D. Neumann-Walter, H. J. Grützmacher, T. Otto, T. Zevaco and O. Walter, *Catal. Lett.*, 2013, **143**, 673–680, DOI: 10.1007/s10562-013-1010-x.
25. P. J. Fennis, P. H. M. Budzelaar, J. H. G. Frijns and A. G. Orpen, *J. Organomet. Chem.*, 1990, **393**, 287–298, DOI: 10.1016/0022-328X(90)80205-E.
26. R. Fornika, C. Six, H. Görls, M. Kessler, C. Krüger and W. Leitner, *Can. J. Chem.*, 2001, **79**, 642–648, DOI: 10.1139/cjc-79-5/6-642.
27. M. Aydemir, N. Meric, C. Kayan, F. Ok and A. Baysal, *Inorganica Chim. Acta*, 2013, **398**, 1–10, DOI: 10.1016/j.ica.2012.12.005.
28. F. Bonatti and G. Wilkinson, *J. Chem. Soc.*, 1964, 3156–3160, DOI: 10.1039/JR9640003156.

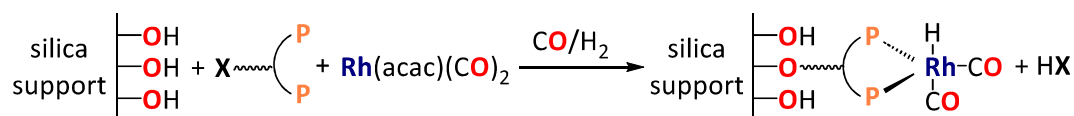
29. T. A. Puckette, *Top. Catal.*, 2012, **55**, 421–425, DOI: 10.1007/s11244-012-9819-x.
30. T. J. Devon, G. W. Phillips, T. A. Puckette, J. L. Stavinoha and J. J. Vanderbilt (to Texas Eastman), US Patent 4 694 109, 1987.
31. D. H. C. Neto, A. A. M. Dos Santos, J. C. S. Da Silva, W. R. Rocha and R. P. Dias, *Eur. J. Inorg. Chem.*, 2020, **2020**, 3907–3916, DOI: 10.1002/ejic.202000799.
32. A. Castellanos-Páez, S. Castillón, C. Claver, P. W. N. M. Van Leeuwen and W. G. J. De Lange, *Organomet.*, 1998, **17**, 2543–2552, DOI: 10.1021/om971059q.
33. M. Rosales, A. González, Y. Guerrero, I. Pacheco and R. A. Sánchez-Delgado, *J. Mol. Catal. A: Chem.*, 2007, **270**, 241–249, DOI: 10.1016/j.molcata.2007.01.044.
34. S. Komiya and F. Fukuoka, *Synthesis of Organometallic Compounds*, John Wiley & Sons Ltd, Chichester, 1997.
35. C. S. Seu, D. Ung, M. D. Doud, C. E. Moore, A. L. Rheingold and C. P. Kubiak, *Organomet.*, 2013, **32**, 4556–4563, DOI: 10.1021/om400472s.
36. G. Yerlikaya, E. B. Tapanyigit, B. Güzel, O. Şahin and G. Kardaş, *J. Mol. Struct.*, 2019, **1198**, 126889, DOI: 10.1016/j.molstruc.2019.126889.
37. M. T. Reetz, S. R. Waldvogel and R. Goddard, *Tetrahedron Lett.*, 1997, **38**, 5967–5970, DOI: 10.1016/S0040-4039(97)01345-2.
38. L. Dahlenburg and V. Kurth, *J. Organomet. Chem.*, 1999, **585**, 315–325, DOI: 10.1016/S0022-328X(99)00243-0
39. C. Claver, S. Castillón, N. Ruiz, G. Delogu, D. Fabbicand and S. Gladiali, *J. Chem. Soc., Chem. Commun.*, 1993, 1883–1884, DOI: 10.1039/C39930001833.
40. C. Berghof, I. G. Grosu, P. Lönnecke, S. Gómez-Ruiz, L. Silaghi-Dumitrescu and E. Hey-Hawkins, *Inorganica Chim. Acta*, 2011, **374**, 127–133, DOI: 10.1016/j.ica.2010.12.004.
41. Johnson Matthey PGM prices, <https://matthey.com/products-and-markets/pgms-and-circularity/pgm-management>, (accessed 4 May 2024).
42. E. Drent and P. H. M. Budzelaar, *J. Organomet. Chem.*, 2000, **593**, 211–225, DOI: 10.1016/S0022-328X(99)00554-9.
43. Y. Zhang, S. Torker, M. Sigrist, N. Bregović and P. Dydio, *J. Am. Chem. Soc.*, 2020, **142**, 18251–18265, DOI: 10.1021/jacs.0c09254.
44. Y. Zhang, M. Sigrist and P. Dydio, *Eur. J. Org. Chem.*, 2021, **2021**, 5985–5997, DOI: 10.1002/ejoc.202101020.
45. M. Sigrist, Y. Zhang, C. Antheaume and P. Dydio, *Angew. Chem. Int. Ed.*, 2022, **61**, e202116406, DOI: 10.1002/anie.202116406.
46. P. C. Ioannou, C. Arbez-Gindre, M. Zoumpantioti, C. P. Raptopoulou, V. Psycharis, I. D. Kostas and P. Kyritsis, *J. Organomet. Chem.*, 2019, **879**, 40–46, DOI: 10.1016/j.jorganchem.2018.10.006.

47. I. K. Stamatopoulos, M. Kapsi, M. Roulia, G. C. Vougioukalakis, C. P. Raptopoulou, V. Psycharis, I. D. Kostas, L. Kollár and P. Kyritsis, *Polyhedron*, 2018, **151**, 292–298, DOI: 10.1016/j.poly.2018.05.041.
48. I. Stamatopoulos, M. Roulia, K. A. Vallianatou, C. P. Raptopoulou, V. Psycharis, M. Carravetta, C. Papachristodoulou, E. Hey-Hawkins, I. D. Kostas and P. Kyritsis, *ChemistrySelect*, 2017, **2**, 12051–12059, DOI: 10.1002/slct.201702601.
49. J. Vicente, J. A. Abad, J. López-Serrano, P. G. Jones, C. Nájera and L. Botella-Segura, *Organomet.*, 2005, **24**, 5044–5057, DOI: 10.1021/om050451y.
50. A. L. Balch, M. M. Olmstead and S. P. Rowley, *Inorganica Chim. Acta*, 1990, **168**, 255–264, DOI: 10.1016/S0020-1693(00)80952-4.
51. S. B. Owens and G. M. Gray, *J. Organomet. Chem.*, 2008, **693**, 3907–3914, DOI: 10.1016/j.jorganchem.2008.10.003.
52. K. Mikami, T. Miyamoto and M. Hatano, *Chem. Commun.*, 2004, 2082–2083, DOI: 10.1039/b407250b.
53. C. Fliedel, A. Ghisolfi and P. Braunstein, *Chem. Rev.*, 2016, **116**, 9237–9304, DOI: 10.1021/acs.chemrev.6b00153.
54. L. Rubio-Pérez, F. Javier Pérez-Flores, P. Sharma, L. Velasco and A. Cabrera, *Org. Lett.*, 2009, **11**, 265–268, DOI: 10.1021/ol802336m.
55. J. J. R. Frew, K. Damian, H. Van Rensburg, A. M. Z. Slawin, R. P. Tooze and M. L. Clarke, *Chem. Eur. J.*, 2009, **15**, 10504–10513, DOI: 10.1002/chem.200901178.
56. H. Bohnen and B. Cornils, *Adv. Catal.*, 2002, **47**, 1–64, DOI: 10.1016/S0360-0564(02)47005-8.
57. Y. N. Timsina, R. K. Sharma and T. V. Rajanbabu, *Chem. Sci.*, 2015, **6**, 3994–4008, DOI: 10.1039/c5sc00929d.
58. A. Carrick, PhD Thesis, Durham University, 2024.
59. Q. Dong, M. J. Rose, W. Y. Wong and H. B. Gray, *Inorg. Chem.*, 2011, **50**, 10213–10224, DOI: 10.1021/ic201213c.
60. A. K. Mondal, M. Sundararajan and S. Konar, *Dalton Trans.*, 2018, **47**, 3745–3754, DOI: 10.1039/c7dt04007e.
61. M. M. Parsutkar and T. V. Rajanbabu, *J. Am. Chem. Soc.*, 2021, **143**, 12825–12835, DOI: 10.1021/jacs.1c06245.
62. P. Braunstein, H.-P. Kormann, W. Meyer-Zaika, R. Pugin and G. Schmid, *Chem. Eur. J.*, 2000, **6**, 4637–4646, DOI: 10.1002/1521-3765(20001215)6:24<4637::AID-CHEM4637>3.0.CO;2-A.

Chapter 4: Reactivity studies of tetherable phosphines with silica, and synthesis of immobilised phosphine rhodium complexes for applications in hydroformylation

4.1 Introduction to phosphine ligand silica-immobilisation

The aim of this project is the development of transition metal-based heterogeneous catalysts that consist of discrete metal complexes immobilised on a solid support, for applications in hydroformylation. A key consideration in the development of this type of immobilised catalyst is the choice of support and method of metal immobilisation. As discussed in Sections 1.14-1.17 there are many ways to approach this challenge. However, in this work metal complexation to a bidentate phosphine ligand containing a pendant silica-tethering functionality has been employed (Scheme 4.1).



Scheme 4.1. Silica-immobilised catalyst synthesis using a modified bidentate phosphine with pendant tethering functionality, X.

This approach can be justified as it has several potential advantages over other methods of heterogeneous catalysis synthesis. Most fundamentally, this technique maintains a “solution like” metal environment that mimics the homogeneous HRh(CO)₂(P[^]P) type catalysts that have been so successfully employed in industry, leading to hydroformylation becoming the world’s largest homogeneous catalytic process.¹ Accordingly, immobilised catalysts produced using this method are primed to maintain the high activities and selectivities achieved in homogeneous hydroformylation catalysis. Additionally, by employing a tethering functionality that can be covalently bound to the support, a robust immobilised catalyst that is stable to hydroformylation reaction conditions (elevated temperatures and pressures, vigorous stirring for gas-liquid mixing) can be envisioned. In contrast, immobilisation methods that rely on intermolecular forces, have been shown to commonly suffer from high leaching rates of the weakly bound catalyst from the support.²

In order to take advantage of these potential benefits, a support is required that is mechanically stable and inert to hydroformylation reaction conditions, including the reaction substrate and products, so that catalyst stability and performance can be maintained. A simple, facile immobilisation step that does not require harsh reaction

conditions or additional components is also preferred to minimise the additional complexity/processing required to produce an immobilised catalyst relative to a homogeneous catalyst.

There are a vast array of options for solid catalyst supports that have been investigated in hydroformylation alone, including a variety of solid oxides, such as silica, alumina and titania, as well dendrimers, polymer supports and resins, which all have their advantages and disadvantages.^{3–8} However, many of those investigated are “designer” supports that are expensive and can only be produced in relatively small quantities, requiring specialist synthetic techniques in their production, making them unsuitable for large scale industrial application. As such, this work will focus on the investigation of cheap, commercially available fumed silica and γ -alumina supports. Alongside the economic advantages of employing these supports over more specialist options, these oxide materials typically display very good thermal and mechanical stabilities, as well as benefiting from them being well studied and characterised as catalyst supports in the literature.⁹ In particular, this work will mainly employ AEROPERL 300/30 silica as the support of choice. This hydrophilic fumed silica shows high thermal and mechanical stability, whilst providing a high internal surface area and pore volume size ideal for obtaining good catalyst loadings (Table 4.1).¹⁰ Calcination techniques can also be utilised pre-immobilisation to modify the silica surface chemistry, allowing tuning to well defined isolated silanol sites ideal for catalyst immobilisation, as has been previously studied in the Dyer Group.¹¹

Table 4.1. Properties of AEROPERL 300/30 silica.^{10,11}

BET surface area / $\text{m}^2 \text{g}^{-1}$	270 – 330
pH value	4.0 – 6.0
Tapped density / g l^{-1}	280
Average particle size / μm	20 – 60
Pore volume / ml g^{-1}	1.5 – 1.9 ¹⁰ (1.85) ¹¹
Average pore diameter / \AA	260 ¹¹

Many functionalities have been employed for covalently anchoring organic compounds onto silica supports by reaction with surface silica OH groups; however, by far the most widely and successfully applied tethering functionality for immobilisation of organics onto solid oxides are alkoxysilanes *via* so-called silanisation reactions (Figure 4.1).^{12,13} Alkoxysilanes have the advantages of being cheap and commercially available starting materials that can be further functionalised as required, while enabling a very facile silica-tethering reaction using mild conditions. Alkoxysilanes also offer the possibility to form up to three covalent bonds to the silica surface, depending on the alkoxysilane used, potentially improving the robustness of the immobilisation. In addition, reactions of silica with alkoxysilanes can be conveniently monitored by solid-state ²⁹Si NMR spectroscopic analysis to characterise and analyse the resulting modified silica surface. These benefits make immobilisation using alkoxysilanes highly attractive over many other potential tethering functionalities. Additionally, in the context of immobilised phosphines for applications in rhodium-catalysed hydroformylation, alkoxysilanes show orthogonal reactivity to the required phosphine ligand functionalities, and their precursors, making them highly applicable to this field. One disadvantage of alkoxysilanes is their high sensitivity to moisture. In this project however, since that alkoxysilane tethering functionality is being incorporated into an already air-sensitive phosphine compound, additional precautions other than routinely employed use of Schlenk line and glovebox techniques for phosphine handling are not required.

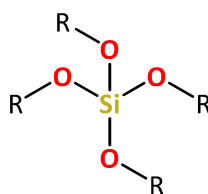
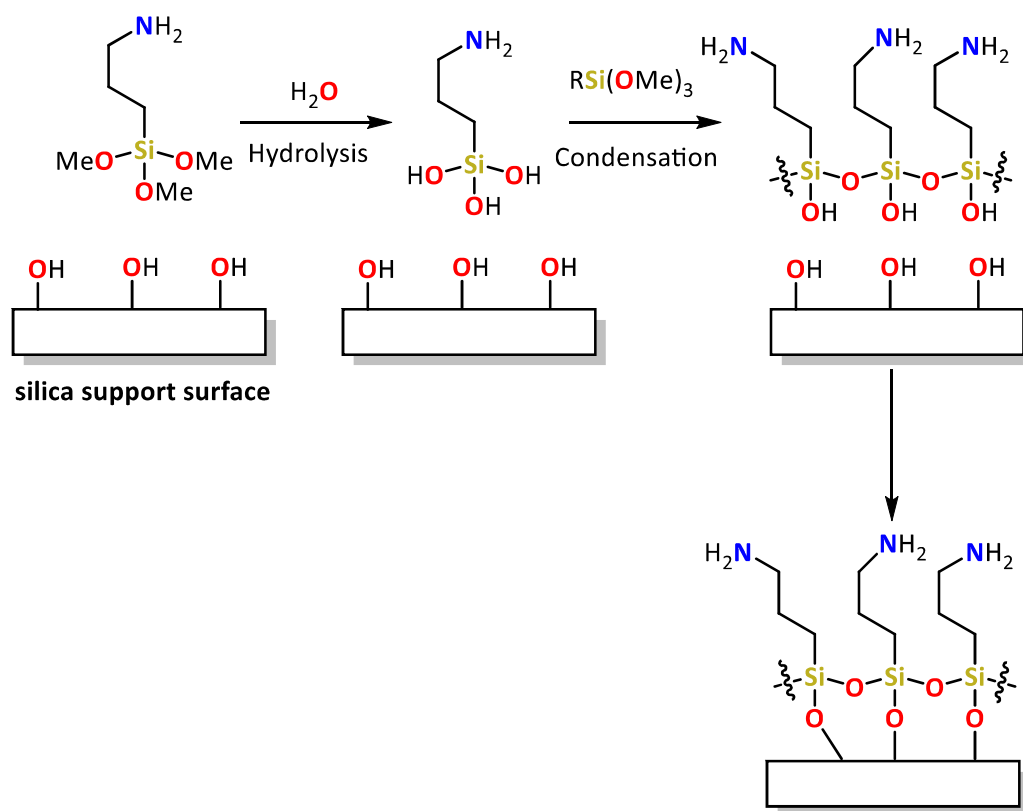


Figure 4.1. Structure of a generic alkoxysilane.

The immobilisation of alkoxysilanes on silica is well documented and understood, with many diverse examples having been reported previously.^{9,12,14–19} In the synthesis of immobilised hydroformylation catalysts this is of vital importance, as without a reliable and robust anchoring of the metal catalyst to the surface, leaching of the catalyst into solution is likely to occur. In turn, this would eliminate all of the advantages of an immobilised catalyst, resulting in difficult catalyst separation and recovery. In particular,

silica functionalisation with aminosilanes, such as (3-aminopropyl)trimethoxysilane, is very popular due to the versatility of the resulting amine functionalised silicas for various applications and further modification.¹² Many studies have been performed to optimize the silanisation reaction conditions, where a number of important variables have been considered, such as: alkoxysilane concentration, reaction temperature and time, the presence of water, the type of solvent and the identity of the alkoxysilane (*e.g.*, the amine functionality in (3-aminopropyl)trimethoxysilane has been shown to catalytically promote alkoxysilane condensation).^{16–19} Different combinations of these variables can lead to very different surface modifications, for example the presence of water leads to hydrolysis of the alkoxysilanes to silanols that can oligomerise before reaction with the surface (Scheme 4.2). Alternatively, under different conditions, still in the presence of water, alkoxysilanes can react with other already surface-bound alkoxysilanes, rather than the support surface itself, leading to vertical polymerisation above the surface (Figure 4.2).



*Scheme 4.2. Alkoxysilane monolayer deposition on a silica surface via hydrolysis and condensation.*¹²

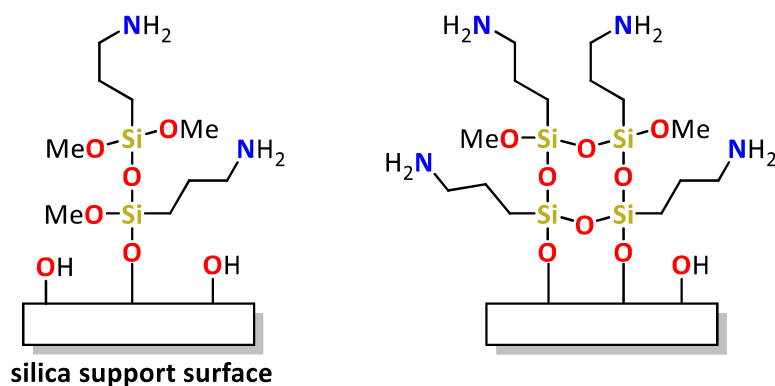


Figure 4.2. Potential vertical polymerisation products of (3-aminopropyl)trimethoxysilane on silica.¹²

For catalyst applications, discrete silane deposition with the maximum number of bonds to the silica surface are desired for improved catalyst stability (Figure 4.3), and therefore water is usually rigorously excluded.²⁰ Depending on the number of bonds made from the alkoxy silane to the silica surface, the silicon environment in the alkoxy silane can be denoted a T^1 , T^2 or T^3 site.

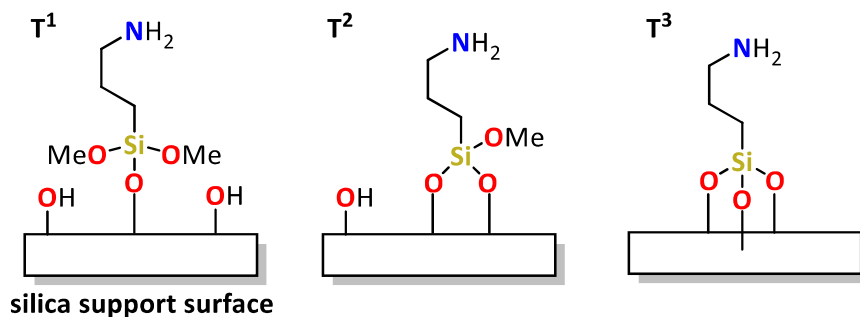


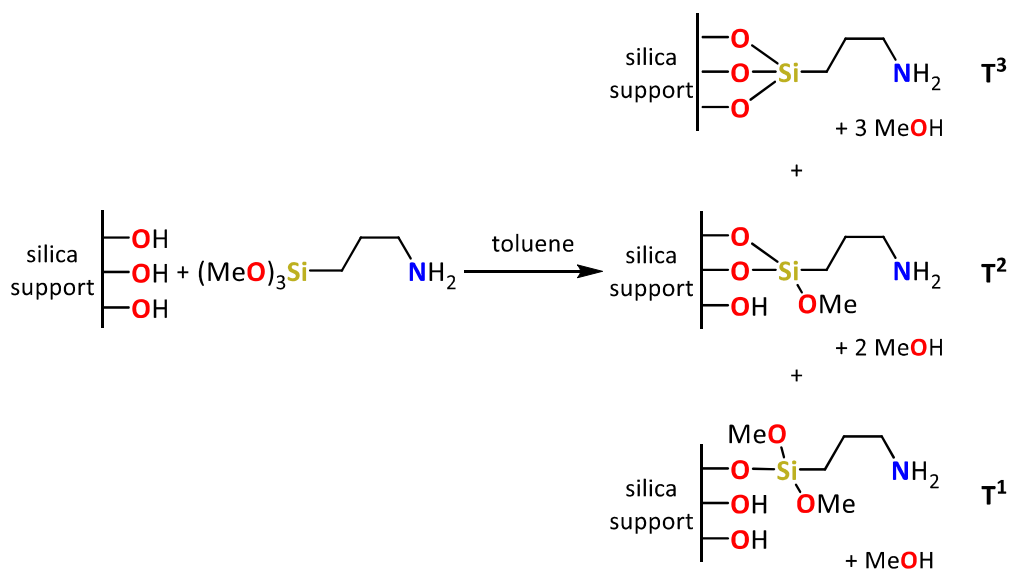
Figure 4.3. Target isolated (3-aminopropyl)trimethoxysilane deposition on silica for catalysis applications, showing different possible bonding modes to the silica surface (T^1 , T^2 and T^3 sites).

An alternative method for incorporation of functionalised alkoxy silanes onto silica supports is the co-condensation of a functionalised silane with tetraethyl orthosilicate during the synthesis of mesoporous silicas, rather than post-synthetically modified existing silicas as described above. This approach has been widely studied for the production of modified silicas in the literature and ensures high levels of incorporation of the desired functionality into the resulting silica framework.²¹ A drawback of this

method, however, is that the majority of the incorporated functionality is not always accessible from the silica surface, limiting this method's application in catalysis.²¹ In this work, only commercially available silica supports were used, due to their consistency of performance and low cost, ensuring that the effect of the tethered phosphine on hydroformylation catalysis could be probed on a consistent support.

4.2 Silica immobilisation of (3-aminopropyl)trimethoxysilane

(3-Aminopropyl)trimethoxysilane is used as a reagent for preparation of several of the ligands described in Chapter 2, including **L1-5**. Therefore, it was selected as a useful model for investigating silica functionalisation with alkoxyxilanes. To this end, (3-aminopropyl)trimethoxysilane was reacted with commercially available AEROPERL 300/30 silica (calcined at 600 °C, properties given in Table 4.2) in toluene and stirred at reflux for 2 hours, in accordance with an adapted literature method (Scheme 4.3).¹⁶ The resulting mixture was filtered and the resulting solid washed thoroughly with toluene before being dried *in vacuo* to afford the surface-modified silica.



Scheme 4.3. Synthesis of surface-modified silica by reaction of AEROPERL 300/30 silica (calcined at 200 °C) with (3-aminopropyl)trimethoxysilane.

The resulting modified silica was analysed by solid-state magic angle spinning ²⁹Si NMR spectroscopy. Due to the low sensitivity of this analysis, a cross-polarisation experiment

was performed, enhancing the signal of ^{29}Si nuclei in close proximity to ^1H nuclei.²² This technique facilitates assignment of the surface ^{29}Si environments that are in low abundance relative to bulk silica, at the expense of quantitative peak integrals, since peak area is no longer directly proportional to the quantity of nuclei in a particular environment. The CP ^{29}Si NMR spectrum (Figure 4.4) shows the presence of three resonances, corresponding to T^1 , T^2 and T^3 silicon environments, alongside those arising from bulk silica. The T^1 , T^2 and T^3 silicon environments correspond to the sites where 1, 2 and 3 methoxysilane groups had reacted with the silica surface, respectively.²³

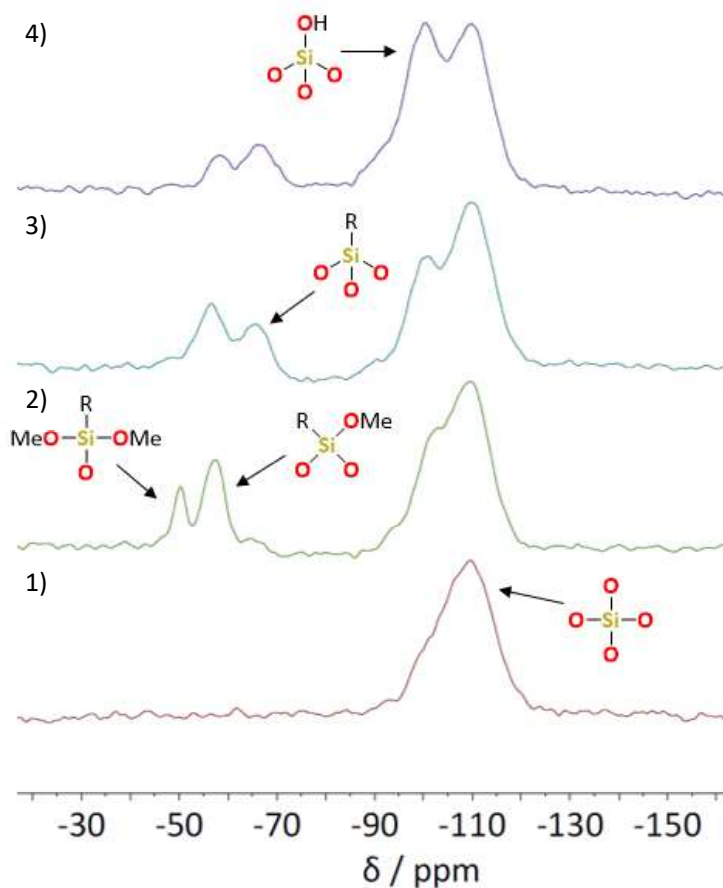
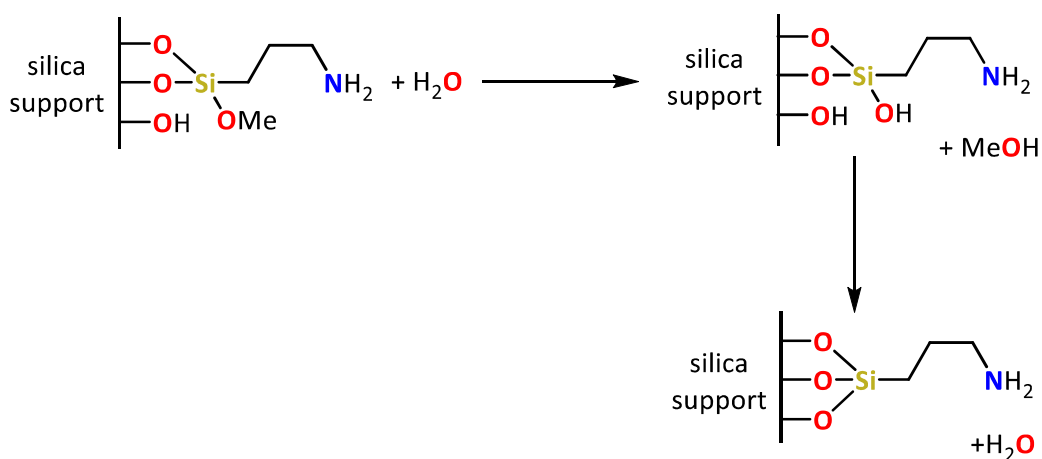


Figure 4.4. SS NMR CP ^{29}Si spectrum acquired at 79 MHz with a spin rate of 6 kHz of AEROPERL 300/30 silica calcined at 600 °C, **1)** before further treatment, **2)** after reaction with 3-aminopropyltrimethoxysilane, **3)** after attempted hydrolysis of tethered amine stirring in water for 30 mins and **4)** after attempted hydrolysis of tethered amine stirring in 1:1 water:methanol for 30 mins.

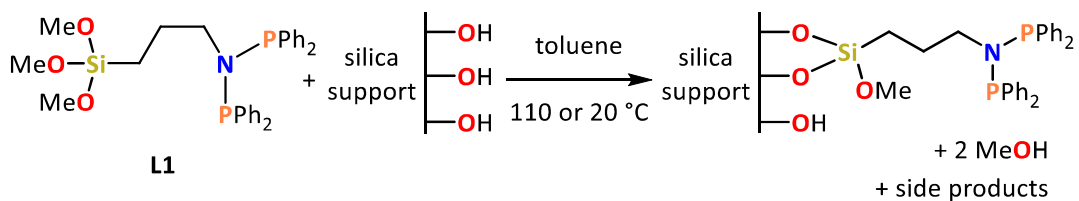
The stability of the surface-bound amine was then investigated by stirring the silica in water for 30 minutes before SS CP ^{29}Si NMR spectroscopic analysis (Figure 4.4). The CP ^{29}Si SS NMR spectrum showed a move from predominantly signals corresponding to T^2 and T^1 site resonances to predominantly T^2 and T^3 species, with approximate overall signal intensity remaining the same, suggesting that no amine was lost from the surface (although quantification is not totally reliable for CP experiments). The increase in surface T^3 sites could be explained by the fact that in solution water promotes oligomerisation of alkoxy silanes, so could also promote the condensation of the trimethoxysilane group with surface silanols to form greater silica-(3-aminopropyl)trimethoxysilane connectivity (Scheme 4.4).¹⁵ The stability of the tethering groups was then investigated in a methanol/water mixture. A sample of the surface-modified silica that had been stirred in a 50:50 water:methanol mixture for 30 minutes was analysed by CP ^{29}Si NMR spectroscopy, which showed an approximate 50% decrease in surface-bound silicon intensity along with significant increase in surface Si-OH groups (Figure 4.4.4). This suggests that the water/methanol mixture had indeed started to hydrolyse $\text{SiO}_2\text{-O-Si-R}$ to reform the original (3-aminopropyl)trimethoxysilane and silica surface silanols. This is not likely to be a significant issue during catalysis however, due to the anhydrous conditions employed for hydroformylation.



*Scheme 4.4. Water-promoted condensation of (3-aminopropyl)trimethoxysilane with silica.*¹⁵

4.3 Silica immobilisation of **L1**: $(\text{Ph}_2\text{P})_2\text{N}(\text{CH}_2)_3\text{Si}(\text{OMe})_3$

After successful immobilisation of test molecule (3-aminopropyl)trimethoxysilane onto silica, the reactivity of the PNP ligand **L1** with silica was investigated, with the goal of developing silica-immobilised hydroformylation catalysts (Scheme 4.5). The same reaction conditions used for the surface binding of (3-aminopropyl)trimethoxysilane onto AEROPERL 300/30 silica (calcined at 600 °C) were used and the resulting product characterised by SS ^{29}Si and ^{31}P NMR spectroscopies. The ^{29}Si NMR spectra showed the presence of surface T^1 , T^2 and T^3 silicon environments (predominantly T^2) in good agreement with the NMR spectrum for the reaction of (3-aminopropyl)trimethoxysilane with silica. This suggested that the immobilisation process had been successful. However, the ^{31}P NMR spectrum of this material shows two signals, one at +59 ppm, corresponding to successfully immobilised **L1** (^{31}P = +62 ppm in solution), alongside a second, larger resonance at +23 ppm, corresponding to an unknown P^{V} side product of immobilisation (Figure 4.5.1), as determined from its chemical shift value. Formation of P^{V} side products when grafting phosphines onto solid oxide supports is a well-known, albeit poorly understood, issue in immobilised catalysis, resulting in species that can no longer bind transition metal catalysts (See section 4.4).²⁴ In order to try and suppress this unwanted phosphine oxidation, the reaction was repeated under milder conditions stirring at room temperature, although this had no appreciable effect on the ^{31}P NMR spectrum of the resulting material. Variation of the silica calcination procedure (200 vs 600 °C) also had no noticeable effect on side product formation. In contrast to this, replacing the silica support with a gamma alumina support was shown to partially suppress side product formation, resulting in the desired immobilised ligand forming as the major product, although a significant amount of side product still remained (Figure 4.5.2).



Scheme 4.5. Reaction of **L1** with AEROPERL 300/30 silica (calcined at 200 or 600 °C).

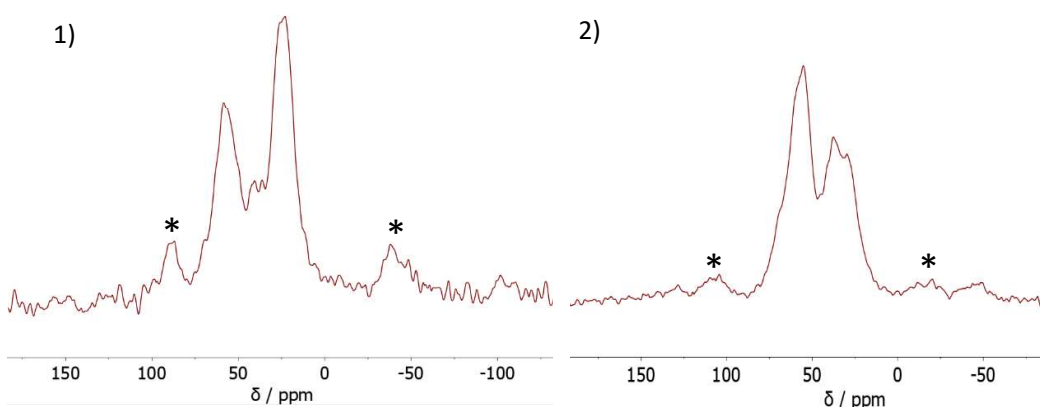


Figure 4.5. SS NMR CP ^{31}P spectrum acquired at 162 MHz with a spin rate of 10 kHz of **L1** on 1); AEROPERL 300/30 silica calcined at 200 °C and 2); gamma alumina calcined at 200 °C. * Denotes spinning sidebands.

4.4 Investigation the effect of the tethering functionality on side product formation during the silica-immobilisation of dppa-type phosphines

The reactivity of dppa-type phosphines with silica was probed by reaction of AEROPERL 300/30 silica (calcined at 200 °C) with **L23**, a bidentate phosphine that does not contain any additional functionality capable of reacting with silica. After heating at reflux in toluene for 4 hours, no reactivity of **L23** was observed according to solution-state ^{31}P NMR spectroscopy (Figure 4.6) (note an unknown impurity present in **L23**, ^{31}P δ = +117 ppm, was shown to react under these conditions producing a new signal in the NMR spectrum at +16 ppm). As methanol is produced as a side product of methoxysilanes reacting with silica, methanol was added to the mixture of silica and **L23** in toluene, in order to better simulate the immobilisation reaction conditions of **L1**. After addition of methanol the mixture was heated at reflux resumed for a further 4 hours, after which time no significant change was observed to the ^{31}P NMR spectrum. This result agrees with literature findings that suggest that the alkoxy silane functionality has to be present in the reaction mixture to promote reactions of phosphines with silica.²⁴

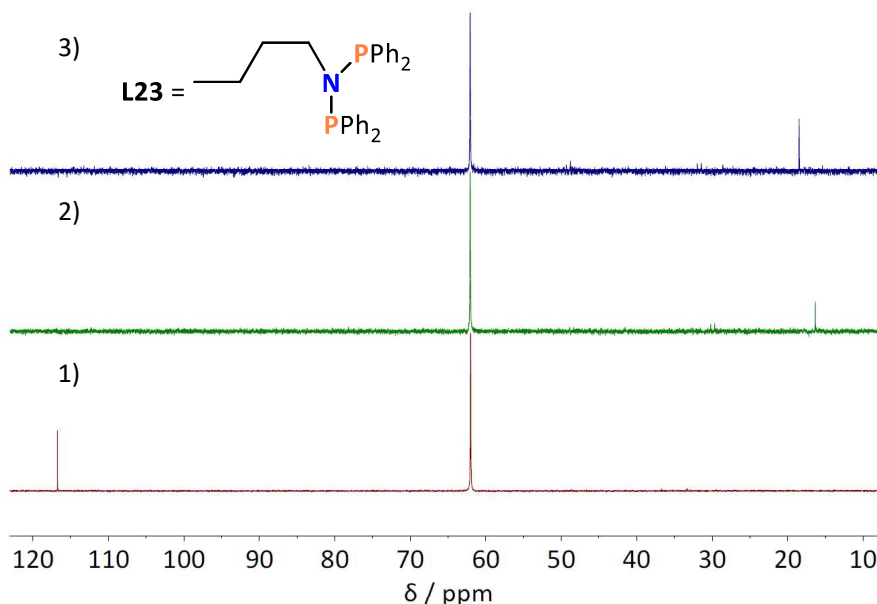


Figure 4.6. $^{31}\text{P}\{^1\text{H}\}$ NMR spectrum (162 MHz, 295 K) of **1**): **L23**, **2**): **L23** after heating at reflux in toluene with AEROPERL 300/30 silica calcined at 200 °C, **3**): **L23** after heating at reflux in toluene with methanol and AEROPERL 300/30 silica calcined at 200 °C.

Work by Blümel *et al.* suggests that the side product produced during the silica-immobilisation of bis(diphenylphosphino)amine type compounds *via* alkoxyasilanes is most likely a species containing a phosphorus atom quaternised by methyl groups from the methoxysilyl functionality (Figure 4.7).²⁵ This type of phosphorus oxidation during immobilisation onto oxide supports has been reported for several phosphine/oxide support combinations.²⁴ In these literature cases, identification of the side product has mostly been performed using ^{31}P CP/MAS and suspension HR-MAS NMR studies, allowing comparison of NMR spectra with those of solution-state test reactions to elucidate the by-product structure (Scheme 4.5).²⁵

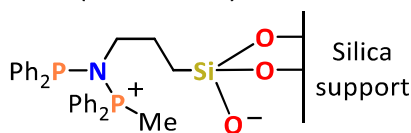
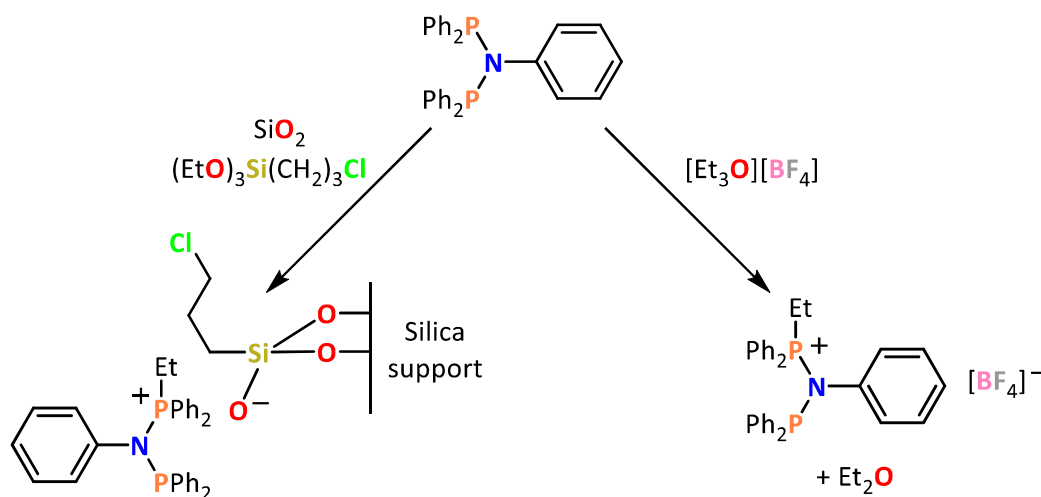


Figure 4.7. Possible side product of the reaction of **L1** with silica, featuring a quaternised phosphorus centre.²⁵

It has been shown by Blümel *et al.* that $(\text{PPh}_2)_2\text{NPh}$ can be alkylated using $[\text{Et}_3\text{O}][\text{BF}_4]$ to give the corresponding quaternary species, which closely matches the observed ^{31}P NMR

spectra obtained during attempted immobilisation of PNP compounds, analogous to **L1**, onto silica (Scheme 4.6).²⁵ It is noted here however, that $[\text{Et}_3\text{O}][\text{BF}_4]$ is a much stronger alkylating agent than the alkoxysilane present during immobilisation reactions. Blümel *et al.* also showed that by mixing a non-tetherable phosphine with silica and the alkoxysilane $(\text{EtO})_3\text{Si}(\text{CH}_2)_3\text{Cl}$, the phosphine become bound to the surface (Scheme 4.6).²⁵ This suggests that the alkylating reaction does not have to occur intramolecularly, but can also occur intermolecularly.²⁵ The possibility of the phosphine reacting with the chloroalkane moiety did not appear to be considered in this study, however.

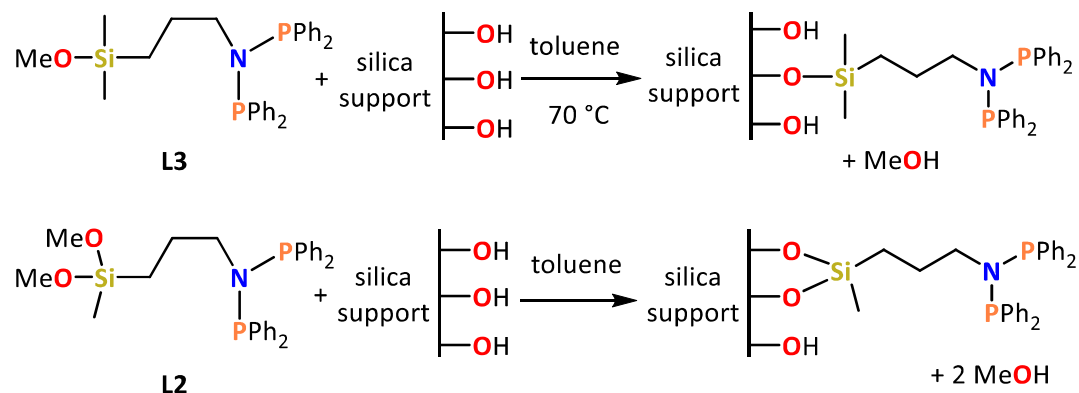


Scheme 4.6. Previously reported model phosphonium-forming reactions of a bis(phosphino)amine.²⁵

Part of the evidence for formation of the quaternised phosphorus side product as described in Figure 4.7, reported by Blümel *et al.*, was a 1:1 ratio of the P^{III} to P^{V} signals in the SS ^{31}P NMR spectrum. However, in our work the observed 2:1 ratio of side product to target product during the immobilisation of **L1** does not agree with this being the identity of the side product.

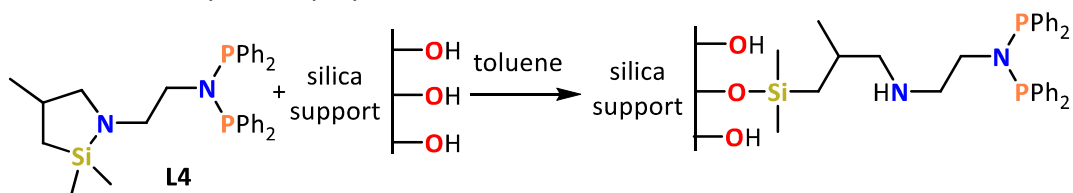
Since the phosphonium side product proposed by Blümel is predicted to form by reaction of pendant OMe groups left over from the immobilisation process, with the phosphine moiety, the degree of side product formation would be expected to decrease when fewer silyl ether groups are introduced into this system. To investigate this, alternative phosphine ligands **L2** and **L3** featuring progressively fewer Si-OMe linkages were prepared (see Section 2.2.1) and reacted with silica (Scheme 4.7). Due to **L3** being

less reactive with silica than the other compounds investigated, as a result its single Si-OMe linkage, the reaction of **L3** with silica was performed at elevated temperature (70 °C).



*Scheme 4.7. Reaction of **L2** and **L3** with AEROPERL 300/30 silica calcined at 200 °C.*

Alongside the alkoxyisilane-functionalised phosphine compounds **L1-3**, it was also of interest to utilise a tethering group that does not feature an alkoxyisilane functionality. To this end, the compound **L4**, featuring a cyclic azasilane tethering functionality, was reacted with silica (Scheme 4.8). The cyclic azasilane functionality has several potential benefits over more traditionally employed alkoxyisilanes for the immobilisation of organics onto silica supports. Cyclic azasilanes, such as **L4**, contain a 5-membered ring containing a reactive Si–N bond that is highly susceptible to ring opening reactions. Reaction with silica surface silanol groups proceeds *via* a ring opening reaction that is driven by the relief of bond-angle strain and steric repulsions, alongside a thermodynamic driving force for the formation of a Si–O over a Si–N bond.²⁶ The ring opening of cyclic azasilanes is 100% atom efficient, resulting in no side products, such as the alcohols produced when alkoxyisilanes are used to tether organics to silica supports. Cyclic azasilanes have additional benefits over alkoxyisilanes in that they have a much weaker tendency to self-polymerise.²⁷



*Scheme 4.8. Reaction of **L4** with AEROPERL 300/30 silica calcined at 200 °C.*

Figure 4.8 shows the ^{31}P NMR spectra of the reactions of **L1-4** with AEROPERL 300/30 silica calcined at 200 °C. In contrast to the expected decrease in side product formation upon reducing the number of Si-OMe linkages in the tether, side product formation increased as the number of Si-OMe linkages decreases from 3-1 for **L1-3**. This result suggests that the P^{V} side products formed during the immobilisation of **L1-3** on silica are not of the type described in Figure 4.8, as these would be expected to be favoured with an increasing number of Si-OMe linkages. However, it was found that side product formation was shown to be suppressed when using the cyclic azasilane-functionalised **L4**. Therefore, this suggests that the alkoxy silane functionality (or the MeOH released as a result of alkoxy silane reactivity with silica) promotes the phosphine oxidation reaction. As oxygen was rigorously excluded in all these experiments, the small amount of P^{V} side product formation ($\approx 10\%$) during the immobilisation of **L4** is likely due to the reaction of the phosphine moieties with surface silanols. The exact nature of the side products formed is unknown, however. As discussed in Chapter 2.2.5, further application of cyclic azasilanes in the immobilisation of phosphines on silica was prevented due to the instability of the other phosphine/phosphite containing cyclic azasilanes prepared.

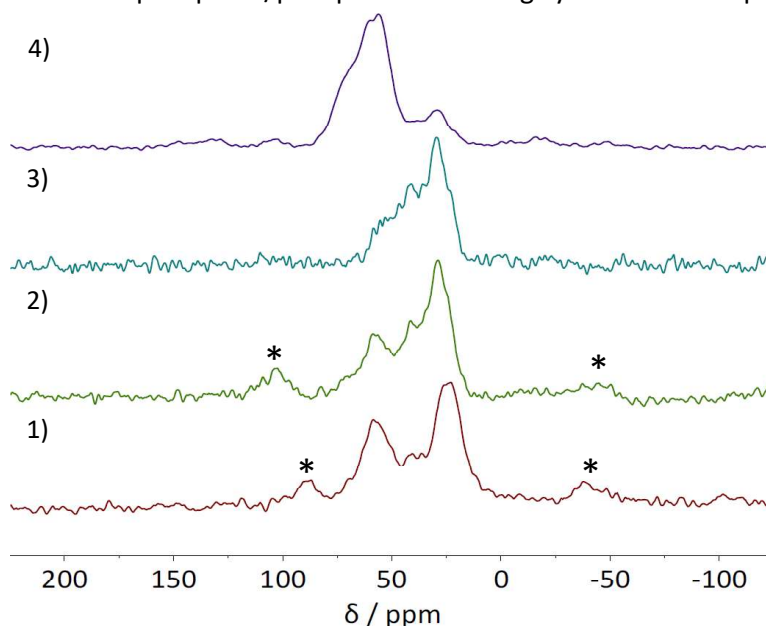
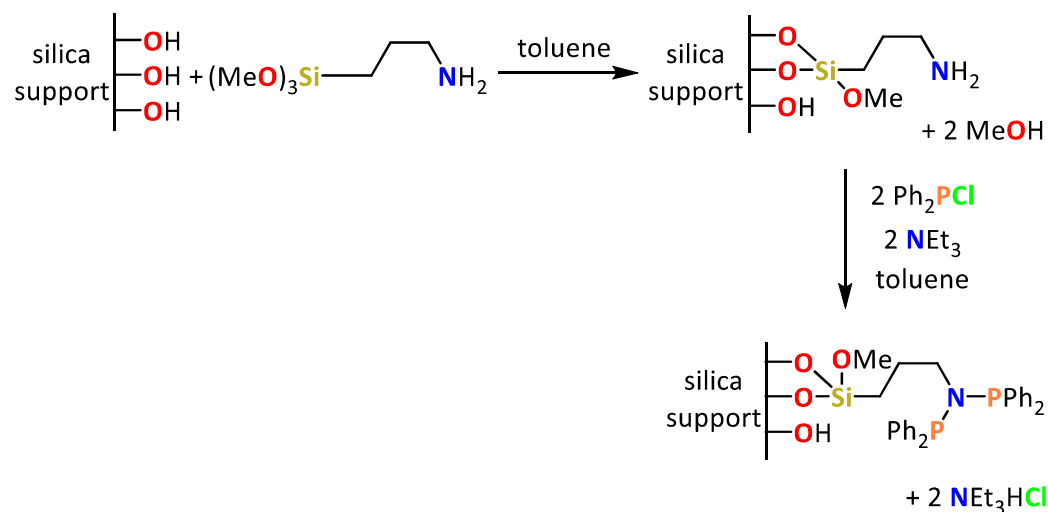


Figure 4.8. SS CP ^{31}P NMR spectrum acquired at 162 MHz with a spin rate of 10 kHz for the products from reaction of AEROPERL 300/30 silica calcined at 200 °C with **1**): **L1**, **2**): **L2**, **3**): **L3** and **4**): **L4**. * Denotes spinning sidebands.

4.5 A two-step synthesis of silica-immobilised **L1**: $(\text{Ph}_2\text{P})_2\text{N}(\text{CH}_2)_3\text{Si}(\text{OMe})_3$, via silica-immobilised (3-aminopropyl)trimethoxysilane

A second method for the production of silica-immobilised **L1** was attempted using two reaction steps. Firstly, (3-aminopropyl)trimethoxysilane was reacted with silica, as detailed in Chapter 4.2, followed by subsequent functionalisation of the immobilised amine by reaction with two equivalent of Ph_2PCl (Scheme 4.9). A similar approach has recently been described in the literature for the synthesis of a silica-immobilised chromium ethylene oligomerisation catalyst.²⁸



*Scheme 4.9. Attempted synthesis of silica immobilised **L1** using a two-step procedure via silica-immobilised (3-aminopropyl)trimethoxysilane.*

In our work, by introducing the phosphine component to the system after the alkoxy silane-silica reaction had already been performed, it was hypothesised that phosphine side reactions with the support could be suppressed. The high-power decoupled (HPDEC) SS ^{31}P NMR spectrum of the resulting material showed this to be the case, with only a small signal at +20 ppm present corresponding to P^{V} species (Figure 4.9). Unfortunately, the desired bidentate phosphine, corresponding to the signal at +60 ppm, was not the major product, which was in fact the monophosphine resulting from a 1:1 reaction of the amine and Ph_2PCl , corresponding to the peak at +40 ppm (Figure 4.10). The fact that the reaction did not go to completion despite a large excess of Ph_2PCl being used, suggests that many of the immobilised amine

functionalities were too sterically hindered by the silica support for complete conversion to the bis(diphenylphosphino)amine to occur.

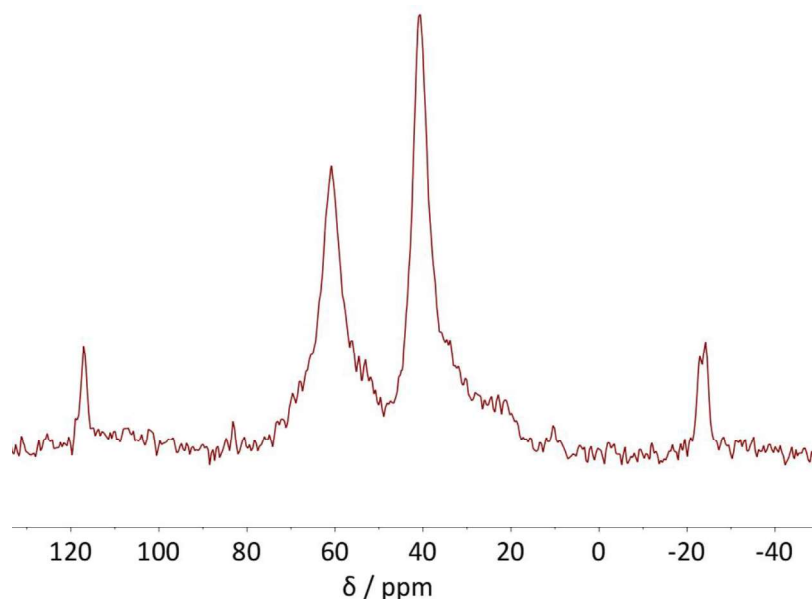


Figure 4.9. HPDEC SS ^{31}P NMR spectrum acquired at 162 MHz with a spin rate of 12 kHz of the reaction of silica-immobilised **L1** prepared by the reaction of (3-aminopropyl)trimethoxysilane-functionalised silica with Ph_2PCI .

The HPDEC SS ^{31}P NMR spectrum of the material also showed two small signals at +117 and -24 ppm that did not appear in the corresponding CP spectrum (Figure 4.9). This suggests that these signals correspond to mobile species (since fast molecular motion reduces CP rate)²² that were not successfully removed during washing of the silica. This assignment is supported by solution-state ^{31}P NMR spectroscopic analysis of an aliquot of the washings, which showed a variety of unattributed signals due to the decomposition of Ph_2PCI , including signals at 117 and -24 ppm. As the phosphine-functionalised silica produced contains multiple species that could potentially bind metals in different ways it was not investigated further for catalyst applications.

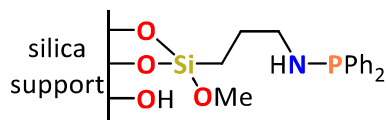
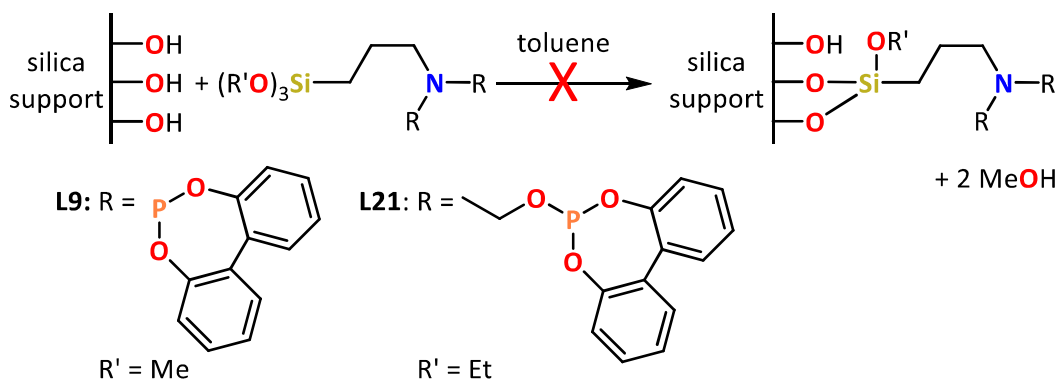


Figure 4.10. Major product in the reaction of Ph_2PCI with silica-immobilised (3-aminopropyl)trimethoxysilane.

4.6 Reactivity of tetherable phosphites **L9**: $(\text{P}(\text{C}_{12}\text{H}_8\text{O}_2)_2\text{N}(\text{CH}_2)_3\text{Si}(\text{OMe})_3$ and **L21**: $((\text{C}_{12}\text{H}_8\text{O}_2)\text{POCH}_2\text{CH}_2)_2\text{N}(\text{CH}_2)_3\text{Si}(\text{OMe})_3$ with silica

In addition to the immobilisation of phosphines on silica, as discussed in Sections 4.3-4.5, also of interest is the immobilisation of phosphites for application as ligands in heterogenised hydroformylation catalysis. Of particular interest is the behaviour of phosphites during immobilisation onto silica relative to their phosphine counterparts. In general, phosphites are more electron-deficient than phosphines, and less susceptible to oxidation reactions, which could potentially provide an advantage during silica-immobilisation.²⁹ However, phosphites can also be prone to hydrolysis reactions, which could have disadvantages during silica-immobilisation.³⁰

Tetherable phosphites **L9**, and **L21** were reacted with AEROPERL 300/30 silica (previously calcined at 200 °C) following an adapted literature procedure, to attempt formation of phosphite-functionalised silicas (Scheme 4.10). The results of these reactions were probed by SS MAS ^{29}Si and ^{31}P NMR spectroscopies to investigate the tethering mode and phosphorus environment of the resulting modified silicas.



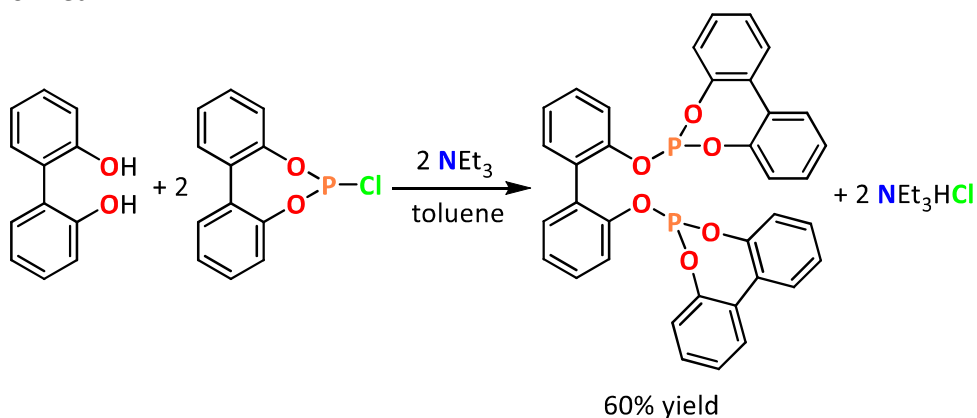
*Scheme 4.10. Attempted immobilisation of **L9** and **L21** onto AEROPERL 300/30 silica previously calcined at 200 °C.*

The ^{29}Si NMR spectra of the **L9**- and **L21**-modified silicas showed the presence of T^1 , T^2 and T^3 silicon environments in each case, suggesting that successful immobilisation of the ligand frameworks had been achieved in both cases. However, the ^{31}P NMR spectra of both samples showed a lone resonance at -8 ppm, with no signals present close to the free-ligand chemical shifts of $+152$ and $+138$ ppm for **L9** and **L21**, respectively. This large change in phosphorus chemical shift upon tethering is unexpected, suggesting that a side reaction had also occurred at the phosphorus atom to give a P^{V} species, that

typically have ^{31}P chemical shifts around 0 ppm for P-O bond-containing species.³¹ These results suggest that phosphites are even more susceptible to side reactions with silica supports than the phosphines described in Sections 4.3 and 4.4, where only partial phosphine oxidation was observed.

4.7 Synthesis and reactivity of **L24**: 2,2'-bis(dibenzo[d,f][1,3,2]dioxaphosphepin-6-yloxy)-1,1'-biphenyl with silica

To gain a better understanding of this phosphite oxidation process occurring in the presence of silica, several test reactions were devised. Firstly, synthesis of a test phosphite, **L24**: 2,2'-bis(dibenzo[d,f][1,3,2]dioxaphosphepin-6-yloxy)-1,1'-biphenyl, featuring the same biphenyl phosphite moiety present in **L9** and **L21**, was performed according to a literature procedure (Scheme 4.11).³² NMR spectroscopic analysis and CHN elemental analysis of the product showed good agreement with reported literature values, including the ^{31}P NMR chemical shift of +144 ppm.³² **L24**, alongside many of its analogues featuring variously-substituted aryl rings, have been previously investigated as ligands for hydroformylation and are currently under patent by Evonik Operations GMBH.³² The design of **L24** for the purpose of this work focused on maintaining as similar phosphorus environment to **L9** and **L21** as possible, whilst removing the tethering functionality. This would allow the reactivity of the phosphite with silica to be observed without any other functionality present that could also potentially react with silica, and also allow solution-state NMR spectroscopic analysis of any reaction products to be performed.



Scheme 4.11. Synthesis of **L24**.

A toluene solution of **L24** was heated under reflux in the presence of silica under conditions identical to those used when investigating the reactivity of test phosphine, **L23**, with silica (see Chapter 4.4). ^{31}P NMR spectroscopic analysis of an aliquot of reaction mixture showed no change to the NMR spectrum of **L24** (Figure 4.11). This suggested that no direct reaction between the phosphite and the silica surface was occurring. To better simulate the tethering reaction conditions experienced during the immobilisation of **L9** and **L21**, a stoichiometric quantity of MeOH was then added to the reaction mixture to mimic the MeOH usually released as a side product of the reaction between an alkoxy silane and silica surface silanols. The reaction mixture was then heated at reflux for a further period of 4 h, after which time ^{31}P NMR spectroscopic analysis of a second aliquot of reaction mixture showed a new signal at +12 ppm with a relative intensity of ~ 0.2 . Unfortunately, attempts to isolate and identify the newly formed species were unsuccessful, as continued heating of the reaction mixture resulted in formation of multiple degradation products.

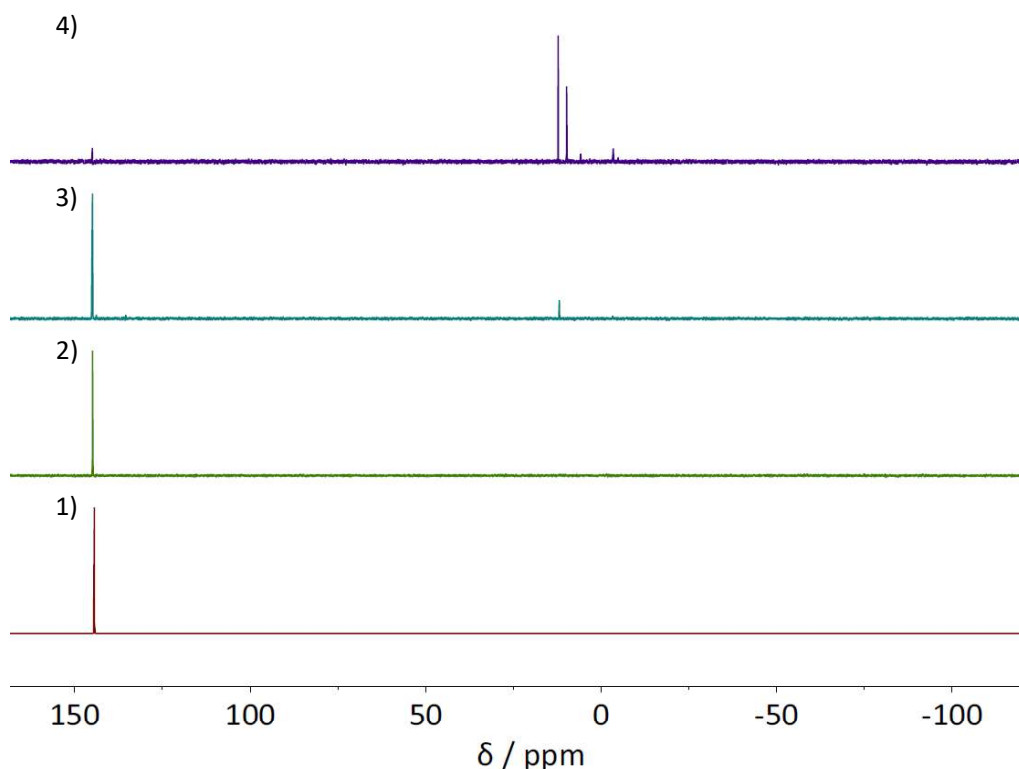
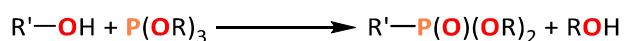


Figure 4.11. $^{31}\text{P}\{^1\text{H}\}$ NMR spectra (162 MHz, CDCl_3 , 300 K) of **1)** **L24**, **2)** **L24** heated at reflux with silica in toluene, **3)** **L24** heated at reflux in toluene with silica and MeOH for 4 hours and **4)** spectrum after extended heating (8 h) of **L24** with silica and MeOH.

The rearrangement of non-alkoxysilane-functionalised **L24** in the presence of silica is much slower than the analogous rearrangements of **L9** and **L21**. This supports the data described in Section 4.4 where phosphine **L23**, was shown to be stable in the presence of silica, while alkoxysilane-functionalised compounds **L1-3** underwent side reactions. However, in this case, phosphite **L24** has a slightly different phosphorus environment to phosphites **L9** and **L21**, which could also potentially affect its reactivity. These results do suggest, however, that phosphites are not stable to the silica-tethering reaction conditions and therefore will require protecting before further work into immobilisation can be performed.

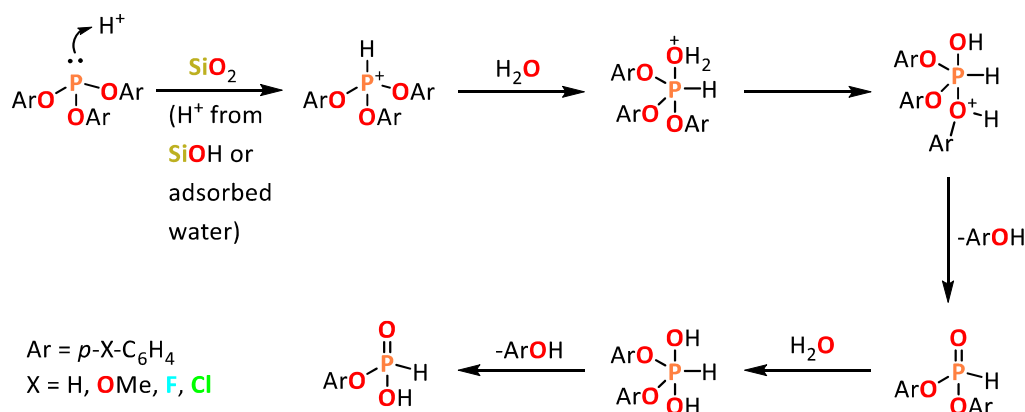
4.8 Possible phosphorus oxidation pathways for phosphites on silica

One possible explanation for the observed reactivity of **L9** and **L21** with silica could be that these phosphites are reacting with the alcohol formed during the tethering reaction in an alcohol-based Michaelis–Arbuzov reaction (Scheme 4.12). This type of reaction has been reported previously in the literature for small alkyl phosphites, such as methyl and ethyl derivatives.³³ It has recently been shown that alcohol-based Michaelis–Arbuzov reaction can be extended to other substrates, such as phenylphosphites, when catalytic I[−] from *n*-Bu₄NI is supplied.³⁴ The Michaelis–Arbuzov reaction is unlikely to be occurring during the tethering of **L9** and **L21** onto silica however, as no I[−] source is present.



*Scheme 4.12. General alcohol-based Michaelis–Arbuzov reaction.*³³

Another possible pathway for phosphite degradation on silica is by reaction with silica surface SiOH groups and residual water adsorbed to the silica surface to form hydrogen phosphonates (Scheme 4.13).³⁵ During the immobilisation of **L9** and **L21** onto silica methanol is released as a side product that could also act potentially act as a proton source or nucleophile, suggesting that methanolysis rather than hydrolysis of the phosphite could also potentially occur.



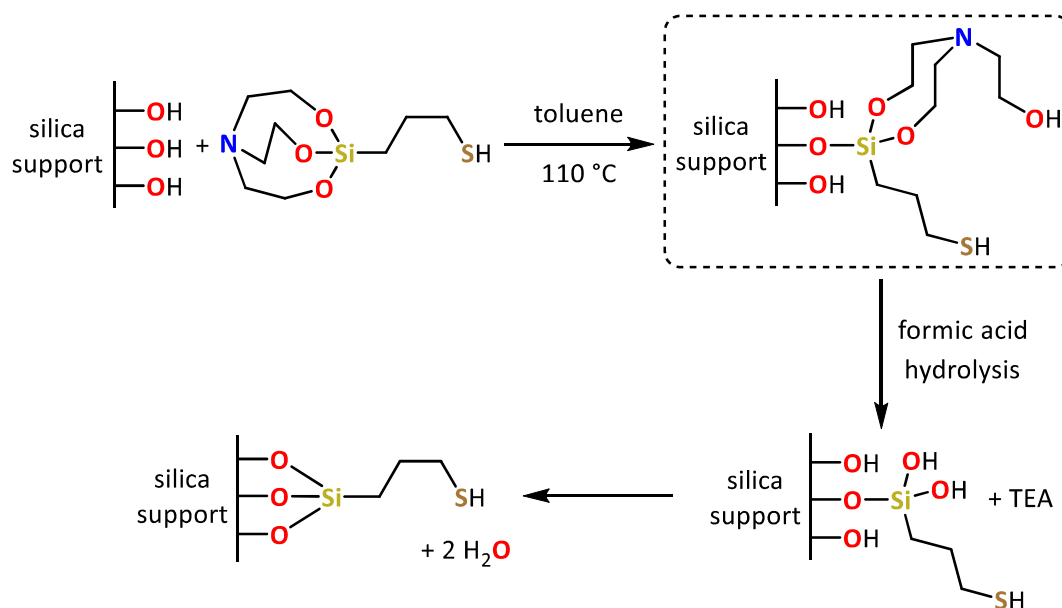
Scheme 4.13. Proposed mechanism for phosphite hydrolysis to aryloxy hydrogen phosphonates in the presence of silica adapted from Ghosh and Greer.³⁵

4.9 Introducing the silatrane functionality as a convenient silica tethering group

The work described in this chapter so far detailed the application of alkoxysilanes (and cyclic azasilanes) as tethering groups for the immobilisation of organic compounds onto oxide supports for applications in immobilised catalysis. However, over the course of this project the silatrane functionality was also investigated as a tethering functionality for the immobilisation of phosphines onto oxide supports. This use of silatranes in organic and inorganic chemical synthesis can provide several benefits over using alkoxysilanes, due to their significantly greater stability towards water and other nucleophiles, and self-condensation.³⁶ The more favourable physical properties of silatrane also greatly improves their ease of handling and purification relative to alkoxysilanes, which tend to be viscous, sticky solids that are difficult to physically manipulate.³⁷ Silatranes are essentially protected trialkoxysilanes and are known to react more slowly with oxide supports than alkoxysilanes.³⁸ Nevertheless, immobilisation of functionalised silatranes on silica has been successfully achieved in the literature, predominantly during development of novel antifouling coatings.^{38,39}

A recent example of a silatrane being used to functionalise silica was 3-mercaptopropylsilatrane by Lämmerhofer *et al.* (Scheme 4.14).⁴⁰ Using a combination of CHNS elemental analysis and SS NMR spectroscopic analysis, it was shown that reaction of the silatrane with silica in anhydrous toluene resulted in partial hydrolysis of

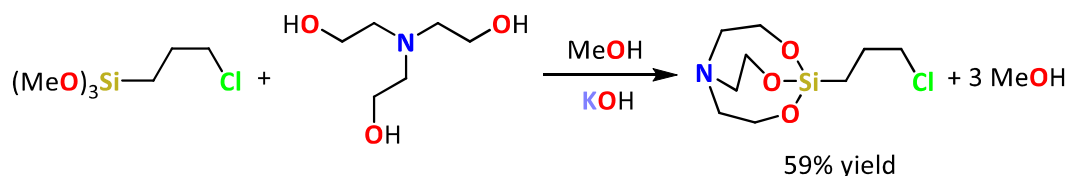
the silatrane functionality, as a result of forming Si-O bonds with the silica surface, when reaction times of up to 7 hours were employed. In order to fully hydrolyse the silatrane, and liberate triethanolamine, a weak acid, such as formic acid, was required. Addition of the acid resulted in formation of three bonds to the silica surface as evidenced by the presence of silicon T³ sites in the resulting SS NMR spectrum and loss of nitrogen from the silica according to CHNS elemental analysis.



Scheme 4.14. 3-mercaptopropylsilatrane silica-immobilisation reaction pathway before and after acid catalyst addition adapted from Lämmerhofer et al.⁴⁰

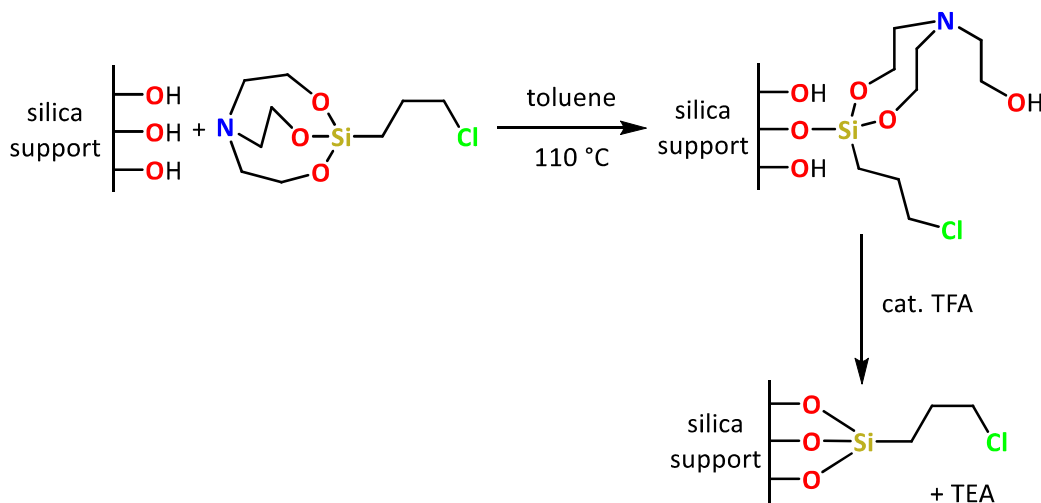
4.10 3-Chloropropylsilatrane synthesis and immobilisation on silica

In order to investigate the synthesis and subsequent reactivity of silatranes with silica we selected 3-chloropropylsilatrane as an initial silatrane synthesis target, as it could potentially be used as a building block for further ligand synthesis through functionalisation at the chloro group. Also, the simple structure makes it an ideal test compound for initial investigations into immobilisation of silatranes. 3-Chloropropylsilatrane was synthesised using a modified literature procedure by reaction of 3-chloropropyltrimethoxysilane with triethanolamine (TEA) in the presence of a KOH catalyst (Scheme 4.15).⁴¹ Subsequent ¹H and ¹³C NMR spectroscopic and CHN elemental analyses of the product showed good agreement with literature data.²⁵



Scheme 4.15. Synthesis of 3-chloropropylsilatrane.

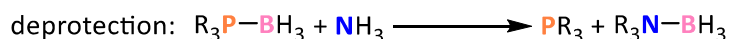
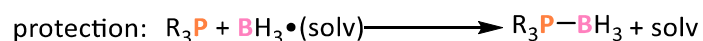
The reactivity of 3-chloropropylsilatrane with silica was investigated by reaction with AEROPERL 300/30 silica (previously calcined at 200 °C) in toluene following a procedure adapted from Lämmerhofer *et al* (Scheme 4.16).⁴⁰ After heating at reflux in toluene for 4 hours, only a trace amount of triethanolamine (the byproduct from complete silatrane hydrolysis) was observed by ¹H NMR spectroscopic analysis of an aliquot of the liquid reaction mixture, as would be expected according to Lämmerhofer *et al*. A catalytic amount of trifluoroacetic acid (TFA) was then added to the reaction mixture and the mixture heated at reflux for a further three hours. After workup, CP and HPDEC SS ²⁹Si NMR spectroscopic analysis of the product indicated the presence of Si T² alongside predominantly T³ sites, in agreement with Lämmerhofer *et al.*, suggesting that full hydrolysis of the silatrane had occurred. These results indicate that the silatrane functionality is a useful tool for the immobilisation of organic compounds to silica supports with the potential to be expanded to the immobilisation of phosphine ligands and metal complexes for applications in hydroformylation catalysis.



Scheme 4.16. Silica-immobilisation of 3-chloropropylsilatrane.

4.11 Investigations into utilising phosphine-borane protecting groups in the synthesis of silica-immobilised phosphines

So far, the contents of this chapter have focused on the preparation of phosphine-modified silicas as catalyst supports. Using this strategy, the functionalised support could be further modified for various catalysis applications by addition of the appropriate metal precursors. Unfortunately, attempts to selectively immobilise phosphines on silica in this work routinely suffered from the occurrence of significant side reactions between the immobilised phosphines and the silica support, forming species unsuitable for the desired catalyst applications. To avoid these issues, alternative synthetic strategies were considered, such as protecting the phosphines as borane adducts during immobilisation. Phosphine-borane adducts are commonly used to protect phosphorus(III) compounds due to their convenient synthesis from their parent phosphines and BH_3 solvates, and facile deprotection using amines as competing Lewis bases (Scheme 4.17).⁴² Phosphorus-borane adducts exhibit significantly improved stability to air and moisture over phosphines, as well as modified reactivity in numerous other processes, allowing significantly easier handling, as well as greater reactivity control than with their corresponding parent phosphines.⁴³

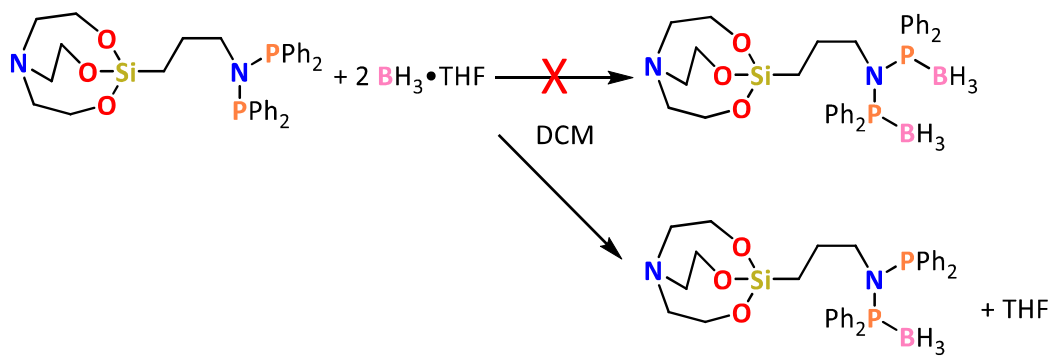


*Scheme 4.17. General formation and deprotection of phosphine-borane adducts.*⁴²

Consequently, in order to explore ways in which the observed formation of side products during the attempted immobilisations detailed in Chapters 4.3-4.7 could be circumvented, phosphine protection as their borane adducts before immobilisation was targeted. It was envisioned that by protecting the phosphorus atoms as borane adducts, the phosphorus reactivity observed during tethering to silica could be attenuated, since the phosphorus lone pair is not available to react.

4.11.1 Attempted synthesis of $L5(BH_3)_2$: $((BH_3)PPh_2)_2N(CH_2)_3Si(OCH_2CH_2)_3N$

Synthesis of the **L5** phosphine-borane adduct, $L5(BH_3)_2$, was attempted by stirring **L5** with two equivalents of $BH_3 \cdot THF$ in DCM overnight at ambient temperature, following a modified literature procedure (Scheme 4.18).⁴⁴



Scheme 4.18. Attempted synthesis of $L5(BH_3)_2$; synthesis of $L5(BH_3)$.

Both ^{31}P and ^{11}B NMR spectroscopy of an aliquot of the reaction mixture showed two peaks in the spectra, corresponding to selective formation of the mono-borane, with half the $BH_3 \cdot THF$ starting material remaining. Upon layering the reaction mixture with hexane, colourless crystals suitable for XRD analysis were obtained. The resulting crystal structure supported the NMR spectral assignment that the mono-borane product had been produced (Figure 4.12).

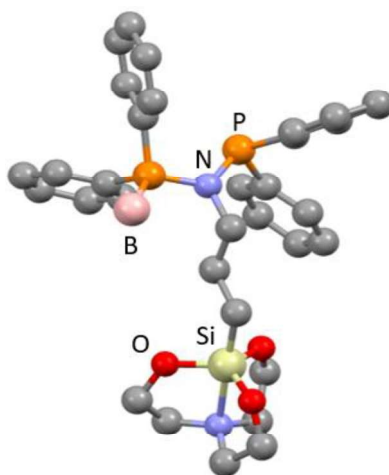
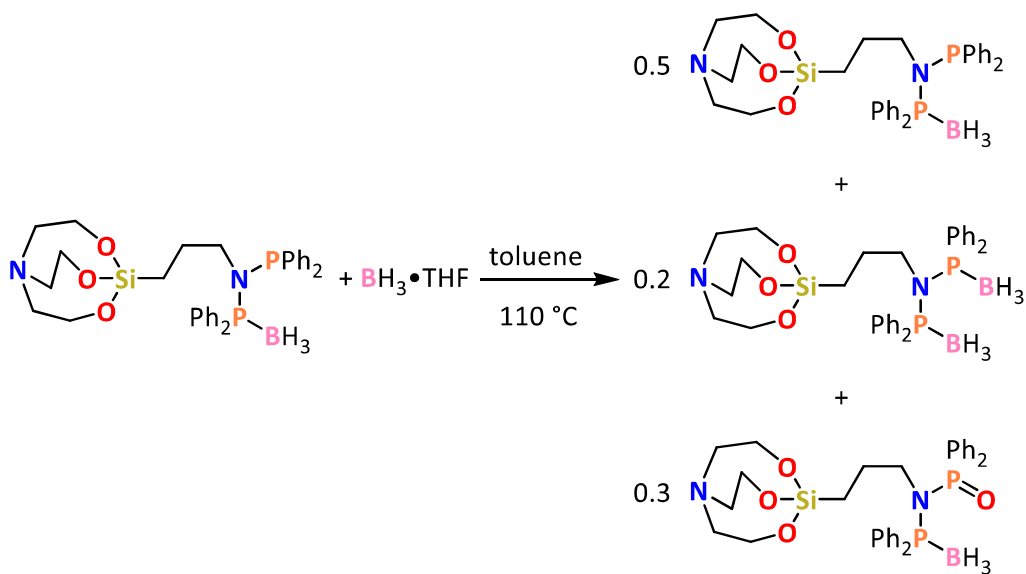


Figure 4.12. Molecular structure of $L5(BH_3)$. Hydrogens omitted for clarity. Selected bond angles / °: P-N-P 121.7(2); N-P-B 112.4(2). Selected bond lengths / Å: P-B 1.917(4); P-N 1.688(3), 1.720(3); Si-N 2.190(3); Si-C 1.879(3).

The molecular structure of **L5**(BH₃) (Figure 4.12) shows the same formal phosphorus lone pair orientation as determined for **L5** (*i.e.* staggered). The BH₃ group bonds to the phosphorus lone pair facing away from the PNP moiety, presumably due to steric considerations. The PNP angle of 121.7(2)° is reasonably close to the 120.08(8)° angle found in **L5**, suggesting that addition of BH₃ does not introduce significant strain into the system. The P-B bond length of 1.917(4) Å is in good agreement with typical BH₃-PR₃ bonds in the literature, typically 1.93 Å.⁴⁵

To encourage formation of the desired di-borane adduct, the obtained mono-borane was reacted with another equivalent of BH₃•THF in toluene at reflux for 48 hours (Scheme 4.19). Subsequently, ³¹P and ¹¹B NMR spectroscopy of an aliquot of the reaction mixture showed that the mono-borane was still the major species present in solution. Upon layering the reaction mixture with hexane, colourless crystals suitable for XRD analysis were again obtained. The crystal structure corresponded to the mono-borane with disorder around the second phosphorus atom (Figure 4.13). These data are consistent with the crystals comprising a mixture of the mono- and di-borane, and the mixed phosphine-borane phosphine oxide, present in a 0.5:0.2:0.3 ratio. Formation of the oxidation product likely resulted from reaction of **L5**(BH₃) with trace O₂ present in the solvent. Due to the small quantities present and similar nature of these compounds, separation was not attempted.



Scheme 4.19. Attempted synthesis of **L5**(BH₃)₂ in toluene at reflux.

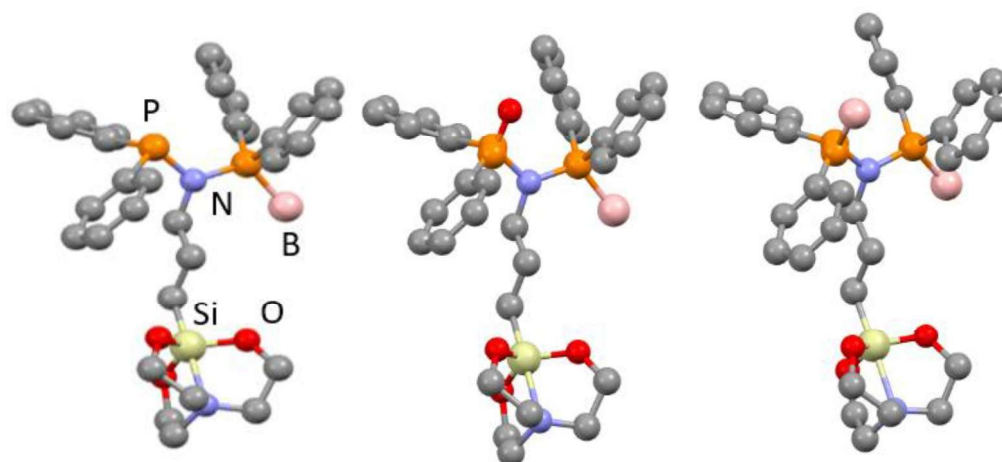
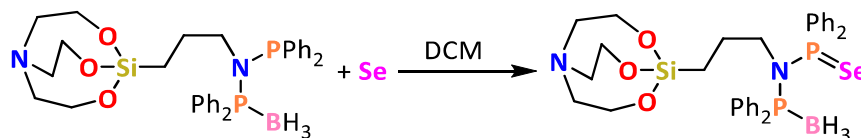


Figure 4.13. Molecular structure of **L5**(BH₃) with disordered phosphorus lone pair, *P:P=O:P-B* 0.5:0.3:0.2. Hydrogens omitted for clarity. Selected bond angles / °: *P-N-P* 121.1(1); *N-P-B* 113.14(8), 123.5(9). Selected bond lengths / Å: *P-B* 1.916(2), 1.915(4); *P-N* 1.686(1), 1.716(3); *P=O* 1.371(5), *Si-N* 2.176(1); *Si-C* 1.875(2).

It is not clear why attempted synthesis of the **L5**(BH₃) failed, as many di-phosphine and di-phosphite di-boranes have been successfully produced using similar methods in the literature.^{46,47} However, there are very few *bis*(borane)-protected PNP-type compounds that have been reported. Two *bis*(borane) PNP examples have been described previously; however these both possess an H atom at the amine moiety.^{44,48} As far as the author is aware, no examples of PNP mono-borane adducts have been previously reported in the literature.

One possible explanation for the observed reactivity of **L5** with BH₃•THF could be that formation of the di-borane is disfavoured due to steric reasons. To investigate this, **L5**(BH₃) was reacted with elemental selenium (Se empirical covalent radius 115 pm, *cf.* B = 85 pm. B-H bond length = 119 ppm)⁴⁹ in an NMR tube (Scheme 4.20). Full conversion to the phosphorus selenide was observed after sonication for 30 minutes, as determined by ³¹P NMR spectroscopy. The ³¹P NMR spectrum showed a broad singlet corresponding to the P-BH₃ (δ ³¹P = +73; ν_{1/2} = 103 Hz) and a doublet with satellites (δ ³¹P = +67; ²J_{PP} = 13 Hz) corresponding to the P-Se moiety. A |¹J_{SeP}| value of 779 Hz was measured, in good agreement with the |¹J_{SeP}| value of 782 Hz measured for **L5**, suggesting that the presence of the borane does not have a large impact on the basicity of the phosphine adjacent to it and that, to a first approximation, that steric factors potentially hinder

formation of the *bis*(borane) adduct. The fact that the phosphorus atom is free to react with selenium also suggests that the borane in **L5**(BH₃) is not bridging between the two phosphorus atoms, and hence occupying both phosphorus lone pairs. This is supported by the molecular structure of **L5**(BH₃) where the borane is located on a single phosphorus atom.

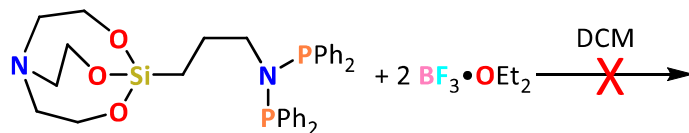


*Scheme 4.20. Synthesis of **L5**(BH₃)(Se).*

Another consideration in the reactivity of **L5**(BH₃) with BH₃•THF is the nature of the P-N bond in **L5**(BH₃). The molecular structure of **L5**(BH₃) (Figure 4.12) shows a trigonal planar geometry of the nitrogen atom. This suggests delocalisation of the nitrogen lone pair into the two N-P bonds, giving rise to some multiple bond character between the nitrogen and the phosphorus atoms, as is commonly seen for PNP compounds.⁵⁰ Further evidence for this is provided by the molecular structure of **L5**(BH₃), which highlights the shortening of the P-N bond distance (1.718(1) to 1.688(3) Å) upon phosphorus-borane adduct formation. This is consistent with increased P-N multiple bond character resulting from a more electron-deficient phosphorus atom arising from P-BH₃ Lewis adduct formation. However, as the P-N bond length of the uncoordinated phosphorus in **L5** and **L5**(BH₃) are within 3σ, 1.718(1) and 1.720(3) Å respectively, the coordination of BH₃ to one phosphorus does not appear to have a large impact on the electronics of the uncoordinated phosphorus, as was indicated by the similar $|^1J_{\text{SeP}}|$ constants in **L5**Se₂ and **L5**(BH₃)(Se). In light of these findings, it seems unlikely that the reason that **L5**(BH₃)₂ formation is disfavoured is trivial in nature.

In order to further investigate whether electronic effects were having a large impact on the borane adduct-forming reaction, BH₃ was replaced with the much more Lewis acidic BF₃, while maintaining similar reactant size, BH₃ vs. BF₃ (Scheme 4.21). The reaction was performed according to an adapted literature procedure, using DCM solvent and BF₃•OEt₂ as the BF₃ source.⁵¹ ³¹P NMR spectroscopy of an aliquot of reaction mixture indicated complete decomposition of the phosphine starting material after 12 h, and

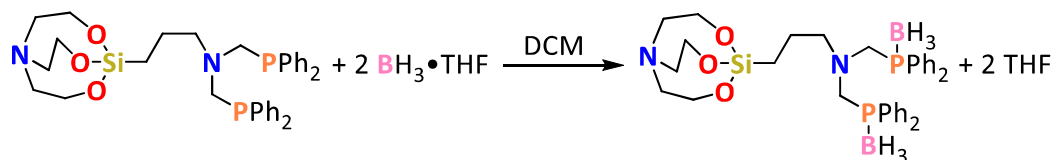
hence the reaction was abandoned. This may be a result of the phosphine- BF_3 adduct reacting with the DCM solvent, which has been shown to occur for certain phosphine- BF_3 adducts in the literature.⁵¹ Unfortunately, **L5** is insoluble in hexane, which is the only other solvent that has been reported for the synthesis of phosphine- BF_3 adducts.



Scheme 4.21. Attempted reaction of **L5** with $\text{BF}_3 \cdot \text{THF}$.

4.11.2 Synthesis of $\text{L17}(\text{BH}_3)_2$ ($\text{Ph}_2\text{P}(\text{BH}_3)\text{CH}_2)_2\text{N}(\text{CH}_2)_3\text{Si}(\text{OCH}_2\text{CH}_2)_3\text{N}$)

To investigate the effect of P[^]P bite angle on the reactivity of diphosphines with $\text{BH}_3 \cdot \text{THF}$, the borane protection of the PCNCP **L17** was attempted. It was envisioned the reaction would afford the *bis*(borane) derivative, as **L17** does not display the unique behaviour associated to PNP compounds due to their partial P-N multiple bond character.⁵⁰ Thus, **L17** was reacted with $\text{BH}_3 \cdot \text{THF}$ in DCM using the same procedure as when reacting **L5** with $\text{BH}_3 \cdot \text{THF}$ (Scheme 4.22). Indeed, after overnight stirring, ^{31}P and ^{11}B NMR spectroscopic analysis of an aliquot of the crude reaction mixture confirmed that complete conversion to the desired *bis*(borane) derivative had been achieved. The target compound $\text{L17}(\text{BH}_3)_2$ was then precipitated by addition of hexane and isolated by filtration.



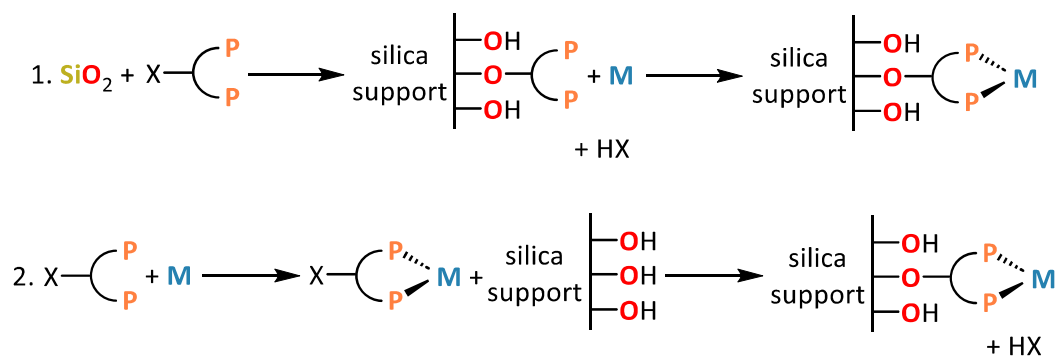
Scheme 4.22. Synthesis of $\text{L17}(\text{BH}_3)_2$.

Successful protection of **L17** as its diphosphine borane using $\text{BH}_3 \cdot \text{THF}$ follows the typically expected behaviour for phosphine compounds. This provides further evidence that the unique steric and electronic properties of PNP type compounds is the origin of their differing reactivity with boranes. Seeing as phosphine protection as phosphine boranes was not a trivial process that could be applied to all the phosphine ligands

investigated in this work, immobilisation of borane protected phosphines for applications in immobilised catalysis were not investigated further.

4.12. Synthesis of silica-immobilised rhodium(I) complexes

Immobilisation of phosphines on silica followed by addition of the desired metal precursor (Scheme 4.23.1) provides a versatile way to produce a variety of immobilised catalysts for different applications depending on the identity of the metal used. An alternative approach to this is formation of the desired metal complex prior to immobilisation on the catalyst support (Scheme 4.23.2). Although this approach is less flexible than the aforementioned method, requiring synthesis and isolation the desired complex before immobilisation, it may have an advantage in that the phosphine lone pairs are coordinated to the metal deterring other reactivity. This approach was shown to eliminate side reactions between immobilised dppa-type phosphine ligands and a silica support when complexed to NiCl_2 before addition to the support.²⁵ Therefore, several rhodium complexes described in Chapter 3 were reacted with silica to produce immobilised rhodium complexes whilst trying to minimise phosphine oxidation.

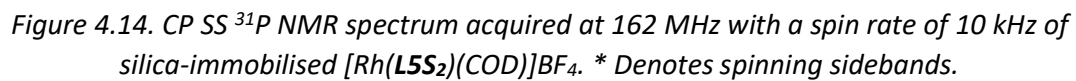
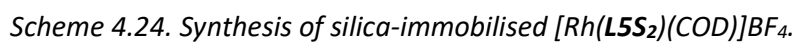


Scheme 4.23. Synthesis of a generic metal (M) immobilised on silica via a tetherable phosphine ligand by; 1. Immobilised phosphine synthesis followed by metal complexation; 2. Phosphine-metal complexation followed by silica-immobilisation.

4.12.1 Silica immobilisation of $[\text{Rh}(\text{L5S}_2)(\text{COD})]\text{BF}_4$

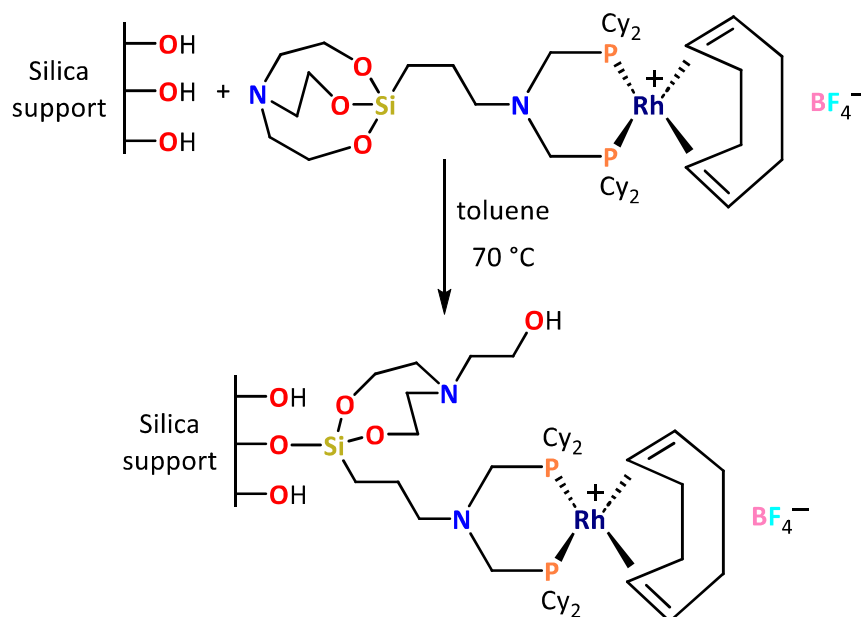
Immobilisation of $[\text{Rh}(\text{L5S}_2)(\text{COD})]\text{BF}_4$ on silica was performed according to the general method detailed in Scheme 4.23.2 (Scheme 4.24). As the phosphorus atoms in this complex are P^{V} , it was envisioned that side reaction with the silica support could be avoided, allowing silatrane-immobilisation of metal complexes to be studied without further complications. Acidic conditions were not employed in this reaction to avoid decomposition of the complex, therefore only partial hydrolysis of the silatrane was expected upon reaction with silica.

Due to the poor solubility of $[\text{Rh}(\text{L5S}_2)(\text{COD})]\text{BF}_4$ in toluene and sparing solubility in PhCl, the reaction with AEROPERL 300/30 silica (calcined at 200 °C) was performed in a DCM/PhCl solvent mixture at 70 °C. After 4 h the silica had turned yellow due to incorporation of the rhodium complex onto the silica surface. In contrast, when the reaction was attempted in only DCM heated to reflux, no reaction was observed, suggesting that 40 °C is too low a temperature to enable reaction between silica and the silatrane functionality. SS ^{31}P NMR spectroscopic analysis (Figure 4.14) indicated successful incorporation of $[\text{Rh}(\text{L5S}_2)(\text{COD})]\text{BF}_4$ onto the silica surface through the presence of a signal at +71 ppm, in good agreement with the solution state NMR spectroscopic analysis of the complex. In addition to this signal, a second minor signal at +59 ppm was observed in the NMR spectrum corresponding to the free ligand. This suggests that the sulfur donor ligand **L5S₂** may be fairly labile, and that some rhodium was lost during the immobilisation reaction or washing process. This result brings concerns with respect to metal leaching during catalysis, which will be discussed in Section 5.5.2.



4.12.2 Silica immobilisation of $[\text{Rh}(\text{L19})(\text{COD})]\text{BF}_4$

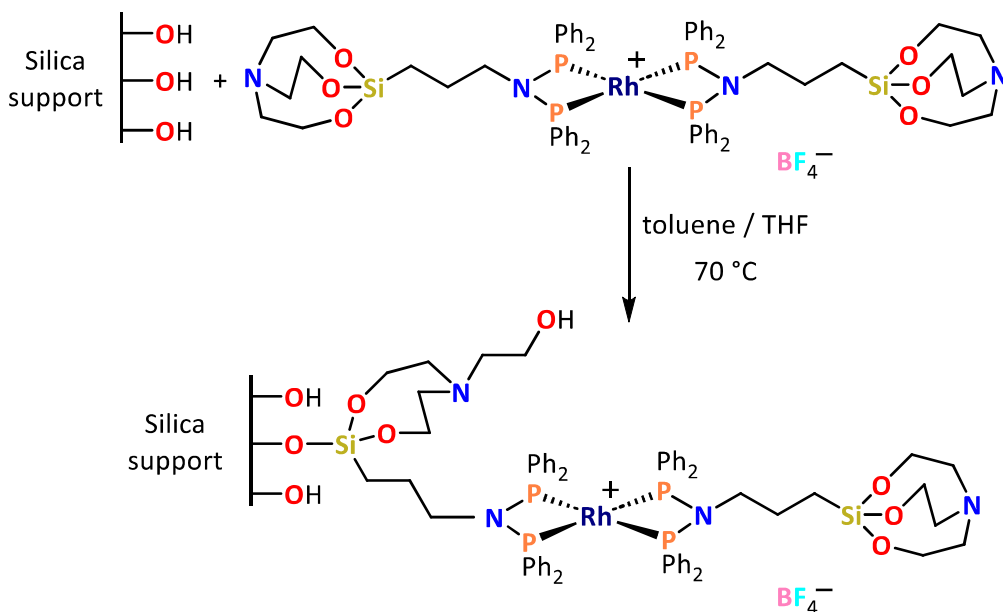
Immobilisation of the phosphine-ligated complex $[\text{Rh}(\text{L19})(\text{COD})]\text{BF}_4$ was performed by reaction of $[\text{Rh}(\text{L19})(\text{COD})]\text{BF}_4$ with AEROPERL 300/30 silica (calcined at 200 °C) in toluene at 70 °C (Scheme 4.25). This temperature was selected as it was the minimum temperature that silatrane reactivity with silica was observed (see Section 4.12.1). After stirring the solution for 2 h, it had become colourless and the silica yellow, suggesting complete immobilisation of the rhodium complex onto silica. Subsequent SS ^{31}P NMR spectroscopic analysis showed a resonance at +8 ppm corresponding to immobilised $[\text{Rh}(\text{L19})(\text{COD})]\text{BF}_4$. Additionally, a complicated resonance at +57 ppm was also observed in an approximate 1:2 ratio with the resonance at +8 ppm. The exact species responsible for the resonance at +57 ppm cannot be identified with the available data, although it is in the appropriate range for P^{V} species containing the $-\text{CH}_2\text{P}^{\text{t}}\text{Bu}_2$ fragment, of around +60 ppm.⁵² This suggests that phosphorus oxidation was observed during the reaction of $[\text{Rh}(\text{L19})(\text{COD})]\text{BF}_4$ with silica, most likely indicating that the phosphine ligand is labile. As **L19** is an electron-rich alkyl phosphine, this may also increase the favourability of oxidation reactions relative to less electron rich phosphines.



Scheme 4.25. Synthesis of silica-immobilised $[\text{Rh}(\text{L19})(\text{COD})]\text{BF}_4$.

4.12.3 Silica immobilisation of $[\text{Rh}(\text{L5})_2]\text{BF}_4$

$[\text{Rh}(\text{L5})_2]\text{BF}_4$ was reacted with AEROPERL 300/30 silica (calcined at 200 °C) in a toluene/THF solvent mixture at 70 °C, required in order to fully solubilise the $[\text{Rh}(\text{L5})_2]\text{BF}_4$ (Scheme 4.26). After 4 h, the solution became colourless and the silica yellow, suggesting that the reaction was complete. SS ^{31}P NMR spectroscopic analysis confirmed that immobilisation of the complex had been successful (Figure 4.15), with a resonance at +65 ppm corresponding to immobilised $[\text{Rh}(\text{L5})_2]\text{BF}_4$. The signal is expected to be a doublet as $^1J_{\text{RhP}}$ coupling is observed in solution; however, the line broadening inherent with SS NMR spectroscopic analysis means that a singlet is observed in the solid state (FWHM = 1120 Hz). Alongside the resonance attributed to $[\text{Rh}(\text{L5})_2]\text{BF}_4$, a small (<10%) broad resonance centred at +40 ppm that could not be assigned was observed.



Scheme 4.26. Synthesis of silica-immobilised $[\text{Rh}(\text{L5})_2]\text{BF}_4$.

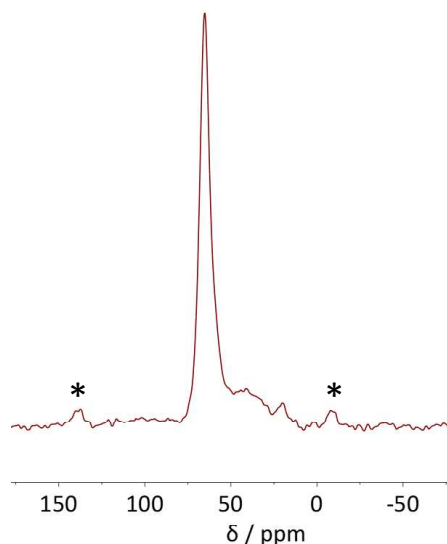


Figure 4.15. CP SS ^{31}P NMR spectrum acquired at 162 MHz with a spin rate of 12 kHz of silica-immobilised $[\text{Rh}(\text{L5})_2]\text{BF}_4$. * Denotes spinning sidebands.

When comparing the silica-immobilisation of $[\text{Rh}(\text{L5})_2]\text{BF}_4$ to that of PNP ligands **L1-L4**, described in Section 4.4, a large increase in selectivity for desired product is observed when tethering $[\text{Rh}(\text{L5})_2]\text{BF}_4$. This shows the positive effect of immobilising a complex rather than free ligand on the stability of phosphines during immobilisation onto silica. It is hypothesised that further reducing the reaction temperature during the silica-immobilisation of rhodium complexes, such as $[\text{Rh}(\text{L5})_2]\text{BF}_4$, could eliminate side product formation altogether; however this is not possible while using the silatrane functionality as the tethering group. Indeed, it has previously been shown that side reactions of phosphines and phosphine-containing complexes with silica during their immobilisation using alkoxysilane tethering groups can be suppressed by lowering the reaction temperature.²⁴

As $[\text{Rh}(\text{L5})_2]\text{BF}_4$ contains two equivalents of **L5**, there is additional complexity in the pathway for its silica-immobilisation relative to complexes containing only one equivalent of tetherable ligand. This gives rise to another possible product to the one shown in Scheme 4.26, where both silatrane functionalities have reacted with the silica (Figure 4.16). Unfortunately, due to the low abundance of the silatrane group on the silica surface and low sensitivity of the ^{29}Si nuclei for NMR spectroscopic analysis, sufficient signal could not be obtained in the SS ^{29}Si NMR spectrum to determine which, or indeed if both of these binding modes are present. The flexible nature of the alkyl

spacer in the ligand backbones suggests that both modes of immobilisation onto the support could be possible. Additionally, from the molecular structure of $[\text{Rh}(\text{L5})_2]\text{BF}_4$ its dimensions were calculated to be $19 \text{ \AA} \times 10 \text{ \AA} \times 9 \text{ \AA}$, suggesting that the complex should comfortably fit within the silica pores, allowing both silatrane functionalities to react (pore vol. = $1.85 \text{ cm}^3 \text{ g}^{-1}$, avg. pore diameter = 260 \AA).^{10,11}

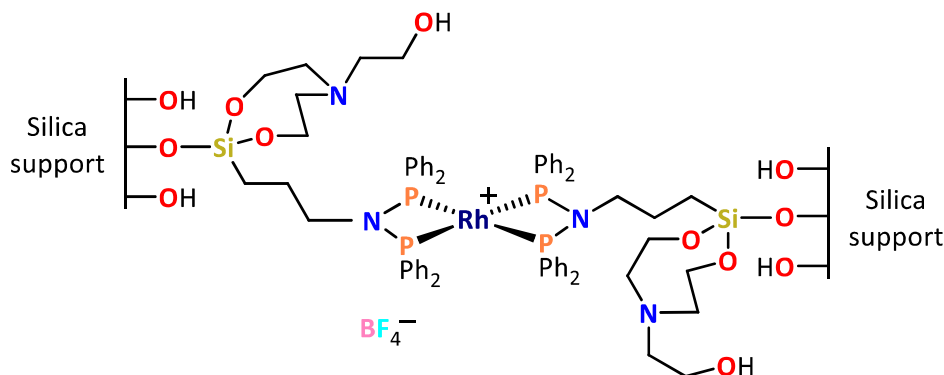
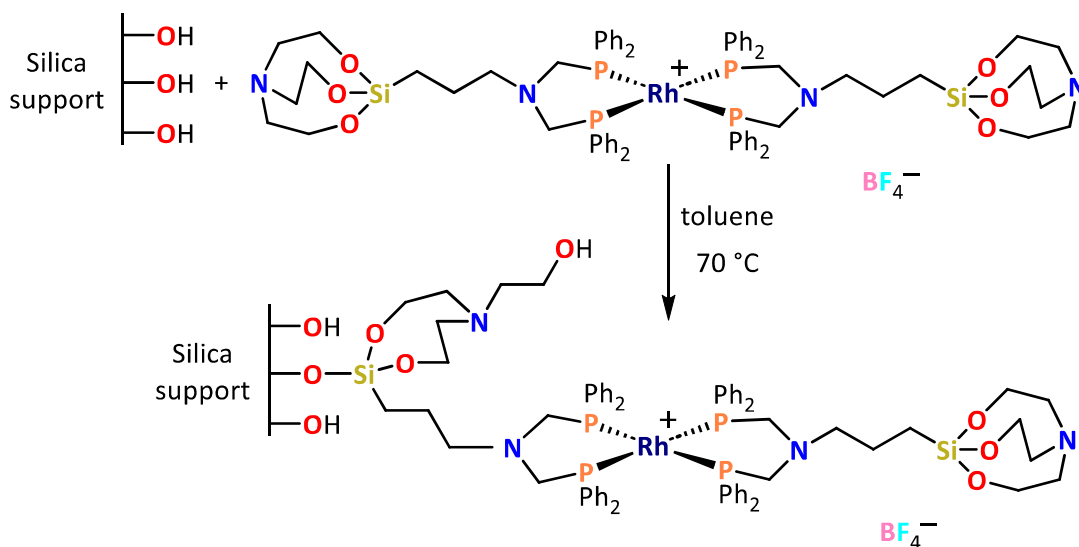


Figure 4.16. Alternative possible product for the reaction of $[\text{Rh}(\text{L5})_2]\text{BF}_4$ with silica.

4.12.4 Silica immobilisation of $[\text{Rh}(\text{L17})_2]\text{BF}_4$

The reaction of $[\text{Rh}(\text{L17})_2]\text{BF}_4$ with AEROPERL 300/30 silica calcined at 200°C was performed in toluene at 70°C (Scheme 4.27) following the same procedure that was used for the immobilisation of $[\text{Rh}(\text{L5})_2]\text{BF}_4$ (see section 4.12.3). The resulting sample was characterised by SS ^{31}P NMR spectroscopic analysis, which showed a single resonance at +8 ppm, corresponding to immobilised $[\text{Rh}(\text{L17})_2]\text{BF}_4$, confirming clean immobilisation of the complex (>95%). SS ^{29}Si NMR spectroscopic analysis was not able to ascertain whether one or both of the silatrane functionalities in the complex had reacted with silica, as was the case for the silica-immobilised $[\text{Rh}(\text{L5})_2]\text{BF}_4$ produced (see Section 4.12.3). The immobilised complexes detailed in Section 4.12 were investigated as catalysts for 1-octene hydroformylation to assess their capabilities with respect to catalyst activity, selectivity and stability to leaching, see Chapter 5 for details.



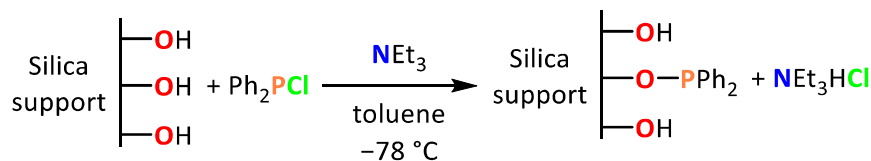
Scheme 4.27. Synthesis of silica-immobilised $[Rh(L5)_2]BF_4$.

4.13 Investigating the reaction of Ph_2PCl with silica

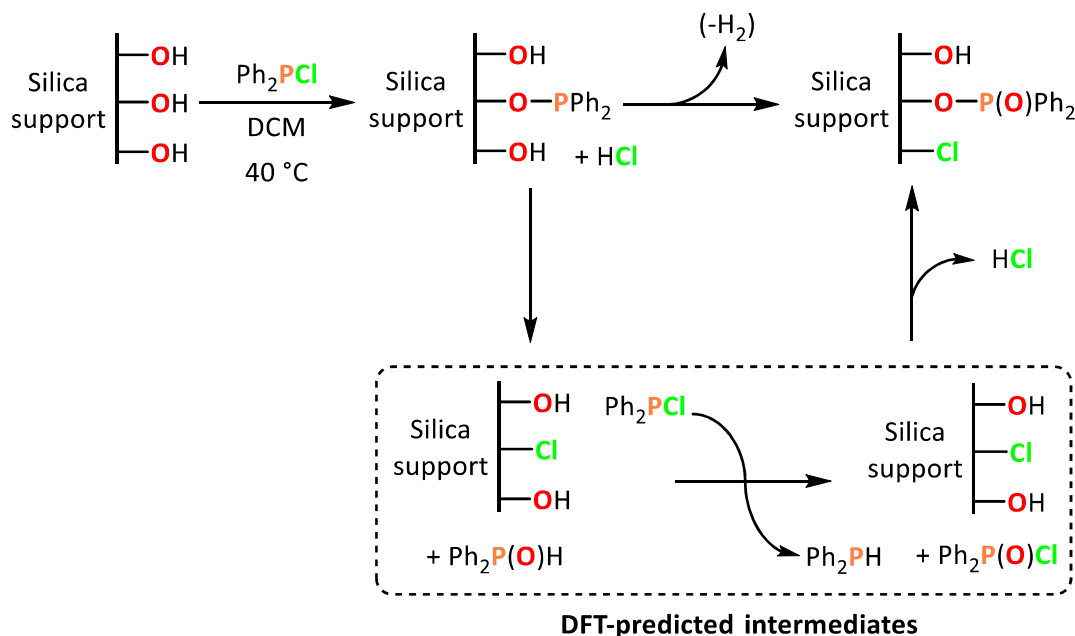
Despite great interest in the phosphine-functionalisation of surfaces for applications in immobilised catalysis using pendant tethering groups, such as alkoxy silanes, surprisingly, very little work has been done on covalently attaching phosphine moieties directly onto a surface.⁵³ Usually, an organic linker with a dedicated tethering functionality is employed to separate the immobilised phosphine from the silica surface.^{20,24} However, one possible way to achieve direct phosphine functionalisation onto a silica surface is by the reaction of a chlorophosphine with silica surface silanols (Scheme 4.28). This approach offers a potentially cheap, facile method of producing a phosphine-functionalised support for applications in catalysis.

To the best of the author's knowledge, the only reported direct immobilisation of a phosphine onto silica *via* a Si-O-PR₂ linkage involved using Ph_2PCl to generate a diphenylphosphine moiety on silica, reported by Verdonck *et al.* for the coordination of $RuCl_3$.⁵⁴ In the study FTIR and XPS experiments were used to suggest that the addition of Ph_2PCl yielded discrete Si-O-PPh₂ moieties on the silica surface that could be later used as ligands for coordination of ruthenium in a monodentate or bidentate fashion. More recent work investigating these claims was performed by Fontaine *et al.* using multinuclear NMR spectroscopy, attenuated total reflection infrared spectroscopy (ATR-

IR), and computational DFT methods to better understand the behaviour of Ph_2PCl immobilised on silica surfaces.⁵³ Subsequent analysis by Fontaine *et al.* suggested that addition of PPh_2Cl to silica leads to immobilisation followed by oxidation of the phosphine to $-\text{P}(\text{O})\text{Ph}_2$, even in the absence of oxygen, due to side reactions with the silica support. This results in a species not useful for applications in immobilised hydroformylation catalysis. In both the studies by Verdonck *et al.* and Fontaine *et al.*, the reaction of PPh_2Cl with silica was performed in refluxing DCM, with no *in situ* base present to neutralise the HCl produced during the reaction. As phosphines are well known to undergo side reactions with silica surfaces, especially at elevated temperatures (as discussed in Section 4.3), it is perhaps not surprising that this was exacerbated further upon the introduction of HCl to the system. This was taken into account in DFT studies by Fontaine *et al.* where a mechanism for the oxidation of the silica-immobilised diphenylphosphine moiety was predicted, which involved HCl (Scheme 4.29).⁵³ Therefore, it was of interest to us to repeat these experiments at -78°C with the addition of NEt_3 as an *in situ* base, to determine whether this would suppress the phosphine oxidation side reactions (Scheme 4.28).



*Scheme 4.28. The reaction of Ph_2PCl with silica, featuring NEt_3 as an *in situ* base.*



Scheme 4.29. The reaction of Ph_2PCl with silica and subsequent phosphine oxidation showing intermediates predicted using DFT by Fontaine *et al.*⁵³

SS ^{31}P NMR spectroscopic analysis of the phosphine modified silica was performed (Figure 4.17) showing significantly different results than those of Fontaine *et al.* A single resonance at +22 ppm was reported in the prior work, where an *in situ* base was not used, corresponding to silica- $\text{OP}(\text{O})\text{Ph}_2$.⁵³ While this was still observed in our current work (overlapping with a spinning sideband), suggesting that some oxidation of the phosphine had occurred, it corresponds to the minor product. The major resonance is located at +104 ppm, corresponding to surface bound PPh_2 . Literature values of solution-state ^{31}P NMR chemical shifts of +95 ppm for $\text{Ph}_2\text{POSiMe}_3$ and +108 ppm for $(\text{Ph}_2\text{PO})_4\text{Si}$ suggest that is a reasonable chemical shift to attribute to silica-bound PPh_2 .^{55,56} Integration of the NMR spectra suggests a 63% selectivity for target product, although this may not be completely reliable due to the nature of the CP experiment. Attempts to further increase the reaction selectivity by tuning the support used were unsuccessful. Changing the silica calcination temperature from 200 to 600°C resulted in a small decrease in selectivity to 55%, while changing the support type to gamma alumina drastically reduced selectivity for surface bound $-\text{OPPh}_2$ to 5%.

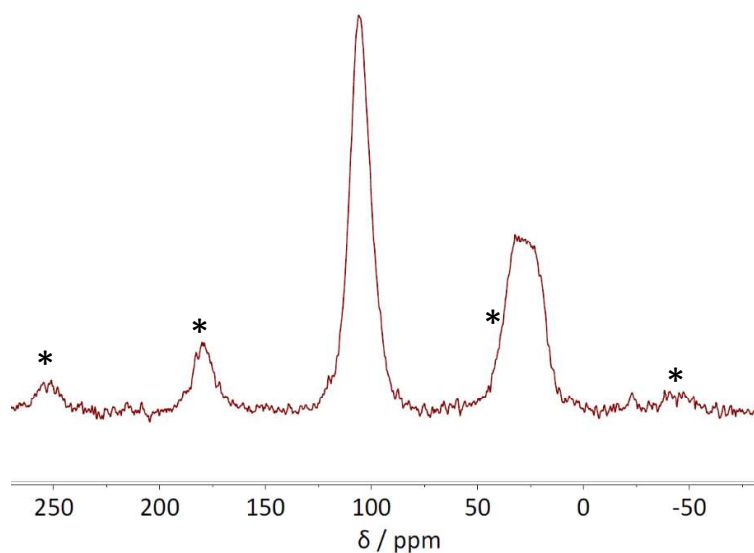
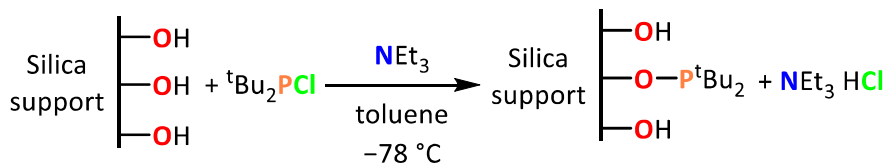


Figure 4.17. CP SS ^{31}P NMR spectrum acquired at 162 MHz with a spin rate of 10 kHz of the reaction of Ph_2PCl with AEROPERL 300/30 silica (calcined at 200 °C) in the presence of NEt_3 . * Denotes spinning sidebands.

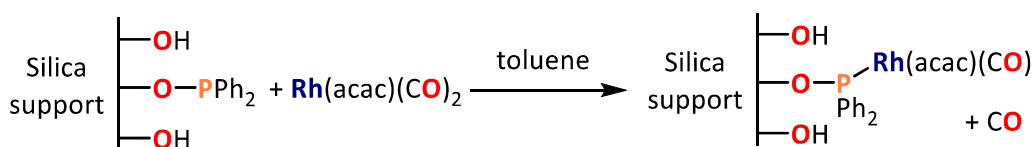
The effect the identity of the chlorophosphine has on reactions of chlorophosphines with silica was investigated using $^t\text{Bu}_2\text{PCl}$ under analogous conditions to those used for Ph_2PCl (Scheme 4.30). It was hypothesised that increasing the steric bulk of the phosphine moiety may reduce the ability for side reactions with the support to occur. However, SS CP ^{31}P NMR spectroscopic analysis of the resulting solid indicated that this was not the case. Rather than the expected phosphinite ^{31}P NMR signal at ≈ 150 ppm, a lone resonance at +39 ppm was instead observed corresponding to an unknown side product of immobilisation.⁵⁷ The large difference in reactivity between $^t\text{Bu}_2\text{PCl}$ and Ph_2PCl with silica, suggests that either increasing phosphine steric bulk or electron donating ability favours oxidative side reactions with the silica support; however this process remains not fully understood.



Scheme 4.30. Attempted synthesis of silica immobilised P^tBu_2 .

4.14 Rh(acac)(CO)₂ complexation with silica-PPh₂

Synthesis of an immobilised hydroformylation catalyst was performed by reaction of the PPh₂-functionalised silica, resulting from the reaction of silica with Ph₂PCl, with Rh(acac)(CO)₂ (Scheme 4.31). Upon stirring in toluene for 2 h, the suspended solid turned from white to orange and CO gas bubbles were observed, suggesting successful anchoring of rhodium onto the silica surface. SS CP ³¹P NMR spectroscopic analysis of the product showed an additional resonance to original PPh₂-modified silica at +82 ppm, corresponding to monodentate PPh₂ coordination of a Rh(acac)(CO) fragment. Interestingly, the majority of the PPh₂ moieties were shown to have not reacted with Rh(acac)(CO)₂, suggesting that for the most part, the silica-PPh₂ moieties were too sterically hindered and therefore inaccessible to the rhodium source. This is presumably a result of the direct immobilisation of the phosphine onto the silica surface without an intervening organic linker, limiting the freedom of movement to the PPh₂ moiety. This could also explain why no bidentate silica-PPh₂ coordination onto the rhodium was observed. The hydroformylation catalyst performance of this supported complex compared to the bidentate ligand-coordinated supported complexes described earlier in this chapter is of great interest, particularly in regard to catalyst stability to metal leaching (see Chapter 5.3.2).



Scheme 4.31. Reaction of silica-PPh₂ with Rh(acac)(CO)₂.

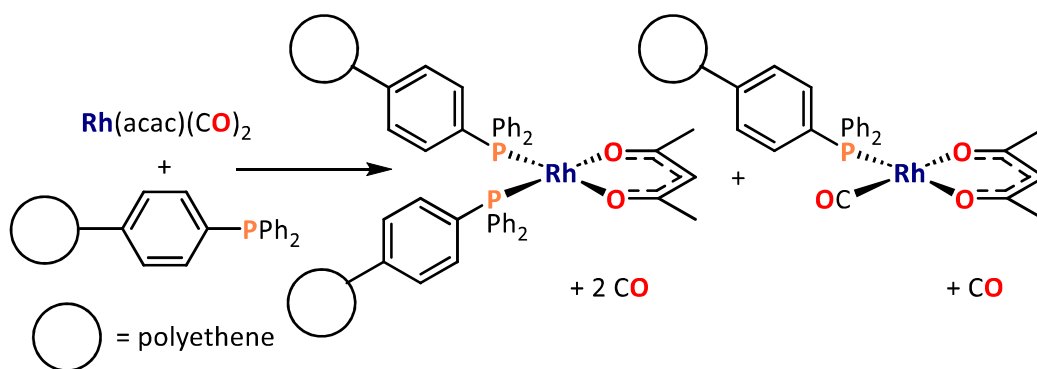
4.15 Synthesis of a FibrecatTM supported rhodium complex

An alternative to the silica supports employed in this Chapter for the development of immobilised discrete metal complexes is the application of a polymer catalyst support. This approach has been investigated for a wide variety of metals and catalytic applications, including hydroformylation, in the literature.^{58–60} One polymer support that has previously been used in immobilised hydroformylation catalysis is FibrecatTM, a

triphenyl phosphine modified, polyethene support prepared by radiation grafting with high-energy electrons.⁶

FibreCat™ fibres, functionalised with PPh₃, (although no longer commercially available) were provided by Johnson Matthey PLC. To produce a polymer supported hydroformylation pre-catalyst as a comparison to the silica-supported pre-catalysts prepared, a solution of Rh(acac)(CO)₂ in toluene was added to FibreCat™ fibres and allowed to stir for 3 h, producing an orange solid alongside a pale green solution (Scheme 4.32). After work up, SS ³¹P NMR spectroscopic analysis showed three signals, corresponding to immobilised but uncoordinated PPh₃ (−6 ppm), immobilised Rh(acac)(PPh₃)₂ (+30 ppm) and immobilised Rh(acac)(PPh₃)(CO) (+42 ppm), in good agreement with the work by Zeelie *et al.*⁶

The synthesis of a literature immobilised catalyst allows for like for like comparisons of our catalyst testing data to the literature's to be made, which is useful to help validate our results (see Chapter 5). A comparison in catalyst performance of polymer-supported and silica-supported catalysts is also of interest in this work and will also be discussed in Chapter 5.



Scheme 4.32. Synthesis of FibreCat™-supported Rh(acac)(PPh₃)(CO) and Rh(acac)(PPh₃)₂.

4.16 Determination of heterogeneous catalyst rhodium loadings

The rhodium contents of the solid catalysts reported in this Chapter were determined by ICP-OES analysis, following HF digestion, performed at Johnson Matthey, Sonning (Table 4.2). Much higher catalyst loadings were achieved for the FibreCat™ and silica-

PPh₂ catalysts, than the other silica-supported catalysts prepared (4.46 and 2.49% respectively). This is likely due to the two-step immobilisation procedure employed for these catalysts whereby the ligand was first grafted onto the support and then complexed with Rh(acac)(CO)₂. Alternately, the immobilisation of pre-formed rhodium complexes with relatively large phosphine ligands is likely to limit the amount of silica surface accessible to these species, resulting in a fewer surface-immobilised ligands and thus immobilised rhodium complexes. The catalysts loadings achieved show good agreement with literature values of Fibrecat™ and silica-immobilised rhodium catalyst loadings.^{6,20} No further optimisation of the silica loadings were performed in this work.

Table 4.2. Heterogeneous catalyst rhodium leaching after 1 h hydroformylation reaction.

Catalyst	Catalyst rhodium content / Wt. %
Fibrecat™ + Rh(acac)(CO) ₂	4.46
Rh(acac)(CO) ₂ + silica-PPh ₂	2.49
Sil-[Rh(L5) ₂]BF ₄	0.53
Sil-[Rh(L17) ₂]BF ₄	0.35
Sil-[Rh(L19)(COD)]BF ₄	0.31
Sil-[Rh(L5S ₂)(COD)]BF ₄	0.76

Errors: ± 0.02%.

4.17 Chapter 4 summary

In this chapter, investigations into the reactivity of a wide range of phosphines and phosphine complexes with silica and alumina were described in the development of heterogeneous hydroformylation catalysts.

(3-Aminopropyl)trimethoxysilane was reacted with AEROPERL 300/30 silica calcined at 600 °C to investigate the surface binding mode of the alkoxysilane, which showed a mixture of T¹, T² and T³ sites. The number of T³ sites was shown to increase when the sample was exposed to water/methanol mixture.

Phosphine **L1** was reacted with AEROPERL 300/30 silica calcined at 600 and 200 °C, and a gamma alumina support calcined at 200 °C, showing differing degrees of phosphine side reactions, resulting in P^V phosphorus environments. The effect of the silica tethering group on these side reactions was investigated by reaction of **L1-4** with AEROPERL 300/30 silica (calcined at 200 °C), which showed that a cyclic azasilane silica tethering group drastically reduced side product formation relative to an alkoxysilane tethering group. An alternative two-step procedure for the immobilisation of **L1** onto silica was performed by reaction of silica-bound (3-aminopropyl)trimethoxysilane with Ph₂PCl in the presence of NEt₃, resulting in predominantly silica bound -N(H)PPh₂. Reaction of phosphoramidite ligands, **L9** and **L21**, containing an alkoxysilane functionality, with AEROPERL 300/30 silica (calcined at 200 °C) resulted in complete rearrangement to P^V phosphorus species.

3-Chloropropylsilatrane was reacted with AEROPERL 300/30 silica calcined at 200 °C in order to study the binding mode of silatranes with silica, with results suggesting a single bond to the surface is formed under anhydrous conditions, while addition of a weak acid results in complete silatrane hydrolysis, liberating an equivalent of triethanolamine and forming three bonds to the silica surface.

Phosphine-boranes were investigated as a method to protect phosphines during immobilisation onto silica. Reaction of **L5** with two equivalents BH₃•THF selectively produced **L5**(BH₃), rather than the expected **L5**(BH₃)₂. Reaction of **L5**(BH₃) with elemental grey selenium produced **L5**(BH₃)Se, indicating that the uncoordinated phosphine's lone pair in **L5**(BH₃) is available for bonding. **L17** was observed to undergo a facile reaction with BH₃•THF to selectively form **L17**(BH₃)₂, suggesting that the unexpected reactivity of **L5** with BH₃•THF was due to a combination of the unique steric and electronic properties of the small bite-angle PNP diphosphine.

The immobilisation of pre-formed rhodium complexes [Rh(**L5S**₂)(COD)]BF₄, [Rh(**L19**)(COD)]BF₄, [Rh(**L5**)₂]BF₄ and [Rh(**L17**)₂]BF₄ onto AEROPERL 300/30 silica (calcined at 200 °C) was performed to produce heterogeneous hydroformylation catalyst precursors, showing a large suppression in the formation of P^V side products relative to immobilisation of the corresponding phosphines with no metal present.

The reactivity of Ph_2PCI with silica in the presence of NEt_3 was investigated as a low-cost method of immobilising phosphine ligands on a solid oxide support. The resulting phosphine-modified silica was reacted with $\text{Rh}(\text{acac})(\text{CO})_2$ to produce a hydroformylation catalyst precursor in the form of $\text{Rh}(\text{acac})(\text{CO})\text{PPh}_2\text{-SiO}_2$.

As a comparison to the silica-immobilised catalysts produced, a polymer supported catalyst with literature precedent was prepared by complexation of $\text{Rh}(\text{acac})(\text{CO})_2$ with Fibrecat™ PPh_3 -modified polyethene fibres, in preparation for catalyst testing (see Chapter 5).

4.18 Chapter 4 references

1. C. Li, W. Wang, L. Yan and Y. Ding, *Front. Chem. Eng.*, 2018, **12**, 113–123, DOI: 10.1007/s11705-017-1672-9.
2. S. Hanf, L. A. Rupflin, R. Gläser and S. A. Schunk, *Catalysts*, 2020, **10**, 1–36, DOI: 10.3390/catal10050510.
3. F. Marras, J. Wang, M. O. Coppens and J. N. H. Reek, *Chem. Commun.*, 2010, **46**, 6587–6589, DOI: 10.1039/c0cc00924e.
4. P. Li, W. Thitsartarn and S. Kawi, *Ind. Eng. Chem. Res.*, 2009, **48**, 1824–1830, DOI: 10.1021/ie800715k.
5. X. Hu, Y. Shi, Y. Zhang, B. Zhu, S. Zhang and W. Huang, *Catal. Commun.*, 2015, **59**, 45–49, DOI: 10.1016/j.catcom.2014.09.043.
6. T. A. Zeelie, A. Root and A. O. I. Krause, *Appl. Catal. A: Gen.*, 2005, **285**, 96–109, DOI: 10.1016/j.apcata.2005.02.010.
7. J. Balué and J. C. Bayón, *J. Mol. Catal. A: Chem.*, 1999, **137**, 193–203, DOI: 10.1016/S1381-1169(98)00124-1.
8. T. T. Adint and C. R. Landis, *J. Am. Chem. Soc.*, 2014, **136**, 7943–7953, DOI: 10.1021/ja501568k.
9. J. Feng, Y. Yan, D. Chen, W. Ni, J. Yang, S. Ma and W. Mo, *Compos. B Eng.*, 2011, **42**, 1821–1825, DOI: 10.1016/j.compositesb.2011.06.023.
10. AEROPERL 300/30 data sheet, <https://glenncorp.com/wp-content/uploads/2013/12/AEROPERL-300-30.pdf>, (accessed January 2024).
11. A. Smith, PhD Thesis, Durham University, 2024.
12. Y. Millot, A. Hervier, J. Ayari, N. Hmili, J. Blanchard and S. Boujday, *J. Am. Chem. Soc.*, 2023, **145**, 6671–6681, DOI: 10.1021/jacs.2c11390.

13. S. Björklund and V. Kocherbitov, *Sci. Rep.*, 2017, **7**, 1–11, DOI: 10.1038/s41598-017-10090-x.
14. M. Sypabekova, A. Hagemann, D. Rho and S. Kim, *Biosensors*, 2023, **13**, 36, DOI: 10.3390/bios13010036.
15. B. Arkles, J. R. Steinmetz, J. Zazyczny and P. Mehta, *J. Adhes. Sci. Technol.*, 1992, **6**, 193–206, DOI: 10.1163/156856192X00133.
16. E. A. Smith and W. Chen, *Langmuir*, 2008, **24**, 12405–12409, DOI: 10.1021/la802234x.
17. G. Jakša, B. Štefane and J. Kovač, *Appl. Surf. Sci.*, 2014, **315**, 516–522, DOI: 10.1016/j.apsusc.2014.05.157.
18. R. M. Pasternack, S. R. Amy and Y. J. Chabal, *Langmuir*, 2008, **24**, 12963–12971, DOI: 10.1021/la8024827.
19. J. A. Howarter and J. P. Youngblood, *Langmuir*, 2006, **22**, 11142–11147, DOI: 10.1021/la061240g.
20. A. J. Sandee, J. N. H. Reek, P. C. J. Kamer and P. W. N. M. Van Leeuwen, *J. Am. Chem. Soc.*, 2001, **123**, 8468–8476, DOI: 10.1021/ja010150p.
21. A. J. Sandee, L. A. Van Der Veen, J. N. H. Reek, P. C. J. Kamer, M. Lutz, A. L. Spek and P. W. N. M. Van Leeuwen, *Angew. Chem. Int. Ed.*, 1999, **38**, 3231–3235, DOI: 10.1002/(SICI)1521-3773(19991102)38:21<3231::AID-ANIE3231>3.0.CO;2-B.
22. W. Kolodziejski and J. Klinowski, *Chem. Rev.*, 2002, **102**, 613–628, DOI: 10.1021/cr000060n.
23. K. Albert and E. Bayer, *J. Chromatogr. A*, 1991, **544**, 345–370, DOI: 10.1016/S0021-9673(01)83995-9.
24. J. Blümel, *Inorg. Chem.*, 1994, **33**, 5050–5056, DOI: 10.1021/ic00100a033.
25. T. Posset, F. Rominger and J. Blümel, *Chem. Mater.*, 2005, **17**, 586–595, DOI: 10.1021/cm048236f.
26. L. Ju and N. C. Strandwitz, *J. Mater. Chem. C*, 2016, **4**, 4034–4039, DOI: 10.1039/c5tc03896k.
27. Y. Pan, A. Maddox, T. Min, F. Gonzaga, J. Goff and B. Arkles, *Chem. Asian J.*, 2017, **12**, 1198–1203, DOI: 10.1002/asia.201700137.
28. W. Tan, R. Yue, Y. Kong, F. Zhang, Y. Wang and B. Luan, (for Shandong Chambroad Petrochemicals Co Ltd) CN Patent, 112742480B, 2022.
29. C. A. Tolman, *Chem. Rev.*, 1977, **77**, 313–348, DOI: 10.1021/cr60307a002.
30. B. Zhang, H. Jiao, D. Michalik, S. Kloß, L. M. Deter, D. Selent, A. Spannenberg, R. Franke and A. Börner, *ACS Catal.*, 2016, **6**, 7554–7565, DOI: 10.1021/acscatal.6b02185.
31. O. Kühl, *Phosphorus-31 NMR Spectroscopy*, Springer, Berlin, 2008.
32. R. Frank, A. Börner, S. Kloss and D. Selent (for Evonik Operations GMBH), US patent 20220056059A1, 2021.

33. J. Cason and W. N. Baxter, *J. Org. Chem.*, 1958, **23**, 1302–1305, DOI: 10.1021/jo01103a017.
34. X. Ma, Q. Xu, H. Li, C. Su, L. Yu, X. Zhang, H. Cao and L. B. Han, *Green Chem.*, 2018, **20**, 3408–3413, DOI: 10.1039/c8gc00931g.
35. G. Ghosh and A. Greer, *J. Phys. Org. Chem.*, 2020, **33**, 1–9, DOI: 10.1002/poc.4115.
36. M. G. Voronkov, V. M. Dyakov and S. V. Kirpichenko, *J. Organomet. Chem.*, 1982, **233**, 1–147, DOI: 10.1016/S0022-328X(00)86939-9.
37. K. L. Materna, B. J. Brennan and G. W. Brudvig, *Dalton Trans.*, 2015, **44**, 20312–20315, DOI: 10.1039/c5dt03463a.
38. T. J. Lee, L. K. Chau and C. J. Huang, *Langmuir*, 2020, **36**, 5935–5943, DOI: 10.1021/acs.langmuir.0c00745.
39. C. J. Huang and Y. Y. Zheng, *Langmuir*, 2019, **35**, 1662–1671, DOI: 10.1021/acs.langmuir.8b01981.
40. C. Geibel, J. Theiner, M. Wolter, M. Kramer, W. Lindner and M. Lämmerhofer, *J. Chromatogr. A*, 2021, **1653**, 1–13, DOI: 10.1016/j.chroma.2021.462418.
41. M. G. Voronkov and V. M. Dyakov, US Patent 4 048 206A, 1977.
42. G. C. Lloyd-Jones and N. P. Taylor, *Chem. Eur. J.*, 2015, **21**, 5423–5428, DOI: 10.1002/chem.201406585.
43. A. Staubitz, A. P. M. Robertson, M. E. Sloan and I. Manners, *Chem. Rev.*, 2010, **110**, 4023–4078, DOI: 10.1021/cr100105a.
44. M. Fritz, L. Maser, B. Ringler, C. von Hänisch and R. Langer, *Z. Anorg. Allg. Chem.*, 2020, **646**, 992–998, DOI: 10.1002/zaac.202000034.
45. P. P. Power, *Angew. Chem. Int. Ed. Engl.*, 1990, **29**, 449–460, DOI: 10.1002/anie.199004491.
46. M. Van Overschelde, E. Vervecken, S. G. Modha, S. Cogen, E. Van der Eycken and J. Van der Eycken, *Tetrahedron*, 2009, **65**, 6410–6415, DOI: 10.1016/j.tet.2009.05.063.
47. T. Reetz, *J. Am. Chem. Soc.*, 1960, **82**, 5039–5042, DOI: 10.1021/ja01504a007.
48. H. Nöth and E. Fluck, *Z. Naturforsch.*, 1984, **39b**, 744–753, DOI: 10.1515/znb-1984-0609.
49. (a) J. C. Slater, *J. Chem. Phys.*, 1964, **41**, 3199–3204, DOI: 10.1063/1.1725697. (b) K. Kawaguchi, *J. Chem. Phys.*, 1992, **96**, 3411–3415, DOI: 10.1063/1.461942.
50. M. R. Crawley, A. E. Friedman and T. R. Cook, *Inorg. Chem.*, 2018, **57**, 5692–5700, DOI: 10.1021/acs.inorgchem.8b00787.
51. J. Burt, J. W. Emsley, W. Levason, G. Reid and I. S. Tinkler, *Inorg. Chem.*, 2016, **55**, 8852–8864, DOI: 10.1021/acs.inorgchem.6b01375.
52. A. S. Ionkin, W. J. Marshall, B. M. Fish, M. F. Schiffhauer and F. Davidson, *J. Am. Chem. Soc.*, 2007, **129**, 9210–9215, DOI: 10.1021/ja071644a.

53. H. Staub, I. Del Rosal, L. Maron, F. Kleitz and F. G. Fontaine, *J. Phys. Chem. C*, 2012, **116**, 25919–25927, DOI: 10.1021/jp309900n.
54. P. Smet, F. Verpoort, G. De Doncker, A. R. Bossuyt, L. Fiermans and L. Verdonck, *Appl. Spectrosc.*, 1997, **51**, 1807–1813, DOI: 10.1366/000370297193987.
55. J. Zhang and L. Han, *Org. Lett.*, 2020, **22**, 4633–4637, DOI: 10.1021/acs.orglett.0c01384.
56. X. Xu, J. Zhang, X. Wang, T. Wang, Y. Liu and L. Han, *Phosphorus, Sulfur, Silicon Relat. Elem.*, 2024, **199**, 23–26, DOI: 10.1080/10426507.2023.2263132.
57. B. C. Vicente, Z. Huang, M. Brookhart, A. S. Goldman and S. L. Scott, *Dalton Trans.*, 2011, **40**, 4268–4274, DOI: 10.1039/C0DT01369B.
58. I. C. Howard, C. Hammond and A. Buchard, *Polym. Chem.*, 2019, **10**, 5894–5904, DOI: 10.1039/c9py01472a.
59. N. Kann, *Molecules*, 2010, **15**, 6306–6331, DOI: 10.3390/molecules15096306.
60. C. U. Pittman and W. D. Honnick, *J. Org. Chem.*, 1980, **45**, 2132–2139, DOI: 10.1021/jo01299a600.

Chapter 5: 1-Octene hydroformylation using homogeneous and silica- immobilised rhodium and palladium complex catalysts

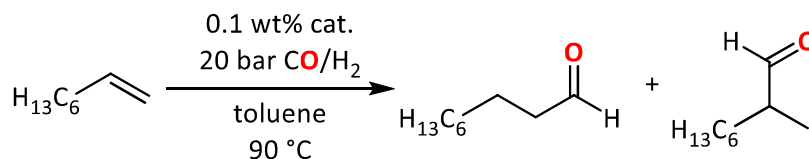
5.1 Aims of hydroformylation catalyst testing

The work so far described in this thesis has focused on the development of silica-immobilised rhodium phosphine and diphosphine complexes. In this chapter, the performance of these systems as hydroformylation catalysts is investigated, due to their potential to enable more facile catalyst separation and recycling than current industrially-used homogeneous catalysts.¹ To determine the catalytic performance of these novel catalysts, several key parameters were investigated including catalyst activity, reaction kinetic profiles, selectivity and stability with respect to metal leaching (for the heterogeneous systems). Also, a comparison between the immobilised catalysts and their analogous homogeneous catalysts is of particular interest.

5.2 Homogeneous hydroformylation catalysis results and discussion

5.2.1 Rh-catalysed homogeneous hydroformylation reaction conditions

Rh-catalysed hydroformylation of 1-octene (a convenient and commonly employed substrate for hydroformylation testing)² was performed in a Parr 300 ml stainless steel autoclave batch reactor fitted with a Teflon liner, under industry relevant conditions of 90 °C and 20 bar (1:1 H₂:CO) pressure, with 0.1 mole percent catalyst relative to 1-octene, in dry/degassed toluene solvent (Scheme 5.1).³ Catalyst, liquid reagents and solvent were introduced into the autoclave under an argon atmosphere. The autoclave was then sealed and pressurised/depressurised with synthesis gas (H₂:CO = 1:1, 5 bar) five times, and then finally pressurised with synthesis gas to 20 bar and heated to 90 °C for one hour. After the reaction was finished, the autoclave was cooled to room temperature (≈1 h) and depressurised. Pressure was maintained throughout the reactions using a mass flow controller connected to a pressure transducer. The reactor was stirred using a gas entraining stirrer at 1350 RPM. In all experiments, the only observed products were C₉ aldehydes and isomerised octenes (no alcohols or alkanes detected). To simplify analysis and quantification, internal octene isomers were grouped during GC analyses.



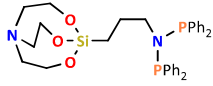
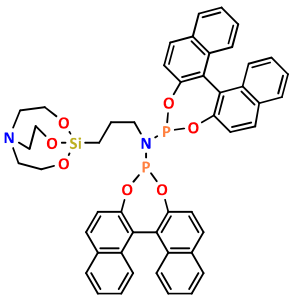
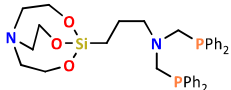

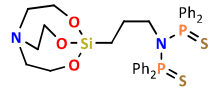
Scheme 5.1. 1-Octene hydroformylation reaction conditions used in the screening of rhodium catalysts in this thesis.

To ascertain a baseline catalyst performance and to enable comparisons to the literature, preliminary experiments were performed using $\text{RhCl}(\text{PPh}_3)_3$, a well-studied hydroformylation catalyst (See Section 5.2.2).⁴ Under the reaction conditions mentioned above, aldehyde production with this catalyst precursor showed a *pseudo* zero-order dependence on octene concentration, as determined by GC-FID analysis of the reaction mixture, with aliquots taken at 15-minute intervals over 1 hour (conversions up to 50%). This observation of pseudo zero order kinetics has previously been made for similar reaction conditions in the literature while using a Rh/PPh_3 catalyst with modified triphenylphosphine ligands featuring bulky oligomeric silsesquioxane functionalities.⁵ To investigate whether mass transport effects were the origin of the *pseudo* zero-order dependence of aldehyde production on octene concentration, hydroformylation reactions were performed using varying gas entraining stirrer rotation speeds ranging from 1000 to 2000 RPM. However, the speed of stirring in this range had no effect on catalyst activity, suggesting that the system was not suffering from mass transport limitations due to insufficient gas-liquid mixing.⁶ Further evidence for our hydroformylation reactions not suffering from limiting mass transport effects was later provided when different catalysts were employed, each showing differing activities under the same reaction conditions.

5.2.2 Comparison of catalyst performance in homogeneous hydroformylation

Homogeneous 1-octene hydroformylation catalyst testing was performed for the rhodium complexes described in Chapter 3, alongside $\text{RhCl}(\text{PPh}_3)_3$ and $\text{Rh}(\text{acac})(\text{CO})_2/\text{PPh}_3$ (Table 5.1).

Table 5.1. Comparison of homogeneous hydroformylation of 1-octene with various catalysts.

Catalyst (numbered ligands shown)	CHO TOF / h ⁻¹	CHO selectivity at 1 h / %	iso-alkene selectivity at 1 h / %	<i>l:b</i> ratio
RhCl(PPh ₃) ₃	84	39	61	3.0
Rh(acac)(CO) ₂ + 2 PPh ₃	667	91	9	2.5
[Rh(L5) ₂]BF ₄ 	65	13	87	2.7
[Rh(L12) ₂]BF ₄ 	0	-	-	-
Rh(acac)(CO) ₂ + L12	124	54	46	8.0
[Rh(L17) ₂]BF ₄ 	674	55	45	2.7
[Rh(L19)(COD)]BF ₄ 	573	66	34	2.5
[Rh(L5S ₂)(COD)]BF ₄ 	240	24	76	1.0

Conditions: 90 °C, 20 bar (1:1 H₂:CO), 1-octene (0.032 mol, 5 ml), [1-octene]/[Rh] = 1000, toluene (95 ml), t = 1 h, nonane (1 ml, internal standard). Errors: ±2-8%; average of 3 runs. TOF values calculated as moles of the aldehyde produced / (moles of catalyst × time).

Hydroformylation of 1-octene using Rh(acac)(CO)₂ + 2 PPh₃ (Table 5.1, entry 2) showed good agreement in terms of aldehyde selectivity, TOF and linear:branched (*l:b*) ratio

with results reported by Trzeciak and Alsalahi using the same catalyst (Table 5.2).⁷ This good agreement in catalyst performance, despite the slightly different reaction conditions used in this work and the work by Trzeciak and Alsalahi, suggests that our experimental set-up was appropriate and performed well. Additionally, 1-octene hydroformylation using $\text{RhCl}(\text{PPh}_3)_3$ (Table 5.1, entry 1) showed good agreement in terms of the *l:b* ratios obtained with results from Wilkinson *et al.* for the hydroformylation of 1-pentene, who obtained an *l:b* ratio of 2.8.⁴ A comparison of our catalyst activity to that obtained by Wilkinson was not possible, as only a 100% conversion after 16 h was reported by Wilkinson.

Table 5.2 Hydroformylation of 1-octene using $\text{Rh}(\text{acac})(\text{CO})_2/\text{PPh}_3$ by Trzeciak and Alsalahi under various conditions.⁷

catalyst	CHO selectivity / %	CHO TOF / h^{-1}	<i>l:b</i> ratio
$\text{Rh}(\text{acac})(\text{CO})_2/\text{PPh}_3^{\text{a}}$	92	545	3.6
$\text{Rh}(\text{acac})(\text{CO})_2/\text{PPh}_3^{\text{b}}$	88	703	4.0

Conditions: 80 °C, 10 bar (1:1 H_2 :CO), 1-octene (0.01 mol, 1.5 mL), [Rh] (2.3×10^{-5} mol), ($\text{PPh}_3 = 1.6 \times 10^{-4}$ mol), [1-octene]/[Rh] = 440, [PPh_3]/[Rh] = 6.8, *t* = 1 h.^a Toluene solvent (volume unspecified), ^b no solvent.

Once the performance of our hydroformylation set-up was established with $\text{Rh}(\text{acac})(\text{CO})_2 + 2 \text{PPh}_3$, hydroformylation experiments using the novel catalyst systems developed in this work (see Chapter 3) were performed. The complex $[\text{Rh}(\text{L5})_2]\text{BF}_4$, featuring small bite-angle PNP ligand, **L5**, displayed a relatively low TOF for aldehyde formation of 65 h^{-1} , but functions as a moderately active alkene isomerisation catalyst ($416 \pm 21 \text{ h}^{-1}$). This is consistent with the recorded performance of the previously reported catalyst, $[\text{Rh}(\text{cod})_2]\text{OTf}/(\text{Ph}_2\text{P})_2\text{NPr}$, containing a small bite-angle PNP ligand, which was also found to be more active for 1-octene isomerisation than hydroformylation.⁸ In that work $[\text{Rh}(\text{cod})_2]\text{OTf}/(\text{Ph}_2\text{P})_2\text{NPr}$ achieved a TOF for aldehydes of 1920 h^{-1} and octene isomerisation TOF of 11580 h^{-1} , resulting in a low aldehyde selectivity of 14% (Conditions: 100 °C, 40 bar (1:1 H_2 :CO), 1-octene (1.27 mol, 200 ml), $\text{Rh} = 1.90 \times 10^{-4}$ mol, data at 50%). However, it was reported that the internal octenes

produced were converted to aldehydes over extended times (45 h). In the same study, *l:b* ratios varied from 3:1 to 4:1 at 50% conversion depending on the conditions used, decreasing to 2:1 at 100% conversion, as 2-octene underwent hydroformylation, in good agreement with our data.⁸ The large difference in catalytic activity between $[\text{Rh}(\text{L5})_2]\text{BF}_4$ and $[\text{Rh}(\text{cod})_2]\text{OTf}/(\text{Ph}_2\text{P})_2\text{NPr}$ is unexpected as the proposed active catalyst species have very similar structures, both $\text{HRh}(\text{CO})_2(\text{PNP})$ complexes (Figure 5.1). The observed difference is proposed to be predominantly due to the different reaction conditions employed where the higher temperature, pressure and 1-octene concentration used with the $[\text{Rh}(\text{cod})_2]\text{OTf}/(\text{Ph}_2\text{P})_2\text{NPr}$ catalyst are likely to enhance activity. Due to time constraints, no optimisation of hydroformylation reaction conditions were performed in our work. However, improvement in catalyst performance through such optimisation is expected to be possible.

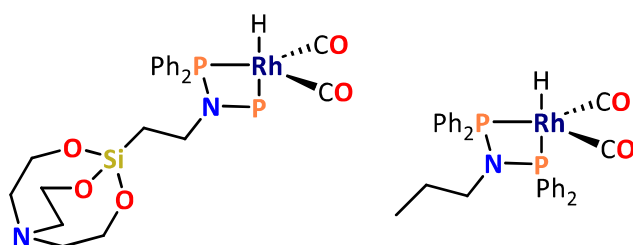


Figure 5.1. Proposed hydroformylation active catalyst species $\text{HRh}(\text{CO})_2(\text{L5})$ (left) and $\text{HRh}(\text{CO})_2((\text{Ph}_2\text{P})_2\text{NPr})$ (right).

The highest catalyst activity observed from our experiments under our defined operating conditions (Table 5.1) resulted from using $[\text{Rh}(\text{L17})_2]\text{BF}_4$ as the catalyst, giving a TOF of 674 h^{-1} . In addition to its hydroformylation activity, $[\text{Rh}(\text{L17})_2]\text{BF}_4$ was also shown to be a highly active isomerisation catalyst, giving 45% selectivity to internal octenes after a one-hour reaction. However, over extended reaction times (24 h), selectivity for aldehydes increased to >98%, due to hydroformylation reactions gradually consuming the various octene isomers present in the reaction mixture. As a result of the hydroformylation of internal octenes, after the first hour of reaction the aldehyde *l:b* ratio decreased from 3:1 to 2:1 after 24 h.

A comparison in the catalyst performance of $[\text{Rh}(\text{L17})_2]\text{BF}_4$ with $[\text{Rh}(\text{L19})(\text{COD})]\text{BF}_4$, both of which contain PCNCP ligands (Figure 5.2), shows $[\text{Rh}(\text{L17})_2]\text{BF}_4$ to give a moderately

higher aldehyde TOF and *i:b* ratio (Table 5.1). Despite this, $[\text{Rh}(\textbf{L17})_2]\text{BF}_4$ displayed a lower aldehyde selectivity after 1 h than $[\text{Rh}(\textbf{L19})(\text{COD})]\text{BF}_4$, something attributed to a higher propensity for alkene isomerisation, at the expense of aldehyde formation. The lower activity of $[\text{Rh}(\textbf{L19})(\text{COD})]\text{BF}_4$ compared to $[\text{Rh}(\textbf{L17})_2]\text{BF}_4$ is likely to be primarily an electronic effect, due to $[\text{Rh}(\textbf{L19})(\text{COD})]\text{BF}_4$ incorporating more Lewis basic PCy_2 groups relative to the PPh_2 groups of $[\text{Rh}(\textbf{L17})_2]\text{BF}_4$ (see Section 3.2.1 for a discussion on ligands Lewis basicity quantified *via* $|^1J_{\text{SeP}}|$ coupling constants of corresponding phosphorus selenides). More electron-rich metal centres are known to suppress CO dissociation from $\text{HRh}(\text{P}^{\wedge}\text{P})(\text{CO})_2$ complexes, thus hindering alkene coordination, which is believed to be the origin of this reduction in olefin turnover.⁹

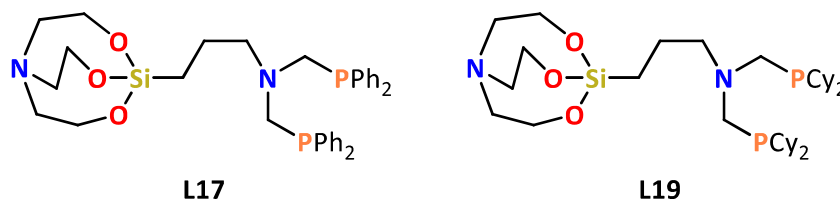
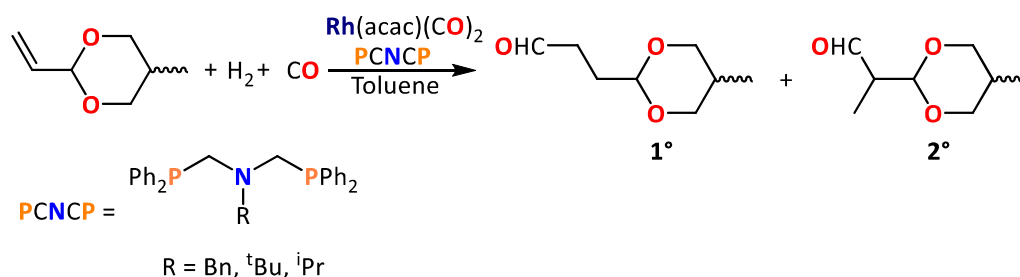


Figure 5.2. Structures of **L17** and **L19** (repeated here for clarity).

Out of the novel homogeneous catalyst systems employed, $[\text{Rh}(\textbf{L17})_2]\text{BF}_4$ has the most similar catalyst performance to the widely used $\text{Rh}(\text{acac})(\text{CO})_2/\text{PPh}_3$ catalyst system, albeit with higher alkene isomerisation rates (Table 5.1). This similar performance of the two systems is in agreement with the steric-electronic map described in Chapter 3 (Section 3.2.4), where, out of the ligands investigated, **L17** was shown to be closest in steric-electronic space to $2 \times \text{PPh}_3$.

A direct comparison of the catalyst performance of $[\text{Rh}(\textbf{L17})_2]\text{BF}_4$ with previously reported PCNCP-ligated catalysts is limited, since there are only a few literature examples of PCNCP ligands used in hydroformylation. One report describes use of an electron-poor alkene substrate, vinylmethyldioxane (VMD), (Scheme 5.2, Table 5.3).¹⁰ Hydroformylation of VMD results in a vastly different hydroformylation product distribution than 1-octene due to the differing electronic characters of the two compounds, with hydroformylation of VMD favouring formation of the branched aldehyde. Additionally, alkene isomerisation of VMD is not possible, simplifying the possible reaction products relative to 1-octene by eliminating internal alkene formation.

TOFs of aldehyde production were not reported for the hydroformylation of VMD, although greater than 90% conversion was reported after 4 hours for all experiments. Reaction times were reportedly not optimised however, so the activity of the catalyst is unknown. Nevertheless, these data show reasonable agreement with the data from the hydroformylation of 1-octene using $[\text{Rh}(\text{L17})_2]\text{BF}_4$, where 55% conversion to aldehydes was observed after 1 h, albeit with a five times higher catalyst loading, but at 30 °C lower temperature relative to the system employing the VMD substrate.



Scheme 5.2. Rhodium-catalysed hydroformylation of VMD, using a $\text{Rh}(\text{acac})(\text{CO})_2$ / PCNCP catalyst.¹⁰

Table 5.3. Hydroformylation of VMD using a $\text{Rh}(\text{acac})(\text{CO})_2$ / PCNCP catalyst system.¹⁰

Ligand	Selectivity / %		Conversion / %
	1°	2°	
PCNCP ^{Bn}	28	72	96
PCNCP ^{tBu}	27	73	90
PCNCP ^{iPr}	23	77	92

Conditions: [VMD] = 5.0 mmol, [VMD]/[Rh] = 5000, L/Rh = 5, 120 °C, 20 bar syngas pressure, 4 h in toluene (10 ml).

Another report of the use of PCNCP ligands in hydroformylation investigated the PCNCP-containing rhodium catalyst, $[\text{Rh}(\text{PCNCP}^{\text{Ph}})(\text{COD})]\text{BF}_4$, comparing its catalytic performance against that of $[\text{Rh}(\text{dppp})(\text{COD})]\text{BF}_4$, using 1-octene as substrate (Table 5.4, ligands shown in Figure 5.3).¹¹ The ligand with a nitrogen atom in the backbone, PCNCP^{Ph}, was found to give a much higher hydroformylation activity, 240 h⁻¹, relative to dppp, which has a solely carbon atom ligand backbone, 57 h⁻¹. In contrast, the *l:b* ratio of the aldehydes produced was found to be largely independent of the ligand used. The

origin of the differing catalytic performance of the two complexes with regard to TOF is not well understood; however it was tentatively concluded to be an electronic effect, since the steric bulk around the metal centre imposed by the two ligands is likely to be comparable.¹¹

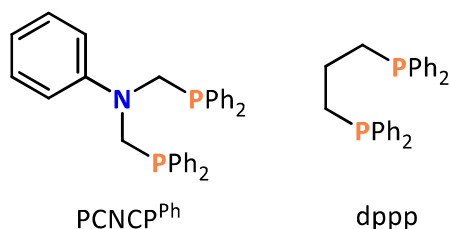


Figure 5.3. Structures of PCNCP^{Ph} and dppp .¹¹

In our work, a comparison of $[\text{Rh}(\mathbf{L17})_2]\text{BF}_4$ with $[\text{Rh}(\text{PCNCP}^{\text{Ph}})(\text{COD})]\text{BF}_4$ shows a much higher activity for the $[\text{Rh}(\mathbf{L17})_2]\text{BF}_4$ system (674 h^{-1} , $I:b = 2.7:1$). These differences are likely predominantly due to the differing reaction conditions employed for the two catalysts, with $[\text{Rh}(\mathbf{L17})_2]\text{BF}_4$ investigated at a higher temperature, but lower pressure (90°C , 20 bar syngas). A more detailed comparison of the performance of the two catalysts is not possible due to the limited experimental detail reported for the $[\text{Rh}(\text{PCNCP}^{\text{Ph}})(\text{COD})]\text{BF}_4$ catalyst (catalyst loading and volume of solvent used not reported). Further discussion of the novel phosphine-ligated homogeneous hydroformylation catalysts considered in this Section, such as the $[\text{Rh}(\mathbf{L17})_2]\text{BF}_4$, is provided in Section 5.6 where they are compared to their heterogeneous analogues.

Table 5.4. Hydroformylation of 1-octene using a $[\text{Rh}(\text{COD})_2]\text{BF}_4$ / P^*P catalyst system.¹¹

Ligand	TOF / h^{-1}	$I:b$ ratio
PCNCP^{Ph}	240	1.6:1
dppp	57	1.7:1

Conditions: 60°C , 100 bar syngas pressure ($\text{CO}:\text{H}_2$ 1:1), 18 h in toluene (volume unspecified).

5.2.3 Sulfur donor ligands in homogeneous hydroformylation catalysis results and discussion

The application of sulfur donor ligands in hydroformylation remains a poorly explored area of research, particularly with regards to neutral, bidentate sulfur ligands. Therefore, the catalytic performance of sulfur donor ligand-containing catalyst, $[\text{Rh}(\text{L5S}_2)(\text{COD})]\text{BF}_4$ (Figure 5.4), in 1-octene hydroformylation was of interest. Hydroformylation using $[\text{Rh}(\text{L5S}_2)(\text{COD})]\text{BF}_4$ showed good catalytic activity of 240 h^{-1} , significantly higher than its sulfur-free analogue $[\text{Rh}(\text{L5})_2]\text{BF}_4$ (note: S[^]S bite angle in **L5S₂** = 96° , P[^]P bite angle in **L5** = 70°).

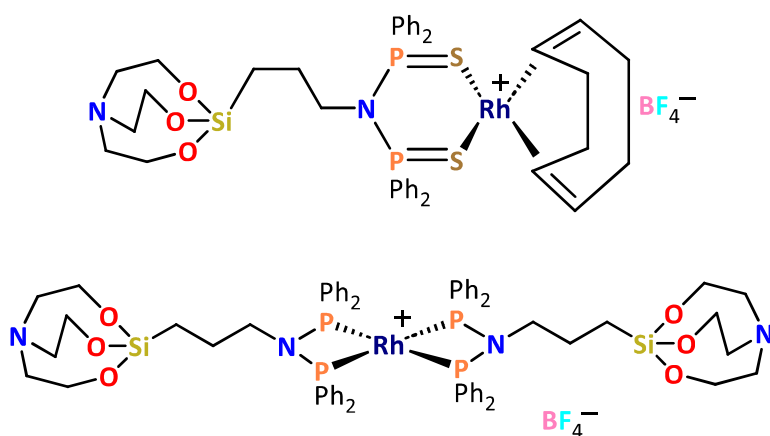
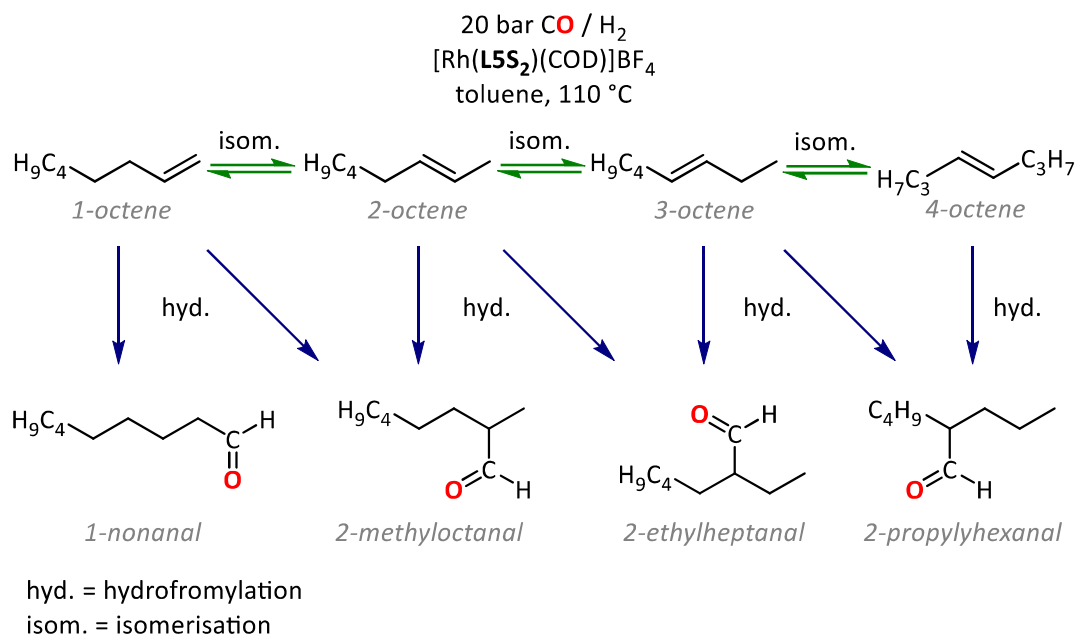


Figure 5.4. Structures of $[\text{Rh}(\text{L5S}_2)(\text{COD})]\text{BF}_4$ (top) and $[\text{Rh}(\text{L5})_2]\text{BF}_4$ (bottom).

Compared to the phosphine ligands investigated in this work $[\text{Rh}(\text{L5S}_2)(\text{COD})]\text{BF}_4$ resulted in a much lower *l:b* ratio after 1 h of 1:1 rather than $\approx 3:1$. This *l:b* ratio was shown to steadily decrease over the course of the reaction, starting from 2.5:1 at 15 minutes, and is a result of significant hydroformylation of internal alkenes as the reaction progresses. A high alkene isomerisation activity of $2161 \pm 70 \text{ h}^{-1}$ is likely a major factor in the low *l:b* ratio obtained, which resulted in 76% conversion to internal alkenes after 15 minutes. After this time, the percentage of internal octenes in the reaction mixture was found to remain approximately constant due to similar rates of 1-octene isomerisation and hydroformylation of internal octenes. As a result of the high isomerisation and hydroformylation activity of $[\text{Rh}(\text{L5S}_2)(\text{COD})]\text{BF}_4$, 2-ethylheptanal and 2-propylhexanal were also observed by GC-FID analysis, unlike for all the phosphine complex-catalysed reactions investigated in this work (Scheme 5.3).



Scheme 5.3. Formation of various aldehyde isomers during the hydroformylation of 1-octene using [Rh(LSS₂)(COD)]BF₄.

Literature examples of sulfur-ligated metal centres for hydroformylation are sparse, particularly for neutral, bidentate sulfur ligands in monometallic complexes.¹² Additionally, literature on the use of sulfur ligands in hydroformylation typically employs additional ligands, such as PPh₃ or P(OMe)₃, to improve catalyst activity and selectivity, with phosphine ligands required to initiate any catalytic activity in some cases.^{12,13} One example from the literature is the chiral complex [Rh(COD)(Me₂binas)]BF₄, which was investigated for the hydroformylation of styrene and showed complete selectivity for aldehydes, with up to 93% selectivity for the branched-aldehyde isomer at low temperatures and high pressures (Figure 5.5, Table 5.5).^{14,15} Since the alkene in styrene cannot be isomerised, the alkene isomerisation ability of this catalyst does not appear to have been investigated. Additionally, as a TOF for hydroformylation was not reported, comparisons in performance with that of [Rh(LSS₂)(COD)]BF₄ are limited. Nevertheless, the catalytic performance of [Rh(LSS₂)(COD)]BF₄ is competitive with our phosphine-ligated systems (e.g., [Rh(L5)₂](BF₄)), showing promise for application as an immobilised catalyst (see Section 5.3.2).

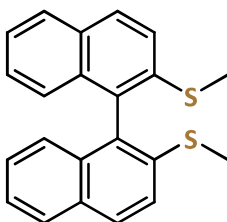


Figure 5.5. Structure of Me_2binas .

Table 5.5. Hydroformylation of styrene using $[\text{Rh}(\text{COD})(\text{Me}_2\text{binas})]\text{BF}_4$.¹⁴

	P / bar	T / °C	t / h	Conversion / %	<i>b</i> -selectivity / %	<i>e.e</i> / %
1 ^a	30	80	24	98	51	6
2 ^b	80	40	3	60	93	3

Conditions: THF solvent, (1:1 H_2 :CO), styrene/Rh = 400. ^a Rh/(S[^]S) = 1/1. ^b Rh/(S[^]S) = 1/4.

5.2.4 $[\text{Rh}(\text{P}^{\wedge}\text{P})_2]\text{BF}_4$ catalyst induction periods

During the hydroformylation of 1-octene catalysed by $[\text{Rh}(\text{L5})_2]\text{BF}_4$ and $[\text{Rh}(\text{L17})_2]\text{BF}_4$ a ~25 min induction period was observed before any catalysis occurred, whereas no induction period was observed when using catalysts $[\text{Rh}(\text{L19})(\text{COD})]\text{BF}_4$ or $[\text{Rh}(\text{L5S}_2)(\text{COD})]\text{BF}_4$ (Figure 5.6). The origin of this induction period is explained by formation of the active catalyst species from $[\text{Rh}(\text{P}^{\wedge}\text{P})_2]\text{BF}_4$ pre-catalysts requiring dissociation of one diphosphine ligand to enable octene coordination (Scheme 5.4).^{16,17} The formation of the hydride carbonyl has been reported to take up to 2 h for $[\text{Rh}(\text{P}^{\wedge}\text{P})_2]^+$ cations in the literature (under 20 bar syngas 1:1 $\text{CO}:\text{H}_2$ at 60 °C in toluene, $\text{P}^{\wedge}\text{P}$ = (2*S*,4*S*)-bis(diphenylphosphine)pentane, see Section 3.3.6).¹⁶

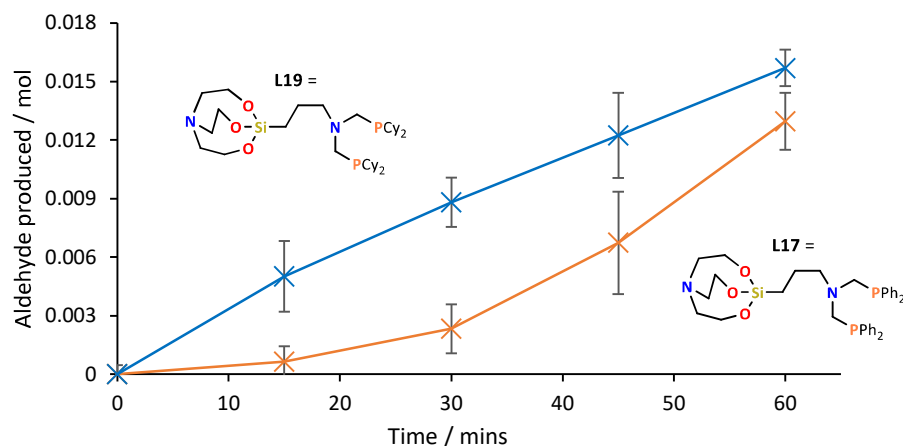
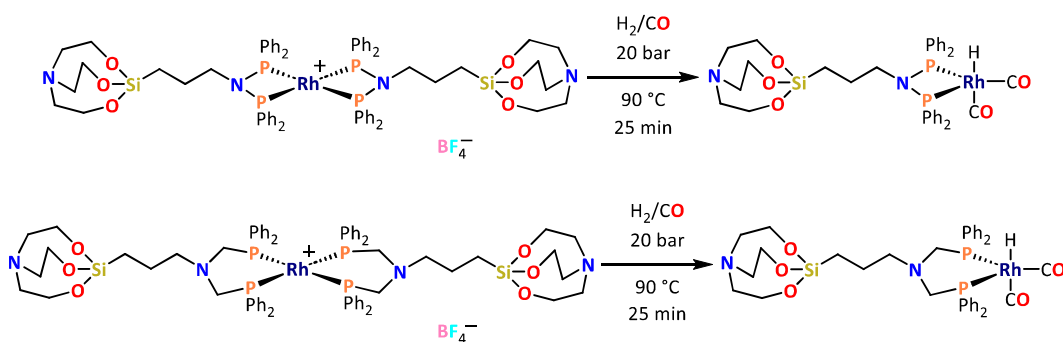


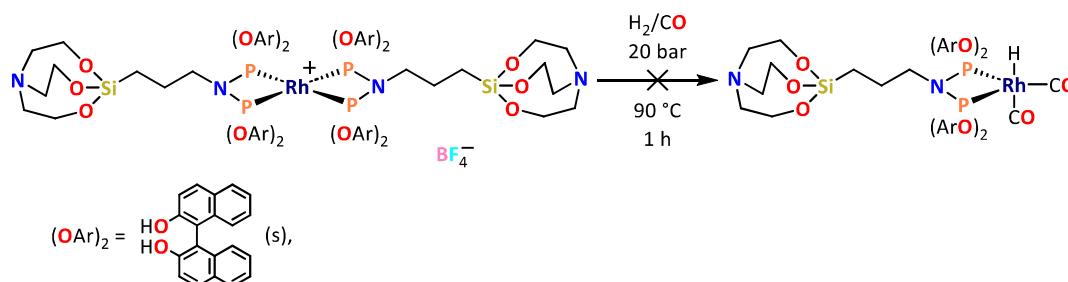
Figure 5.6. C_9 aldehyde production over time for the hydroformylation of 1-octene with **blue**: $[Rh(L19)(COD)]BF_4$ and **orange**: $[Rh(L17)_2]BF_4$. Conditions: 90 °C, 20 bar (1:1 $H_2:CO$), $[1\text{-octene}]/[Rh] = 1000$, in toluene.



Scheme 5.4. Proposed catalyst activation of $[Rh(L5)_2]BF_4$ (top) and $[Rh(L17)_2]BF_4$ under hydroformylation conditions.

In contrast to the observed behaviour of $[Rh(L5)_2]BF_4$ and $[Rh(L17)_2]BF_4$ under hydroformylation conditions, for which formation of an active catalyst species took ~25 min, experiments employing $[Rh(L12)_2]BF_4$ resulted in no catalytic activity under the reaction conditions employed. It is proposed that this is due to **L12** dissociation not occurring, preventing formation of an active catalyst species (Scheme 5.5). To investigate this, the catalyst $Rh(L12)(acac)$ was generated *in situ* from a 1:1 mixture of $Rh(acac)(CO)_2$ and **L12**, with the resulting species showing a modest TOF of 124 h^{-1} , but high *i:b* ratio of 8. This result indicates that $[Rh(L12)_2]BF_4$ is indeed inactive for catalysis due to very slow dissociation of **L12**, since catalytic activity was observed when the stoichiometry of phosphine present was reduced, which would inhibit the formation of $[Rh(L12)_2]BF_4$. The difference in catalyst induction behaviour between $[Rh(L5)_2]BF_4$ and

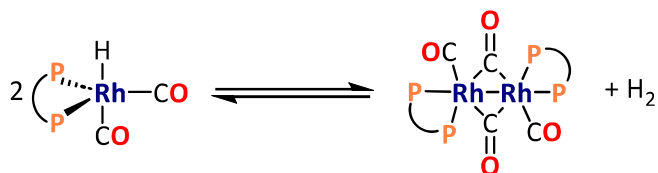
$[\text{Rh}(\text{L12})_2]\text{BF}_4$ is unexpected, since both catalysts have similar structures (both containing PNP ligands). The observed difference in reactivity is therefore likely due to the difference in electronics character of the ligands in each complex, with the phosphoramidite ligand, **L12**, being a weaker Lewis base than **L5** (see Section 3.2.1).



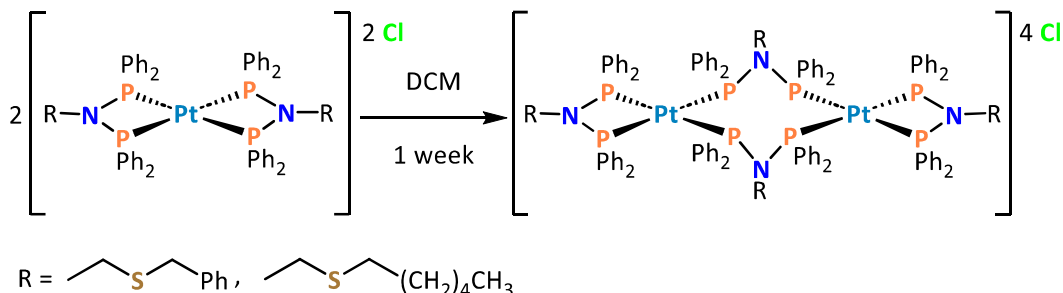
Scheme 5.5. Attempted catalyst activation of $[\text{Rh}(\text{L12})_2]\text{BF}_4$ under hydroformylation conditions (90 °C, 20 bar (1:1 H_2/CO), $[1\text{-octene}]/[\text{Rh}] = 1000$, in toluene).

5.2.5 Hydroformylation activity comparison of PNP- and PCNCP-containing catalysts

The low activity of the PNP ligand-containing catalysts, lower than that of $\text{RhCl}(\text{PPh}_3)_3$ ($[\text{Rh}(\text{L5})_2]\text{BF}_4$ TOF = 65 h^{-1} , $\text{RhCl}(\text{PPh}_3)_3$ TOF = 84 h^{-1}), which is known to have its rate suppressed by the presence of halide, and much lower than $[\text{Rh}(\text{L17})_2]\text{BF}_4$ (TOF = 674 h^{-1}), is unexpected. One possible explanation for this low activity could be the formation of inactive dimers under hydroformylation conditions. Rhodium complex dimerisation is a widely known and common pathway for rhodium hydroformylation catalyst deactivation, and is particularly prevalent under low hydrogen pressure and high rhodium concentrations (Scheme 5.6).¹⁸ Indeed, the unique chemistry of small bite-angle PNP ligands, such as **L5**, is known to favour forming dimeric species with many different metal centres under different reaction conditions by acting as a bridging ligand.¹⁹ For example, *bis*(dppa)platinum(II) complexes have been shown to gradually convert to dppa-bridged platinum dimers when they are left to stand in a DCM solution (Scheme 5.7).²⁰



Scheme 5.6. Previously reported reversible dimer formation of rhodium hydroformylation catalysts; the equilibrium is controlled by the nature of the bidentate phosphine ligand.¹⁸



Scheme 5.7. Slow dimerisation of $[Pt(PNP)_2]Cl_2$ complexes in solution.²⁰

Additionally, cationic rhodium(I) dimers featuring terminal and bridging PNP ligands, of the type $[Rh_2(PNP)_2(\mu-PNP)_2]^{2+}$, have been previously synthesised with various counter anions (Figure 5.7).^{21,22} It was shown that formation of these dimeric species could be controlled by the steric bulk of the PNP ligands employed. When methylamine PNP ligand, $MeN(P(OMe)_2)_2$, was reacted with various rhodium precursors, such as $[RhCl(COD)]_2$ or $[Rh(COD)(acetone)_2]ClO_4$, $[Rh_2(PNP)_2(\mu-PNP)_2]^{2+}$ was found to form selectively in all cases, regardless of whether the ligand to metal ratio used was 1:1 or 2:1. Meanwhile, analogous reactions with a more bulky phenylamine PNP ligand, $PhN(P(OMe)_2)_2$, resulted in mononuclear rhodium complexes, as was also observed during the synthesis of **L5** and **L12** in this work.²²

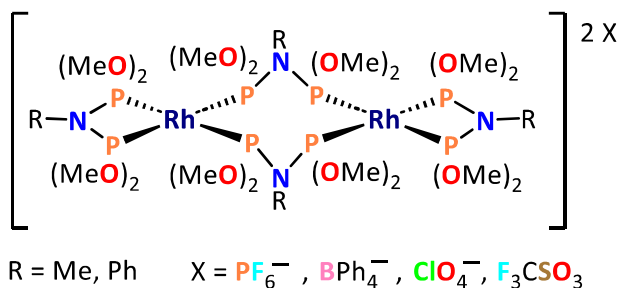


Figure 5.7. Structure of previously reported $[Rh_2(PNP)_2(\mu-PNP)_2]^{2+}$ rhodium(I) cations with various counter anions.^{21,22}

Interestingly, the different ligand bite angle between the PNP- and PCNCP-containing catalysts $[\text{Rh}(\text{L5})_2]\text{BF}_4$ and $[\text{Rh}(\text{L17})_2]\text{BF}_4$ does not appreciably affect the *l:b* ratio of the aldehyde products produced (both 2.7:1) under the reaction conditions investigated (see Section 5.2.2, Table 5.1). Typically, larger bite angle ligands result in higher aldehyde *l:b* ratios, something that is generally attributed to more favourable (eq),(eq), rather than (eq),(ax) phosphine coordination of the rhodium centre in the catalyst, which in turn has both a steric and electronic impact upon product regiochemistry.²³ However, a complex combination of factors are likely to also play a significant role in the resultant aldehyde regioselectivity of rhodium-catalysed hydroformylation.²³ Indeed, our results suggest that ligand bite angle is not the only factor controlling aldehyde *l:b* ratio in our experiments.

5.3 Heterogeneous hydroformylation catalysis results and discussion

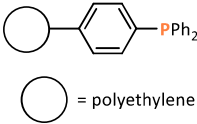
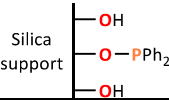
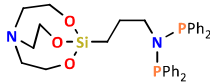
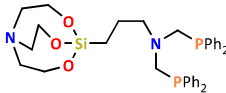

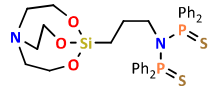
5.3.1 Rhodium-catalysed heterogeneous hydroformylation reaction conditions

Investigation of the catalytic performance of the heterogeneous catalysts described in Chapter 4 for hydroformylation required implementation of an adapted experimental procedure to that used for homogeneous catalysis testing discussed in Section 5.2. To introduce the catalyst into the autoclave the autoclave was first assembled and purged with argon, before being unsealed and the solid catalyst quickly added from a nitrogen-filled vial. The autoclave was then re-sealed and evacuated and backfilled with argon before liquid reagents were added *via* the septum inlet. Otherwise, the hydroformylation reaction procedure was the same for the homogeneous and heterogeneous catalysts. Note that the average particle size of the AEROPERL 300/30 silica used was 20-60 μm , and that stirring was sufficient to generate a fine dispersal of the material during analysis.²⁴ A test reaction showed that unmodified silica displayed no catalytic activity for 1-octene hydroformylation or isomerisation under the conditions employed (90 °C, 20 bar (1:1 H_2 :CO), in toluene).

5.3.2 Heterogeneous hydroformylation catalyst activity comparison

Heterogeneous hydroformylation catalyst testing was performed for the silica-immobilised rhodium complexes described in Chapter 4, alongside a previously reported FibrecatTM-immobilised catalyst (Table 5.6, entry 1).²⁵ FibrecatTM is a polyethylene fibre grafted with triphenylphosphine ligands (see section 4.15).

Table 5.6. Heterogeneous hydroformylation of 1-octene using various catalysts.

Catalyst (ligands shown)	CHO TOF / h ⁻¹	CHO selectivity at 1 h / %	<i>l:b</i> ratio at 1 h	[1-octene]/[Rh]
Fibrecat TM + Rh(acac)(CO) ₂  ○ = polyethylene	114	81	3.1	295
Rh(acac)(CO) ₂ + silica-PPh ₂ 	200	31	3.0	441
Sil-[Rh(L5) ₂](BF ₄) 	135	15	2.9	1553
Sil-[Rh(L17) ₂](BF ₄) 	682	75	2.6	2353
Sil-[Rh(L19)(COD)]BF ₄ 	384	50	2.6	2666
Sil-[Rh(L5S2)(COD)]BF ₄ 	212	26	1.1	1004

Conditions: 90 °C, 20 bar (1:1 H₂:CO), 1-octene (0.032 mol, 5 ml), toluene (95 ml), t = 1 h, nonane (1 ml, internal standard). Errors ±2-9%; data in table calculated as an average of 3 separate runs.

Previously, a FibrecatTM/Rh(acac)(CO)₂ catalyst has been reported by Zeelie for the hydroformylation of ethene in a fixed bed reactor, and showed up to 96% selectivity for propanal (with 4% ethane produced).²⁵ The reaction conditions used were 5 bar pressure at 110 °C, with a feed flow of 7 l/h consisting of 1:2:2:2 molar ratio of Ar, CO, H₂ and C₂H₄. The catalyst loading was 0.5 g (3.0 to 7.7 wt.% Rh), and the reaction time 20 h.²⁵ In our hands, using the same FibrecatTM/Rh(acac)(CO)₂ catalyst for the hydroformylation of 1-octene in a batch reactor using the conditions described (Table 5.6), we observed a lower selectivity for aldehyde production than was reported by Zeelie of 81% (19% internal octenes). This lower selectivity for aldehydes is predominantly due to 1-octene isomerisation to internal alkenes, which undergo significantly slower hydroformylation, whereas ethene cannot isomerise. Additionally, it must be noted that, as a result of its much smaller size than octene, the coordination of ethene to a metal centre during hydroformylation catalysis is less constrained by the steric demands of the complex, which is likely to have an effect on the regiochemistry of the resulting aldehydes produced.²⁶

A comparison of hydroformylation catalyst performance for the polymer-supported FibrecatTM/Rh(acac)(CO)₂ and silica-supported silica-PPh₂/Rh(acac)(CO)₂ in our work shows several interesting findings. Notably, the silica-PPh₂-supported catalyst exhibited almost twice the activity for aldehyde production than the FibrecatTM-supported system, 200 ± 18 vs 114 ± 8 h⁻¹. However, the selectivity for aldehydes of the silica-PPh₂/Rh(acac)(CO)₂ catalyst was significantly lower than the FibrecatTM/Rh(acac)(CO)₂ catalyst at 31% relative to 81%, something resulting from the high alkene isomerisation activity of the silica-supported system. This difference in catalyst performance could originate from the different properties of the supported phenyl phosphine ligands. The silica-supported phosphine is likely to be more electron-deficient and sterically hindered than the FibrecatTM-supported phosphine, as the phosphorus atom is directly bound to the silica surface through an electron withdrawing Si-O-P linkage, resulting in a Si-O-PPh₂ functionality, as was determined by ³¹P SS NMR (see Section 4.13). Meanwhile, the FibrecatTM-supported PPh₃ is connected to the support *via* one of its phenyl groups, providing an aryl spacer between the phosphorus donor atom and the support surface.

Overall, the catalyst testing results of the heterogeneous systems prepared as part of this project (Table 5.7) show a similar trend in catalyst activity and selectivity to their analogous homogeneous catalysts (see Section 5.4). The PCNCP-containing catalysts, Sil-[Rh(**L19**)(COD)]BF₄ and Sil-[Rh(**L17**)₂]BF₄, gave significantly higher TOFs than the PNP-containing catalyst, Sil-[Rh(**L5**)₂]BF₄, and the sulfur-donor-ligand-containing Sil-[Rh(**L5S2**)(COD)]BF₄, with Sil-[Rh(**L17**)₂]BF₄ providing the best overall catalyst activity of $682 \pm 48 \text{ h}^{-1}$. In order to assess the overall most effective immobilised hydroformylation catalyst, the stability and lifetime of the catalyst also has to be considered alongside activity and selectivity (see Sections 5.3.4 and 5.3.5).

5.3.3 Homogeneous vs heterogeneous [Rh(P[^]P)₂]BF₄ catalyst induction period comparison

Interestingly, the catalysts Sil-[Rh(**L5**)₂]BF₄ and Sil-[Rh(**L17**)₂]BF₄ exhibited significantly shorter induction periods than their homogeneous analogues, as summarised in Figure 5.8, which compares [Rh(**L17**)₂]BF₄ with Sil-[Rh(**L17**)₂]BF₄. As discussed in Section 5.3.1, based on previous reports in the literature, the origin of the induction period prior to the onset of catalysis is likely to correlate with the time required to displace one equivalent of diphosphine in order to form the active catalyst species, which contains only one bidentate phosphine ligand (Scheme 5.8).^{16,27} It is not readily apparent why this process is more facile while [Rh(**L5**)₂]BF₄ and [Rh(**L17**)₂]BF₄ are immobilised on silica, however. One factor to consider is that immobilisation is likely to deter formation of inactive dimeric species, which could impact the activation of these catalysts (as discussed in Sections 5.2.4 and 5.4).

Unfortunately, understanding the formation of an active catalyst species from Sil-[Rh(**L5**)₂]BF₄ and Sil-[Rh(**L17**)₂]BF₄ is complicated by the fact that SS ²⁹Si NMR spectroscopic analysis of the pre-catalysts could not determine whether silica-immobilisation was achieved *via* one or both phosphine ligands (see Section 4.12.3). As a result, two pathways to form the active, immobilised catalysts species from Sil-[Rh(**L5**)₂]BF₄ and Sil-[Rh(**L17**)₂]BF₄ are possible depending on the silica-immobilisation mode of the complex (Schemes 5.8 and 5.9). Further complications arise since the location of the immobilised complexes is also uncertain, with immobilisation on the

external silica surface or inside the silica pore structure both possible (Figure 5.9). Note, the dimensions of the molecular structure of $[\text{Rh}(\text{L5})_2]\text{BF}_4$, $19 \text{ \AA} \times 10 \text{ \AA} \times 9 \text{ \AA}$, suggest that it can diffuse inside AEROPERL 300/30 silica (average pore diameter 260 \AA). A combination of these possible binding modes and locations on the silica means that understanding the exact catalyst species produced during catalysis, and their formation pathway is difficult. As a result, understanding the origin of the difference in the length of induction of $[\text{Rh}(\text{L5})_2]\text{BF}_4$ and $[\text{Rh}(\text{L17})_2]\text{BF}_4$ compared to $\text{Sil}-[\text{Rh}(\text{L5})_2]\text{BF}_4$ and $\text{Sil}-[\text{Rh}(\text{L17})_2]\text{BF}_4$ is very challenging.

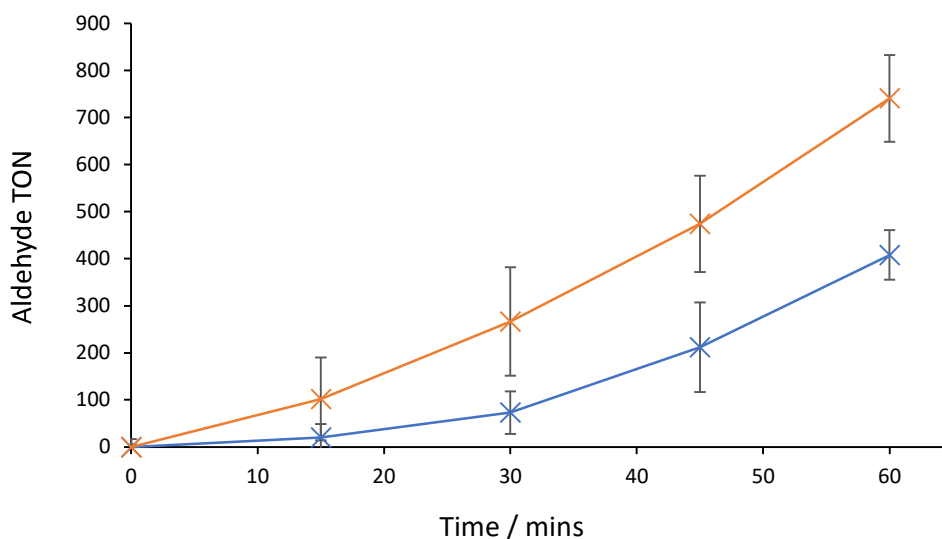
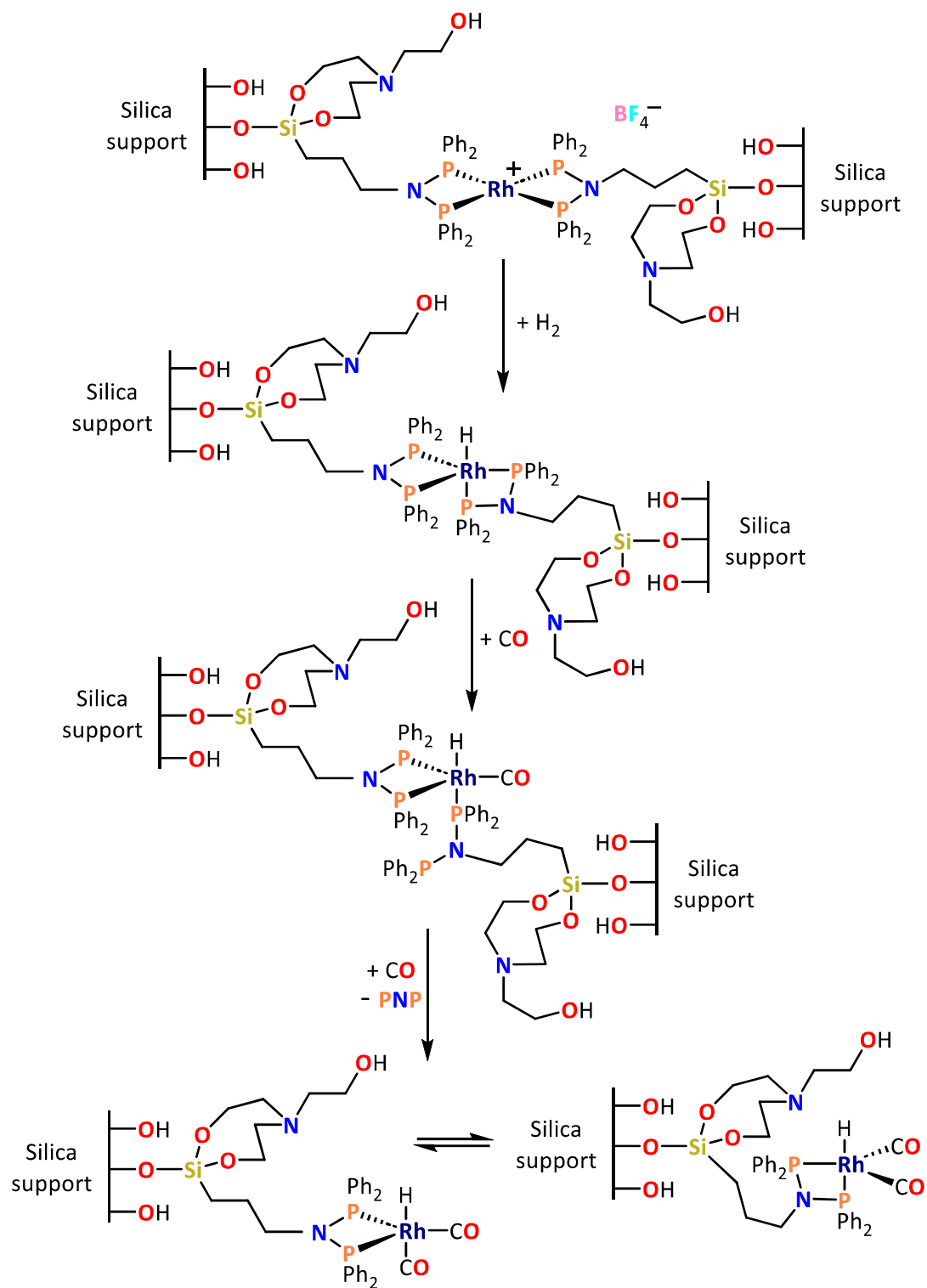
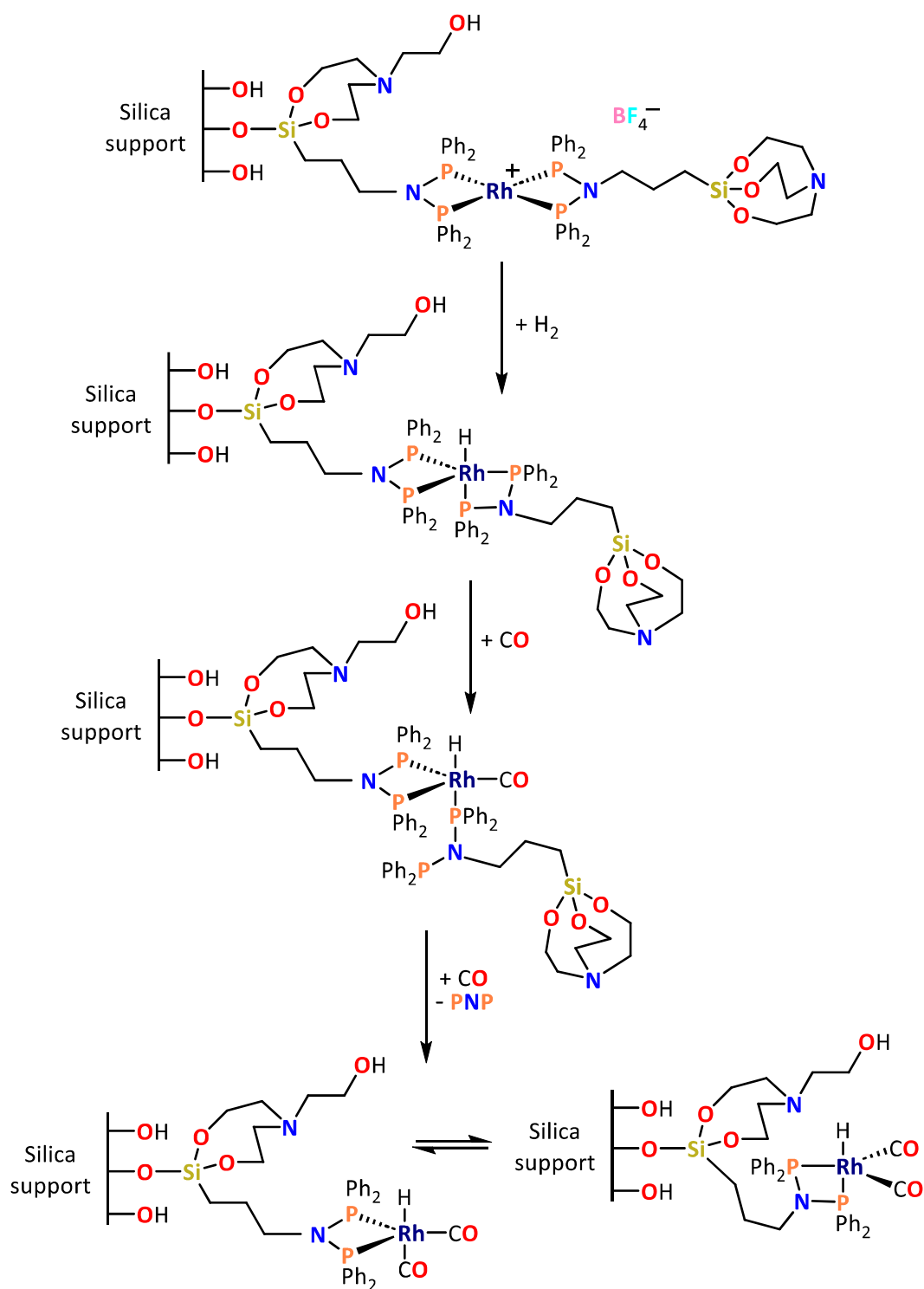


Figure 5.8. C_9 aldehyde production over time for the hydroformylation of 1-octene with
orange: silica-supported $[\text{Rh}(\text{L17})_2]\text{BF}_4$ and *blue*: $[\text{Rh}(\text{L17})_2]\text{BF}_4$.



Scheme 5.8. Active catalyst formation under hydroformylation conditions for $\text{Sil}-[\text{Rh}(\text{L5})_2]\text{BF}_4$ immobilised via both phosphine ligands.



Scheme 5.9. Active catalyst formation under hydroformylation conditions for $\text{Sil}[\text{Rh}(\text{L5})_2]\text{BF}_4$ immobilised via one phosphine ligand.

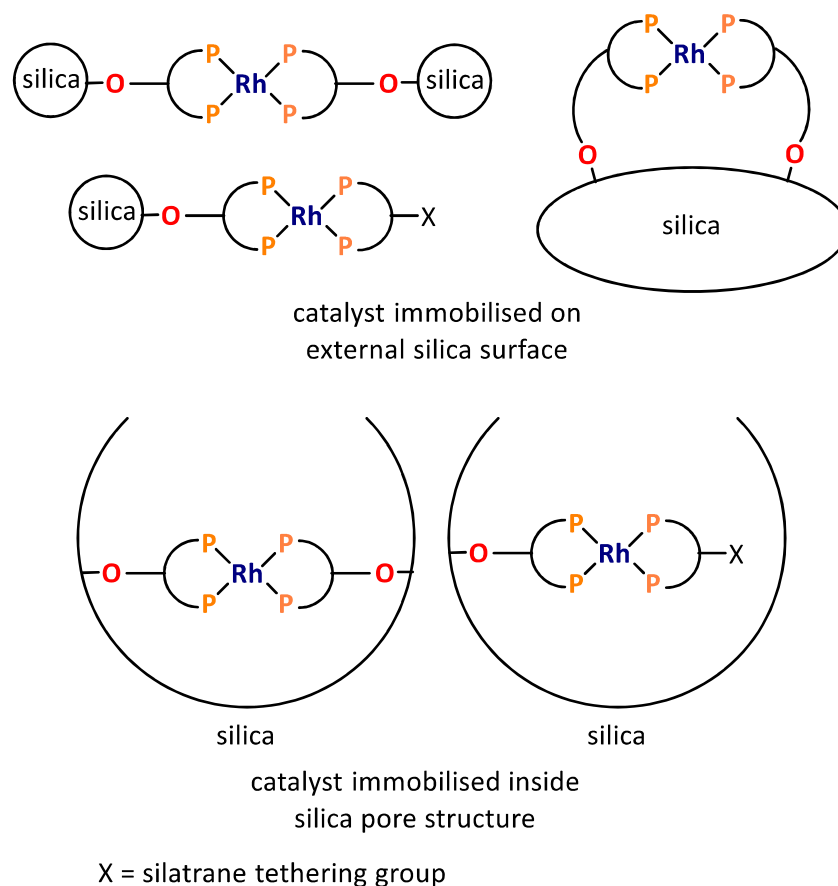


Figure 5.9. Possible silica binding modes of $\text{Sil}[\text{Rh}(\text{L5})_2]\text{BF}_4$ and $\text{Sil}[\text{Rh}(\text{L17})_2]\text{BF}_4$.

Previously, several factors have been shown to affect the length of induction periods for hydroformylation catalysts of different types, including temperature, syngas pressure, rhodium concentration and the presence of additional ligands and halides.^{4,6,28–32} It is possible that these factors could also contribute to the reduced induction periods of the catalysts $[\text{Rh}(\text{L5})_2]\text{BF}_4$ and $\text{Sil}[\text{Rh}(\text{L17})_2]\text{BF}_4$ once silica-immobilised. For example, $\text{Sil}[\text{Rh}(\text{L5})_2]\text{BF}_4$ and $\text{Sil}[\text{Rh}(\text{L17})_2]\text{BF}_4$ could potentially experience an artificially high syngas pressure within the silica pore structure, which may promote ligand exchange of the immobilised rhodium complexes. This can be rationalised by the fact that hydrogen (uptake 2.0 wt.% at 45 bar, 77 k), and carbon monoxide (uptake 2.7 wt.% at 5 bar, 298 k) have both been shown to physisorb to porous silica by weak interaction with silica surface silanols, potentially enhancing their local concentration at the silica surface.^{33,34} The potential for this effect to occur is largely dependent on the location of the immobilised rhodium complexes on/within the silica support material, however, as it

much more likely to be a significant effect inside the silica pore structure than on the external silica surface.

Another potential cause of the reduction in induction period of the silica immobilised catalysts relative to that of their homogeneous analogues is the presence of additional species able to act as ligands on the silica surface. ^{31}P SS NMR spectroscopic analysis of $\text{Si}[\text{Rh}(\text{L5})_2]\text{BF}_4$ and $\text{Si}[\text{Rh}(\text{L17})_2]\text{BF}_4$ pre-catalysts indicates the presence of small amounts of immobilised phosphine oxide species, formed as side products of immobilisation (see Chapter 4), which could potentially interact with the immobilised rhodium. Indeed, the presence of phosphine oxides, such as Ph_3PO , have been shown to reduce induction periods for the formation of the active hydroformylation catalyst $\text{HCo}(\text{CO})_4$ from $\text{Co}_2(\text{CO})_8$ under mild conditions, unlike phosphines.³¹ It is unknown, however, whether surface-immobilised phosphine oxides would be physically close enough to interact with immobilised rhodium complexes or if they would have a similar effect of reducing induction periods for rhodium catalysts as with $\text{Co}_2(\text{CO})_8$. Other potential ligands present on the silica surface include silica surface silanols, and alcohols produced by partial hydrolysis of silatranes upon silica-immobilisation of the rhodium complexes. These functionalities could also potentially interact with the immobilised rhodium centres and influence the catalyst formation pathway, and are likely to be more accessible than immobilised phosphine oxides. For example, silica surface silanols have been previously shown to tether $\text{RhCo}_3(\text{CO})_{12}$ clusters onto a silica surface by nucleophilic attack at cobalt.³⁵ This suggests that interactions between silica surface silanols and metal complexes may also be possible in our systems and could potentially affect the length of catalyst induction periods. It is important to note that in our work ^{31}P and ^{29}Si SS NMR spectroscopic analysis did not indicate the presence of any directly surface bound rhodium species *via* Rh-O linkages in any of our catalyst precursors, however. Work by van Leeuwen *et al.* showed that silica-immobilisation of a rhodium Xantphos complex also resulted in no ionic silica-rhodium interactions, unlike when $\text{Rh}(\text{acac})(\text{CO})_2$ was added directly to a phosphine-functionalised silica (see Section 1.16), in good agreement with the immobilised catalysts investigated in our work.³⁶

Without additional studies, it is not possible to determine the origin of the significantly shorter catalyst induction periods exhibited by $\text{SiI}[\text{Rh}(\text{L5})_2]\text{BF}_4$ and $\text{SiI}[\text{Rh}(\text{L17})_2]\text{BF}_4$ than their homogeneous analogues (see Future work).

5.3.4 Investigating rhodium loss from heterogeneous catalysts during hydroformylation reactions

Investigations were conducted to assess the stability of the supported catalysts by determining the loss of rhodium from the support into the reaction solution over the course of a 1 h hydroformylation experiment. To achieve this, a sample of the reaction solution was collected *via* the autoclave dip tube after catalysis and analysed by ICP-OES analysis at Durham University, to quantify the amount of solubilised rhodium lost from the support after a 1 h hydroformylation experiment. The results of these experiments are summarised in Table 5.7 alongside initial catalyst loadings (see Section 4.16). To prepare the collected reaction solution for ICP-OES analysis, the sample was filtered to ensure no solid catalyst was present, then dried *in vacuo* and the residue dissolved in HCl (see experimental section for further details).

The FibrecatTM-supported sample showed the smallest amount of leaching at 0.72%, despite the rhodium being coordinated by monodentate ligands rather than the bidentate ligands used for the majority of the catalysts investigated. This contrasts with our prediction of bidentate ligands improving the stability of the immobilised catalysts, suggesting that other factors may also be important in controlling catalyst stability with respect to metal leaching from phosphine-immobilised hydroformylation catalysts. It is likely that the chemical nature of the support plays a key role in the catalysts resistance to rhodium leaching in this case. The polyethylene FibrecatTM support is expected to be much more inert than the silica supports, as it does not possess any functionality that is likely to react with phosphines or phosphine rhodium complexes, which may aid overall catalyst stability. A strong argument for this is the fact that, as described in Chapter 4, the synthesis of silica-immobilised phosphines was very challenging due to phosphine oxidation caused by side reactions with the silica support. Although this effect was suppressed when the phosphine was complexed by rhodium before immobilisation of

the resulting complex, it is unknown if the formation of unidentified P^V species, due to the reaction of immobilised phosphines with the silica support, could be observed/promoted under hydroformylation reaction conditions.

Table 5.7. Heterogeneous catalyst rhodium leaching after 1 h hydroformylation reaction.

Catalyst	Catalyst rhodium loading / mg	Catalyst rhodium loading / Wt. %	Rhodium leached / mg	Rhodium leached / %
FibreCat™ + Rh(acac)(CO) ₂	11.2	4.46	0.08	0.72
Rh(acac)(CO) ₂ + silica-PPh ₂	7.5	2.49	2.16	29
Sil-[Rh(L5) ₂]BF ₄	2.1	0.53	0.03	1.4
Sil-[Rh(L17) ₂]BF ₄	1.4	0.35	0.02	1.4
Sil-[Rh(L19)(COD)]BF ₄	1.2	0.31	0.42	34
Sil-[Rh(L5S ₂)(COD)]BF ₄	3.0	0.76	0.09	3.0

Note: A standard mass of the different catalysts was used in the hydroformylation experiments because the rhodium content of the catalysts was not known at the time (400 mg for silica catalysts, 250 mg for the FibreCat™ catalyst, 300 mg for Rh(acac)(CO)₂ + silica-PPh₂). Errors: catalyst rhodium content \pm 0.02%, rhodium leached \pm 0.1%.

Another consideration in the comparatively low rhodium leaching observed for the FibreCat™-supported rhodium system is the excess of uncoordinated “PPh₃” on the support, as evidenced by ³¹P SS NMR spectroscopic analysis of the sample before catalysis ([Rh]/[P] \approx 1:3). During catalysis these free “PPh₃” sites could potentially capture any released rhodium species and prevent them from leaching from the system in what amounts to a “release and capture” type process. The best performing silica-supported catalysts with respect to leaching, Sil-[Rh(L5)₂]BF₄ and Sil-[Rh(L5)₂]BF₄, could

also potentially benefit from this “release and capture” effect to a lesser extent due to them each containing two equivalents of diphosphine per rhodium centre, whereas Sil-[Rh(**L19**)(COD)]BF₄ and Sil-[Rh(**L5S2**)(COD)]BF₄ have a 1:1 ratio of immobilised ligand to rhodium.

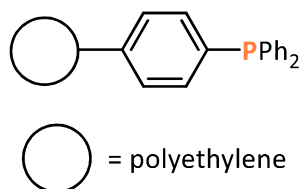


Figure 5.10. Structure of Fibrecat™ (repeated here for clarity).

It is possible that several other factors could also contribute to the leaching performance of the catalyst for the silica-supported catalysts. These include the type of silica used and any pretreatment, the silica functionalisation reaction type and conditions, and the identity of the immobilised rhodium complex. However, these factors were not investigated in this work and remain areas of potential future interest (see Future work).

Both the silica-PPh₂-supported catalyst and Sil-[Rh(**L19**)(COD)]BF₄ system showed high leaching of rhodium from the support, 29% and 34% respectively, indicating poor catalyst stability. For the silica-PPh₂-supported catalyst the large steric demand of the silica-bound phosphine may hinder strong coordination to rhodium, resulting in facile loss of rhodium from the surface. This contrasts to the Fibrecat™-supported catalyst (Figure 5.10) where the steric hinderance of the support is likely to be less due to the aryl spacer between the support backbone and phosphine donor centres. Meanwhile, electron-rich phosphines, such as **L19**, are known to be more susceptible to oxidation reactions than less electron-rich phosphines, which may increase their susceptibility to decomposition on silica.³⁷ However, due to time constraints and the difficulty in isolating the catalyst in an air-sensitive manner back out from the autoclave, no post-catalysis catalyst characterisation was performed in order to try and elucidate the decomposition pathways of the catalysts used in this work.

The high levels of rhodium loss from silica-PPh₂/Rh(acac)(CO)₂ and Sil-[Rh(**L19**)(COD)]BF₄ during hydroformylation of 1-octene are similar in magnitude to the rhodium leaching reported for the hydroformylation of cyclohexene with a silica-immobilised Wilkinson's

catalyst (Figure 5.11, top), where 41% of rhodium was lost after a 20 h reaction.³⁸ In contrast, a previously reported modified Wilkinson's catalyst immobilised *via* a sulfur donor (Figure 5.11, bottom) was shown to be more resistant to leaching, resulting in 13% rhodium loss after 20 h under the same conditions (100 °C, 28 bar (1:1 H₂:CO), cyclohexene (12 ml), THF (55 ml), t = 20 h).³⁸ In contrast, in our work, the sulfur-ligated catalyst, Sil-[Rh(**L5S2**)(COD)]BF₄, showed 3.0% rhodium leaching after 1 h, whereas Sil-[Rh(**L5**)₂]BF₄ showed 1.4%.

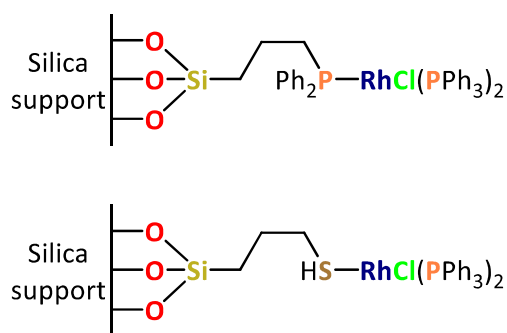


Figure 5.11. Immobilised Wilkinson's catalyst analogues for hydroformylation of cyclohexene using modified phosphine and thiol donor motifs.³⁸

Superior resistance to leaching than the previously mentioned immobilised Wilkinson's catalysts has been reported in the literature for a silica-immobilised RhCl(CO)(PPh₃)₂ catalyst, tethered *via* a PPh₂ moiety attached to the silica surface *via* alkyl chains of various lengths C₁-C₁₁ (Figure 5.12) (Table 5.8).³⁹ The extent of rhodium leaching was shown to decrease to a minimum of 2.9% over 8 catalyst recycles as the alkyl spacer was increased to the maximum, C₁₁. A comparison of the rhodium loss after one cycle of Sil-[Rh(**L5**)₂]BF₄ and Sil-[Rh(**L17**)₂]BF₄, both 1.4%, to Sil-C₅-PPh₂-RhCl(CO)(PPh₃) (0.41%) shows lower levels of rhodium loss for the literature system. Note that in these examples the length of the immobilisation tether is similar (5 atoms between Si and P for Sil-[Rh(**L17**)₂]BF₄ and Sil-C₅-PPh₂-RhCl(CO)(PPh₃), 4 atoms for Sil-[Rh(**L5**)₂]BF₄). A possible explanation for this difference in rhodium leaching between Sil-[Rh(**L5**)₂]BF₄/Sil-[Rh(**L17**)₂]BF₄, and Sil-C₅-PPh₂-RhCl(CO)(PPh₃) is the large excess of immobilised ligand employed relative to rhodium used in the Sil-C_x-PPh₂-RhCl(CO)(PPh₃) systems resulting from phosphine modification of the silica support prior to rhodium complexation. As mentioned earlier in this section, using a large excess of ligand is potentially an

important factor in preventing rhodium leaching, through a “release and capture” type process. To enable a more full comparison of the leaching behaviour of $\text{Sil}-[\text{Rh}(\text{L5})_2]\text{BF}_4$ and $\text{Sil}-[\text{Rh}(\text{L17})_2]\text{BF}_4$, to $\text{Sil}-\text{C}_5\text{-PPh}_2\text{-RhCl}(\text{CO})(\text{PPh}_3)$, additional studies on the rhodium loss of $\text{Sil}-[\text{Rh}(\text{L5})_2]\text{BF}_4$ and $\text{Sil}-[\text{Rh}(\text{L17})_2]\text{BF}_4$ over several catalyst runs is required (see Future work) to assess the long-term stability to rhodium leaching of these catalysts.

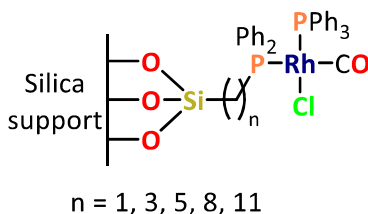


Figure 5.12. silica-immobilised $\text{RhCl}(\text{CO})(\text{PPh}_3)_2$ catalysts immobilised via different length alkyl chains.³⁹

Table 5.8. Rhodium leaching from silica-immobilised $\text{RhCl}(\text{CO})(\text{PPh}_3)_2$ catalysts with varying length alkyl chain tethers after 1-octene hydroformylation.³⁹

Catalyst	Catalyst cycle times	Total rhodium leaching / %	Rhodium leaching per cycle / %
$\text{Sil}-\text{C}_1\text{-PPh}_2\text{-Rh}$	3	4.0	1.30
$\text{Sil}-\text{C}_3\text{-PPh}_2\text{-Rh}$	8	3.8	0.48
$\text{Sil}-\text{C}_5\text{-PPh}_2\text{-Rh}$	8	3.3	0.41
$\text{Sil}-\text{C}_8\text{-PPh}_2\text{-Rh}$	8	3.0	0.38
$\text{Sil}-\text{C}_{11}\text{-PPh}_2\text{-Rh}$	8	2.9	0.36

Conditions: 120 °C, 50 bar (1:1 $\text{H}_2\text{:CO}$), 1-octene (0.032 mol, 5 ml), toluene (15 ml), $t = 1$ h, isopropyl alcohol (1 ml, internal standard). Rhodium leaching determined by ICP-MS.

5.3.5 $\text{Sil}-[\text{Rh}(\text{L17})_2]\text{BF}_4$ catalyst recycling study

In order to study catalyst lifetimes, a recycling experiment was performed where the same $\text{Sil}-[\text{Rh}(\text{L17})_2]\text{BF}_4$ catalyst was reused five times. Recycling was performed by allowing the solid catalyst to settle out on the autoclave bottom at the end of the reaction, then siphoning off the liquid fraction from the autoclave *via* the catalyst dip tube. For each run conversion to aldehydes at one hour was calculated using GC-FID

data (Figure 5.13). Unfortunately, this method could not ensure that no catalyst was lost between runs. Fresh toluene, octene and nonane internal standard were then added for each run. After addition of fresh reagents to the autoclave for each run, gas chromatography was performed on an aliquot of the reaction mixture to ensure that the initial reaction mixture was consistent for each run and that product accumulation in the autoclave was not occurring (*e.g.* that all the previous reaction mixture was successfully removed).⁴⁰ $\text{SiI}[\text{Rh}(\text{L17})_2]\text{BF}_4$ was selected as the catalyst for the recycling experiments as it provided the best performance in terms of catalyst activity, selectivity and resistance to leaching of the novel catalysts investigated.

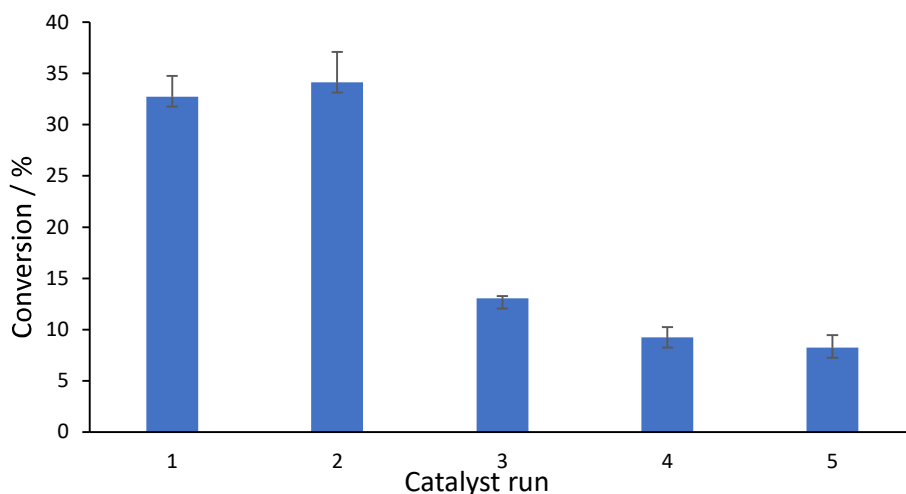
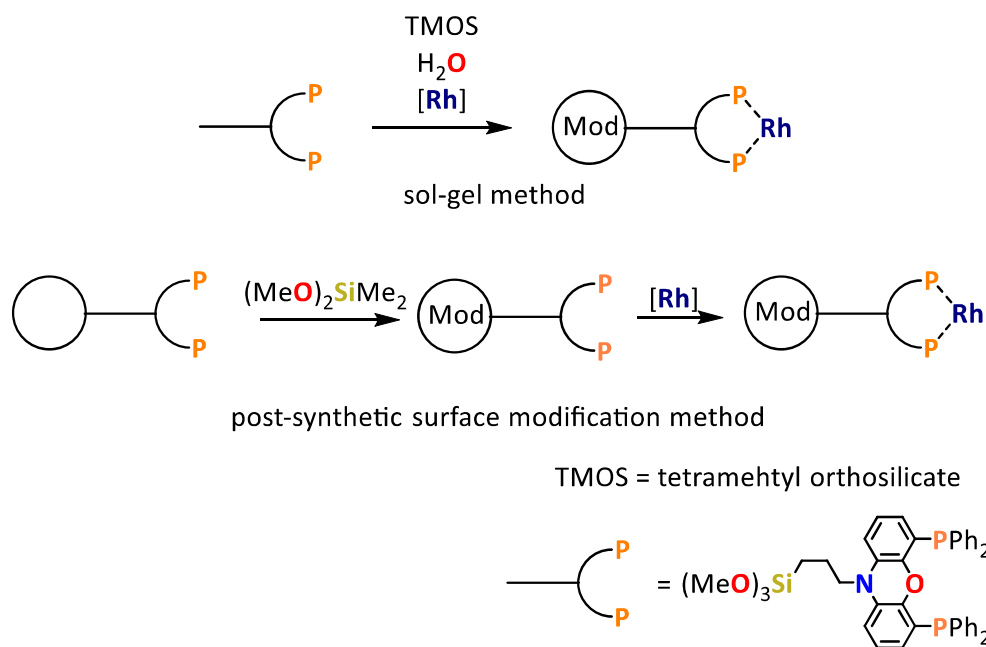


Figure 5.13. 1-Octene conversion to aldehydes using $\text{SiI}[\text{Rh}(\text{L17})_2]\text{BF}_4$ as a function of catalyst recycle (some loss of catalyst during GC sample collection and recycling expected). Conditions: 90 °C, 20 bar (1:1 H_2 :CO), 1-octene (0.032 mol, 5 ml), toluene (95 ml), $t = 1$ h, nonane (1 ml, internal standard), $\text{SiI}[\text{Rh}(\text{L17})_2]\text{BF}_4$ (400 mg, 0.35 Wt.% Rh).

The preliminary recycling study shows a consistent conversion to aldehydes of 33% for the first two catalysis runs, followed by a large decrease to 13% during run 3, with aldehyde conversion reducing further to 8% after 5 runs, approximately one quarter of the conversion delivered by the fresh catalyst. In the first run the induction period observed for *bis*(diphosphine)-containing catalysts needs to be considered, which will result in a lower-than-expected turnover for the first catalyst run (See section 5.2.4). Overall, these results suggest poor recyclability of the catalyst; however these experiments were performed with no optimisation of the reaction conditions or of the

method of catalyst recovery. Additionally, it is possible that some catalyst could be lost upon each recycle and subsequent GC sample collection, which would result in a lower than expected catalyst turnover on subsequent runs; however an alternative method to separate the catalyst from the reaction mixture without exposure to air could not be established for our reactor set-up in a reasonable time frame.

In comparison to the results obtained for recycling $\text{SiI}[\text{Rh}(\text{L17})_2]\text{BF}_4$, the previously reported by van Leeuwen hydroformylation of 1-octene using a silica-immobilised catalyst grafted *via* a bidentate NiXantphos ligand, prepared using the sol-gel method (Scheme 5.10), showed no reduction in conversion until the 4th cycle, where a 38% reduction in catalyst TOF was observed.³⁶ Alternatively, when the catalyst was prepared by post-synthetic surface modification of silica, a 38% reduction in catalyst TOF was observed on the 3rd cycle. These catalyst recycling experiments were performed by removing the reaction solution from the solid catalyst (located in the autoclave) with a 1.2 mm syringe, then washing the catalyst with 5 mL of toluene, before addition of fresh reagents to the autoclave for subsequent catalysis. These recycling experiments were performed at lower temperature (80 °C), higher pressure (50 bar 1:1 H_2 :CO), and with a larger ratio of ligand to rhodium (10:1) than for the recycling $\text{SiI}[\text{Rh}(\text{L17})_2]\text{BF}_4$, all of which have been shown to improve catalyst stability for various hydroformylation catalyst systems in the literature.^{3,41,42} Optimisation of the hydroformylation reaction conditions, such as reaction temperature and pressure, alongside catalyst recovery method remains an area of future interest in our work, using catalyst $\text{SiI}[\text{Rh}(\text{L17})_2]\text{BF}_4$ to further maximise catalyst lifetime, in addition to assessing the recyclability of the other heterogeneous catalysts developed in this work (see Future work).



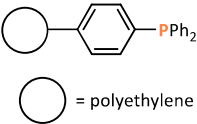
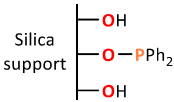
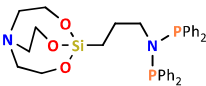
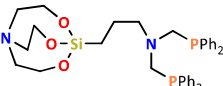
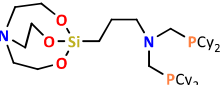
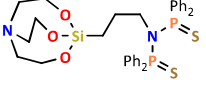
Scheme 5.10. Different methods of silica-immobilised hydroformylation catalyst synthesis reported by van Leeuwen.³⁶

5.4 Hydroformylation activity comparison between homogeneous and analogous silica-immobilised catalysts

In order to assess the effect of silica-immobilisation on catalyst performance, a comparison of homogeneous and analogous heterogeneous catalysts was performed. To facilitate this comparison, Table 5.9 contains the combined homogeneous and heterogeneous catalysis results previously presented in Tables 5.1 and 5.6.

Comparing the heterogeneous catalysts to their homogeneous analogues, the *l*:*b* ratio is shown to be consistent within error. This suggests that the immobilised metal centre is far enough removed from the silica surface, as a result of the phosphine linker ligand, for the silica to have any effect on catalyst *l*:*b* ratio.

Table 5.9. Comparison of homogeneous and heterogeneous hydroformylation of 1-octene with various catalysts.

Catalyst (rhodium loading / mg)	Ligand	CHO TOF / h ⁻¹	CHO selectivity at 1 h / %	<i>l</i> : <i>b</i> ratio at 1 h
FibreCat™ + Rh(acac)(CO) ₂ (11.2)		114	81	3.1
RhCl(PPh ₃) ₃	PPh ₃	84	39	3.0
Rh(acac)(CO) ₂ + silica-PPh ₂ (7.5)		200	31	3.0
Rh(acac)(CO) ₂ + 2 PPh ₃	PPh ₃	667	91	2.5
Sil-[Rh(L5) ₂]BF ₄ (2.1)		135	15	2.9
[Rh(L5) ₂]BF ₄		65	13	2.7
Sil-[Rh(L17) ₂]BF ₄ (1.4)		682	75	2.6
[Rh(L17) ₂]BF ₄		674	55	2.7
Sil-[Rh(L19)(COD)]BF ₄		384	50	2.6
[Rh(L19)(COD)]BF ₄ (1.2)		573	66	2.5
Sil-[Rh(L5S2)(COD)]BF ₄ (3.0)		212	26	1.1

Conditions: 90 °C, 20 bar (1:1 H₂:CO), 1-octene (0.032 mol, 5 ml), toluene (95 ml), t = 1 h, nonane (1 ml, internal standard), homogeneous catalysts: [1-octene]/[Rh] = 1000.

Several different trends in catalyst activity are observed between the homogeneous and heterogeneous analogues of the different catalysts investigated. [Rh(L17)₂]BF₄ showed no statistically significant change in catalyst activity when in solution or immobilised on

silica, with TOF values of 674 ± 23 to $682 \pm 48 \text{ h}^{-1}$ determined for the homogeneous and heterogeneous catalysts, respectively. Similarly, the activity of the $[\text{Rh}(\text{L5S}_2)(\text{COD})]\text{BF}_4$ catalyst was shown to be consistent within error for the homogeneous and silica-immobilised catalysts, with TOF values of $240 \pm 16 \text{ h}^{-1}$ and $212 \pm 19 \text{ h}^{-1}$ determined, respectively. These results suggest that mass transport effects, which are commonly a major limitation in heterogeneous catalyst systems, resulting in suppression of catalyst activity, are not rate limiting in these systems.^{43–45} Potentially, this could suggest that all the metal complexes are immobilised onto the external silica surface, rather than inside the silica pores (average pore diameter 260 \AA) where mass transport may be limited, or that diffusion within the silica pores is facile.

The catalytic activity of $[\text{Rh}(\text{L19})(\text{COD})]\text{BF}_4$ was found to decrease from $573 \pm 47 \text{ h}^{-1}$ to $384 \pm 17 \text{ h}^{-1}$ when immobilised on silica. This differing behaviour upon immobilisation of $[\text{Rh}(\text{L19})(\text{COD})]\text{BF}_4$ compared to $[\text{Rh}(\text{L17})_2]\text{BF}_4$ and $[\text{Rh}(\text{L5S}_2)(\text{COD})]\text{BF}_4$ is likely due to the poor stability of $\text{Si}-[\text{Rh}(\text{L19})(\text{COD})]\text{BF}_4$ under hydroformylation reaction conditions, as was seen during the leaching study (see Section 5.3.4). As the catalyst decomposition products have not been identified, their subsequent effect on catalysis is also unknown.

Surprisingly, the activity of $[\text{Rh}(\text{L5})_2]\text{BF}_4$ was shown to more than double from $65 \pm 5 \text{ h}^{-1}$ to $135 \pm 11 \text{ h}^{-1}$ upon silica-immobilisation. Increases in catalyst activity relative to homogeneous catalysis upon immobilisation are rare and indicate a shift in catalyst behaviour, as typically a decrease in activity is to be expected.⁴⁶ For $[\text{Rh}(\text{L5})_2]\text{BF}_4$ the origin of the enhanced rate of the immobilised catalyst is likely due to a suppression of catalyst deactivation caused by dimerisation, by isolating catalyst sites away from each other on the silica support (see Section 5.2.5). This was not verified experimentally, but similar effects have been seen previously where a silica-immobilised Wilkinson's catalyst showed an increased catalyst lifetime compared to its homogeneous analogue.³⁸ This was attributed to the suppression of catalyst deactivation pathways.

Hydroformylation using rhodium complexes immobilised onto silica *via* bidentate phosphine ligands has previously been investigated by van Leeuwen *et al.* for the Xantphos complex $\text{Rh}(\text{acac})(\text{Xantphos})$ (Table 5.10).³⁶ The catalyst showed a very high *I:b* ratio of 37:1 in solution and 32:1 when the catalyst was immobilised onto silica, much higher than was observed for the catalysts investigated in this work. This may in part be

due to the low alkene isomerisation activity of the Xantphos catalyst, making hydroformylation of internal alkenes less likely. Unlike the silica-immobilised catalysts investigated in this work, immobilisation of the Xantphos complex onto silica resulted in a very large 95% decrease in catalyst activity. This difference in behaviour suggests that large mass transport limitations may be operative for the Xantphos-based system that are not present in the catalysts presented in this work. One consideration is the type of silica support used; in our work the AEROPERL 300/30 silica employed has an average pore diameter of 260 Å, whereas in the work by van Leeuwen *et al.* a smaller average pore diameter of 60 Å was used. The smaller pore size used by van Leeuwen *et al.* possibly results in hindered substrate diffusion through the silica and results in mass transport effects during catalysis. This is most likely to play a significant role on catalyst activity if the catalyst sites are located within the silica framework rather than the external surface.

Table 5.10. Hydroformylation of 1-octene with a silica-immobilised Xantphos complex.³⁶

catalyst	time	TOF / h ⁻¹	I/b ratio	Aldehyde / %	Alcohol / %	Octene isomers / %
immobilised	22	13.2	37	93.3	5.1	1.6
homogeneous	2	283	32	96.2	0	3.7

Conditions: 80 °C, 50 bar (1:1 H₂:CO), ligand/Rh = 10, 1-octene/Rh = 673, Rh content = 10 µmol, toluene 10 ml.

5.5 Palladium-catalysed hydroformylation preliminary investigation

An investigation into the catalyst performance of the PdI₂(P[^]P) complexes described in Chapter 3 was of interest, as these complexes could potentially be used as lower cost catalysts relative to the currently industrially used rhodium complexes. Production of an immobilised palladium catalyst could possibly reduce catalyst costs further by facilitating improved catalyst recycling capabilities. Due to time constraints, in this work only a preliminary investigation of homogeneous hydroformylation catalysis with a PdI₂(P[^]P) complex was performed. PdI₂(**L19**) (Figure 5.14) was selected as the catalyst,

as the phosphine sterics and electronics of **L19** most closely match those of the highest performing ligands reported in the literature for $\text{PdI}_2(\text{PR}_3)_2$ -catalysed hydroformylation, *i.e.* monodentate alkyl phosphines, such as PCy_3 .⁴⁷

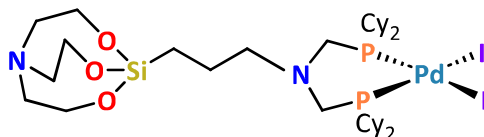


Figure 5.14. Structure of $\text{PdI}_2(\text{L19})$.

Hydroformylation reactions described in the literature using $\text{PdI}_2(\text{PR}_3)_2$ catalysts employ harsher reaction conditions of 110 °C and a 100 bar pressure of syngas, harsher than those employed for the rhodium-catalysed hydroformylation described so far in this Chapter.⁴⁷ Since high reaction pressures are generally undesirable due to increased operating costs and safety requirements, it was of interest to determine the minimum pressure required for catalyst activity of the $\text{PdI}_2(\text{PR}_3)_2$ systems at 110 °C.⁴⁸ To this end, a 1-octene hydroformylation experiment using $\text{PdI}_2(\text{L19})$ as a catalyst was performed with the reaction monitored at increasing syngas pressures (Table 5.11). Initially, the reaction was pressurised to 20 bar for 24 h (the same pressure used for the rhodium catalysts). No catalyst activity was observed after this time and so subsequently the pressure was increased to 50 bar and the test continued for a further 72 h. After this extended reaction time 38% of the 1-octene had been consumed; however this was predominantly due to alkene isomerisation, with only 7% conversion to aldehydes being achieved. Finally, the reaction pressure was increased to 100 bar, which resulted in a further 2% conversion to aldehydes over 1 h, corresponding to a TOF of 16 h^{-1} over this final 1 h period, while the alkene isomerisation activity increased to 48 h^{-1} . Further optimisation of the reaction conditions or catalyst were not performed.

Table 5.11. Hydroformylation of 1-octene with $\text{Pdl}_2(\text{L19})$.

Time / h (pressure / bar)	Reaction composition			Aldehyde <i>l:b</i> ratio
	1-octene / %	Internal octenes / %	C ₉ Aldehyde / %	
0	100	trace	0	-
24 (at 20 bar)	100	trace	0	-
96 (72 h at 50 bar)	62	31	7	3:1
97 (1 h at 100 bar)	54	37	9	3:1

Conditions: 110 °C, (1:1 H₂:CO), 1-octene (0.032 mol, 5 ml), toluene (95 ml), $\text{Pdl}_2(\text{L19})$ (0.04 g, 3.9×10^{-5} mol), t = 1 h, nonane (1 ml, internal standard).

A $\text{Pdl}_2(\text{PCy}_3)_2$ catalyst was recently investigated by Dydio *et al.* for the hydroformylation of propene under the following conditions: 2.5 mM Pdl_2 , 5 mM PCy, 2 mL anisole, 20 bar CO, 80 bar H₂, 110 °C, resulting in a TOF of 32 h⁻¹ and *l:b* ratio of 1:3 (*l:b* ratio was shown to increase significantly at lower temperatures up to 1:50 at 80 °C, at the cost of drastically reduced activity).⁴⁷ This result suggests that $\text{Pdl}_2(\text{L19})$ is competitive with other $\text{Pdl}_2(\text{PR}_3)_2$ catalysts and hence is an interesting area for future work in which silica-immobilisation of $\text{Pdl}_2(\text{L19})$ could be investigated alongside catalyst lifetime and stability (see Future work).

5.6 Chapter 5 summary

In this chapter the results of homogeneous and heterogeneous hydroformylation of 1-octene using rhodium catalysts have been detailed under industrially relevant conditions of: 90 °C, 20 bar (1:1 H₂:CO), 1-octene (0.032 mol, 5 ml), [1-octene]/[Rh] = 1000, toluene (95 ml), t = 1 h, nonane (1 ml, internal standard).

The homogeneously-catalysed hydroformylation of 1-octene with $\approx 90^\circ$ bite angle PCNCP ligand-containing catalysts, $[\text{Rh}(\text{L17})_2]\text{BF}_4$ and $[\text{Rh}(\text{L19})(\text{COD})]\text{BF}_4$, showed the highest

catalyst activities of the novel complexes investigated, of 674 ± 23 and $573 \pm 47 \text{ h}^{-1}$ respectively, values comparable to those achieved using an *in situ* generated $\text{HRh}(\text{CO})_2(\text{PPh}_3)_2$ catalyst ($667 \pm 31 \text{ h}^{-1}$). Meanwhile the smaller bite angle (*ca.* 70°) PNP-ligated $[\text{Rh}(\text{L5})_2]\text{BF}_4$ showed a much lower catalyst activity of $65 \pm 5 \text{ h}^{-1}$, while $[\text{Rh}(\text{L12})_2]\text{BF}_4$ displayed no catalyst activity under the conditions investigated. It was shown that an active catalyst could be generated *in situ* from a 1:1 mixture of $\text{Rh}(\text{acac})(\text{CO})_2$ and **L12**, however, achieving a TOF of $124 \pm 8 \text{ h}^{-1}$ and *l:b* ratio of 8. The disulfur donor-ligand-containing catalyst, $[\text{Rh}(\text{L5S}_2)(\text{COD})]\text{BF}_4$, was shown to be a highly active alkene isomerisation catalyst with a TOF of $2161 \pm 70 \text{ h}^{-1}$. It was also a modest hydroformylation catalyst with a TOF of $240 \pm 16 \text{ h}^{-1}$, active for hydroformylation of both internal and terminal alkenes, resulting in an aldehyde *l:b* ratio of 1:1, much lower than the phosphine-containing catalysts investigated. An induction period of *ca.* 25 minutes was observed for the bis(diphosphine) catalysts, $[\text{Rh}(\text{L17})_2]\text{BF}_4$ and $[\text{Rh}(\text{L5})_2]\text{BF}_4$, corresponding to the time required to displace one equivalent of diphosphine ligand in order to form the active catalyst species. In contrast no induction period was observed for the $[\text{Rh}(\text{L}^\wedge\text{L})(\text{COD})]\text{BF}_4$ catalysts.

Heterogeneous catalysis using the silica-immobilised rhodium complexes showed a similar trend in catalytic performance to their homogeneous analogues, with Sil- $[\text{Rh}(\text{L17})_2]\text{BF}_4$ and Sil- $[\text{Rh}(\text{L19})(\text{COD})]\text{BF}_4$ providing the highest TOFs of 682 ± 48 and $384 \pm 17 \text{ h}^{-1}$, respectively, followed by Sil- $[\text{Rh}(\text{L5S}_2)(\text{COD})]\text{BF}_4$ with $212 \pm 19 \text{ h}^{-1}$ and Sil- $[\text{Rh}(\text{L5})_2]\text{BF}_4$ with 135 h^{-1} . Meanwhile, the FibrecatTM-supported catalyst was shown to have the highest aldehyde selectivity of 81%, but the lowest activity of $114 \pm 8 \text{ h}^{-1}$. A silica- PPh_2 supported catalyst displayed a higher TOF of $200 \pm 18 \text{ h}^{-1}$, but a much lower aldehyde selectivity of 31%, due to alkene isomerisation being the dominant reaction.

In contrast to their analogous homogeneous catalysts, Sil- $[\text{Rh}(\text{L5})_2]\text{BF}_4$ and Sil- $[\text{Rh}(\text{L17})_2]\text{BF}_4$ showed a significantly reduced induction period. The origin of this effect is poorly understood, but may be due to the presence of potentially coordinating ligands on the silica surface, such as silanols, phosphine oxides, or silica-bound CO. It is proposed that interaction with these species could potentially enhance the rate of diphosphine substitution from $[\text{Rh}(\text{P}^\wedge\text{P})_2]\text{BF}_4$ complexes, required to form hydroformylation-active $\text{HRh}(\text{P}^\wedge\text{P})(\text{CO})_2$ complexes.

Catalyst leaching studies showed that the FibrecatTM-supported catalyst was most resilient to leaching, losing 0.72% rhodium content after a 1 h reaction, followed by Sil-[Rh(**L17**)₂]BF₄ and Sil-[Rh(**L5**)₂]BF₄ at 1.4%. Sil-[Rh(**L19**)(COD)]BF₄ and the silica-PPh₂-supported catalysts showed the worst leaching performance with 34 and 29% rhodium loss after 1 h, respectively.

The recycling performance of Sil-[Rh(**L17**)₂]BF₄ was investigated, showing no loss in activity after one recycle, followed by a subsequent large decrease in catalytic activity down to approximately 25% of initial activity after five runs.

Preliminary studies using the palladium hydroformylation catalyst PdI₂(**L19**) showed an aldehyde activity of 16 h⁻¹ and l:b ratio of 3:1 at 110 °C and 100 bar (1:1 H₂:CO) in good agreement with literature PdI₂(PR₃)₂ systems.⁴⁷

5.7 Chapter 5 references

1. A. J. Sandee, L. A. Van Der Veen, J. N. H. Reek, P. C. J. Kamer, M. Lutz, A. L. Spek and P. W. N. M. Van Leeuwen, *Angew. Chem. Int. Ed.*, 1999, **38**, 3231–3235, DOI: 10.1002/(SICI)1521-3773(19991102)38:21<3231::AID-ANIE3231>3.0.CO;2-B.
2. K. Raghuvanshi, C. Zhu, M. Ramezani, S. Menegatti, E. E. Santiso, D. Mason, J. Rodgers, M. E. Janka and M. Abolhasani, *ACS Catal.*, 2020, **10**, 7535–7542, DOI: 10.1021/acscatal.0c01515.
3. R. Franke, D. Selent and A. Börner, *Chem. Rev.*, 2012, **112**, 5675–5732, DOI: 10.1021/cr3001803.
4. D. Evans, J. A. Osborn and G. Wilkinson, *J. Chem. Soc. A*, 1968, 3133–3142, DOI: 10.1039/J19680003133.
5. M. Janssen, J. Wilting, C. Müller and D. Vogt, *Angew. Chem.*, 2010, **122**, 7904–7907, DOI: 10.1002/ange.201001926.
6. D. Guha, H. Jin, M. P. Dudukovic, P. A. Ramachandran and B. Subramaniam, *Chem. Eng. Sci.*, 2007, **62**, 4967–4975, DOI: 10.1016/j.ces.2006.12.029.
7. W. Alsalahi and A. M. Trzeciak, *J. Mol. Catal. A: Chem.*, 2015, **408**, 147–151, DOI: 10.1016/j.molcata.2015.07.021.
8. E. Piras, B. Powietzka, F. Wurst, D. Neumann-Walter, H. J. Grützmacher, T. Otto, T. Zevaco and O. Walter, *Catal. Lett.*, 2013, **143**, 673–680, DOI: 10.1007/s10562-013-1010-x.

9. L. A. Van Der Veen, M. D. K. Boele, F. R. Bregman, P. C. J. Kamer, P. W. N. M. Van Leeuwen, K. Goubitz, J. Fraanje, H. Schenk and C. Bo, *J. Am. Chem. Soc.*, 1998, **120**, 11616–11626, DOI: 10.1021/ja981969e.
10. J. Ternel, J. L. Dubois, J. L. Couturier, E. Monflier and J. F. Carpentier, *ChemCatChem*, 2013, **5**, 1562–1569, DOI: 10.1002/cctc.201200630.
11. M. T. Reetz, S. R. Waldvogel and R. Goddard, *Tetrahedron Lett.*, 1997, **38**, 5967–5970, DOI: 10.1016/S0040-4039(97)01345-2.
12. J. C. Bayón, C. Claver and A. M. Masdeu-Bultó, *Coord. Chem. Rev.*, 1999, **193**, 73–145, DOI: 10.1016/S0010-8545(99)00169-1.
13. P. Kalck, J. M. Frances, P. M. Pfister, T. G. Southern and A. Thorez, *J. Chem. Soc., Chem. Commun.*, 1983, 510–511, DOI: 10.1039/C39830000510.
14. N. Ruiz, A. Aaliti, J. Fornies-Camer, A. Ruiz, C. Claver, C. J. Cardin, D. Fabbri and S. Gladiali, *J. Organomet. Chem.*, 1997, **545**, 79–87, DOI: 10.1016/S0022-328X(97)00151-4.
15. C. Claver, S. Castellón, N. Ruiz, G. Delogu, D. Fabbri and S. Gladiali, *J. Chem. Soc., Chem. Commun.*, 1993, 1883–1884, DOI: 10.1039/C39930001833.
16. A. Castellanos-Páez, S. Castellón, C. Claver, P. W. N. M. Van Leeuwen and W. G. J. De Lange, *Organomet.*, 1998, **17**, 2543–2552, DOI: 10.1021/om971059q.
17. M. Rosales, A. González, Y. Guerrero, I. Pacheco and R. A. Sánchez-Delgado, *J. Mol. Catal. A: Chem*, 2007, **270**, 241–249, DOI: 10.1016/j.molcata.2007.01.044.
18. P. W. N. M. Van Leeuwen, *Appl. Catal. A-Gen.*, 2001, **212**, 61–81, DOI: 10.1016/S0926-860X(00)00844-9.
19. C. Fliedel, A. Ghisolfi and P. Braunstein, *Chem. Rev.*, 2016, **116**, 9237–9304, DOI: 10.1021/acs.chemrev.6b00153.
20. V. Gallo, P. Mastrolilli, C. F. Nobile, P. Braunstein and U. Englert, *Dalton Trans.*, 2006, 2342–2349, DOI: 10.1039/b514787e.
21. J. T. Mague, *Inorg. Chim. Acta*, 1995, **229**, 17–25, DOI: 10.1016/0020-1693(94)04221-G.
22. J. T. Mague and C. L. Lloyd, *Organometallics*, 1988, **7**, 983–993, DOI: 10.1021/om00094a031.
23. P. Dierkes and P. W. N. M. Van Leeuwen, *J. Chem. Soc., Dalton Trans.*, 1999, 1519–1530, DOI: 10.1039/A807799A.
24. AEROPERL 300/30 data sheet, <https://glenncorp.com/wp-content/uploads/2013/12/AEROPERL-300-30.pdf>, (accessed January 2024).
25. T. A. Zeelie, A. Root and A. O. I. Krause, *Appl. Catal. A: Gen.*, 2005, **285**, 96–109, DOI: 10.1016/j.apcata.2005.02.010.
26. L. Iu, J. A. Fuentes, M. E. Janka, K. J. Fontenot and M. L. Clarke, *Angew. Chem. Int. Ed.*, 2019, **58**, 2120–2124, DOI: 10.1002/ange.201811888.

27. A. Bara-Estaún, C. L. Lyall, J. P. Lowe, P. G. Pringle, P. C. J. Kamer, R. Franke and U. Hintermair, *ChemCatChem*, 2023, **15**, e2022012, DOI: 10.1002/cctc.202201204.
28. Z. K. Lopez-Castillo, R. Flores, I. Kani, J. P. Fackler and A. Akgerman, *Ind. Eng. Chem. Res.*, 2003, **42**, 3893–3899, DOI: 10.1021/ie030176k.
29. Y. Matsui, H. Taniguchi, K. Terada, T. Anezaki and M. Iriuchijima, *Bull. Jpn. Petrol Inst.*, 1977, **19**, 62–67, DOI: 10.1627/jpi1959.19.62.
30. J. Fang, PhD Thesis, University of Kansas, 2009.
31. F. G. Delolo, J. Yang, H. Neumann, E. N. Dos Santos, E. V. Gusevskaya and M. Beller, *ACS Sustain. Chem. Eng.*, 2021, **9**, 5148–5154, DOI: 10.1021/acssuschemeng.1c00205.
32. C. Fyhr and M. Garland, *Organometallics*, 1993, **12**, 1753–1764.
33. D. A. Sheppard and C. E. Buckley, *Int. J. Hydrogen Energy*, 2008, **33**, 1688–1692, DOI: 10.1016/j.ijhydene.2007.12.021.
34. C. Yeom and Y. Kim, *Korean J. Chem. Eng.*, 2018, **35**, 587–593, DOI: 10.1007/s11814-017-0309-5.
35. L. Huang, Y. Xu, G. Piao, A. Liu and W. Zhang, *Catal. Lett.*, 1994, **23**, 87–95, DOI: 10.1007/BF00812134.
36. A. J. Sandee, J. N. H. Reek, P. C. J. Kamer and P. W. N. M. Van Leeuwen, *J. Am. Chem. Soc.*, 2001, **123**, 8468–8476, DOI: 10.1021/ja010150p.
37. B. Stewart, A. Harriman and L. J. Higham, *Organometallics*, 2011, **30**, 5338–5343, DOI: 10.1021/om200070a.
38. L. Huang and S. Kawi, *Catal. Lett.*, 2004, **92**, 57–62, DOI: 10.1023/B:CATL.0000011087.58049.32.
39. W. Zhou and D. He, *Green Chem.*, 2009, **11**, 1146–1154, DOI: 10.1039/b900591a.
40. T. A. Fassbach, J. M. Ji, A. J. Vorholt and W. Leitner, *ACS Catal.*, 2024, **14**, 7289–7298, DOI: 10.1021/acscatal.4c01006.
41. J. B. Claridge, R. E. Douthwaite, M. L. H. Green, R. M. Lago, S. C. Tsang and A. P. E. York, *J. Mol. Catal.*, 1994, **89**, 113–120, DOI: 10.1016/0304-5102(93)E0328-E.
42. R. Tudor and M. Ashley, *Platinum Metals Rev.*, 2007, **51**, 116–126, DOI: 10.1595/147106707X216855.
43. R. Klaewkla, M. Arend and W. F. Hoelderich, in *Mass Transfer - Advanced Aspects*, ed. H. Nakajima, InTech, Rijeka, 2011, ch. 29, 667–684.
44. O. E. Brandt Corstius, M. Kikkert, S. T. Roberts, E. J. Dorskocil, J. E. S. van der Hoeven and P. E. de Jongh, *React. Chem. Eng.*, 2024, 1–13, DOI: 10.1039/d4re00039k.
45. R. Horn, *Modern Methods in Heterogeneous Catalysis - Measurement and Analysis of Kinetic Data*, Fritz-Haber-Institute of the MPG, Berlin, 2007.
46. Â. C. B. Neves, M. J. F. Calvete, T. M. V. D. Pinho E Melo and M. M. Pereira, *Eur. J. Org. Chem.*, 2012, **2012**, 6309–6320, DOI: 10.1002/ejoc.201200709.

47. M. Sigrist, Y. Zhang, C. Antheaume and P. Dydio, *Angew. Chem. Int. Ed.*, 2022, **61**, e202116406, DOI: 10.1002/anie.202116406.
48. RCC International: The storage, handling and processing of dangerous substances, <https://www.rrc.co.uk/media/667814/UNIT%20C%20SAMPLE%20MATERIAL.pdf>, (accessed June 2024).

Future work

Much of the work described in this thesis has focused on the design and synthesis of small bite-angle P[^]P ligands with varied steric and electronic properties for applications in immobilised hydroformylation. However, to broaden this focus further, additional investigations into wider bite angle ligands for immobilised hydroformylation could be performed. As the attempted synthesis of the PCCNCCP compound **L20** was unsuccessful, one modification that could be made to the structure of the compound to make synthesis easier is replacement of the alkoxysilane tethering group with a silatrane functionality to give compound **L25** (Figure F1). As was shown for the synthesis of phosphoramidite PNP and PCNCP compounds, incorporation of the more robust silatrane moiety resulted in better selectivity for the relevant target compounds by suppressing unwanted nucleophilic substitution reactions at the silicon atom, especially from alcohols or water. Incorporation of a silatrane tethering functionality still enables relatively facile silica-immobilisation of the compound, which required moderate reaction temperatures of *ca.* 70 °C, relative to room temperature immobilisation possible using alkoxysilane tethering functionalities. Synthesis of **L25** would allow the subsequent investigation into systematic change of P[^]P bite angle on immobilised hydroformylation by comparing ligand performance of **L25** to **L5** and **L17**.

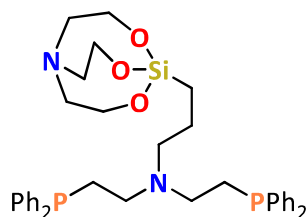


Figure F1. Structure of **L25**.

The synthesis of additional wide bite angle phosphites could also be performed to enable comparison to small bite-angle phosphoramidites **L11** and **L12**. One such ligand target is the compound **L26**, featuring an acacH-derived carbon backbone that could be functionalised with a pendant silatrane tethering group (Figure F2). A modular synthesis could be employed, enabling tuning of the sterics and electronics of the phosphorus centres by application of different parent alcohols in the synthesis of the phosphite moieties. By increasing the library of tetherable ligands for immobilised hydroformylation, more data can be gathered on the key ligand structural features that effect catalyst performance. This knowledge can then be applied during the development of new hydroformylation catalyst processes, enabling precise tuning of the system to maximise catalyst performance in terms of activity, selectivity and stability.

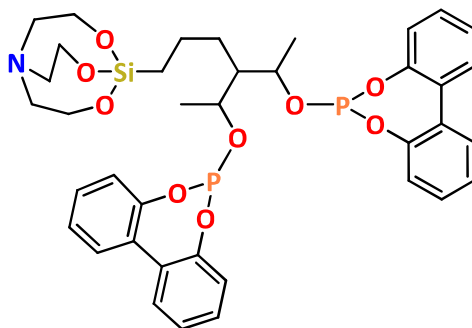


Figure F2. Structure of **L26**.

Further catalyst testing is also of great interest to gain additional insight into the performance of the catalysts previously developed. Of particular importance would be to investigate the immobilised catalysts developed in this work in a fixed bed reactor setup for the hydroformylation of propene, to mimic how these catalysts would likely be used in an industrial setting. More in depth catalyst recycling and leaching studies would also be beneficial, which could be combined with post-reaction characterisation of the catalysts, by solid-state NMR spectroscopic analysis, for example, to further elucidate the behaviour of the catalyst and identify possible catalyst decomposition pathways. This would also require development of an improved method for reaction sampling and catalyst separation during recycling studies to mitigate the catalyst loss of these processes in the test autoclave system employed.

This work could be complemented by further studies investigating the effect of the catalyst immobilisation conditions on subsequent catalysts performance, particularly in regard to catalyst stability. Developing a greater understanding of whether the catalyst is immobilised on the external silica surface or within the silica pore structure would result in significantly better understanding of these catalyst systems. Additionally, better understanding of catalyst structure may also help elucidate the effect the origin of the differing lengths of catalyst induction period of catalysts $[\text{Rh}(\text{L5})_2]\text{BF}_4$ and $[\text{Rh}(\text{L17})_2]\text{BF}_4$ when in solution or silica-immobilised.

A complete study of the $\text{PdI}_2(\text{P}^\wedge\text{P})$ complexes described in the work as hydroformylation catalysts is also desired, including further optimisation of the reaction conditions and catalyst to maximise activity for hydroformylation. Synthesis and catalyst testing of silica-immobilised $\text{PdI}_2(\text{P}^\wedge\text{P})$ complexes could then be investigated and their catalytic performance compared to the rhodium catalysts described in this work, to determine the overall most effective catalyst.

Chapter 6: Experimental

6.1 General considerations

Unless otherwise stated, all reactions were conducted under an atmosphere of dry nitrogen or argon using standard Schlenk-line and glove box (Saffron Scientific and InertTechnologies) techniques. Air- and moisture-sensitive NMR-scale reactions were conducted in NMR tubes fitted with Youngs' taps. All solvents excluding THF and PhCl were dried using an Innovative Technologies Solvent Purification System facility. THF was dried by heating at reflux over sodium wire with benzophenone as indicator, followed by distillation. PhCl was dried over P₂O₅ and distilled. 1-Octene, d₈-THF, C₆D₆ and CD₂Cl₂ were dried over CaH₂ and vacuum transferred. All solvents and liquid reagents were deoxygenated using the freeze-pump-thaw method prior to use. NEt₃ was dried with 3Å molecular sieves and distilled. Ph₂PCl was purified by vacuum transfer. Ultrapure type I water was used for all reactions involving water. Fibrecat™, Rh(acac)(CO)₂ and RhCl₃ were provided by Johnson Matthey and used as received. PdCl₂(COD) and PdCl₂(MeCN)₂ were prepared from PdCl₂ provided by Johnson Matthey.¹ BISBI was obtained from Strem Chemicals and used as received. All other reagents were used as received from Sigma-aldrich, Fisher Scientific or Fluorochem.

Solution phase NMR spectra were collected on a Bruker Avance 400 spectrometer at ambient temperatures (293 K) operating at 399.95, 100.58, 161.91, 128.32 and 376.27 MHz for ¹H, ¹³C, ³¹P, ¹¹B and ¹⁹F respectively. Chemical shifts were referenced to residual *protio* impurities in the deuterated solvent (¹H), ¹³C shift of the solvent (¹³C{¹H}) or to external 85% H₃PO₄ aqueous solution (³¹P, ³¹P{¹H}), external CFCl₃ (¹⁹F) or external BF₃·Et₂O (¹¹B). Chemical shifts are reported in ppm and coupling constants in Hz. Solvent residual proton shifts used are: CDCl₃ 7.26 (s); C₆D₆, 7.15 (s); (CD₃)₂CO, 2.05 (s) and CD₂Cl₂, 5.35 (s).² Solvent residual carbon shifts employed: CDCl₃, 77.0 (t); C₆D₆, 128.0 (t); (CD₃)₂CO, 206.2 (s), 29.8 (sept) and CD₂Cl₂, 53.0 (quin).¹¹⁸ Solid-state NMR spectra were obtained on a Varian VNMRS spectrometer using a 6 mm (o.d.) rotor or a Bruker Avance III HD spectrometer using a 4 mm (o.d.) probe at 79.44 MHz and 161.99 MHz for ²⁹Si and ³¹P respectively. Chemical shifts are reported in ppm relative to external tetrakis(trimethylsilyl)silane at -9.9 ppm for silicon spectra and relative to external 85 % H₃PO₄ at 0 ppm for phosphorus spectra. Cross polarisation spectra were recorded with

a 10 ms contact time and recycle delay of 1 s for ^{29}Si nuclei and a contact time of 1 ms and recycle delay of 5 s for ^{31}P nuclei.

Infrared spectra were collected on a FT-IR Perkin-Elmer Spectrum RXI with an ATR attachment. Approximately 2 mg of sample was placed on the crystal and secured with the screw down arm before measurements were performed.

Crystallographic data were obtained in Durham using a Bruker D8Venture_Mo Diffractometer with confocal optics Mo-K α (λ 0.71073 Å) at -180(1) °C. All calculations were performed using the Olex2 software package except for refinement, which was performed using SHELXL. All structures were collected and solved by Dr Andrei Batsanov, Dr Dmitry Yufit or Dr Toby Blundell (Durham Chemistry Department). Steric maps were generated and %V_{bur} calculated using the web software SambVca 2.1.³

CHN Elemental analysis was performed by Dr Emily Unsworth of Durham University using an Exeter CE-440 Elemental Analyser using a horizontal furnace, with static combustion in pure oxygen. The instrument was calibrated with acetanilide before each batch of samples. Please note that CHN elemental analysis could not be performed on any of the viscous oils produced in this work.

Gas chromatography was performed using an HP 5890-II GC-FID instrument equipped with a HP-PONA column (50 m length, 0.2 mm i.d., 0.5 μm film thickness). Experiments were performed at 45 °C with the temperature held constant for 5 mins, followed by an increase to 60 °C at a ramp rate of 5 °C min⁻¹. The temperature was held at 60 °C for 6 mins then increased to 150 °C at a ramp rate of 5 °C min⁻¹, then further increased to 300 °C at a ramp rate of 30 °C min⁻¹.

ICP-OES analyses of supported catalysts was performed at Johnson Matthey TC, Sonning by Aikaterini Droungou. For silica-supported catalysts, samples were prepared in duplicate. ~0.05 g of the sample was weighed on Zr crucible and was fused with ~3 g of sodium peroxide (obtained from Fisher Scientific). The fusion system used was Fluxana Vitriox. The melt was leached in 15 cm³ conc. HCl (obtained from Fisher Scientific) in UHP water, and the leachates were transferred to 100 cm³ vol. flasks and made to volume with UHP water. A range of Rh standards was prepared (1, 5, and 15 ppm) and matrix matched (15% HCl in UHP water plus 3 g sodium peroxide which has

also been through the fusion machine), and an aliquot of each sample replicate was analysed by ICP-OES (Agilent 5110), in radial viewing mode. Yttrium was used as internal standard.

For the Fibrecat supported sample; the sample was prepared in triplicate. ~0.05 g of the sample was weighed in a digestion tube and 10 cm³ inverse aqua regia (IAR, 7.5 ml HNO₃, 2.5 cm³ HCl; both acids obtained from Fisher Scientific) was added. The tubes were placed in the Ultrawave Reactor (Milestone Ultrawave ECR Microwave High Pressure Reactor) for ~50 min and full digestion was accomplished. The digests were transferred to 100 cm³ vol. flasks and made to volume with UHP water. A range of Rh standards was prepared (5, 15, and 25 ppm) and matrix matched (10% IAR in UHP water), and an aliquot of each sample replicate was analysed by ICP-OES (Agilent 5800), in radial viewing mode. Yttrium was used as internal standard.

ICP experiments to determine catalyst leaching were performed at Durham University by Dr Emily Unsworth. Samples preparation was as follows: hydroformylation reaction solution was collected after 1 h and filtered through a glass wool plug to remove any silica. 20 cm³ of solution was added to a Schlenk flask that had been washed out three times with distilled water prior to use. All volatile components were then removed *in vacuo*, followed by addition of 5 ml of 10 % HCl and heating to 80 °C for 1 h to ensure full digestion of the metal. The contents of the Schlenk flask were washed into volumetric flasks (pre-washed three times with HCl and three times with distilled water) and the solutions made up to the mark with distilled water and the prepared solutions were submitted to the ICP-OES service for analysis. The instrument used for ICP-OES analysis was a Agilent 5800 VDV equipped with a vertical torch, cyclonic spray chamber and concentric nebulizer. The instrument was used in axial mode and the standards were prepared by diluting a commercially available (Aldrich) 1000ppm rhodium stock standard solution.

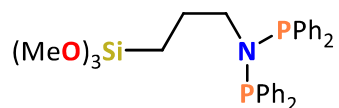
6.2 Chapter 2 experimental

6.2.1 Synthesis of PNP-type ligands

6.2.1.1 General procedure for the synthesis of dppa-type compounds L1-5

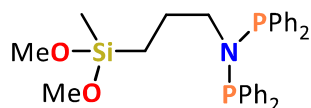
The appropriate primary amine (1 eq., ~10 mmol) and NEt_3 (2.1 - 5 eq.) were dissolved in toluene or THF (40 cm^3). The solution was cooled to -40 or -78 $^\circ\text{C}$ and Ph_2PCl (2 eq.) added dropwise. The solution was allowed to warm to room temperature and then stirred overnight, producing a white solid and pale-yellow solution. The mixture was filtered and the solid washed with toluene (3×5 cm^3). The combined washings were then dried *in vacuo* to give the desired product, which was then stored in the glovebox.

6.2.1.1.1 Synthesis of L1



Obtained as a pale yellow viscous oil (2.01 g, 62%); ^1H NMR (400 MHz, CD_2Cl_2) 0.20 – 0.28 (2H, m, SiCH_2), 1.14 – 1.26 (2H, m, $\text{CH}_2\text{CH}_2\text{CH}_2$), 3.20 – 3.33 (2H, m, CH_2N), 3.40 (9H, s, $\text{Si}(\text{OCH}_3)_3$), 7.31 – 7.41 (12H, m, phenyl), 7.41 – 7.50 (8H, m, phenyl); $^{31}\text{P}\{^1\text{H}\}$ NMR (162 MHz, CD_2Cl_2) δ : +62; $^{13}\text{C}\{^1\text{H}\}$ NMR (101 MHz, CD_2Cl_2), 6.04 (s, SiCH_2), 24.38 (s, $\text{CH}_2\text{CH}_2\text{CH}_2$), 50.17 (s, $\text{Si}(\text{OCH}_3)_3$), 55.82 (t, $^2J_{\text{PC}} = 10.5$ Hz, CH_2N), 128.07 (t, $^3J_{\text{PC}} = 3.1$ Hz, aryl-C), 128.74 (s, aryl-C), 132.70 (t, $^2J_{\text{PC}} = 11.0$ Hz, aryl-C), 139.78 (t, $^1J_{\text{PC}} = 6.3$ Hz, aryl-C). NMR spectroscopic analysis showed good agreement with reported literature values.⁴

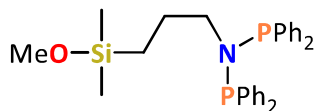
6.2.1.1.2 Synthesis of L2



Obtained as a colourless oil (3.3 g, 65%); ^1H NMR (400 MHz, CD_2Cl_2) -0.10 (3H, s, SiCH_3), 0.19 – 0.26 (2H, m, SiCH_2), 1.09 – 1.21 (2H, m, $\text{CH}_2\text{CH}_2\text{CH}_2$), 3.23 – 3.45 (2H, m, CH_2N),

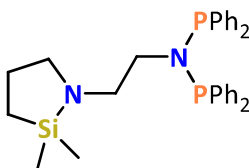
3.37 (6H, s, OCH₃), 7.36 – 7.41 (12H, m, phenyl), 7.43 – 7.49 (8H, m, phenyl); ³¹P{¹H} NMR (162 MHz, CD₂Cl₂) δ: +62; ¹³C{¹H} NMR (101 MHz, CD₂Cl₂) –6.20 (s, SiCH₃), 9.90 (s, SiCH₂), 24.56 (t, ³J_{PC} = 3.2 Hz, CH₂CH₂CH₂), 49.84 (s, OCH₃), 56.04 (t, ²J_{PC} = 10.6 Hz, CH₂N), 128.07 (t, ³J_{PC} = 3.1 Hz, aryl-C), 128.75 (s, aryl-C), 132.71 (t, ²J_{PC} = 10.9 Hz, aryl-C), 139.81 (t, ¹J_{PC} = 6.3 Hz, aryl-C).

6.2.1.1.3 Synthesis of L3



Obtained as a colourless oil (2.4 g, 69%); ¹H NMR (400 MHz, CD₂Cl₂) –0.10 (6H, s, SiCH₃), 0.15 – 0.21 (2H, m, SiCH₂), 1.03 – 1.14 (2H, m, CH₂CH₂CH₂), 3.22 – 3.32 (2H, m, CH₂N), 3.26 (3H, s, OCH₃), 7.34 – 7.40 (12H, m, phenyl), 7.42 – 7.48 (8H, m, phenyl); ³¹P{¹H} NMR (162 MHz, CD₂Cl₂) δ: +62; ¹³C{¹H} NMR (101 MHz, CD₂Cl₂) –3.13 (s, SiCH₃), 12.69 (s, SiCH₂), 25.09 (t, ³J_{PC} = 3.2 Hz, CH₂CH₂CH₂), 49.91 (s, OCH₃), 56.23 (t, ²J_{PC} = 10.5 Hz, CH₂N), 128.05 (t, ³J_{PC} = 3.1 Hz, aryl-C), 128.73 (s, aryl-C), 132.69 (t, ²J_{PC} = 11.0 Hz, aryl-C), 139.84 (t, ¹J_{PC} = 6.4 Hz, aryl-C).

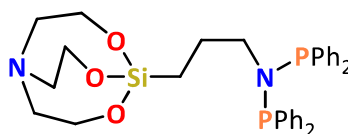
6.2.1.1.4 Synthesis of L4



Obtained as a colourless oil (2.2 g, 43%); ¹H NMR (400 MHz, CD₂Cl₂) –0.12 (3H, s, SiCH₃), –0.09 (3H, s, SiCH₃), 0.05 – 0.25 (2H, m, SiCH₂), 0.96 (3H, d, ³J_{HH} = 6.5 Hz, CHCH₃), 1.89 – 1.97 (1H, m, CHCH₃), 2.18 (1H, t, ²J_{HH} = 8.9 Hz, CHCH(H)N), 2.35 – 2.42 (2H, m, CH₂CH₂N), 2.58 (1H, dd, ²J_{HH} = 8.9 Hz, ³J_{HH} = 6.2 Hz, CHCH(H)N), 3.24 – 3.35 (2H, m, CH₂CH₂N), 7.35 – 7.41 (12H, m, phenyl), 7.43 – 7.50 (8H, m, phenyl); ³¹P{¹H} NMR (162 MHz, CD₂Cl₂) δ: +63; ¹³C{¹H} NMR (101 MHz, CD₂Cl₂) –0.95 (s, SiCH₃), –0.09 (s, SiCH₃), 21.30 (s, CHCH₃), 21.63 (s, CHCH₃), 32.12 (s, SiCH₂), 48.18 (t, ²J_{PC} = 3.2 Hz, CH₂N(PPh₂)₂), 52.19 (t, ³J_{PC} = 9.4

Hz, SiNCH₂CH₂), 128.11 (q, ²J_{PC} = 3.42 Hz, aryl-C), 128.73 (s, aryl-C), 128.77 (s, aryl-C), 132.67 (t, ²J_{PC} = 11.1 Hz, aryl-C), 132.74 (t, ³J_{PC} = 11.0 Hz, aryl-C), 139.70 (t, ¹J_{PC} = 10.5 Hz, aryl-C), 139.71 (t, ¹J_{PC} = 10.4 Hz, aryl-C).

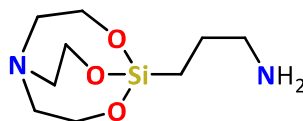
6.2.1.1.5 Synthesis of L5



Isolated as a white solid that was recrystallized from DCM/hexane and dried *in vacuo* (2.6 g, 64%). Single crystals suitable for XRD analysis were obtained by layering a solution of the compound in DCM with hexane at -20 °C; ν_{\max} /cm⁻¹ 3051 (C-H aromatic), 2944 (C-H), 2840 (C-H), 1584 (C=C), 1566 (C=C), 1432 (P-Ph), 908 (P-N); ¹H NMR (400 MHz, CDCl₃) 0.06 – 0.12 (2H, m, SiCH₂), 1.39 – 1.49 (2H, m, CH₂CH₂CH₂), 2.70 (6H, t, ³J_{HH} = 5.8 Hz, OCH₂CH₂N), 3.15 – 3.26 (2H, m, CH₂N(PPh₂)₂), 3.61 (6H, t, ³J_{HH} = 5.8 Hz, OCH₂CH₂N), 7.23 – 7.29 (12H, m, phenyl), 7.35 – 7.41 (8H, m, phenyl); ³¹P{¹H} NMR (162 MHz, CDCl₃) δ : +61; ¹³C{¹H} NMR (101 MHz, CDCl₃) 12.70 (s, SiCH₂), 26.29 (t, ³J_{PC} = 4.2 Hz, CH₂CH₂CH₂), 51.13 (s, OCH₂CH₂N), 56.10 (t, ²J_{PC} = 10.0 Hz, CH₂N(PPh₂)₂), 57.71 (s, OCH₂CH₂N), 127.85 (t, ³J_{PC} = 3.0 Hz, aryl-C), 128.33 (s, aryl-C), 132.82 (t, ³J_{PC} = 11.1 Hz, aryl-C), 140.16 (d, ¹J_{PC} = 12.9 Hz, aryl-C). Anal. Calcd for C₃₃H₃₈N₂O₃P₂Si·0.67CH₂Cl₂: C, 61.56; H, 6.04; N, 4.26. Found: C, 61.86; H, 5.58; N, 4.39 %.

Single crystals of O(Ph₂PO)₂ suitable for XRD analysis were obtained from a solution of L5 in DCM layered with hexane left to stand in air.

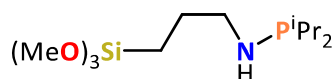
6.2.1.2 Synthesis of (3-aminopropyl)silatrane



Triethanolamine (6 cm³, 0.05 mol), (3-aminopropyl)trimethoxysilane (8 cm³, 0.05 mol) and KOH (0.05 g, 0.9 mmol) were dissolved in toluene (30 cm³) and heated to 80 °C for

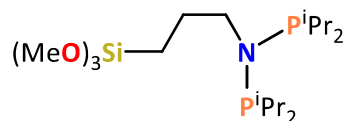
4 h. Methanol produced was removed as it formed using Dean-Stark apparatus. The crude product was dried *in vacuo* then recrystallized from toluene, then chloroform and dried *in vacuo* to give a white solid (5.6 g, 52%); $\nu_{\max}/\text{cm}^{-1}$ 3355 (N-H), 2922 (C-H), 2858 (C-H); ^1H NMR (400 MHz, CDCl_3) δ : 0.38 – 0.46 (2H, m, SiCH_2), 1.23 (2H, s, br, NH_2), 1.49 – 1.58 (2H, m, $\text{CH}_2\text{CH}_2\text{CH}_2$), 2.64 (2H, t, $^3J_{\text{HH}} = 7.0$ Hz, CH_2NH_2), 2.82 (6H, t, $^3J_{\text{HH}} = 5.8$ Hz, $\text{OCH}_2\text{CH}_2\text{N}$), 3.78 (6H, t, $^3J_{\text{HH}} = 5.8$ Hz, $\text{OCH}_2\text{CH}_2\text{N}$); $^{13}\text{C}\{^1\text{H}\}$ NMR (101 MHz, CDCl_3) δ : 12.99 (s, SiCH_2), 29.88 (s, $\text{CH}_2\text{CH}_2\text{CH}_2$), 45.79 (s, CH_2NH_2), 51.12 (s, $\text{OCH}_2\text{CH}_2\text{N}$), 57.82 (s, $\text{OCH}_2\text{CH}_2\text{N}$). Anal. Calcd for $\text{C}_9\text{H}_{20}\text{N}_2\text{O}_3\text{Si}$: C, 46.52; H, 8.68; N, 12.06. Found: C, 46.32; H, 8.24; N, 12.08 %. CHN elemental analysis and NMR spectroscopic analysis are in good agreement with reported literature values.⁵

6.2.1.3 Attempted synthesis of L6 – synthesis of L6X



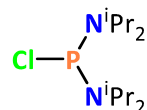
(3-Aminopropyl)trimethoxysilane (2.0 cm^3 , 11.5 mmol) and NEt_3 (4.0 cm^3 , 28 mmol) were dissolved in THF (30 cm^3). The solution was cooled to -40°C and $i\text{Pr}_2\text{PCL}$ (3.7 cm^3 , 23 mmol) added dropwise. The solution was allowed to warm to room temperature and then stirred for 18 h, after which time ^{31}P NMR spectroscopy of an aliquot of reaction mixture showed only one equivalent of $i\text{Pr}_2\text{PCL}$ had reacted. A second equivalent (3-aminopropyl)trimethoxysilane (2.0 cm^3 , 11.5 mmol) was added to the reaction mixture at -40°C and stirred overnight at room temperature, after which the solution was filtered and the resulting solid residue washed with THF ($3 \times 5 \text{ cm}^3$). The combined washing were dried *in vacuo* to give a colourless oil (5.17 g, 76%); ^1H NMR (400 MHz, C_6D_6) 0.63 – 0.69 (2H, m, SiCH_2), 0.96 – 1.07 (12H, m, $\text{CH}(\text{CH}_3)_2$), 1.44 (2H, septet of doublets, $^3J_{\text{HH}} = 7.1$ Hz, $^2J_{\text{PH}} = 1.1$ Hz, $\text{PCH}(\text{CH}_3)_2$), 1.58 – 1.68 (2H, m, $\text{CH}_2\text{CH}_2\text{CH}_2$) 2.85 – 2.95 (2H, m, CH_2N) 3.44 (9H, s, $\text{Si}(\text{OCH}_3)_3$); $^{31}\text{P}\{^1\text{H}\}$ NMR (162 MHz, CDCl_3) δ : +64; $^{13}\text{C}\{^1\text{H}\}$ NMR (101 MHz, C_6D_6), 6.13 (s, SiCH_2), 17.20 (d, $^2J_{\text{PC}} = 7.7$ Hz, $\text{PCH}(\text{CH}_3)_2$), 19.03 (d, $^3J_{\text{PC}} = 20.1$ Hz, $\text{CH}_2\text{CH}_2\text{CH}_2$), 26.48 (d, $^3J_{\text{PC}} = 18.5$ Hz, $\text{PCH}(\text{CH}_3)_2$), 50.42 (s, $\text{Si}(\text{OCH}_3)_3$), 51.45 (d, $^2J_{\text{PC}} = 22.7$ Hz, CH_2N).

6.2.1.4 Second attempted synthesis of L6



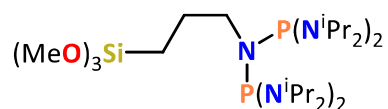
(3-Aminopropyl)trimethoxysilane (2.0 cm³, 11.5 mmol) and NEt₃ (4.0 cm³, 28.0 mmol) were dissolved in DCM (30 cm³). The solution was cooled to -40 °C and ⁱPr₂PCl (3.7 cm³, 23 mmol) added dropwise. The solution was allowed to warm to room temperature and then stirred for 18 h, after which time ³¹P NMR spectroscopy of an aliquot of reaction mixture showed a mixture of the monosubstituted product **L6X** and an iminobisphosphine side product, so the reaction was abandoned.

6.2.1.5 Synthesis of bis(diisopropylamino)chlorophosphine



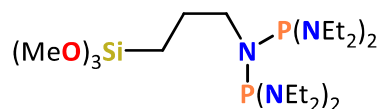
PCl₃ (7.0 cm³, 80 mmol) was dissolved in toluene (50 cm³) and cooled to 0 °C, followed by slow addition of HNⁱPr₂ (45.0 cm³, 320 mmol) through a pressure equalising dropping funnel. Toluene (25 cm³) was then washed through the dropping funnel. The reaction was heated at reflux overnight to give an orange solution and white precipitate. The solution was filtered and the solid washed with toluene (25 cm³). The combined filtrate and washings were dried *in vacuo*, leaving an orange solid. Upon washing with MeCN (4 × 20 cm³) the product was isolated as a white solid (12.23 g, 57%); ¹H NMR (400 MHz, CD₂Cl₂) δ: 1.23 (6H, d, ³J_{HH} = 6.9 Hz, CH(CH₃)₂), 1.29 (6H, d, ³J_{HH} = 6.8 Hz, CH(CH₃)₂), 3.65 – 3.79 (2H, m, NCH(CH₃)₂); ³¹P{¹H} NMR (162 MHz, CD₂Cl₂) δ: +141; ¹³C{¹H} NMR (101 MHz, CD₂Cl₂), 22.67 (d, ³J_{PC} = 11.8 Hz, CH₃), 23.74 (d, ³J_{PC} = 5.52 Hz, PCH₂), 47.45 (d, ²J_{PC} = 13.0 Hz, NCH(CH₃)₂); Anal. Calcd for C₁₂H₂₈ClN₂P: C, 54.02; H, 10.58; N, 10.50. Found: C, 53.97; H, 10.75; N, 10.73 %. NMR spectroscopic analysis and CHN elemental analysis are in good agreement with reported literature values.⁶

6.2.1.6 Attempted synthesis of L7



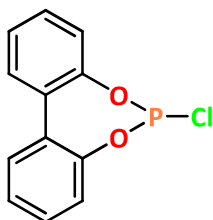
(3-Aminopropyl)trimethoxysilane (0.2 cm³, 1.2 mmol) and NEt₃ (0.34 cm³, 2.4 mmol) were dissolved in toluene (20 cm³). The solution was cooled to −40 °C and (iPr₂N)₂PCl (0.625 g, 2.3 mmol) added dropwise. The solution was allowed to warm to room temperature and then stirred for 18 h, after which time ³¹P NMR spectroscopic analysis showed that no reaction had occurred. The reaction mixture was then heated at reflux for 2 hours, still resulting in no reaction by ³¹P NMR spectroscopic analysis, so the experiment was abandoned.

6.2.1.7 Attempted synthesis of L8



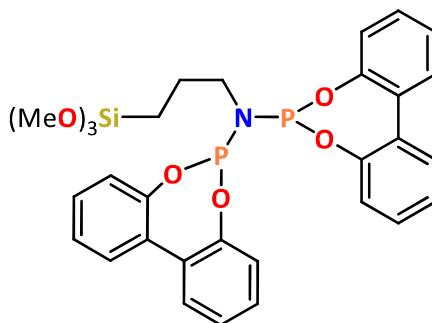
(3-Aminopropyl)trimethoxysilane (2.0 cm³, 11.5 mmol) and NEt₃ (3.5 cm³, 25.1 mmol) were dissolved in DCM (40 cm³). The solution was cooled to −40 °C and (Et₂N)₂PCl (4.8 cm³, 22.9 mmol) added dropwise. The solution was allowed to warm to room temperature and then stirred for 18 h, after which time ³¹P NMR spectroscopic analysis showed no reaction had occurred. The reaction mixture was then heated at reflux for 2 hours, resulting in decomposition of the start material by ³¹P NMR spectroscopy, hence the reaction was abandoned.

6.2.1.8 Synthesis of 2,2'-biphenol phosphochloridite



2,2-Biphenol (10.05 g, 53 mmol) was azeotropically dried with toluene ($3 \times 5 \text{ cm}^3$), then dissolved in toluene (40 cm^3). Following addition of PCl_3 (10.0 cm^3 , 100 mmol) and NEt_3 (5.5 cm^3 , 50 mmol), the solution was heated at reflux for 2 hours. Once cooled to room temperature, the resulting mixture was filtered and the solid washed with toluene ($3 \times 5 \text{ cm}^3$). The combined washings were then dried *in vacuo* and the crude product purified by removal of an impurity by sublimation to give a white solid (10.14 g, 75%); ^1H NMR (400 MHz, CDCl_3) 7.24 – 7.29 (2H, m, aryl), 7.35 – 7.48 (4H, m, aryl) 7.50 – 7.56 (2H, m, aryl); $^{31}\text{P}\{^1\text{H}\}$ NMR (162 MHz, CD_2Cl_2) δ : +179; $^{13}\text{C}\{^1\text{H}\}$ NMR (101 MHz, CD_2Cl_2), 122.23 (d, $^3J_{\text{PC}} = 2.2 \text{ Hz}$, aryl-C), 126.30 (d, $^4J_{\text{PC}} = 1.1 \text{ Hz}$, aryl-C), 129.50 (s, aryl-C), 130.21 (d, $^4J_{\text{PC}} = 1.5 \text{ Hz}$, aryl-C), 130.95 (d, $^3J_{\text{PC}} = 3.6 \text{ Hz}$, aryl-C), 149.25 (d, $^2J_{\text{PC}} = 5.6 \text{ Hz}$, aryl-C); Anal. Calcd for $\text{C}_{12}\text{H}_8\text{O}_2\text{ClP}$: C, 57.51; H, 3.22; N, 0.00. Found: C, 57.61; H, 3.32; N, 0.10 %. CHN elemental analysis and NMR spectroscopic analysis are in good agreement with reported literature values.⁷

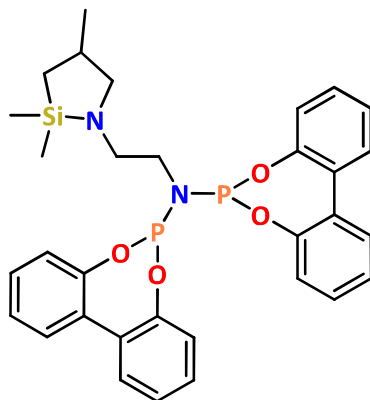
6.2.1.9 Synthesis of L9



(3-Aminopropyl)trimethoxysilane (0.9 cm^3 , 4.9 mmol) and NEt_3 (1.5 cm^3 , 11.0 mmol) were dissolved in toluene (40 cm^3). The solution was cooled to -40°C and 2,2'-biphenol phosphochloridite (2.47 g, 9.8 mmol) added dropwise. The solution was allowed to warm to room temperature and then stirred for 18 h, producing a white solid and pale-yellow solution. The solution was filtered and the resulting solid washed with toluene ($3 \times 5 \text{ cm}^3$) and the combined washings dried *in vacuo* to give a pale-yellow viscous oil. The oil was dissolved in DCM (5 cm^3) and upon addition of hexane (5 cm^3) with vigorous stirring, a white solid precipitated which was dried *in vacuo* to give a white solid (2.2 g, 73%). Single crystals suitable for XRD analysis were obtained by layering a solution of

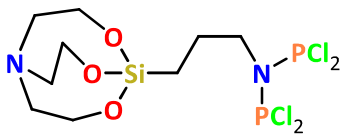
the compound in DCM with hexane; ν_{\max} /cm⁻¹ 3061 (C-H aromatic), 2943 (C-H), 2840 (Si-OMe), 1602 (C=C), 1567 (C=C), 1046 (P-O), 913 (P-N); ¹H NMR (400 MHz, CDCl₃) 0.64 – 0.71 (2H, m, SiCH₂), 1.58 – 1.68 (2H, m, CH₂CH₂CH₂), 2.99 – 3.13 (2H, m, CH₂N), 3.61 (9H, s, Si(OCH₃)₃), 7.20 – 7.35 (8H, m, aryl), 7.42 – 7.57 (8H, m, aryl); ³¹P{¹H} NMR (162 MHz, CD₂Cl₂) δ : +152; ¹³C{¹H} NMR (101 MHz, CD₂Cl₂) 8.42 (s, SiCH₂), 28.03 (s, CH₂CH₂CH₂), 48.35 (t, ²J_{PC} = 9.2 Hz, CH₂N), 52.08 (s, Si(OCH₃)₃), 123.94 (s, aryl-C), 127.02 (s, aryl-C), 131.34 (s, aryl-C), 131.89 (s, aryl-C) 132.75 (s aryl-C), 152.77 (t, ²J_{PC} = 2.3 Hz, aryl-C); Anal. Calcd for C₃₀H₃₁NO₇P₂Si: C, 59.30; H, 5.14; N, 2.31. Found: C, 58.08; H, 5.29; N, 2.61 %.

6.2.1.10 Attempted synthesis of L10



2-(2,2,4-Trimethyl-1,2-azasilolidin-1-yl)ethan-1-amine (1.95 cm³, 5.0 mmol) and NEt₃ (1.4 cm³, 10 mmol) are dissolved in toluene (30 cm³) and cooled to –78 °C, followed by dropwise addition of 2,2'-biphenolphosphochloridite (2.5 g, 10 mmol). The resulting mixture was allowed to warm to room temperature and stirred overnight, after which an aliquot of reaction mixture was analysed by ³¹P NMR spectroscopy and showed complete conversion of the starting material. After filtration and subsequent removal of all volatile components *in vacuo*, ³¹P NMR spectroscopy indicated decomposition of the target compound and the reaction was abandoned; ³¹P{¹H} NMR (162 MHz, C₆D₆) δ : +153.

6.2.1.11 Synthesis of Bis(dichlorophosphino)amino-3-propylsilatrane

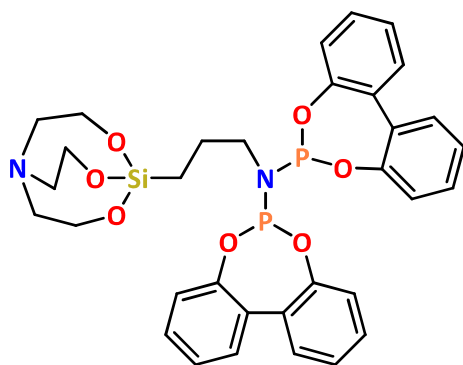


(3-Aminopropyl)silatrane (0.85 g, 3.7 mmol) and NEt_3 (2.0 cm^3 , 15 mmol) were dissolved in toluene (10 cm^3) and the solution added dropwise to a solution of PCl_3 (0.32 cm^3 , 3.7 mmol) in toluene (15 cm^3) at -78°C . The resulting mixture was allowed to warm to room temperature and stirred overnight. Following filtration, the resulting solution was dried *in vacuo*, then DCM (5 cm^3) and hexane (10 cm^3) added to give a colourless solution and red oil. The colourless solution was filtered and dried *in vacuo* to give a white solid (0.6 g, 37%); ^1H NMR (400 MHz, CDCl_3) 0.46 (2H, t, $^3J_{\text{HH}} = 8.0$ Hz SiCH_2), 1.95 – 2.06 (2H, m, $\text{CH}_2\text{CH}_2\text{CH}_2$), 2.84 (6H, t, $^3J_{\text{HH}} = 5.8$ Hz, $\text{OCH}_2\text{CH}_2\text{N}$), 3.72 – 3.83 (8H, m, $\text{CH}_2\text{CH}_2\text{CH}_2\text{N} + \text{OCH}_2\text{CH}_2\text{N}$); $^{31}\text{P}\{^1\text{H}\}$ NMR (162 MHz, CDCl_3) +166; $^{13}\text{C}\{^1\text{H}\}$ NMR (101 MHz, CDCl_3) 13.55 (s, SiCH_3), 27.52 (t, $^3J_{\text{PC}} = 3.1$ Hz, $\text{CH}_2\text{CH}_2\text{CH}_2$), 51.05 (s, $\text{OCH}_2\text{CH}_2\text{N}$), 51.78 (t, $^2J_{\text{PC}} = 7.1$ Hz, $\text{CH}_2\text{CH}_2\text{CH}_2\text{N}$), 57.66 (s, $\text{OCH}_2\text{CH}_2\text{N}$).

6.2.1.12 General procedure for the synthesis of compounds L11 and L12

2,2-Biphenol or (S)-1,1'-Bi-2-naphthol (1 eq., 5.4 mmol) and NEt_3 (2.7 cm^3 , 19 mmol) were dissolved in toluene (30 cm^3) and cooled to -78°C , followed by dropwise addition of a solution of bis(dichlorophosphino)amino-3-propylsilatrane (1 eq., 2.8 mmol) in toluene (10 cm^3). The resulting mixture was allowed to warm up to room temperature and stirred overnight. Upon filtering, the resulting solution was dried *in vacuo*. The crude product was then recrystallised from DCM / hexane (5 cm^3 / 10 cm^3) and dried *in vacuo* to give a white solid.

6.2.1.12.1 Synthesis of L11



Isolated as a white solid (0.45 g, 25%); single crystals suitable for XRD analysis were obtained by layering a solution of the compound in CDCl_3 with hexane (Figure 6.1); $\nu_{\text{max}}/\text{cm}^{-1}$ 2982 (C-H), 2874 (C-H), 1603 (C=C), 1581 (C=C), 1051 (P-O), 910 (P-N); ^1H NMR (400 MHz, CDCl_3) $-0.01 - 0.06$ (2H, m, SiCH_2), $1.71 - 1.83$ (2H, m, $\text{CH}_2\text{CH}_2\text{CH}_2$), 2.74 (6H, t, $^3J_{\text{HH}} = 5.7$ Hz, $\text{OCH}_2\text{CH}_2\text{N}$), $2.96 - 3.09$ (2H, m, $\text{CH}_2\text{CH}_2\text{CH}_2\text{N}$), 3.68 (6H, t, $^3J_{\text{HH}} = 5.7$ Hz, $\text{OCH}_2\text{CH}_2\text{N}$), $7.22 - 7.32$ (12H, m, aryl), $7.35 - 7.41$ (4H, m, aryl), 7.45 (4H, dd, $^3J_{\text{HH}} = 7.7$ Hz, $^4J_{\text{HH}} = 1.6$ Hz, aryl); $^{31}\text{P}\{^1\text{H}\}$ NMR (162 MHz, CDCl_3) $+151$; $^{13}\text{C}\{^1\text{H}\}$ NMR (101 MHz, CDCl_3) 13.49 (s, SiCH_3), 28.78 (t, $^3J_{\text{PC}} = 3.3$ Hz, $\text{CH}_2\text{CH}_2\text{CH}_2$), 47.15 (t, $^2J_{\text{PC}} = 10.9$ Hz, $\text{CH}_2\text{CH}_2\text{CH}_2\text{N}$), 51.07 (s, $\text{OCH}_2\text{CH}_2\text{N}$), 57.72 (s, $\text{OCH}_2\text{CH}_2\text{N}$), 122.38 (s, aryl-C), 124.76 (s, aryl-C), 129.17 (s, aryl-C), 129.80 (s, aryl-C), 131.11 (t, $^2J_{\text{PC}} = 1.5$ Hz, aryl-C), 151.07 (t, $^1J_{\text{PC}} = 2.2$ Hz, aryl-C). Anal. Calcd for $\text{C}_{33}\text{H}_{34}\text{N}_2\text{O}_7\text{P}_2\text{Si}$: C, 59.99; H, 5.19; N, 4.24. Found: C, 60.39; H, 5.55; N, 3.91 %.

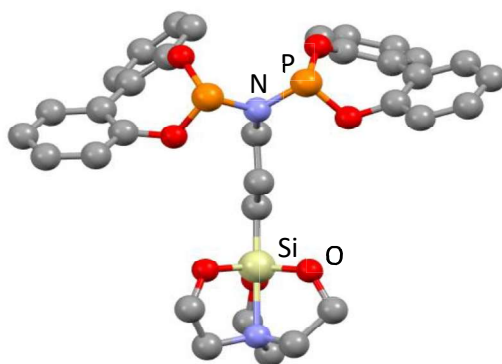
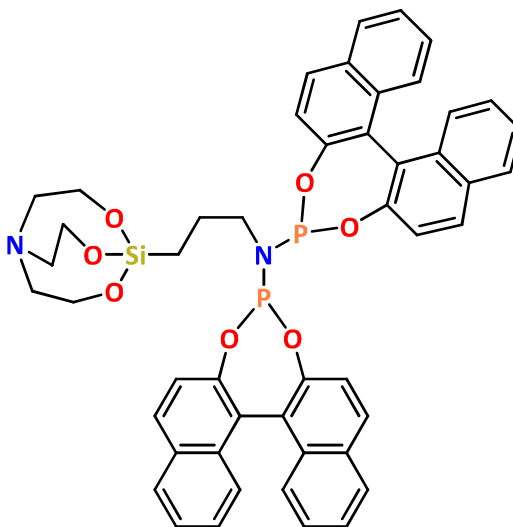


Figure 6.1. Molecular structure of **L11**. Hydrogens omitted for clarity.

Selected bond angles / °: P-N-P 110.1(2); P-N-C 125.1(3), 123.7(3).

Selected bond distances / Å: P-N 1.703(3), 1.687(3); C-N 1.490(4); P-O 1.633(3), 1.647(3), 1.647(3), 1.637(3).

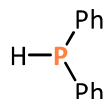
6.2.1.12.2 Synthesis of L12



Isolated as a white solid (2.42 g, 67%); ν_{\max} / cm^{-1} 2955 (C-H), 2866 (C-H), 1618 (C=C), 1587 (C=C), 1057 (P-O), 883 (P-N); ^1H NMR (400 MHz, CDCl_3) -0.18 – 0.04 (2H, m, SiCH_2), 1.75 – 1.89 (2H, m, $\text{CH}_2\text{CH}_2\text{CH}_2$), 2.66 (6H, t, $^3J_{\text{HH}} = 5.7$ Hz, $\text{OCH}_2\text{CH}_2\text{N}$), 2.79 – 2.93 (2H, m, $\text{CH}_2\text{CH}_2\text{CH}_2\text{N}$), 3.62 (6H, t, $^3J_{\text{HH}} = 5.7$ Hz, $\text{OCH}_2\text{CH}_2\text{N}$), 7.17 – 7.45 (12H, m, aryl), 7.35 – 7.41 (4H, m, aryl), 7.52 (2H, d, $^3J_{\text{HH}} = 8.8$ Hz, aryl) 7.69 (2H, d, $^3J_{\text{HH}} = 8.8$ Hz, aryl), 7.85 – 7.99 (8H, m, aryl); $^{31}\text{P}\{^1\text{H}\}$ NMR (162 MHz, CDCl_3) +149; $^{13}\text{C}\{^1\text{H}\}$ NMR (101 MHz, CDCl_3) 13.02 (s, SiCH_3), 28.92 (t, $^3J_{\text{PC}} = 3.2$ Hz, $\text{CH}_2\text{CH}_2\text{CH}_2$), 47.25 (s, $\text{CH}_2\text{CH}_2\text{CH}_2\text{N}$), 51.05 (s, $\text{OCH}_2\text{CH}_2\text{N}$), 57.69 (s, $\text{OCH}_2\text{CH}_2\text{N}$), 122.08 (s, aryl-C), 122.31 (s, aryl-C), 122.45 (s, aryl-C), 124.32 (t, $^1J_{\text{PC}} = 2.6$ Hz, aryl-C), 124.50 (s, aryl-C), 124.84 (s, aryl-C), 125.83 (s, aryl-C), 125.99 (s, aryl-C), 127.07 (s, aryl-C), 127.17 (s, aryl-C), 128.30 (s, aryl-C), 128.36 (s, aryl-C), 130.11 (s, aryl-C), 130.25 (s, aryl-C), 130.84 (s, aryl-C), 131.44 (s, aryl-C), 132.56 (s, aryl-C), 132.79 (s, aryl-C), 149.15 (s, aryl-C), 149.60 (t, $^1J_{\text{PC}} = 3.1$ Hz, aryl-C). Anal. Calcd for $\text{C}_{49}\text{H}_{42}\text{N}_2\text{O}_7\text{P}_2\text{Si}$: C, 68.36; H, 4.92; N, 3.25. Found: C, 66.82; H, 4.78; N, 2.85 %. CHN result affected by silicon grease in sample.

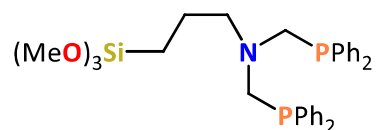
6.2.2 Synthesis of PCNCP-type compounds

6.2.2.1 Synthesis of HPPH_2



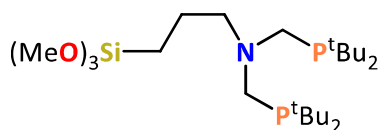
Triphenylphosphine (21.44 g, 81.4 mmol) and lithium wire (1.32 g, 184 mmol) were added to THF (200 cm³) at 0 °C under argon and then stirred for 18 h at room temperature. The resulting mixture was filtered and the filtrate dried *in vacuo*. The residue was dissolved in Et₂O (150 cm³), followed by careful addition of degassed water (150 cm³) at 0 °C. The organic layer was then separated and dried over activated 4Å molecular sieves. The crude product was then purified by vacuum distillation (53 °C, 0.05 mbar) to give a colourless oil (9.7 g, 64%); ¹H NMR (400 MHz, CDCl₃) 7.41 (6H, m, phenyl), 7.58 – 7.66 (4H, m, phenyl); ³¹P{¹H} NMR (162 MHz, CDCl₃) δ: –40. NMR spectroscopic analysis are in good agreement with reported literature values.⁸

6.2.2.2 Synthesis of L13



(3-Aminopropyl)trimethoxysilane (1.0 cm³, 4.6 mmol), paraformaldehyde (0.34 g, 11.5 mmol) and HPPH₂ (1.6 cm³, 9.2 mmol) were heated at reflux in toluene (25 cm³) for 1 h. MeOH (15 cm³) was then added to aid dissolution of the paraformaldehyde and the solution heat at reflux again for 1 h. After cooling to room temperature, the solvent was removed *in vacuo* and the resulting oil dissolved in Et₂O (15 cm³) then filtered. The filtrate was dried *in vacuo* to give a yellow viscous oil (1.00 g, 50%); ¹H NMR (400 MHz, CD₂Cl₂) 0.48 – 0.56 (2H, m, SiCH₂), 1.45 – 1.65 (2H, m, CH₂CH₂CH₂), 2.89 (2H, t, ³J_{HH} = 7.3 Hz, CH₂CH₂N), 3.54 (9H, s, Si(OCH₃)₃), 3.63 (4H, d, ²J_{PH} = 3.1 Hz, NCH₂P), 7.32 – 7.38 (12H, m, phenyl), 7.43 – 7.50 (8H, m, phenyl); ³¹P{¹H} NMR (162 MHz, CD₂Cl₂) δ: –29; ¹³C{¹H} NMR (101 MHz, CD₂Cl₂), 6.44 (s, SiCH₂), 19.57 (s, CH₂CH₂CH₂), 50.29 (s, Si(OCH₃)₃), 58.55 (dd, ¹J_{PC} = 9.5 Hz, ³J_{PC} = 5.5 Hz, NCH₂P), 59.16 (t, ³J_{PC} = 8.9 Hz, CH₂N) 128.32 (d, ³J_{PC} = 7.0 Hz, aryl-C), 128.46 (s, aryl-C), 133.05 (d, ²J_{PC} = 18.5 Hz, aryl-C), 138.45 (d, ¹J_{PC} = 13.6 Hz, aryl-C).

6.2.2.3 Attempted synthesis of L14

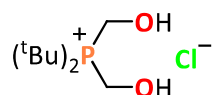


(3-Aminopropyl)trimethoxysilane (1.0 cm³, 4.6 mmol), paraformaldehyde (0.35 g, 11.6 mmol) and HP^tBu₂ (1.30 g, 9.2 mmol) were heated at reflux in toluene (25 cm³) and MeOH (15 cm³) overnight. Subsequent ³¹P NMR spectroscopic analysis showed decomposition of the product and the reaction was abandoned.

6.2.2.4 General procedure for the synthesis of dialkylbis(hydroxymethyl)phosphonium chloride salts

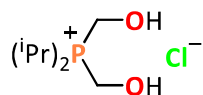
Paraformaldehyde (2 eq, ~20 mmol) and a secondary phosphine (1 eq.) were dissolved in water (10 cm³), followed by addition of 1 M HCl (1 eq.) at 0 °C. The mixture was allowed to warm to room temperature and stirred overnight, then the solvent was removed *in vacuo*. The residue was washed with Et₂O (3 × 5 cm³) and dried *in vacuo* to give a white solid.

6.2.2.4.1 Synthesis of di-*tert*-butylbis(hydroxymethyl)phosphonium chloride:



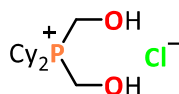
Isolated as a white solid (1.54 g, 66%); $\nu_{\text{max}}/\text{cm}^{-1}$ 3209 (O-H), 3130 (O-H br), 2975 (C-H); ¹H NMR (400 MHz, D₂O) 1.51 (18H, d, ³J_{PH} = 14.7 Hz, C(CH₃)₃), 4.72 (4H, d, ²J_{PH} = 1.6 Hz PCH₂); ³¹P{¹H} NMR (162 MHz, D₂O) δ : +36; ¹³C{¹H} NMR (101 MHz, D₂O), 26.30 (s, C(CH₃)₃), 33.08 (d, ¹J_{PC} = 30.5 Hz, PC(CH₃)₃), 50.95 (d, ¹J_{PC} = 52.4 Hz, PCH₂); Anal. Calcd for C₁₀H₂₄ClO₂P: C, 49.48; H, 9.97; N, 0.00. Found: C, 49.28; H, 9.98; N, 0.00 %. NMR spectroscopic analysis and CHN elemental analysis are in good agreement with reported literature values.⁹

6.2.2.4.2 Synthesis of di-*iso*-propylbis(hydroxymethyl)phosphonium chloride:



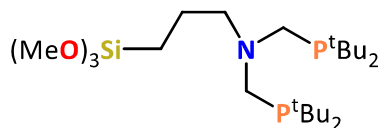
Isolated as a white solid (1.61 g, 63%); $\nu_{\max}/\text{cm}^{-1}$ 3104 (O-H br), 2980 (C-H), 2895 (C-H); ^1H NMR (400 MHz, D_2O) 1.30 (12H, dd, $^3J_{\text{PH}} = 16.3$ Hz, $^3J_{\text{HH}} = 7.3$ Hz, $\text{CH}(\text{CH}_3)_2$), 2.65 – 2.83 (2H, m, $\text{CH}(\text{CH}_3)_2$), 4.56 (4H, d, $^2J_{\text{PH}} = 1.9$ Hz, PCH_2); $^{31}\text{P}\{^1\text{H}\}$ NMR (162 MHz, D_2O) δ : +36; $^{13}\text{C}\{^1\text{H}\}$ NMR (101 MHz, D_2O), 15.20 (s, $\text{CH}(\text{CH}_3)_2$), 18.10 (d, $^1J_{\text{PC}} = 39.44$ Hz, $\text{PCH}(\text{CH}_3)_2$), 49.40 (d, $^1J_{\text{PC}} = 55.9$ Hz, PCH_2); Anal. Calcd for $\text{C}_8\text{H}_{20}\text{ClO}_2\text{P}$: C, 44.76; H, 9.39; N, 0.00. Found: C, 44.37; H, 9.45; N, 0.00 %. NMR spectroscopic analysis and CHN elemental analysis are in good agreement with reported literature values.⁹

6.2.2.4.3 Synthesis of dicyclohexylbis(hydroxymethyl)phosphonium chloride:



Isolated as a white solid (2.07 g, 80%); $\nu_{\max}/\text{cm}^{-1}$ 3153 (O-H br), 2926 (C-H), 2857 (C-H); ^1H NMR (400 MHz, D_2O) 1.1 – 1.95 (20H, m, Cy), 2.51 (2H, qt, $^3J_{\text{HH}} = 12.7$ Hz, $^3J_{\text{HH}} = 2.9$ Hz PCH), 4.53 (4H, d, $^2J_{\text{PH}} = 1.9$ Hz, PCH_2); $^{31}\text{P}\{^1\text{H}\}$ NMR (162 MHz, D_2O) δ : +29; $^{13}\text{C}\{^1\text{H}\}$ NMR (101 MHz, D_2O), 24.81 (s, $\text{PCHCH}_2\text{CH}_2\text{CH}_2$), 25.43 (d, $^3J_{\text{PC}} = 4.0$ Hz, $\text{PCHCH}_2\text{CH}_2\text{CH}_2$), 25.71 (d, $^2J_{\text{PC}} = 12.2$ Hz, PCHCH_2), 27.18 (d, $^1J_{\text{PC}} = 38.0$ Hz, PCH), 49.18 (d, $^1J_{\text{PC}} = 56.6$ Hz, PCH_2); Anal. Calcd for $\text{C}_{14}\text{H}_{28}\text{ClO}_2\text{P}$: C, 57.04; H, 9.57; N, 0.00. Found: C, 56.92; H, 9.57; N, 0.00 %. NMR spectroscopic analysis and CHN elemental analysis are in good agreement with reported literature values.⁹

6.2.2.5 Second attempted synthesis of L14

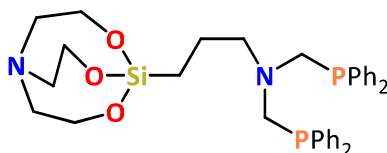


bis(*tert*-butyl)Hydroxymethylphosphonium chloride (1.5 g, 6.2 mmol) and NEt₃ (0.9 cm³, 6.4 mmol) were dissolved in MeOH (15 cm³) and stirred for 10 mins. (3-aminopropyl)trimethoxysilane (0.5 cm³, 3.1 mmol) was then added and the reaction heated to reflux for 1 h. ³¹P spectroscopic analysis of an aliquot of reaction mixture showed an unidentified side product that could not be removed and the reaction was abandoned.

6.2.2.6 General procedure for the synthesis of PCNCP compounds L17, L18 and L19

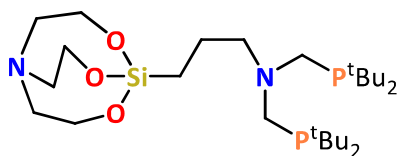
(3-Aminopropyl)silatrane (1.0 g, 4.3 mmol), paraformaldehyde (0.26 g, 8.6 mmol) and HPPH₂ (1.5 cm³, 8.6 mmol) were heated at reflux in a toluene (25 cm³) and MeOH (15 cm³) solvent mixture overnight. After cooling to room temperature, the solvent was removed *in vacuo* and the crude solid recrystallized from DCM/pentane and dried *in vacuo* to give a white solid.

6.2.2.6.1 Synthesis of L17



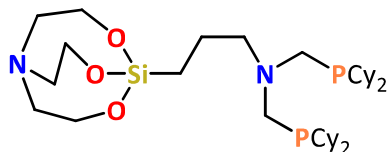
Isolated as a white solid. Single crystals suitable for XRD analysis were obtained by layering a solution of the compound in DCM with hexane (2.0 g, 74%); ν_{\max} /cm⁻¹ 3051 (C-H aromatic), 2927 (C-H), 2876 (C-H), 1582 (C=C); ¹H NMR (400 MHz, CDCl₃) 0.30 – 0.38 (2H, m, SiCH₂), 1.58 – 1.66 (2H, m, CH₂CH₂CH₂), 2.80 (6H, t, ³J_{HH} = 5.8 Hz, OCH₂CH₂N), 2.84 – 2.90 (2H, m, CH₂CH₂N), 3.60 (4H, d, ²J_{PH} = 2.8 Hz, NCH₂P), 3.76 (6H, t, ³J_{HH} = 5.8 Hz, OCH₂CH₂N), 7.24 – 7.30 (10H, m, phenyl), 7.37 – 7.46 (10H, m, phenyl); ³¹P{¹H} NMR (162 MHz, CDCl₃) δ : -28; ¹³C{¹H} NMR (101 MHz, CD₂Cl₂) 13.69 (s, SiCH₂), 21.34 (s, CH₂CH₂CH₂), 50.96 (s, OCH₂CH₂N), 57.63 (s, OCH₂CH₂N), 58.55 (dd, ¹J_{PC} = 9.4 Hz, ³J_{PC} = 4.9 Hz, NCH₂P), 59.74 (s, CH₂N), 128.16 (s, aryl-C), 128.24 (d, ³J_{PC} = 2.1 Hz, aryl-C), 133.05 (d, ²J_{PC} = 18.5 Hz, aryl-C), 138.79 (d, ¹J_{PC} = 13.4 Hz, aryl-C). Anal. Calcd for C₃₅H₄₂N₂O₃P₂Si: C, 66.86; H, 6.73; N, 4.46. Found: C, 66.02; H, 6.54; N, 4.83 %.

6.2.2.6.2 Synthesis of L18



Isolated as a white solid (1.3 g, 55%); ν_{\max} /cm⁻¹ 2935 (C-H), 2862 (C-H); ¹H NMR (400 MHz, CDCl₃) 0.33 – 0.40 (2H, m, SiCH₂), 1.17 (36H, d, ³J_{PH} = 10.6 Hz, PC(CH₃)₃) 1.55 – 1.63 (2H, m, CH₂CH₂CH₂), 2.71 – 2.78 (2H, m, CH₂CH₂N), 2.80 (4H, s, br, NCH₂P), 2.80 (6H, t, ³J_{HH} = 5.8 Hz, OCH₂CH₂N), 3.76 (6H, t, ³J_{HH} = 5.8 Hz, OCH₂CH₂N); ³¹P{¹H} NMR (162 MHz, CDCl₃) δ : +12; ¹³C{¹H} NMR (101 MHz, CD₂Cl₂) 13.40 (s, SiCH₂), 19.63 (s, CH₂CH₂CH₂), 29.98 (d, ²J_{PC} = 13.3 Hz, PC(CH₃)₃), 31.43 (d, ¹J_{PC} = 21.1 Hz, PC(CH₃)₃), 51.29 (s, OCH₂CH₂N), 57.63 (s, br, NCH₂P), 57.98 (s, OCH₂CH₂N), 60.32 (s, CH₂N). Anal. Calcd for C₂₇H₅₈N₂O₃P₂Si: C, 59.09; H, 10.65; N, 5.10. Found: C, 58.46; H, 10.30; N, 5.48 %.

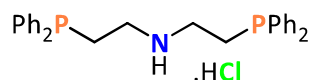
6.2.2.6.3 Synthesis of L19



During work-up the compound found to be soluble in DCM/pentane, therefore the solvent was removed *in vacuo* and the crude solid washed with MeOH (15 cm³), filtered and dried *in vacuo* to give a white solid (2.2 g, 41%); ν_{\max} /cm⁻¹ 2916 (C-H), 2862 (C-H); ¹H NMR (400 MHz, CDCl₃) 0.31 – 0.40 (2H, m, SiCH₂), 1.15 – 1.31 (20H, m, Cy-H), 1.48 – 1.61 (6H, m, CH₂CH₂CH₂ + Cy-H), 1.63 – 1.88 (20H, m, Cy-H), 2.59 – 2.66 (2H, m, CH₂N(CH₂PPh₂)₂), 2.80 (6H, t, ³J_{HH} = 5.8 Hz, OCH₂CH₂N), 2.82 (4H, s, br, NCH₂P), 3.76 (6H, t, ³J_{HH} = 5.8 Hz, OCH₂CH₂N); ³¹P{¹H} NMR (162 MHz, CDCl₃) δ : -18; ¹³C{¹H} NMR (101 MHz, CD₂Cl₂) 13.38 (s, SiCH₂), 21.11 (s, CH₂CH₂CH₂), 26.66 (s, Cy-C), 27.45 (d, ³J_{PC} = 9.1 Hz, Cy-C), 29.78 (dd, ²J_{PC} = 11.6 Hz, Cy-C), 32.85 (d, ¹J_{PC} = 12.9 Hz, Cy-C), 51.24 (s, OCH₂CH₂N), 52.11 (t, ¹J_{PC} = 7.0 Hz, NCH₂P), 57.96 (s, OCH₂CH₂N), 60.39 (s, CH₂CH₂CH₂N). Anal. Calcd for C₃₅H₆₆N₂O₃P₂Si : C, 64.38; H, 10.19; N, 4.29. Found: C, 64.52; H, 10.18; N, 3.58 %.

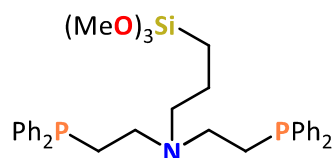
6.2.3 Synthesis of wide bite angle tetherable phosphines

6.2.3.1 Synthesis of bis(2-(diphenylphosphino)ethyl)amine hydrochloride



Diphenylphosphine (3.0 cm³, 17.0 mmol) and potassium *tert*-butoxide (2.78 g, 24.9 mmol) were stirred in THF (30 cm³) for 5 min, followed by addition of bis(2-chloroethyl)amine (1.37 g, 7.7 mmol). The resulting solution was heated at reflux overnight, then added to hexane (50 cm³) and washed with 10% NaOH (50 cm³) and brine (50 cm³). After separation, the organic layer was stirred with 2M HCl (50 cm³) to give a white precipitate. The precipitate was filtered and recrystallised from hot MeCN (10 cm³) to give a white solid (1.34 g, 35%); ν_{\max} /cm⁻¹ 3064 (C-H), 2969 br (N-H) 1433 (P-Ph); ¹H NMR (400 MHz, CDCl₃) 2.48 (4H, m, PCH₂), 2.95 (4H, s, br, NCH₂), 7.23 – 7.33 (12H, m, phenyl), 7.34 – 7.42 (8H, m, phenyl), 9.98 (2H, s, NH₂); ³¹P{¹H} NMR (162 MHz, CDCl₃) δ : -21; ¹³C{¹H} NMR (101 MHz, CDCl₃) 23.87 (d, ¹J_{PC} = 16.2 Hz, PCH₂), 44.20 (d, ²J_{PC} = 26.3 Hz, NCH₂), 128.82 (d, ³J_{PC} = 7.0 Hz, aryl-C), 129.2 (s, aryl-C), 132.65 (d, ²J_{PC} = 19.5 Hz, aryl-C), 136.02 (d, ¹J_{PC} = 12.4 Hz, aryl-C); Anal. Calcd for C₂₈H₃₀ClNP₂: C, 70.36; H, 6.33; N, 2.93. Found: C, 69.58; H, 5.98; N, 3.41 %. NMR spectroscopic analysis are in good agreement with reported literature values.¹⁰

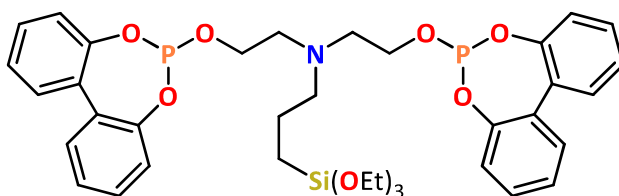
6.2.3.2 Attempted synthesis of L20



bis(2-(Diphenylphosphino)ethyl)amine hydrochloride (0.19 g, 0.4 mmol) was dissolved in THF (10 cm³) and stirred at -78 °C, followed by addition of ⁿBuLi (0.4 cm³, 0.8 mmol). The solution was allowed to warm to room temperature and stirred for 30 mins to produce a yellow solution. The solution was re-cooled to -78 °C, followed by dropwise addition of (3-chloropropyl)trimethoxysilane (0.1 cm³, 0.4 mmol) and warming to room temperature, producing a colourless solution. Further stirring for 6 hours was

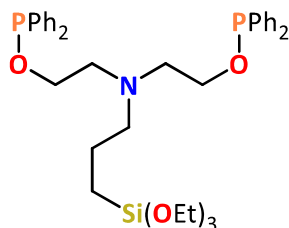
undertaken, after which the solution was filtered, and the filtrate dried *in vacuo* to give an orange oil. ^1H NMR spectroscopic analysis showed the presence of unknown impurities that could not be removed and the reaction was abandoned.

6.2.3.3 Synthesis of L21



bis(2-Hydroxyethyl)-3-aminopropyltriethoxysilane, 62% in ethanol (3.25 cm³, 6.0 mmol) was dried *in vacuo* then dissolved in MeCN (30 cm³). NEt₃ (1.7 cm³, 12.5 mmol) was added and the solution cooled to –40 °C, followed by dropwise addition of a solution of 2,2'-biphenol phosphochloridite (2.95 g, 12.0 mmol) dissolved in MeCN (10 cm³). The solution was allowed to warm up to room temperature and stirred overnight. Subsequently, the solvent was removed *in vacuo*, followed by extraction into toluene (3 × 10 cm³). Upon addition of hexane (30 cm³) a yellow precipitate was observed, and the solution was filtered. The filtrate was dried *in vacuo* to give a colourless oil (1.25 g, 28%); ^1H NMR (400 MHz, C₆D₆) 0.76 (2H, t, $^3J_{\text{HH}} = 7.0$ Hz, SiCH₂), 0.95 (9H, t, $^3J_{\text{PH}} = 7.1$ Hz, SiOCH₂CH₃) 1.44 (2H, t, $^3J_{\text{HH}} = 7.0$ Hz, CH₂CH₂CH₂), 1.74 – 1.84 (2H, m, CH₂CH₂CH₂N), 1.86 – 2.01 (4H, m, NCH₂CH₂O), 3.35 – 3.54 (4H, m, NCH₂CH₂O), 3.76 – 3.85 (6H, m, OCH₂CH₃), 6.90 – 7.23 (16H, m, aryl); $^{31}\text{P}\{^1\text{H}\}$ NMR (162 MHz, C₆D₆) δ : + 138; $^{13}\text{C}\{^1\text{H}\}$ NMR (101 MHz, C₆D₆), 9.03 (s, SiCH₂), 19.04 (s, CH₂CH₂CH₂), 21.11 (s, OCH₂CH₃), 51.25 (s, CH₂CH₂CH₂N), 52.08 (s, NCH₂CH₂O), 58.79 (s, OCH₂CH₃), 60.50 (d, $^2J_{\text{PC}} = 2.7$ Hz, NCH₂CH₂O), 121.89 (s, aryl-C), 124.81 (s, aryl-C), 129.16 (s, aryl-C), 129.94 (d, $^3J_{\text{PC}} = 1.1$ Hz, aryl-C), 131.20 (d, $^3J_{\text{PC}} = 3.3$ Hz, aryl-C), 150.49 (d, $^3J_{\text{PC}} = 5.6$ Hz, aryl-C).

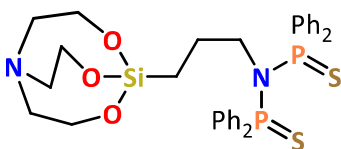
6.2.3.4 Attempted synthesis of L22



bis(2-Hydroxyethyl)-3-aminopropyltriethoxysilane, 62% in ethanol (4.07 cm³, 7.5 mmol) was dried *in vacuo* then dissolved in MeCN (30 cm³). NEt₃ (3.4 cm³, 25 mmol) was added and the solution cooled to -40 °C, followed by dropwise addition of chlorodiphenylphosphine (2.75 cm³, 15.0 mmol). The solution was allowed up to warm up to room temperature and stirred overnight. ³¹P NMR spectroscopic analysis of an aliquot of the reaction mixture showed only start material, so the reaction was heated to reflux for 1 h. ³¹P NMR spectroscopic analysis of a second aliquot of reaction mixture showed decomposition of the phosphine and hence the reaction was abandoned.

6.2.4 Synthesis of tetherable sulfur ligands

6.2.4.1 Synthesis of L5S₂



L5 (0.50 g, 0.8 mmol) and elemental sulfur S₈ (0.05 g, 1.6 mmol) were dissolved in THF (10 cm³) and stirred for 48 h. Hexane (10 cm³) was added resulting in a white solid that was isolated and dried *in vacuo* to give the target compound (0.43 g, 79%); $\nu_{\text{max}}/\text{cm}^{-1}$ 3051 (C-H aromatic), 2972 (C-H), 2881 (C-H), 1588 (C=C), 1435 (P-Ph), 907 (P-N), 644 (P=S); ¹H NMR (400 MHz, CDCl₃) -0.35 (2H, t, ³J_{HH} = 7.5 Hz, SiCH₂), 1.50 (2H, p, ³J_{HH} = 7.5 Hz, CH₂CH₂CH₂), 2.70 (6H, t, ³J_{HH} = 5.8 Hz, OCH₂CH₂N), 3.36 – 3.53 (2H, m, CH₂N(PPh₂)₂), 3.57 (6H, t, ³J_{HH} = 5.8 Hz, OCH₂CH₂N), 7.25 – 7.43 (12H, m, phenyl), 7.95 – 8.05 (8H, m, phenyl); ³¹P{¹H} NMR (162 MHz, CDCl₃) δ : +69; ¹³C{¹H} NMR (101 MHz, CDCl₃) 12.63 (s, SiCH₂), 25.74 (s, CH₂CH₂CH₂), 51.02 (s, OCH₂CH₂N), 53.18 (s, CH₂N(PPh₂)₂), 57.52 (s, OCH₂CH₂N), 127.65 (s, aryl-C), 128.96 (t, ³J_{PC} = 6.2 Hz aryl-C),

132.79 (s, aryl-C), 133.91 (t, $^2J_{PC}$ = 6.4 Hz, aryl-C). Anal. Calcd for $C_{33}H_{38}N_2O_3P_2S_2Si$: C, 59.62; H, 5.76; N, 4.21. Found: C, 58.48; H, 5.84; N, 4.01 %.

6.3 Chapter 3 experimental

6.3.1 General procedure for preparation of diphosphinediselenides

Elemental grey Se powder (25 mg, 0.031 mmol) was added to solution of the desired bidentate phosphine (0.02 g, 0.07 mmol) in CD_2Cl_2 (0.7 cm^3) in a Youngs NMR tube to give a pale-yellow solution, followed by sonication until complete conversion to the diselenide derivative was observed. The product was not isolated as only the $|^1J_{SeP}|$ coupling constant is of interest.

Single crystals of $BISBI(Se)_2$ suitable for XRD analysis were obtained from a CD_2Cl_2 solution (Figure 6.2).

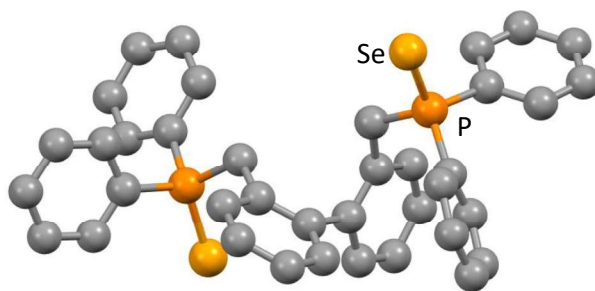


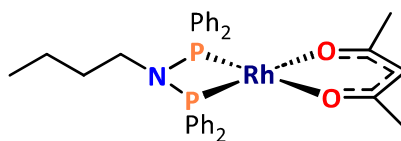
Figure 6.2. *Molecular structure of $BISBI(Se)_2$. Hydrogens omitted for clarity. Selected bond lengths / Å: Se-P 2.117(1), 2.104(1).*

Table 17. $^{31}\text{P}\{^1\text{H}\}$ NMR chemical shifts and $|^1J_{\text{SeP}}|$ coupling constants measured in CD_2Cl_2 at 162 MHz.

Compound	δ / ppm	$ ^1J_{\text{SeP}} $ / Hz
L1(Se)₂	+67	786
L2(Se)₂	+67	785
L3(Se)₂	+67	786
L4(Se)₂	+68	787
L5(Se)₂	+67	786
L13(Se)₂	+24	732
L17(Se)₂	+26	729
L18(Se)₂	+67	688
L19(Se)₂	+46	684
L9(Se)₂	+77	1012
L11(Se)₂	+78	1010
L12(Se)₂	+80	1010
L21(Se)₂	+77	1031
L6X(Se)	+87	752
BISBI(Se)₂	+34	738

6.3.2 Synthesis of rhodium(I) complexes

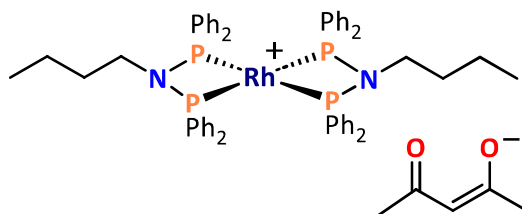
6.3.2.1 Attempted Synthesis of Rh(acac)(L23)



A solution of **L23** (0.07 g, 0.15 mmol) in THF (15 cm³) was added to a solution of Rh(acac)(CO)₂ (0.05 g, 0.15 mmol) in THF (15 cm³) and the resulting solution stirred for 12 h. ^{31}P NMR spectroscopic analysis of an aliquot of reaction mixture showed a mixture

of products; $^{31}\text{P}\{^1\text{H}\}$ NMR (162 MHz, unlocked) δ : +64 (d, $^1J_{\text{RhP}} = 173$ Hz, $\text{Rh}(\text{acac})(\text{L23})$), +67 ppm (d, $^1J_{\text{RhP}} = 120$ Hz, $[\text{Rh}(\text{L23})_2][\text{acac}]$).

6.3.2.2 Synthesis of $[\text{Rh}(\text{L23})_2][\text{acac}]$



A young's NMR tube was charged with **L23** (0.022 g, 0.05 mmol), $\text{Rh}(\text{acac})(\text{COD})$ (0.008 g, 0.05 mmol) and THF (0.7 cm^3). The resulting solution was sonicated for 1 h, then all volatile components were removed *in vacuo* to give a brown solid (0.015 g, 55%); ^1H NMR (400 MHz, CDCl_3) δ : 0.54 (6H, t, $^3J_{\text{HH}} = 7.4$ Hz, CH_2CH_3), 0.82 (4H, sextet, $^3J_{\text{HH}} = 7.4$ Hz, $\text{CH}_2\text{CH}_2\text{CH}_3$), 0.96 – 1.08 (4H, m, $\text{CH}_2\text{CH}_2\text{CH}_2$), 2.04 (3H, s, COCH_3), 2.37 (3H, s, COCH_3), 2.72 – 2.85 (4H, m, CH_2N), 5.59 (1H, s, COCHCO), 7.21 – 7.34 (31H, m, phenyl) 7.48 – 7.56 (9H, m, phenyl); $^{31}\text{P}\{^1\text{H}\}$ NMR (162 MHz, CDCl_3) δ : + 67 (d, $^1J_{\text{RhP}} = 120$ Hz); $^{13}\text{C}\{^1\text{H}\}$ NMR (101 MHz, CDCl_3) δ : 13.33 (s, CH_2CH_3), 20.00 (s, $\text{CH}_2\text{CH}_2\text{CH}_3$), 28.01 (s, COCH_3), 31.85 (s, $\text{CH}_2\text{CH}_2\text{CH}_2$), 49.61 (s, NCH_2), 100.47 (s, COCHCO), 129.05 (t, $^3J_{\text{PC}} = 2.6$ Hz, aryl-C), 131.68 (s, aryl-C), 132.26 (t, $^1J_{\text{PC}} = 13$ Hz, aryl-C), 132.53 (t, $^2J_{\text{PC}} = 3.9$ Hz, aryl-C).

6.3.2.3 Optimised synthesis of $\text{Rh}(\text{acac})(\text{L23})$

A solution of **L23** (0.12 g, 0.2 mmol) in THF (15 cm^3) was added dropwise to a solution of $\text{Rh}(\text{acac})(\text{COD})$ (0.05 g, 0.15 mmol) in THF (15 cm^3) at -78°C . The solution was allowed to warm up to room temperature and stirred for 2 h. ^{31}P NMR spectroscopic analysis of an aliquot of reaction mixture showed $\approx 90\%$ selectivity for $\text{Rh}(\text{acac})(\text{L23})$; $^{31}\text{P}\{^1\text{H}\}$ NMR (162 MHz, unlocked) δ : +63 (d, $^1J_{\text{RhP}} = 173$ Hz, $\text{Rh}(\text{acac})(\text{L23})$), +67 ppm (d, $^1J_{\text{RhP}} = 120$ Hz, $[\text{Rh}(\text{L23})_2][\text{acac}]$).

6.3.2.4 General procedure for the attempted synthesis of Rh(acac)(P[^]P) complexes

Rh(acac)(CO)₂ or Rh(acac)(COD) (0.1 g, 0.4 mmol) and P[^]P (1 eq., 0.4 mmol) were dissolved in THF (15 cm³) and stirred for 4 days. The solvent was removed *in vacuo* and the resulting solid washed with hexane (3 × 5 cm³) and Et₂O (3 × 5 cm³), then dried *in vacuo*. NMR spectroscopic analysis showed various impurities in each sample.

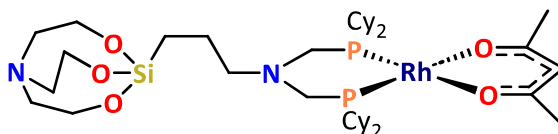
Rh(acac)(L1): ³¹P{¹H} NMR (162 MHz, unlocked) +63 (d, ¹J_{RhP} = 170 Hz), +75 (d, ¹J_{RhP} = 177 Hz).

Rh(acac)(L9): ³¹P{¹H} NMR (162 MHz, unlocked) +147 (d, ¹J_{RhP} = 262 Hz).

Rh(acac)(L13): ³¹P{¹H} NMR (162 MHz, unlocked) +31 (d, ¹J_{RhP} = 172 Hz), +33 (d, ¹J_{RhP} = 172 Hz), +36 (d, ¹J_{RhP} = 180 Hz).

Rh(acac)(L21): ³¹P{¹H} NMR (162 MHz, unlocked) +147 (d, ¹J_{RhP} = 285 Hz), +156 (d, ¹J_{RhP} = 296 Hz).

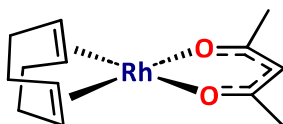
6.3.2.5 Synthesis of Rh(acac)(L19)



Rh(acac)(CO)₂ (0.1 g, 0.4 mmol) and **L19** (0.25 g, 0.4 mmol) were dissolved in THF (15 cm³) and stirred for 3 h. The solvent was removed *in vacuo* and the resulting solid washed with hexane (3 × 5 cm³) and Et₂O (3 × 5 cm³), then dried *in vacuo* to give a yellow solid (0.13 g, 38%); ν_{max} /cm⁻¹ 2919 (C-H), 2849 (C-H), 1952 (C=O); ¹H NMR (400 MHz, d⁸-THF) 0.22 – 0.29 (2H, m, SiCH₂), 1.19 – 1.40 (12H, m, Cy-H + SiCH₂CH₂), 1.48 – 1.72 (12H, m, Cy-H), 1.78 (6H, s, COCH₃), 1.79 – 1.90 (18H, m, Cy-H), 1.97 – 2.06 (4H, m, Cy-H), 2.34 (4H, s, br, NCH₂P), 2.41 (2H, s, br, CH₂CH₂CH₂N), 2.79 (6H, t, ³J_{HH} = 5.7 Hz, OCH₂CH₂N), 3.67 (6H, t, ³J_{HH} = 5.7 Hz, OCH₂CH₂N), 5.21 (1H, s, COCHCO); ³¹P{¹H} NMR (162 MHz, d⁸-THF) +42 (d, ¹J_{RhP} = 185.9 Hz); ¹³C{¹H} NMR (101 MHz, d⁸-THF) 13.76 (s, SiCH₂), 20.50 (s, CH₂CH₂CH₂), 21.18 (s, CH₃CO), 26.69 (s, Cy-C), 27.57 (d, ²J_{PC} = 25.3 Hz, Cy-C), 29.32 (s, Cy-C), 35.62 (d, ¹J_{PC} = 10.2 Hz, Cy-C), 50.92 (s, OCH₂CH₂N), 51.26 (d, ¹J_{PC}

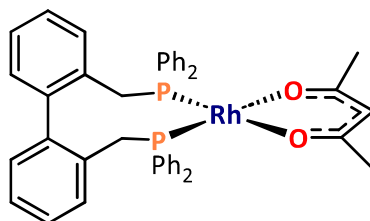
= 41.8 Hz, NCH₂P), 57.54 (s, OCH₂CH₂N), 58.35 (s, CH₂CH₂CH₂N), 98.25 (d, ³J_{RhC} = 77.0 Hz, COCHCO), 182.52 (s, CH₃CO); Anal. Calcd for C₄₀H₇₃N₂O₅P₂RhSi: C, 56.19; H, 8.61; N, 3.28. Found: C, 55.70; H, 8.46; N, 2.53 %.

6.3.2.6 Synthesis of Rh(acac)(COD)



Rh(acac)(CO)₂ (0.30 g, 1.2 mmol) and COD (5 cm³, 40 mmol) were stirred in pet. ether (15 cm³) for 3 h at room temperature. The solvent was then removed *in vacuo* to give a yellow solid (0.34 g, 94%); ν_{\max} /cm⁻¹ 2982 (C-H), 2928 (C-H), 2880 (C-H), 2831 (C-H), 1561 (C=C), 1513 (C=C); ¹H NMR (400 MHz, C₆D₆) δ : 1.52 – 1.66 (4H, m, CHCH₂), 1.78 (6H, s, COCH₃), 2.16 – 2.32 (4H, m, CHCH₂), 4.33 (4H, s, CHCH₂), 5.14 (1H, s, COCHCO); ¹³C{¹H} NMR (101 MHz, C₆D₆) δ : 26.92 (d, ³J_{RhC} = 1.1 Hz, COCH₃), 30.20 (s, CHCH₂), 75.91 (d, ¹J_{RhC} = 14.1 Hz, CHCH₂), 99.42 (d, ³J_{RhC} = 1.9 Hz, COCHCO), 186.36 (s, CH₃CO); Anal. Calcd for C₁₃H₁₉O₂Rh: C, 50.34; H, 6.17. Found: C, 51.40; H, 6.28 %. NMR spectroscopic analysis are in good agreement with reported literature values.¹¹

6.3.2.7 Attempted synthesis of Rh(acac)(BISBI)

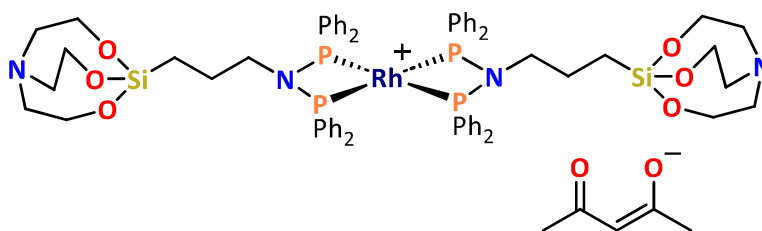


A solution of BISBI (0.09 g, 0.2 mmol) in THF (10 cm³) was added dropwise to a solution of Rh(acac)(COD) (0.05 g, 0.2 mmol) in THF (10 cm³) at –78 °C. The resulting solution was allowed to warm to room temperature and stirred for 3 h. ³¹P NMR spectroscopic analysis of an aliquot of reaction mixture subsequently showed a mixture of products and the reaction was abandoned.

6.3.2.8 General procedure for the synthesis of $[\text{Rh}(\text{P}^{\wedge}\text{P})_2]\text{acac}$ complexes

$\text{Rh}(\text{acac})(\text{CO})_2$ (0.05 g, 0.2 mmol) and $\text{P}^{\wedge}\text{P}$ (1 equiv., 0.2 mmol) were dissolved in THF (20 cm^3) and stirred overnight. The solvent was removed *in vacuo* to give the target product.

6.3.2.8.1 Synthesis of $[\text{Rh}(\text{L5})_2]\text{acac}$

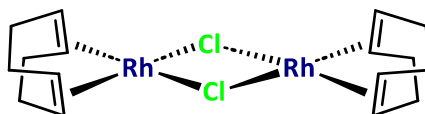


Single crystals of $[\text{Rh}(\text{L5})_2]\text{Cl}$ suitable for XRD analysis were obtained by layering a solution of $[\text{Rh}(\text{L5})_2]\text{acac}$ in DCM with hexane; yellow solid (0.27 g, 74%); $\nu_{\text{max}}/\text{cm}^{-1}$ 3068 (C-H aromatic), 2930 (C-H), 2880 (C-O), 1585 (C=C), 1574 (C=C), 1433 (P-Ph), 912 (P-N); ^1H NMR (400 MHz, CD_6D_6) 0.00 (4H, t, $^3J_{\text{HH}} = 7.1\text{ Hz}$, SiCH_2), 1.35 (4H, p, $^3J_{\text{HH}} = 7.1\text{ Hz}$, $\text{CH}_2\text{CH}_2\text{CH}_2$), 1.93 (6H, s, br, CH_3CO), 2.17 (12H, t, $^3J_{\text{HH}} = 5.9\text{ Hz}$, $\text{OCH}_2\text{CH}_2\text{N}$), 2.80 – 2.92 (4H, m, $\text{CH}_2\text{N}(\text{PPh}_2)_2$), 3.19 (12H, t, $^3J_{\text{HH}} = 5.9\text{ Hz}$, $\text{OCH}_2\text{CH}_2\text{N}$), 4.61 (1H, s, COCHCO), 6.99 (16H, t, $^3J_{\text{HH}} = 7.8\text{ Hz}$, phenyl), 7.15 (8H, s, phenyl), 7.18 – 1.26 (16H, m, phenyl); $^{31}\text{P}\{^1\text{H}\}$ NMR (162 MHz, CD_6D_6) δ : +66 (d, $^1J_{\text{RhP}} = 120\text{ Hz}$); $^{13}\text{C}\{^1\text{H}\}$ NMR (101 MHz, CD_6D_6) 13.28 (s, SiCH_2), 25.79 (s, $\text{CH}_2\text{CH}_2\text{CH}_2$), 30.06 (s, br, CH_3O), 46.23 (s, $\text{CH}_2\text{N}(\text{PPh}_2)_2$), 50.25 (s, $\text{OCH}_2\text{CH}_2\text{N}$), 56.99 (s, $\text{OCH}_2\text{CH}_2\text{N}$), 100.89 (s, COCHCO), 128.59 (t, $^3J_{\text{PC}} = 2.5\text{ Hz}$, aryl-C), 131.02 (s, aryl-C), 132.67 (t, $^2J_{\text{PC}} = 4.3\text{ Hz}$, aryl-C), 136.04 (s, aryl-C); Anal. Calcd for $\text{C}_{71}\text{H}_{83}\text{N}_4\text{O}_8\text{RhSi}_2$: C, 60.76; H, 5.96; N, 3.99. Found: C, 59.91; H, 5.76; N, 3.76 %.

6.3.2.8.2 Synthesis of $[\text{Rh}(\text{L17})_2]\text{acac}$: A mixture of $[\text{Rh}(\text{L17})_2]\text{acac}$ and $\text{Rh}(\text{acac})(\text{L17})$ was produced as determined by ^{31}P NMR spectroscopic analysis of an aliquot of the crude reaction mixture and the reaction was abandoned.

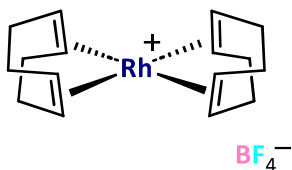
6.3.2.8.3 Synthesis of $[\text{Rh}(\text{L18})_2]\text{acac}$: A mixture of $[\text{Rh}(\text{L18})_2]\text{acac}$ and $\text{Rh}(\text{acac})(\text{L18})$ was produced as determined by ^{31}P NMR spectroscopic analysis of an aliquot of the crude reaction mixture and the reaction was abandoned.

6.3.2.9 Synthesis of $[\text{Rh}_2\text{Cl}_2(\text{COD})_2]$



RhCl_3 (3.0 g, 11.4 mmol) 1,5-cyclooctadiene (6 cm^3 , 48 mmol) were dissolved in ethanol (30 cm^3) and the solution was heated at reflux for 3 h. After cooling to room temperature, the mixture was filtered and the resulting solid washed with acetic acid (1 \times 5 cm^3) and ethanol (3 \times 5 cm^3) then dried *in vacuo* to give an orange/yellow solid (2.07 g, 74%); ^1H NMR (400 MHz, CDCl_3) 1.71 – 1.82 (8H, m, CH_2), 2.44 – 2.58 (8H, m, CH_2), 4.23 (8H, s, br, $\text{CH}=\text{CH}$); $^{13}\text{C}\{^1\text{H}\}$ NMR (101 MHz, CDCl_3) 30.88 (s, CH_2), 78.71 (d, $^1J_{\text{RhP}} = 13.8$ Hz, $\text{CH}=\text{CH}$). NMR spectroscopic analyses are in good agreement with reported literature values.¹²

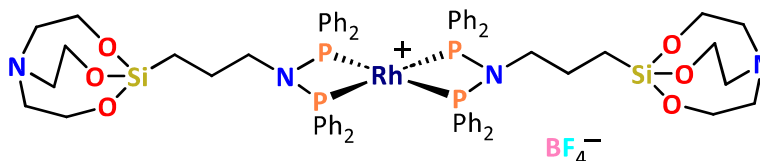
6.3.2.10 Synthesis of $[\text{Rh}(\text{COD})_2]\text{BF}_4$



$\text{Rh}_2\text{Cl}_2(\text{COD})_2$ (2.0 g, 4.1 mmol) and COD (1.0 cm^3 , 8.2 mmol) were dissolved in DCM (20 cm^3). A solution of AgBF_4 (1.6 g, 8.2 mmol) in DCM (40 cm^3) was then added dropwise and the solution stirred for 30 mins. The resulting mixture was then filtered and dried *in vacuo*. The crude product was then washed with diethyl ether (3 \times 5 cm^3) and dried *in vacuo* affording a red solid (2.92 g, 89%); ν_{max} / cm^{-1} 2922 (C-H), 2842 (C-H), 1556 br (C=C); ^1H NMR (400 MHz, CDCl_3) 2.44 – 2.57 (8H, m, CH_2), 2.58 – 2.71 (8H, m, CH_2), 5.37 (8H, s, br, $\text{CH}=\text{CH}$); $^{11}\text{B}\{^1\text{H}\}$ NMR (128 MHz, CDCl_3) -0.9 (s, br); $^{19}\text{F}\{^1\text{H}\}$ NMR (376 MHz, CDCl_3) -153.3 (s); $^{13}\text{C}\{^1\text{H}\}$ NMR (101 MHz, CDCl_3) 29.75 (s, CH_2), 107.54 (d, $^1J_{\text{RhP}} = 7.7$ Hz, $\text{CH}=\text{CH}$); Anal. Calcd for $\text{C}_{16}\text{H}_{24}\text{BF}_4\text{Rh}$: C, 47.33; H, 5.96. Found: C, 47.24; H, 5.79 %. NMR

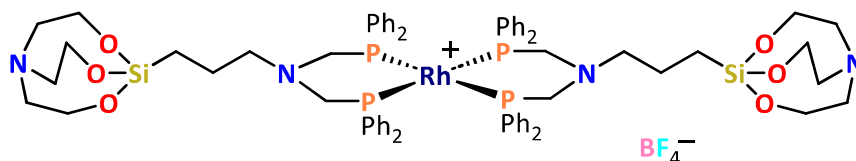
spectroscopic analysis and CHN elemental analysis showed are in agreement with reported literature values.¹³

6.3.2.11 Synthesis of $[\text{Rh}(\text{L5})_2]\text{BF}_4$



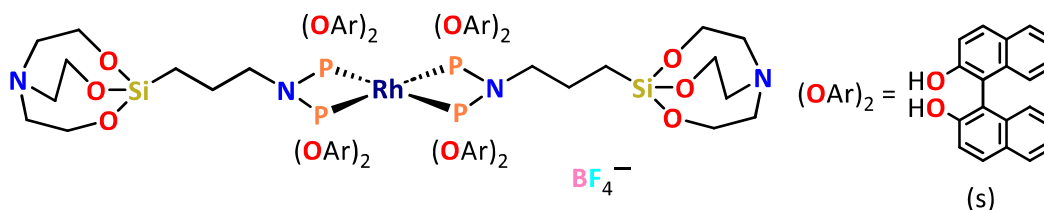
L5 (0.15 g, 0.2 mmol) was dissolved in THF (10 cm³) and added dropwise to a solution of $[\text{Rh}(\text{COD})_2]\text{BF}_4$ (0.10 g, 0.2 mmol) in THF (10 cm³). The mixture was stirred for 30 mins after which time NMR spectroscopic analysis of the crude reaction mixture showed conversion to $[\text{Rh}(\text{L5})_2]\text{BF}_4$ rather than $[\text{Rh}(\text{COD})(\text{L5})]\text{BF}_4$. A second equivalent of **L5** (0.15 g, 0.2 mmol) was then added and the resulting solution stirred for 1 h, then filtered. The filtrate was dried *in vacuo* to give a yellow solid (0.22 g, 64%); $\nu_{\text{max}}/\text{cm}^{-1}$ 3059 (C-H aromatic) 2964 (C-H), 2873 (C-H), 1632 (C=C), 1589 (C=C), 1436 (P-Ph), 910 (P-N); ¹H NMR (400 MHz, CDCl₃) -0.04 (4H, t, ³J_{HH} = 7.1 Hz, CH₂Si), 1.23 – 1.40 (4H, m, CH₂CH₂CH₂), 2.73 (12H, ³J_{HH} = 5.9 Hz, OCH₂CH₂N), 2.82 – 2.95 (4H, m, CH₂N(PPh₂)₂), 3.51 (12H, ³J_{HH} = 5.9 Hz, OCH₂CH₂N), 7.21 – 7.34 (32H, m, phenyl), 7.44 – 7.51 (8H, m, phenyl); ³¹P{¹H} NMR (162 MHz, CDCl₃) δ : +65 (d, ¹J_{RhP} = 124.5 Hz); ¹¹B{¹H} NMR (128 MHz, CDCl₃) -0.9 (s, br); ¹⁹F{¹H} NMR (376 MHz, CDCl₃) -154.2 (s); ¹³C{¹H} NMR (101 MHz, CDCl₃) 13.00 (s, SiCH₂), 25.65 (s, CH₂CH₂CH₂), 50.66 (s, OCH₂CH₂N), 52.71 (s, CH₂CH₂CH₂N), 57.34 (s, OCH₂CH₂N), 128.73 (t, ³J_{PC} = 2.6 Hz, aryl-C), 130.68 (s, aryl-C), 131.17 (s, aryl-C), 132.82 (t, dist, ²J_{PC} = 3.6 Hz, aryl-C); Anal. Calcd for C₆₆H₇₆BF₄N₄O₆P₄RhSi₂: C, 56.98; H, 5.51; N, 4.03. Found: C, 53.55; H, 5.97; N, 3.06 %. CHN result affected by silicon grease in sample.

6.3.2.12 Synthesis of $[\text{Rh}(\text{L17})_2]\text{BF}_4$



[Rh(COD)₂]BF₄ (0.20 g, 0.5 mmol) and **L17** (0.62 g, 1.0 mmol) were dissolved in THF (20 cm³) and stirred for 3 h. The solvent was removed *in vacuo* and the resulting solid washed with Et₂O (3 x 5 ml) and dried *in vacuo* to give a yellow solid (0.63 g, 74%); ν_{\max} /cm⁻¹ 3052 (C-H aromatic) 2981 (C-H), 2878 (C-H), 1587 (C=C), 1435 (P-Ph); ¹H NMR (400 MHz, CDCl₃) 0.30 – 0.38 (2H, m, SiCH₂), 1.58 – 1.66 (2H, m, CH₂CH₂CH₂), 2.80 (6H, t, ³J_{HH} = 5.8 Hz, OCH₂CH₂N), 2.84 – 2.90 (2H, m, CH₂CH₂N), 3.60 (4H, d, ²J_{PH} = 2.8 Hz, NCH₂P), 3.76 (6H, t, ³J_{HH} = 5.8 Hz, OCH₂CH₂N), 7.24 – 7.30 (10H, m, phenyl), 7.37 – 7.46 (10H, m, phenyl); ³¹P{¹H} NMR (162 MHz, CDCl₃) δ : -28; ¹³C{¹H} NMR (101 MHz, CD₂Cl₂) 13.69 (s, SiCH₂), 21.34 (s, CH₂CH₂CH₂), 50.96 (s, OCH₂CH₂N), 57.63 (s, OCH₂CH₂N), 58.55 (dd, ¹J_{PC} = 9.4 Hz, ³J_{PC} = 4.9 Hz, NCH₂P), 59.74 (s, CH₂N), 128.16 (s, aryl-C), 128.24 (d, ³J_{PC} = 2.1 Hz, aryl-C), 133.05 (d, ²J_{PC} = 18.5 Hz, aryl-C), 138.79 (d, ¹J_{PC} = 13.4 Hz, aryl-C). Anal. Calcd for C₇₀H₈₄BF₄N₄O₆P₄RhSi₂: C, 58.09; H, 5.85; N, 3.87. Found: C, 58.66; H, 6.03; N, 3.59 %.

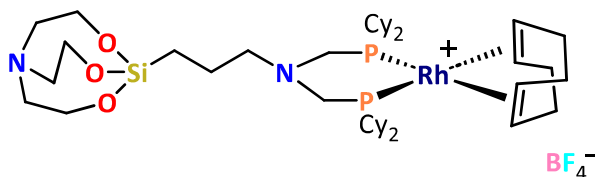
6.3.2.13 Synthesis of [Rh(COD)(L12)]BF₄



L12 (0.21 g, 0.2 mmol) was dissolved in THF (10 cm³) and added dropwise to a solution of [Rh(COD)₂]BF₄ (0.05 g, 0.2 mmol) in THF (10 cm³). The resulting mixture was stirred 2 h, then filtered. The filtrate was dried *in vacuo* to give an orange solid (0.15 g, 64%); ν_{\max} /cm⁻¹ 3067 (C-H aromatic), 2871 (C-H), 1620 (C=C), 1589 (C=C), 1068 (P-O), 870 (P-N); ¹H NMR (400 MHz, d⁸-THF) -0.87 – -0.72 (4H, m, CH₂Si), 0.84 – 0.98 (2H, m, CH₂CH₂CH₂), 1.27 – 1.41 (2H, m, CH₂CH₂CH₂), 1.78 – 1.94 (2H, m, CH₂N(PPh₂)₂), 2.36 – 2.47 (2H, m, CH₂N(PPh₂)₂), 2.62 (12H, ³J_{HH} = 5.9 Hz, OCH₂CH₂N), 3.25 – 3.40 (12H, m, OCH₂CH₂N), 6.78 – 6.82 (4H, m, phenyl), 7.04 – 7.15 (8H, m, phenyl), 7.16 – 7.27 (8H, m, phenyl), 7.31 – 7.37 (4H, m, phenyl), 7.42 – 7.57 (12H, m, phenyl), 7.68 – 7.73 (4H, m, phenyl), 7.97 – 8.02 (4H, m, phenyl), 8.09 – 8.14 (4H, m, phenyl); ³¹P{¹H} NMR (162 MHz, d⁸-THF) δ : +119 (d, ¹J_{RhP} = 198.2 Hz); B¹¹{¹H} NMR (128 MHz, d⁸-THF) -0.9 (s, br); F¹⁹{¹H} NMR (376 MHz, CDCl₃) -153.5 (s); ¹³C{¹H} NMR (101 MHz, d⁸-THF) 13.66 (s, SiCH₂), 26.75

(s, CH₂CH₂CH₂), 50.42 (s, OCH₂CH₂N), 51.88 (s, CH₂CH₂CH₂N), 56.98 (s, OCH₂CH₂N), 119.99 (s, aryl-C), 120.30 (s, aryl-C), 120.95 (s, aryl-C), 121.65 (s, aryl-C), 125.54 (s, aryl-C), 125.67 (s, aryl-C), 126.23 (s, aryl-C), 126.47 (s, aryl-C), 126.52 (s, aryl-C), 126.91 (s, aryl-C), 128.36 (s, aryl-C), 128.54 (s, aryl-C), 130.63 (s, aryl-C), 131.18 (s, aryl-C), 131.31 (s, aryl-C), 131.59 (s, aryl-C), 131.77 (s, aryl-C), 132.00 (s, aryl-C), 145.74 (s, aryl-C), 148.25 (s, aryl-C); Anal. Calcd for C₉₈H₈₄BF₄N₄O₁₄P₄RhSi₂·C₈H₁₂: C, 63.04; H, 4.79; N, 2.77. Found: C, 62.97; H, 4.85; N, 2.59 %.

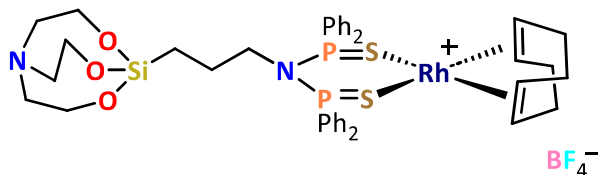
6.3.2.14 Synthesis of [Rh(COD)(L19)]BF₄



L19 (0.64 g, 1.0 mmol) and [Rh(COD)₂]BF₄ (0.20 g, 0.5 mmol) were dissolved in THF (20 cm³) and stirred for 3 h. Subsequently, ³¹P NMR spectroscopic analysis of an aliquot of reaction mixture showed the formation of [Rh(COD)(L19)]BF₄ rather than [Rh(L19)₂]BF₄, so a second equivalent of [Rh(COD)₂]BF₄ (0.20 g, 0.5 mmol) was added to complete conversion to [Rh(COD)(L19)]BF₄ and the reaction stirred for a further 3h. The solvent was then removed *in vacuo* and the resulting solid washed with hexane (3 × 5 cm³), then dried *in vacuo* to give a yellow solid (0.75 g, 75%); ν_{max} /cm⁻¹ 2922 (C-H), 2851 (C-H), 1632 (C=C); ¹H NMR (400 MHz, d⁸-THF) 0.24 – 0.32 (2H, m, SiCH₂), 1.23 – 1.69 (26H, m, Cy-H + SiCH₂CH₂), 1.76 (8H, s, CH₂CH=CH), 1.80 – 1.93 (8H, m, Cy-H), 1.96 – 2.04 (4H, m, Cy-H), 2.06 – 2.16 (4H, m, Cy-H), 2.21 – 2.29 (4H, m, Cy-H), 2.41 (2H, t, ³J_{HH} = 7.4 Hz, CH₂CH₂CH₂N), 2.84 (6H, t, ³J_{HH} = 6.0 Hz, OCH₂CH₂N), 2.92 (4H, s, br, NCH₂P), 3.68 (6H, t, ³J_{HH} = 6.0 Hz, OCH₂CH₂N), 5.27 (4H, s, br, CH₂CH=CH); ³¹P{¹H} NMR (162 MHz, d⁸-THF) δ : +9 (d, ¹J_{RhP} = 139.5 Hz); B¹¹{¹H} NMR (128 MHz, d⁸-THF) –1.1 (s, br); F¹⁹{¹H} NMR (376 MHz, CDCl₃) –153.4 (s); ¹³C{¹H} NMR (101 MHz, d⁸-THF) 13.96 (s, SiCH₂), 21.48 (s, CH₂CH₂CH₂), 26.15 (s, Cy-C), 27.06 (d, ²J_{PC} = 44.6 Hz, Cy-C), 28.89 (s, Cy-C), 30.36 (d, ²J_{RhC} = 11.7 Hz, CH₂CH=CH), 37.26 (d, ¹J_{PC} = 10.1 Hz, Cy-C), 50.32 (s, CH₂CH₂CH₂N), 50.69 (s, OCH₂CH₂N), 56.51 (s, CH₂CH₂CH₂N), 57.38 (s, OCH₂CH₂N), 128.22 (s, CH₂CH=CH); Anal.

Calcd for $C_{43}H_{78}BF_4N_2O_3P_2RhSi$: C, 54.32; H, 8.27; N, 2.95. Found: C, 54.88; H, 8.40; N, 2.35 %.

6.3.2.15 Synthesis of $[Rh(COD)(L5S_2)]BF_4$



L5S₂ (0.16 g, 0.2 mmol) was dissolved in THF (10 cm³) and added dropwise to a solution of $[Rh(COD)_2]BF_4$ (0.10 g, 0.2 mmol) in THF (10 cm³). The mixture was stirred for 30 mins and the resulting precipitate was then filtered and dried *in vacuo* affording a yellow solid (0.18 g, 78%); ν_{max}/cm^{-1} 3064 (C-H aromatic), 2977 (C-H), 2863 (C-H), 1587 (C=C), 1438 (P-Ph), 887 (P-N), 665 (P=S); ¹H NMR (400 MHz, CDCl₃) -0.46 (2H, t, ³J_{HH} = 6.6 Hz, CH₂Si), 0.09 – 1.02 (2H, m, CH₂CH₂CH₂), 1.74 – 1.82 (4H, m, CH₂CH=CH), 1.98 – 2.10 (4H, m, CH₂CH=CH), 2.75 (6H, t, ³J_{HH} = 5.9 Hz, OCH₂CH₂N), 3.20 – 3.36 (2H, m, CH₂N(P(S)Ph₂)₂), 3.49 (6H, t, ³J_{HH} = 5.9 Hz, OCH₂CH₂N), 4.17 (4H, s, br, CH=CH), 7.67 – 7.75 (8H, m, phenyl), 7.78 – 7.88 (12H, m, phenyl); ³¹P{¹H} NMR (162 MHz, CDCl₃) δ : +65 (d, ²J_{RhP} = 4.3 Hz); ¹¹B{¹H} NMR (128 MHz, CDCl₃) -0.8 (s, br); ¹⁹F{¹H} NMR (376 MHz, CDCl₃) -153.9 (s); ¹³C{¹H} NMR (101 MHz, CDCl₃) 12.80 (s, SiCH₂), 25.62 (s, CH₂CH₂CH₂), 30.78 (s, CH₂CH=CH), 50.31 (s, OCH₂CH₂N), 54.71 (s, CH₂CH₂CH₂N), 57.07 (s, OCH₂CH₂N), 84.57 (d, ¹J_{RhC} = 11.9 Hz, CH₂CH=CH), 128.26 (s, aryl-C), 129.50 (t, dist, ³J_{PC} = 6.9 Hz, aryl-C), 132.54 (t, dist, ²J_{PC} = 5.9 Hz, aryl-C), 134.21 (s, aryl-C). Anal. Calcd for $C_{41}H_{50}BF_4N_2O_3P_2RhS_2Si$: C, 51.15; H, 5.24; N, 2.91. Found: C, 51.17; H, 5.30; N, 2.84 %.

6.3.3 Synthesis of Palladium(II) complexes

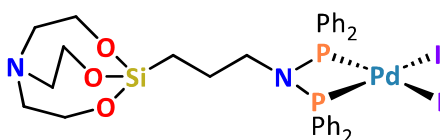
6.3.3.1 General procedure for the synthesis of PdI₂(P[^]P) complexes

PdCl₂(MeCN)₂ or PdCl₂(COD) (1 eq., ~0.4 mmol), P[^]P (1 eq., 0.4 mmol) and NaI (10 eq., ~4 mmol) were dissolved in acetone (20 cm³) and stirred for 3 h. The solvent was removed *in vacuo* and DCM (10 cm³) added resulting in a coloured solution and white

precipitate. Upon filtration of the mixture, hexane (20 cm³) was added to the solution, resulting in a precipitate that was isolated by filtration and dried *in vacuo* to give the target compound.

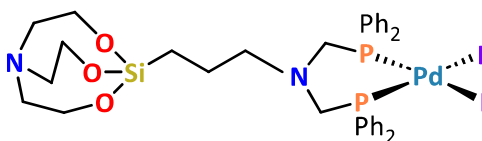
Note: CHN analysis of palladium halide compounds consistently gave lower C, H and N values than expected, despite analysis of single crystals of each compound, suggesting incomplete combustion during analysis.

6.3.3.1.1 Synthesis of PdI₂(L5)



Isolated as an orange solid (0.25 g, 68%). Single crystals suitable for XRD analysis were obtained by layering a solution of the compound in CDCl₃ with hexane; ν_{\max} /cm⁻¹ 3051 (C-H aromatic), 2909 (C-H), 2859 (C-H), 1584 (C=C), 1432 (P-Ph), 904 (P-N); ¹H NMR (400 MHz, CDCl₃) -0.02 (2H, t, ³J_{HH} = 7.4 Hz, SiCH₂), 1.29 – 1.38 (2H, m, CH₂CH₂CH₂), 2.70 (6H, t, ³J_{HH} = 5.9 Hz, OCH₂CH₂N), 2.81 – 2.94 (2H, m, CH₂N(PPh₂)₂), 3.53 (6H, t, ³J_{HH} = 5.9 Hz, OCH₂CH₂N), 7.46 – 7.54 (8H, m, phenyl), 7.58 – 7.64 (4H, m, phenyl), 7.83 – 7.92 (8H, m, phenyl); ³¹P{¹H} NMR (162 MHz, CDCl₃) δ : +23; ¹³C{¹H} NMR (101 MHz, CDCl₃) 10.88 (s, SiCH₂), 25.24 (s, CH₂CH₂CH₂), 50.87 (s, OCH₂CH₂N), 54.86 (s, CH₂N(PPh₂)₂), 57.34 (s, OCH₂CH₂N), 128.63 (s, aryl-C), 128.96 (t, ³J_{PC} = 6.2 Hz aryl-C), 132.79 (s, aryl-C), 133.91 (t, ²J_{PC} = 6.4 Hz, aryl-C); Anal. Calcd for C₃₃H₃₈I₂N₂O₃P₂PdSi: C, 41.25; H, 3.99; N, 2.92. Found: C, 39.02; H, 3.81; N, 2.76 %.

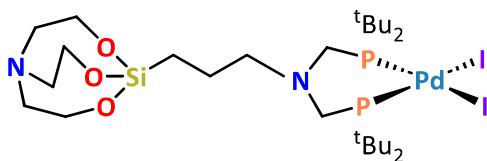
6.3.3.1.2 Synthesis of PdI₂(L17)



Isolated as an orange solid (0.13 g, 75%); Single crystals suitable for XRD analysis were obtained by layering a solution of the compound in DCM with hexane; ν_{\max} /cm⁻¹ 3050

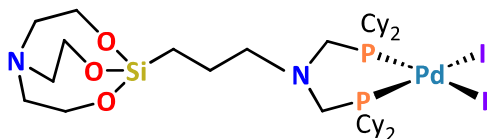
(C-H aromatic), 2937 (C-H), 2863 (C-H), 1621 (C=C), 1585 (C=C), 1431 (P-Ph); ^1H NMR (400 MHz, CDCl_3) 0.14 – 0.22 (2H, m, SiCH_2), 1.37 – 1.48 (2H, m, $\text{CH}_2\text{CH}_2\text{CH}_2$), 2.55 (2H, t, $^3J_{\text{HH}} = 7.9$ Hz, $\text{CH}_2\text{CH}_2\text{CH}_2\text{N}$), 2.80 (6H, t, $^3J_{\text{HH}} = 5.9$ Hz, $\text{OCH}_2\text{CH}_2\text{N}$), 3.42 (4H, d, $^2J_{\text{PH}} = 1.3$ Hz, NCH_2P) 3.72 (6H, t, $^3J_{\text{HH}} = 5.9$ Hz, $\text{OCH}_2\text{CH}_2\text{N}$), 7.36 – 7.42 (8H, m, phenyl), 7.43 – 7.49 (4H, m, phenyl), 7.79 – 7.87 (8H, m, phenyl); $^{31}\text{P}\{^1\text{H}\}$ NMR (162 MHz, CDCl_3) δ : -6; $^{13}\text{C}\{^1\text{H}\}$ NMR (101 MHz, CDCl_3) 13.44 (s, SiCH_2), 19.39 (s, $\text{CH}_2\text{CH}_2\text{CH}_2$), 50.91 (s, $\text{OCH}_2\text{CH}_2\text{N}$), 56.98 (d, $^1J_{\text{PC}} = 47.1$ Hz, NCH_2P), 57.59 (s, $\text{OCH}_2\text{CH}_2\text{N}$), 66.60 (t, $^3J_{\text{PC}} = 9.1$ Hz, $\text{CH}_2\text{CH}_2\text{CH}_2\text{N}$), 128.26 (t, $^3J_{\text{PC}} = 5.5$ Hz, aryl-C), 131.00 (s, aryl-C), 131.60 (d, $^1J_{\text{PC}} = 3.6$ Hz, aryl-C), 134.02 (t, $^2J_{\text{PC}} = 4.8$ Hz, aryl-C); Anal. Calcd for $\text{C}_{35}\text{H}_{42}\text{I}_2\text{N}_2\text{O}_3\text{P}_2\text{PdSi}$: C, 42.51; H, 4.28; N, 2.83. Found: C, 40.00; H, 4.18; N, 2.60 %.

6.3.3.1.3 Synthesis of $\text{PdI}_2(\text{L18})$



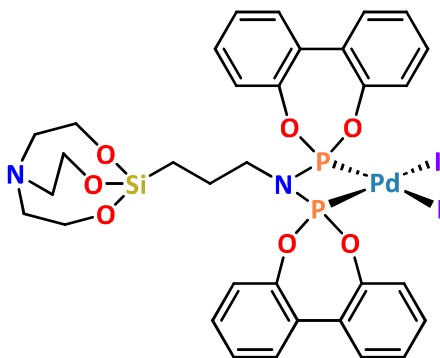
Isolated as a brown solid (0.23 g, 73%). Single crystals suitable for XRD analysis were obtained by layering a solution of the compound in CDCl_3 with hexane; $\nu_{\text{max}}/\text{cm}^{-1}$ 2945 (C-H), 2867 (C-H); ^1H NMR (400 MHz, CDCl_3) 0.34 – 0.41 (2H, m, SiCH_2), 1.60 (36H, d, $^3J_{\text{PH}} = 13.9$ Hz, $\text{C}(\text{CH}_3)_3$), 1.62 – 1.71 (2H, m, $\text{CH}_2\text{CH}_2\text{CH}_2$), 2.70 (2H, t, $^3J_{\text{HH}} = 7.9$ Hz, $\text{CH}_2\text{CH}_2\text{CH}_2\text{N}$), 2.87 (6H, t, $^3J_{\text{HH}} = 5.9$ Hz $\text{OCH}_2\text{CH}_2\text{N}$), 3.04 (4H, d, $^2J_{\text{PH}} = 2.6$ Hz, NCH_2P) 3.81 (6H, t, $^3J_{\text{HH}} = 5.9$ Hz, $\text{OCH}_2\text{CH}_2\text{N}$); $^{31}\text{P}\{^1\text{H}\}$ NMR (162 MHz, CDCl_3) δ : +37; $^{13}\text{C}\{^1\text{H}\}$ NMR (101 MHz, CDCl_3) 13.77 (s, SiCH_2), 20.13 (s, $\text{CH}_2\text{CH}_2\text{CH}_2$), 31.77 (s, $\text{PC}(\text{CH}_3)_3$), 39.42 (d, $^1J_{\text{PC}} = 14.2$ Hz, NCH_2P), 50.99 (s, $\text{OCH}_2\text{CH}_2\text{N}$), 57.70 (s, $\text{OCH}_2\text{CH}_2\text{N}$), 62.61 (s, $\text{CH}_2\text{CH}_2\text{CH}_2\text{N}$). CHN unsuccessful.

6.3.3.1.4 Synthesis of $\text{PdI}_2(\text{L19})$



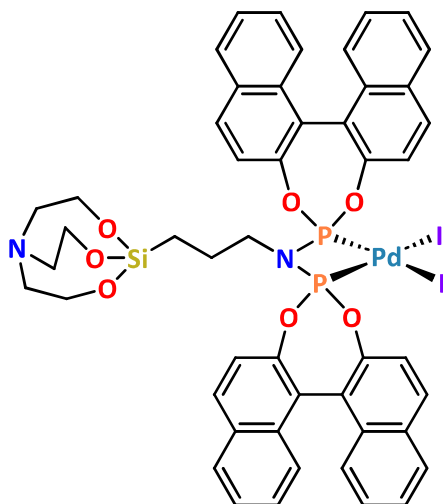
Isolated as a brown solid (0.49 g, 69%). Single crystals suitable for XRD analysis were obtained by layering a solution of the compound in DCM with hexane; $\nu_{\max}/\text{cm}^{-1}$ 3919 (C-H), 2850 (C-H); ^1H NMR (400 MHz, CDCl_3) 0.35 – 0.42 (2H, m, SiCH_2), 1.12 – 1.57 (22H, m, Cy-H + SiCH_2), 1.60 – 1.85 (14H, m, Cy-H), 1.95 – 2.05 (4H, m, Cy-H), 2.35 – 2.47 (4H, m, Cy-H), 2.61 (2H, t, $^3J_{\text{HH}} = 7.7$ Hz, $\text{CH}_2\text{CH}_2\text{CH}_2\text{N}$), 2.74 – 2.79 (2H, m, Cy-H), 2.84 (4H, d, $^2J_{\text{PC}} = 1.6$ Hz, NCH_2P), 2.87 (6H, t, $^3J_{\text{HH}} = 5.8$ Hz, $\text{OCH}_2\text{CH}_2\text{N}$), 3.81 (6H, t, $^3J_{\text{HH}} = 5.8$ Hz, $\text{OCH}_2\text{CH}_2\text{N}$); $^{31}\text{P}\{^1\text{H}\}$ NMR (162 MHz, CDCl_3) +24; $^{13}\text{C}\{^1\text{H}\}$ NMR (101 MHz, CDCl_3) 13.76 (s, SiCH_2), 20.13 (s, $\text{CH}_2\text{CH}_2\text{CH}_2$), 25.88 (s, Cy-C), 27.08 (d, $^2J_{\text{PC}} = 29.8$ Hz, Cy-C), 29.88 (s, Cy-C), 30.86 (s, Cy-C), 48.71 (d, $^1J_{\text{PC}} = 41.8$ Hz, NCH_2P), 51.05 (s, $\text{OCH}_2\text{CH}_2\text{N}$), 57.73 (s, $\text{OCH}_2\text{CH}_2\text{N}$), 66.57 (s, $\text{CH}_2\text{CH}_2\text{CH}_2\text{N}$); Anal. Calcd for $\text{C}_{35}\text{H}_{66}\text{I}_2\text{N}_2\text{O}_3\text{P}_2\text{PdSi}$: C, 41.49; H, 6.57; N, 2.76. Found: C, 41.02; H, 6.64; N, 2.59 %.

6.3.3.1.5 Synthesis of $\text{PdI}_2(\text{L11})$



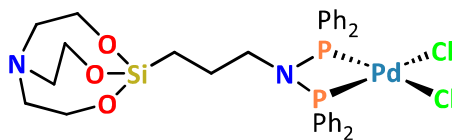
Isolated as a red solid (0.18 g, 63%). Single crystals suitable for XRD analysis were obtained by layering a solution of the compound in CD_2Cl_2 with hexane; $\nu_{\max}/\text{cm}^{-1}$ 3063 (C-H aromatic), 2922 (C-H), 2874 (C-H), 1607 (C=C), 1567 (C=C) 1042 (P-O), 873 (P-N); ^1H NMR (400 MHz, CDCl_3) -0.17 (2H, t, $^3J_{\text{HH}} = 7.9$ Hz, SiCH_2), 1.21 – 1.27 (2H, m, $\text{CH}_2\text{CH}_2\text{CH}_2$), 2.72 (6H, t, $^3J_{\text{HH}} = 5.9$ Hz, $\text{OCH}_2\text{CH}_2\text{N}$), 2.73 – 2.77 (2H, m, $\text{CH}_2\text{N}(\text{PPh}_2)_2$), 3.59 (6H, t, $^3J_{\text{HH}} = 5.9$ Hz, $\text{OCH}_2\text{CH}_2\text{N}$), 7.41 – 7.48 (4H, m, aryl), 7.49 – 7.60 (8H, m, phenyl), 7.64 – 7.69 (2H, m, phenyl), 7.93 – 8.00 (2H, m, phenyl); $^{31}\text{P}\{^1\text{H}\}$ NMR (162 MHz, CDCl_3) δ : +67; $^{13}\text{C}\{^1\text{H}\}$ NMR (101 MHz, CDCl_3); Anal. Calcd for $\text{C}_{33}\text{H}_{34}\text{I}_2\text{N}_2\text{O}_7\text{P}_2\text{PdSi}$: C, 38.82; H, 3.36; N, 2.74. Found: C, 36.76; H, 3.32; N, 2.62 %. $^{13}\text{C}\{^1\text{H}\}$ NMR Singal intensity too low interpretation due to poor solubility of the compound in CDCl_3 .

6.3.3.1.6 Synthesis of PdI₂(L12)



Isolated as a red solid (0.18 g, 62%). Single crystals suitable for XRD analysis were obtained by layering a solution of the compound in CDCl₃ with hexane; ν_{\max} /cm⁻¹ 3069 (C-H aromatic), 2925 (C-H), 2874 (C-H), 1619 (C=C), 1590 (C=C) 1069 (P-O), 890 (P-N); ¹H NMR (400 MHz, CDCl₃) -0.60 – -0.46 (1H, m, SiCH₂), -0.41 – -0.28 (1H, m, SiCH₂), 0.95 – 1.04 (1H, m, CH₂CH₂CH₂), 1.28 – 1.42 (1H, m, CH₂CH₂CH₂), 2.11 – 2.32 (1H, m, CH₂CH₂CH₂N), 2.56 (6H, t, ³J_{HH} = 5.9 Hz, OCH₂CH₂N), 2.67 – 2.82 (1H, m, CH₂CH₂CH₂N), 3.25 – 3.40 (6H, m, OCH₂CH₂N), 7.27 – 7.36 (6H, m, aryl), 7.38 – 7.43 (2H, m, aryl), 7.47 – 7.56 (4H, m, aryl), 7.66 (2H, d, ³J_{HH} = 8.9 Hz, aryl), 7.87 (2H, d, ³J_{HH} = 8.9 Hz, aryl), 7.94 (2H, d, ³J_{HH} = 8.3 Hz, aryl), 7.98 – 8.03 (4H, m, aryl), 8.14 (2H, d, ³J_{HH} = 8.9 Hz, aryl); ³¹P{¹H} NMR (162 MHz, CDCl₃) δ : +68; ¹³C{¹H} NMR (101 MHz, CDCl₃) 13.34 (s, SiCH₂), 26.12 (s, CH₂CH₂CH₂), 50.79 (s, OCH₂CH₂N), 52.58 (s, CH₂CH₂CH₂N), 57.18 (s, OCH₂CH₂N), 119.82.63 (s, aryl-C), 121.37 (s, aryl-C), 121.53 (s, aryl-C), 121.55 (s, aryl-C), 122.55 (s, aryl-C), 126.08 (s, aryl-C), 126.10 (s, aryl-C), 126.75 (s, aryl-C), 126.89 (s, aryl-C), 127.24 (s, aryl-C), 127.45 (s, aryl-C), 128.60 (s, aryl-C), 128.82 (s, aryl-C), 131.42 (s, aryl-C), 131.74 (s, aryl-C), 131.79 (s, aryl-C), 132.19 (s, aryl-C), 132.37 (s, aryl-C), 147.24 (s, aryl-C), 148.42 (s, aryl-C); Anal. Calcd for C₄₉H₄₂I₂N₂O₇P₂PdSi: C, 48.20; H, 3.47; N, 2.29. Found: C, 47.04; H, 3.53; N, 2.18 %.

6.3.3.2 Synthesis of PdCl₂(L5)



L5 (0.175 g, 0.3 mmol) and PdCl₂(MeCN)₂ (0.075 g, 0.3 mmol) were dissolved in DCM (10 cm³) and stirred overnight. The reaction mixture was then layered with Et₂O (15 cm³) resulting in crystals suitable for XRD analysis (Figure 6.3). The crystals were filtered and dried *in vacuo* to give a pale yellow solid (0.12 g, 56%); $\nu_{\text{max}}/\text{cm}^{-1}$ 3050 (C-H aromatic), 2966 (C-H), 2869 (C-H), 1585 (C=C), 1571 (C=C), 890 (P-N); ¹H NMR (400 MHz, CDCl₃) δ : 0.02 (2H, t, ³J_{HH} = 7.3 Hz, SiCH₂), 1.36 – 1.45 (2H, m, CH₂CH₂CH₂), 2.71 (6H, t, ³J_{HH} = 5.9 Hz, OCH₂CH₂N), 2.92 – 3.07 (2H, m, CH₂N(PPh₂)₂), 3.54 (6H, t, ³J_{HH} = 5.9 Hz, OCH₂CH₂N), 7.51 (8H, t, ³J_{HH} = 7.2 Hz, phenyl), 7.62 (4H, t, ³J_{HH} = 7.4 Hz, phenyl), 7.84 – 7.92 (8H, m, phenyl); ³¹P{¹H} NMR (162 MHz, CDCl₃) δ : + 30; ¹³C{¹H} NMR (101 MHz, CDCl₃) δ : 12.92 (s, SiCH₂), 25.63 (s, CH₂CH₂CH₂), 50.83 (s, OCH₂CH₂N), 52.09 (t, ²J_{PC} = 4.4 Hz, CH₂N(PPh₂)₂), 57.35 (s, OCH₂CH₂N), 127.04 (d, ¹J_{PC} = 12.3 Hz aryl-C), 129.25 (t, ³J_{PC} = 6.3 Hz, aryl-C), 133.04 (s, aryl-C), 133.75 (t, ²J_{PC} = 6.7 Hz, aryl-C); Anal. Calcd for C₃₃H₃₈Cl₂N₂O₃P₂PdSi: C, 50.94; H, 4.92; N, 3.60. Found: C, 48.64; H, 4.56; N, 3.51 %.

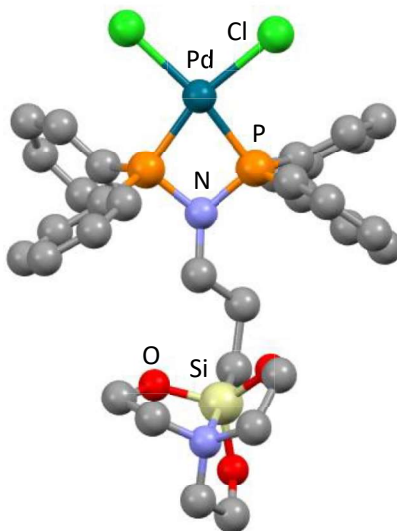


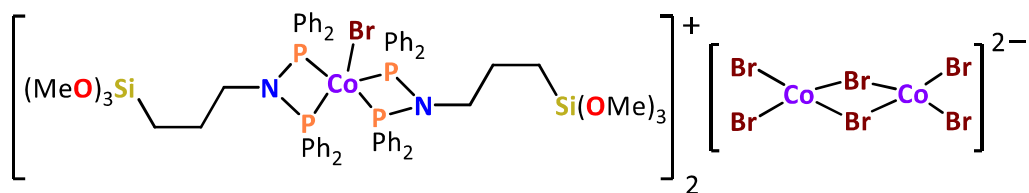
Figure 6.3. Molecular structure of PdCl₂(L5). Hydrogen atoms and alkyl chain disorder omitted for clarity. Selected bond lengths / Å: Pd-P 2.214(1), 2.217(1); P-N 1.691(4), 1.701(4); Selected bond angles / °: P-Rh-P 71.38(5); P-N-P 99.3(2).

6.3.4 Synthesis of cobalt(II) complexes

6.3.4.1 General procedure for synthesis of $\text{CoBr}_2(\text{P}^{\wedge}\text{P})$ complexes

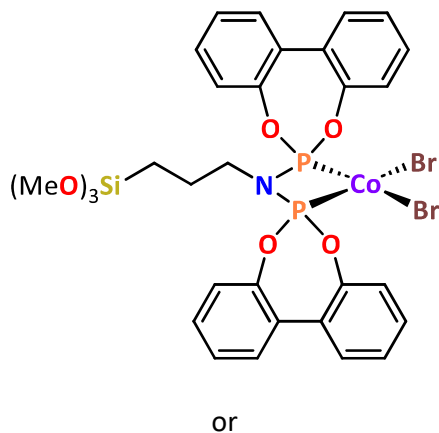
CoBr_2 (1 eq., 0.08 g, 0.4 mmol) and $\text{P}^{\wedge}\text{P}$ (1 eq., 0.4 mmol,) were dissolved in THF (15 cm^3) and stirred overnight. The solvent was then removed *in vacuo* and the resulting solid washed with Et_2O ($3 \times 5 \text{ cm}^3$), then dried *in vacuo* to give the product as a green/brown solid.

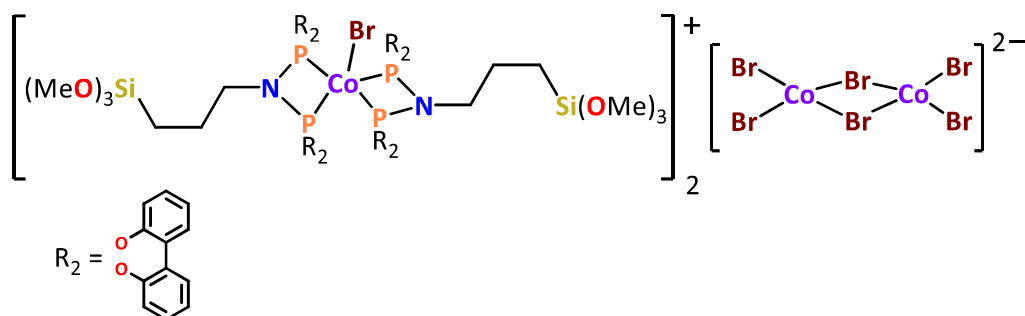
6.3.4.1.1 Synthesis of $\text{CoBr}_2(\text{L1})$



Brown solid (0.15 g, 54%). Single crystals suitable for XRD were obtained from a solution of $[\text{CoBr}_2(\text{L1})]$ in PhCl layered with hexane; $\nu_{\text{max}} / \text{cm}^{-1}$ 3053 (C-H aromatic), 2964 (C-H), 2838 (Si-OMe), 1587 (C=C), 1435 (P-Ph), 869 (P-N); Anal. Calcd for $\text{C}_{30}\text{H}_{35}\text{Br}_2\text{CoNO}_3\text{P}_2\text{Si}$: C, 47.02; H, 4.60; N, 1.83. Found: C, 47.41; H, 4.56; N, 1.95 %.

6.3.4.1.2 Synthesis of $\text{CoBr}_2(\text{L2})$:



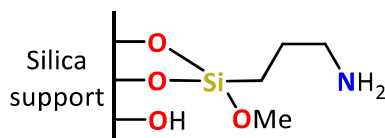


Green solid (0.15 g, 54%); $\nu_{\text{max}} / \text{cm}^{-1}$ 3058 (C-H aromatic), 2970 (C-H), 2840 (Si-OMe), 1605 (C=C), 1567 (C=C), 1044 (P-O), 900 (P-N); Anal. Calcd for $\text{C}_{30}\text{H}_{31}\text{Br}_2\text{CoNO}_7\text{P}_2\text{Si}$: C, 43.60; H, 3.78; N, 1.70. Found: C, 42.60; H, 4.15; N, 1.92 %.

6.4 Chapter 4 experimental

6.4.1 Synthesis and stability testing of silica-immobilised (3-aminopropyl)trimethoxysilane

6.4.1.1 Synthesis of silica-immobilised (3-aminopropyl)trimethoxysilane



(3-Aminopropyl)trimethoxysilane (0.1 cm^3 , 0.75 mmol) and AEROPERL 300/30 silica (0.25 g) were heated at reflux in toluene (10 cm^3) for 2 hours. The resulting mixture was filtered and allowed to cool to room temperature, and the solid washed with toluene (3 x 5 cm^3), before being dried *in vacuo* to give a white solid (0.33 g, 94 %); $\nu_{\text{max}} / \text{cm}^{-1}$ 1076 (Si-O), 807 (Si-O); ^{29}Si CP MAS NMR (79 MHz, versus $\text{Si}(\text{SiCH}_3)_4 = -9.9$ ppm): 51 (T^1), 58 (T^2), 65 (T^3), 109 (Si-O_4). Found: C, 3.02; H, 0.40; N, 0.83 %.

6.4.1.2 Silica-immobilised (3-aminopropyl)trimethoxysilane water stability test

Silica-immobilised (3-aminopropyl)trimethoxysilane (0.10 g) was stirred in water (5 cm^3) for 30 min, then filtered and dried *in vacuo* to give a white solid (0.10 g, 100 %); ^{29}Si CP

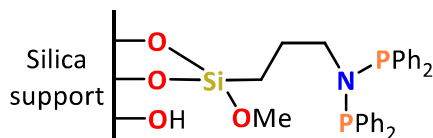
MAS NMR (79 MHz, versus $\text{Si}(\text{SiCH}_3)_4 = -9.9$ ppm): 51 (T^1), 58 (T^2), 65 (T^3), 100 (HO-Si-O_3), 109 (Si-O_4).

6.4.1.3 Silica-immobilised (3-aminopropyl)trimethoxysilane water/methanol stability test

Silica-immobilised (3-aminopropyl)trimethoxysilane (0.10 g) was stirred in a 50/50 mixture of water and methanol (5 cm^3) for 30 min, then filtered and dried *in vacuo* to give a white solid (0.10 g, 100 %); ^{29}Si CP MAS NMR (79 MHz, versus $\text{Si}(\text{SiCH}_3)_4 = -9.9$ ppm): 58 (T^2), 65 (T^3), 100 (HO-Si-O_3), 109 (Si-O_4).

6.4.2 Silica-immobilisation of phosphine compounds

6.4.2.1 Synthesis of silica-immobilised L1



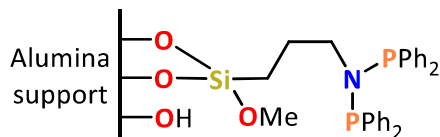
L1 (0.13 g, 0.22 mmol) and AEROPERL 300/30 silica (0.28 g) were heated at reflux in toluene (10 cm^3) for 2 hours or stirred at rt overnight. The resulting mixture was filtered, after cooling to room temperature, and the solid washed with toluene (3 \times 5 cm^3), before being dried *in vacuo* to give a white solid (0.40 g, 98%); $\nu_{\text{max}}/\text{cm}^{-1}$ 2978 (C-H), 1064 (Si-O), 804 (Si-O); ^{29}Si CP MAS NMR (79 MHz, versus $\text{Si}(\text{SiCH}_3)_4 = -9.9$ ppm): 48 (T^1), 56 (T^2), 101 (Si-OH), 108 (Si-O_4); ^{31}P CP MAS NMR (162 MHz, versus 85 % $\text{H}_3\text{PO}_4 = 0.0$ ppm) 23.4 (O=PPh_2), 59.0 (PPh_2). Found: C, 5.55; H, 0.40; N, 0.33 %.

6.4.2.2 Investigation into phosphine-silica reactivity

AEROPERL 300/30 silica (0.1 g), and **L14** (0.05 g, 0.08 mmol) were added to toluene (10 cm^3) and refluxed for 12 h, after which an aliquot of the reaction mixture was analysed by ^{31}P NMR spectroscopy. MeOH (0.007 cm^3 , 0.16 mmol) was added to the bulk mixture,

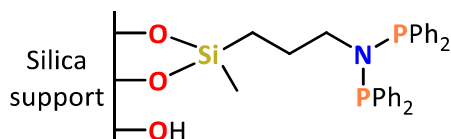
which was stirred at room temperature for 24 h. ^{31}P NMR spectroscopic analysis of a second aliquot of reaction mixture showed complete consumption of start material.

6.4.2.3 Synthesis of alumina-immobilised L1



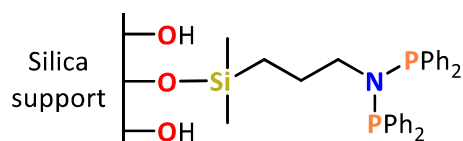
L1 (0.06 g, 0.05 mmol) and alumina (0.26 g) were stirred in toluene (10 cm³) for overnight. The resulting mixture was filtered, and the solid washed with toluene (3 × 5 cm³), before being dried *in vacuo* to give a white solid (0.21 g, 81%); ^{29}Si CP MAS NMR (79 MHz, versus $\text{Si}(\text{SiCH}_3)_4 = -9.9$ ppm): 47 (T^1); $\nu_{\text{max}}/\text{cm}^{-1}$ 1239 (Al-OH), 500 (Al-O); ^{31}P CP MAS NMR (162 MHz, versus 85 % $\text{H}_3\text{PO}_4 = 0.0$ ppm) + 35.8 (PPh_2), + 58.2 (PPh_2); Found: C, 6.11; H, 0.66; N, 0.24 %.

6.4.2.4 Synthesis of silica-immobilised L2



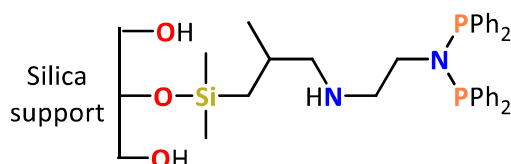
AEROPERL 300/30 silica calcined at 200 °C (0.25 g) and **L2** (25 mg, 0.05 mmol) were added to toluene (10 cm³) and stirred overnight. The suspension was then filtered and washed with toluene (3 × 5 cm³), then dried *in vacuo* to give a white solid (0.11 g, 40 %); $\nu_{\text{max}}/\text{cm}^{-1}$ 1069 (Si-O), 803 (Si-O); ^{29}Si CP MAS NMR (79 MHz, versus $\text{Si}(\text{SiCH}_3)_4 = -9.9$ ppm) -6 ($\text{OSi}(\text{CH}_3)(\text{OMe})\text{CH}_2$), -10 ($\text{O}_2\text{-Si}(\text{CH}_3)\text{CH}_2$), -101 (Si-OH), -109 (Si-O_4); ^{31}P CP MAS NMR (162 MHz, versus 85 % $\text{H}_3\text{PO}_4 = 0.0$ ppm) +29 ($\text{P}(\text{O})\text{Ph}_2$), + 57 (PPh_2); Found: C, 3.11; H, 0.37; N, 0.18 %.

6.4.2.5 Synthesis of silica-immobilised L3



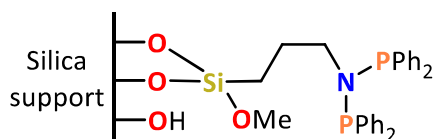
AEROPERL 300/30 silica calcined at 200 °C (0.24 g) and **L3** (22 mg, 0.05 mmol) were added to toluene (10 cm³) and stirred at reflux for 3 h. Upon cooling to room temperature the suspension was filtered and washed with toluene (3 × 5 cm³), then dried *in vacuo* to give a white solid (0.16 g, 62 %); $\nu_{\max}/\text{cm}^{-1}$ 1072 (Si-O), 806 (Si-O); ²⁹Si CP MAS NMR (79 MHz, versus Si(SiCH₃)₄ = −9.9 ppm) +14 (OSi(CH₃)₂CH₂), −100 (Si-OH), −109 (Si-O₄); ³¹P CP MAS NMR (162 MHz, versus 85 % H₃PO₄ = 0.0 ppm) +29 (P(O)Ph₂), +56 (PPh₂). Found: C, 1.29; H, 0.00; N, 0.00 %. CHN experimental error resulted in reported small negative values of H and N %.

6.4.2.6 Synthesis of silica-immobilised L4



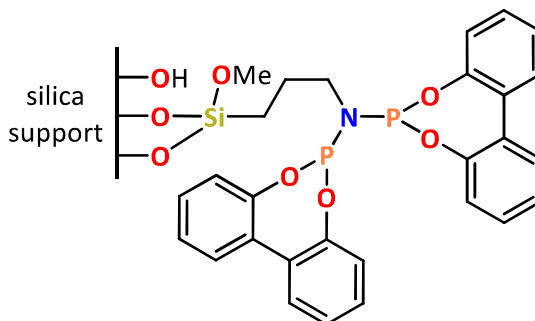
AEROPERL 300/30 silica calcined at 200 °C (0.24 g) and **L4** (20 mg, 0.05 mmol) were added to toluene (10 cm³) and stirred at rt for 3 h. The suspension was then filtered and washed with toluene (3 × 5 cm³), then dried *in vacuo* to give a white solid (0.11 g, 42 %); $\nu_{\max}/\text{cm}^{-1}$ 1064 (Si-O), 801 (Si-O); ²⁹Si CP MAS NMR (79 MHz, versus Si(SiCH₃)₄ = −9.9 ppm) +12 (OSi(CH₃)₂CH₂), −101 (Si-OH), −107 (Si-O₄); ³¹P CP MAS NMR (162 MHz, versus 85 % H₃PO₄ = 0.0 ppm) +29 (P(O)Ph₂), +57 (PPh₂); Found: C, 9.91; H, 0.88; N, 0.67 %.

6.4.2.7 Attempted two-step synthesis of silica-immobilised L1



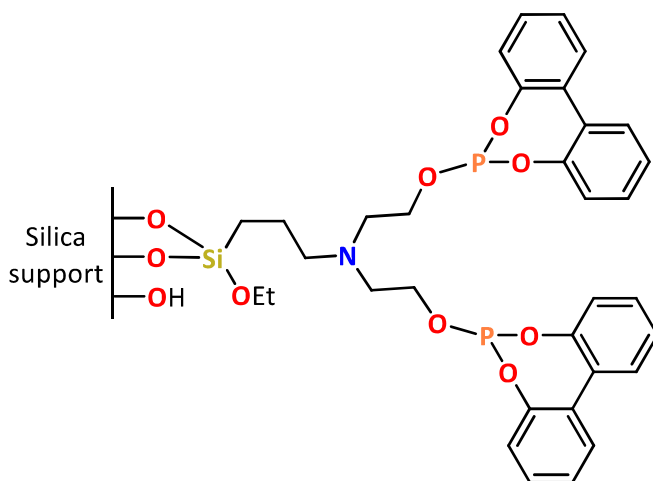
(3-aminopropyl)trimethoxysilane (0.1 cm^3 , 0.22 mmol) and AEROPERL 300/30 silica (0.40 g) were stirred overnight in toluene (10 cm^3). The resulting mixture was filtered, and the solid washed with toluene ($3 \times 5 \text{ cm}^3$). Toluene (10 cm^3) and Net_3 (0.1 cm^3 , 0.7 mmol) and Ph_2PCI (0.1 cm^3 , 0.7 mmol) were then added and the resultant mixture stirred overnight. Following this the solid was filtered and washed with toluene ($3 \times 5 \text{ cm}^3$) and chloroform ($3 \times 5 \text{ cm}^3$) and dried *in vacuo* to give an off-white solid (0.32 g , 80%); $\nu_{\text{max}}/\text{cm}^{-1}$ 1067 (Si-O), 808 (Si-O); ^{29}Si CP MAS NMR (79 MHz, versus $\text{Si}(\text{SiCH}_3)_4 = -9.9 \text{ ppm}$): -50 ($\text{O-Si}(\text{OCH}_3)_2\text{CH}_2$), -58 ($\text{O}_2\text{-Si}(\text{OCH}_3)\text{CH}_2$), -101 (Si-OH), -109 (Si-O_4); ^{31}P CP MAS NMR (162 MHz, versus 85% $\text{H}_3\text{PO}_4 = 0.0 \text{ ppm}$) $+23$ ($\text{P}(\text{O})\text{Ph}_2$), $+40$ (HNPPH_2) $+57$ ($\text{N}(\text{PPh}_2)_2$); Found: C, 14.25; H, 1.24; N, 0.99 %.

6.4.2.8 Attempted synthesis of silica-immobilised L9



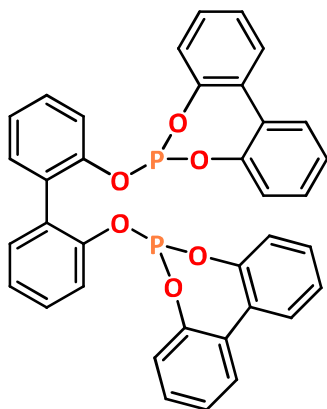
L9 (0.10 g , 0.17 mmol) and AEROPERL 300/30 silica (0.25 g) were heated at reflux in toluene (10 cm^3) for 12 h. The resulting mixture was filtered, after cooling to room temperature, and the solid washed with toluene ($3 \times 5 \text{ cm}^3$), before being dried *in vacuo* to give a white solid (0.11 g , 27%); $\nu_{\text{max}}/\text{cm}^{-1}$ 1067 (Si-O), 811 (Si-O); ^{29}Si CP MAS NMR (79 MHz, versus $\text{Si}(\text{SiCH}_3)_4 = -9.9 \text{ ppm}$): -59 (T^2), -66 (T^3), -102 (Si-OH), -110 (Si-O_4); ^{31}P CP MAS NMR (162 MHz, versus 85% $\text{H}_3\text{PO}_4 = 0.0 \text{ ppm}$) -8.4 , 4.7 ; Found: C, 11.94; H, 1.50; N, 0.32 %.

6.4.2.9 Attempted synthesis of silica-immobilised L21



L21 (0.10 g, 0.14 mmol) and AEROPERL 300/30 silica (0.25 g) were heated at reflux in toluene (10 cm³) for 12 h. The resulting mixture was filtered, after cooling to room temperature, and the solid washed with toluene (3 × 5 cm³), before being dried *in vacuo* to give a white solid (0.11 g, 27 %); $\nu_{\text{max}}/\text{cm}^{-1}$ 1063 (Si-O), 803 (Si-O); ²⁹Si CP MAS NMR (79 MHz, versus Si(SiCH₃)₄ = -9.9 ppm): -59 (T²), -67 (T³), -104 (Si-OH), -109 (Si-O₄); ³¹P CP MAS NMR (162 MHz, versus 85 % H₃PO₄ = 0.0 ppm) -8.1, 2.6; Found: C, 7.31; H, 0.88; N, 0.52 %.

6.4.2.10 Synthesis of L24



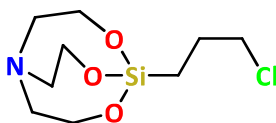
2,2-Biphenol (0.5 g, 3 mmol) was azeotropically dried with toluene (3 × 5 cm³), then dissolved in toluene (30 cm³). After addition of NEt₃ (0.8 cm³, 8 mmol), the solution was cooled to 0 °C and a solution of 2,2-biphenolphosphochloridite (1.4 g, 6 mmol) in toluene

(10 cm³) added dropwise. The reaction mixture was then refluxed for 2 h. Upon Cooling to room temperature, the mixture was filtered and the filtrate dried *in vacuo*. The crude product was then recrystallized from DCM/hexane, filtered and dried *in vacuo* to give the target compound as a white solid (1.04 g, 60%); $\nu_{\max}/\text{cm}^{-1}$ 3067 (aromatic C-H), 3026 (aromatic C-H), 1601 (C=C), 1568 (C=C), 1041 (P-O); ¹H NMR (400 MHz, CDCl₃) δ : 6.85 – 6.93 (4H, m, aryl), 7.18 – 7.27 (10H, m, aryl), 7.30 – 7.44 (10H, m, aryl); ³¹P{¹H} NMR (162 MHz, CDCl₃) δ : +144; ¹³C{¹H} NMR (101 MHz, CDCl₃) δ : 120.70 (t, ²J_{PC} = 5.3 Hz, aryl-C), 122.16 (s, aryl-C), 127.14 (s, aryl-C), 125.13 (s, aryl-C), 129.03 (s, aryl-C), 129.06 (s, aryl-C), 129.72 (s, aryl-C), 130.26 (s, aryl-C), 131.11 (s, aryl-C), 132.34 (s, aryl-C), 149.08 (t, ³J_{PC} = 2.4 Hz, aryl-C), 149.68 (³J_{PC} = 4.4 Hz, aryl-C); Anal. Calcd for C₃₆H₂₄O₆P₂: C, 70.36; H, 3.94. Found: C, 70.18; H, 3.93 %. NMR spectroscopic analysis and CHN elemental analysis are in good agreement with reported literature values.¹⁴

6.4.2.11 Investigation into phosphite-silica reactivity

AEROPERL 300/30 silica (0.1 g), and **L19** (0.05 g, 0.09 mmol) were added to toluene (10 cm³) and heated at reflux for 12 h, after which an aliquot of the reaction mixture was analysed by ³¹P NMR spectroscopy. MeOH (0.009 cm³, 0.18 mmol) was added to the bulk mixture, which was stirred at room temperature for 24 h. ³¹P NMR spectroscopic analysis of a second aliquot of reaction mixture showed no observable change.

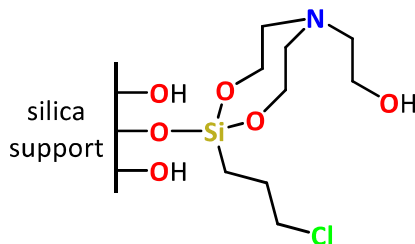
6.4.2.12 Synthesis of (3-chloropropyl)silatrane



Triethanolamine (3.6 cm³, 27.4 mmol) and KOH (0.05 g, 1.0 mmol) were dissolved in MeOH (25 cm³) and stirred at reflux for 1 h. (3-chloropropyl)trimethoxysilane (5.0 cm³, 27.4 mmol) was added to the solution and reflux continued for 1 h further. The solution was allowed to cool to room temperature and pentane (15 cm³) added. Upon cooling to –78 °C a white precipitate was produced, which was isolated by filtration, and dried *in*

vacuo to give the target compound (4.08 g, 59%); ν_{\max} /cm⁻¹ 3061 (C-H aromatic), 2943 (C-H), 2840 (C-H), 1602 (C=C), 1567 (C=C), 1184 (C-H); ¹H NMR (400 MHz, CDCl₃) δ : 0.45 – 0.52 (2H, m, SiCH₂), 1.84 – 1.94 (2H, m, CH₂CH₂CH₂), 2.83 (6H, t, ³J_{HH} = 5.8 Hz, NCH₂), 3.52 (2H, t, ³J_{HH} = 7.5 Hz, CH₂Cl), 3.78 (6H, t, ³J_{HH} = 5.8 Hz, CH₂O); ¹³C{¹H} NMR (101 MHz, CDCl₃) δ : 14.07 (s, SiCH₂), 29.12 (s, CH₂CH₂CH₂), 48.53 (s, CH₂Cl), 51.06 (s, NCH₂), 57.65 (s, OCH₂); Anal. Calcd for C₉H₁₈ClNSi: C, 42.93; H, 7.21; N, 5.56. Found: C, 42.95; H, 6.80; N, 5.32 %. NMR spectroscopic analysis and CHN elemental analysis are in good agreement with reported literature values.¹⁵

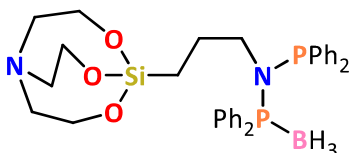
6.4.2.13 Synthesis of silica-immobilised (3-chloropropyl)silatrane



(3-Chloropropyl)silatrane (0.10 g, 0.4 mmol) and AEROPERL 300/30 silica (0.25 g) were heated at reflux in toluene (10 cm³) for 4 h. Upon cooling to room temperature, TFA (0.05 cm³, 0.7 mmol) was added the mixture heated at reflux for a further 4 h. Upon cooling to room temperature and the solid was filtered and washed with toluene (3 × 5 cm³), then dried *in vacuo* to give a white solid (0.26 g, 74%); ²⁹Si CP MAS NMR (79 MHz, versus Si(SiCH₃)₄ = –9.9 ppm): –58 (T²), –68 (T³), –102 (Si-OH), –110 (Si-O₄).

6.4.3 Investigating phosphine protection as BH₃ adducts

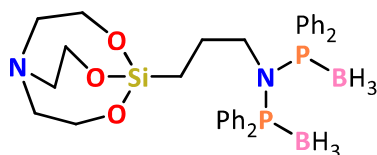
6.4.3.1 Synthesis of L5(BH₃): attempted synthesis of L5(BH₃)₂



L5 (0.35 g, 0.6 mmol) and BH₃.THF (1M in THF, 1.3 cm³, 1.2 mmol) were dissolved in DCM (10 cm³) and stirred overnight. The reaction mixture was then layered with hexane

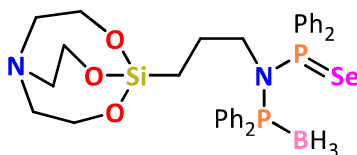
(15 cm³) resulting in crystals suitable for XRD analysis. The crystals were filtered and dried *in vacuo* to give a white solid (0.09 g, 23%); ν_{\max} /cm⁻¹ 3059 (aromatic C-H), 2961 (C-H), 2866 (C-H), 2378 br (B-H), 1588 (C=C), 891 (P-N); ¹H NMR (400 MHz, CDCl₃) δ : -0.05 (2H, t, ³J_{HH} = 7.2 Hz, SiCH₂), 1.02 – 1.12 (2H, m, CH₂CH₂CH₂), 2.66 (6H, t, ³J_{HH} = 5.8 Hz, OCH₂CH₂N), 3.45 – 3.57 (2H, m, CH₂N(PPh₂)₂), 3.60 (6H, t, ³J_{HH} = 5.8 Hz, OCH₂CH₂N), 7.27 – 7.46 (15H, m, phenyl), 7.55 – 7.62 (1H, m, phenyl), 7.66 – 7.82 (3H, m, phenyl), 7.85 – 7.91 (1H, m, phenyl), signals for BH₃ were unresolved; ³¹P{¹H} NMR (162 MHz, CDCl₃) δ : +55 (d, ²J_{PP} = 44.7 Hz, NPPH₂), +75 (s, br, NPPH₂(BH₃)); ¹¹B{¹H} NMR (128 MHz, CDCl₃) -36 (s, br); ¹³C{¹H} NMR (101 MHz, CDCl₃) δ : 12.19 (s, SiCH₂), 26.11 (s, CH₂CH₂CH₂), 51.07 (s, OCH₂CH₂N), 52.28 (s, CH₂N(PPh₂)₂), 57.65 (s, OCH₂CH₂N), 128.02 (d, ²J_{PC} = 6.8 Hz, aryl-C), 128.10 (d, ²J_{PC} = 3.8 Hz, aryl-C), 128.95 (s, aryl-C), 130.90 (d, ³J_{PC} = 2.2 Hz, aryl-C), 132.81 (s, aryl-C), 132.95 (dd, ¹J_{PC} = 10.4 Hz, ³J_{PC} = 2.9 Hz, aryl-C), 133.02 (s, aryl-C), 137.49 (dd, ¹J_{PC} = 17.1 Hz, ³J_{PC} = 3.1 Hz, aryl-C).

6.4.3.2 Second attempted synthesis of L5(BH₃)₂



L5(BH₃) (0.03 g, 0.2 mmol) and BH₃.THF (1M in THF, 1.3 cm³, 1.2 mmol) were dissolved in DCM and stirred at room temperature for 2 h. The reaction mixture was then layered with hexane (15 cm³) resulting in crystals suitable for XRD analysis corresponding to a disordered mixture of **L5**(BH₃), **L5**(BH₃)(O) and **L5**(BH₃)₂ in a 0.5:0.3:0.2 ratio, and the reaction was abandoned.

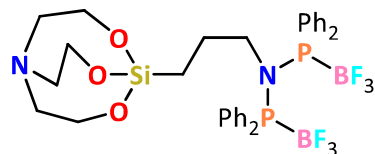
6.4.3.3 Synthesis of L5(BH₃)(Se)



Elemental grey Se powder (25 mg, 0.031 mmol) was added to solution of a **L5**(BH₃) (0.02 g, 0.07 mmol) in CD₂Cl₂ (0.7 cm³) in a Youngs NMR tube to give a pale-yellow solution,

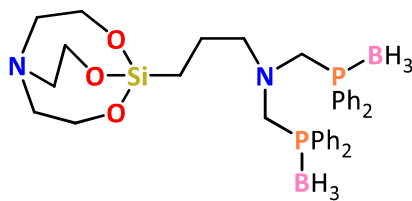
followed by sonication until complete conversion to the selenide derivative was observed. The product was not isolated as only the $|^1J_{\text{SeP}}|$ coupling constant is of interest; $^{31}\text{P}\{^1\text{H}\}$ NMR (162 MHz, CD_2Cl_2) δ : +67 (d with satellites, $^2J_{\text{PP}} = 13$ Hz, $^1J_{\text{SeP}} = 779$ Hz, $\text{P}=\text{Se}$), +73 (s, br, $\text{P}-\text{BH}_3$).

6.4.3.4 Attempted synthesis of $\text{L5}(\text{BF}_3)_2$



L17 (0.1 g, 0.6 mmol) and $\text{BF}_3 \cdot \text{OEt}_2$ (0.04 cm^3 , 0.4 mmol) were dissolved in DCM (10 cm^3) and stirred overnight. ^{31}P and ^{19}F NMR spectroscopic analysis of an aliquot of reaction mixture showed complete decomposition of the start materials and the reaction was abandoned.

6.4.3.5 Synthesis of $\text{L17}(\text{BH}_3)_2$

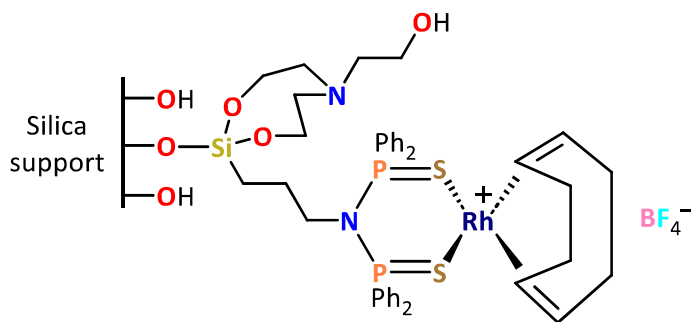


L17 (0.15 g, 0.2 mmol) and $\text{BH}_3 \cdot \text{THF}$ (1M in THF, 0.6 cm^3 , 0.5 mmol) were dissolved in DCM (10 cm^3) and stirred overnight. The reaction mixture was then layered with hexane (15 cm^3) resulting in a colourless oil. The oil was filtered and dried *in vacuo* to give a white solid (0.09 g, 61%); ^1H NMR (400 MHz, CDCl_3) δ : -0.08 – 0.01 (2H, m, SiCH_2), 1.22 – 1.32 (2H, m, $\text{CH}_2\text{CH}_2\text{CH}_2$), 2.59 (2H, t, $^3J_{\text{HH}} = 7.8$ Hz, $\text{CH}_2\text{CH}_2\text{CH}_2\text{N}$), 2.78 (6H, t, $^3J_{\text{HH}} = 5.8$ Hz, $\text{OCH}_2\text{CH}_2\text{N}$), 3.72 (6H, t, $^3J_{\text{HH}} = 5.8$ Hz, $\text{OCH}_2\text{CH}_2\text{N}$), 3.87 (4H, d, $^2J_{\text{PH}} = 1.6$ Hz, NCH_2P), 7.35 – 7.41 (8H, m, phenyl), 7.42 – 7.48 (4H, m, phenyl), 7.64 – 7.70 (8H, m, phenyl), signals for BH_3 were unresolved; $^{31}\text{P}\{^1\text{H}\}$ NMR (162 MHz, CDCl_3) δ : +10; $\text{B}^{11}\{^1\text{H}\}$ NMR (128 MHz, CDCl_3) -38 (s, br); $^{13}\text{C}\{^1\text{H}\}$ NMR (101 MHz, CDCl_3) δ : 12.55 (s, SiCH_2), 21.30 (s, $\text{CH}_2\text{CH}_2\text{CH}_2$), 52.00 (s, $\text{OCH}_2\text{CH}_2\text{N}$), 53.80 (dd, $^1J_{\text{PC}} = 39.6$ Hz, $^3J_{\text{PC}} = 3.6$ Hz, NCH_2P), 57.76 (s, $\text{OCH}_2\text{CH}_2\text{N}$),

60.14 (t, $^3J_{PC} = 4.0$ Hz, $\text{CH}_2\text{CH}_2\text{CH}_2\text{N}$), 128.60 (d, $^2J_{PC} = 9.6$ Hz, aryl-C), 129.20 (s, aryl-C), 130.96 (d, $^3J_{PC} = 2.3$ Hz, aryl-C), 132.79 (d, $^1J_{PC} = 8.5$ Hz aryl-C).

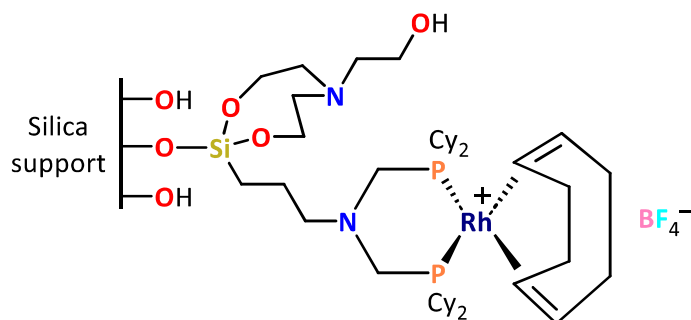
6.4.4 Synthesis of silica-immobilised rhodium hydroformylation catalysts

6.4.4.1 Synthesis of silica-immobilised $[\text{Rh}(\text{L5S}_2)(\text{COD})]\text{BF}_4$



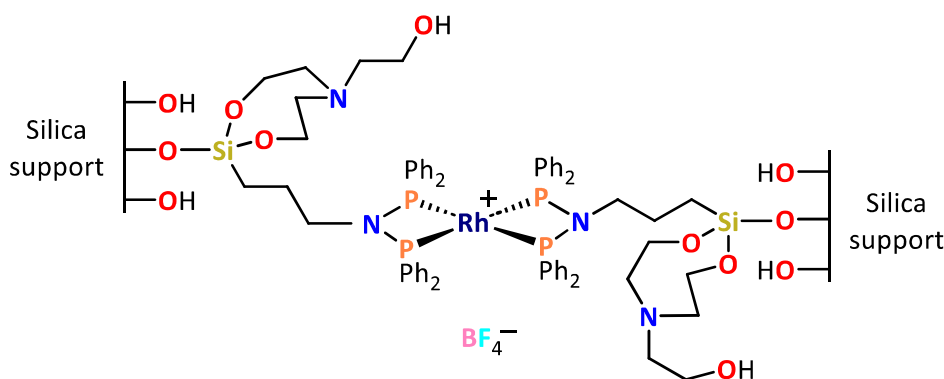
A Schlenk was charged with AEROPERL 300/30 silica calcined at 200 °C (1.0 g), **L5S₂** (0.10 g, 0.1 mmol), toluene (10 cm³) and THF (5 cm³) and stirred at 70 °C for 4 h. After cooling to rt the insoluble silica remained colourless suggesting no reaction had taken place. All volatile components were removed *in vacuo* and PhCl (10 cm³) and DCM (5 cm³) added, and the mixture heated to 70 °C for 4 h, after which time the silica had turned yellow. Upon cooling to rt, the mixture was filtered and the resulting solid washed with PhCl (2 × 5 cm³) and DCM (2 × 5 cm³), then dried *in vacuo* to give a yellow solid (0.94 g, 85%); $\nu_{\text{max}}/\text{cm}^{-1}$ 1069 (Si-O), 803 (Si-O); ^{29}Si CP MAS NMR (79 MHz, versus $\text{Si}(\text{SiCH}_3)_4 = -9.9$ ppm): -101 (Si-OH), -108 (Si-O₄); ^{31}P CP MAS NMR (162 MHz, versus 85 % $\text{H}_3\text{PO}_4 = 0.0$ ppm) $+59$ (RhSPPH₂), $+70$ (SPPH₂); Found: C, 3.98; H, 0.61; N, 0.20 %.

6.4.4.2 Synthesis of silica-immobilised $[\text{Rh}(\text{L19})(\text{COD})]\text{BF}_4$



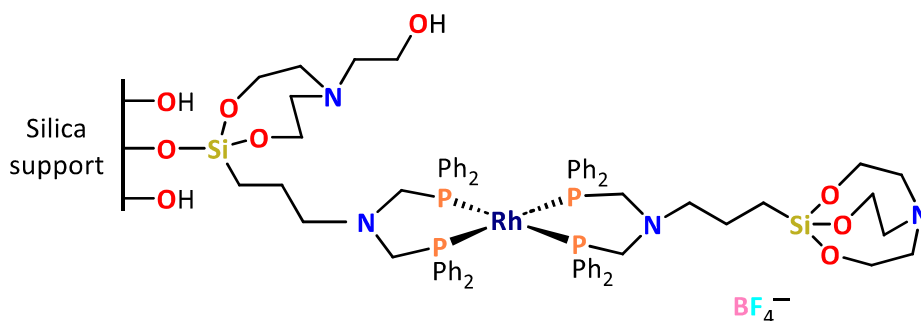
A Schlenk was charged with AEROPERL 300/30 silica calcined at 200 °C (1.2 g), **L19** (0.11 g, 0.11 mmol), toluene (10 cm³) and stirred at 70 °C for 4 h. After cooling to rt and subsequent filtration, the remaining solid was washed with toluene (3 × 5 cm³) and THF (3 × 5 cm³) and dried *in vacuo* to give a yellow solid (1.1 g, 84 %); $\nu_{\max}/\text{cm}^{-1}$ 1072 (Si-O), 812 (Si-O); ²⁹Si CP MAS NMR (79 MHz, versus Si(SiCH₃)₄ = -9.9 ppm): -101 (Si-OH), -109 (Si-O₄); ³¹P CP MAS NMR (162 MHz, versus 85 % H₃PO₄ = 0.0 ppm) +8 (RhPCy₂), +56 (P(O)Cy₂); Found: C, 2.45; H, 0.52; N, 0.06 %.

6.4.4.3 Synthesis of silica-immobilised [Rh(L5)₂]BF₄



A Schlenk was charged with AEROPERL 300/30 silica calcined at 200 °C (0.72 g), [Rh(**L5**)₂]BF₄ (0.06 g, 0.04 mmol) and THF (20 cm³) and stirred at reflux for 4 h. After cooling to rt and subsequent filtration, the remaining solid was washed with THF (3 × 5 cm³) and dried *in vacuo* to give a yellow solid (0.52 g, 65%); $\nu_{\max}/\text{cm}^{-1}$ 2978 (C-H), 1078 (Si-O), 808 (Si-O); ²⁹Si CP MAS NMR (79 MHz, versus Si(SiCH₃)₄ = -9.9 ppm): -100 (Si-OH), -109 (Si-O₄); ³¹P CP MAS NMR (162 MHz, versus 85 % H₃PO₄ = 0.0 ppm) +40 (unknown side product), +65 (RhPPh₂); Found: C, 3.23; H, 0.49; N, 0.17 %.

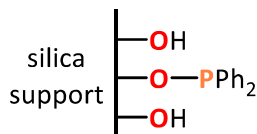
6.4.4.4 Synthesis of silica-immobilised [Rh(L17)₂]BF₄



A Schlenk was charged with AEROPERL 300/30 silica calcined at 200 °C (1.0 g), **L5S₂** (0.10 g, 0.1 mmol), toluene (10 cm³) and THF (5 cm³) and stirred at 70 °C for 4 h. Upon cooling to rt, the mixture was filtered and the resulting solid washed with toluene (2 × 5 cm³) and THF (2 × 5 cm³), then dried *in vacuo* to give a yellow solid (1.08 g, 99%); ν_{\max} /cm⁻¹ 1068 (Si-O), 811 (Si-O); ²⁹Si CP MAS NMR (79 MHz, versus Si(SiCH₃)₄ = -9.9 ppm): -102 (Si-OH), -108 (Si-O₄); ³¹P CP MAS NMR (162 MHz, versus 85 % H₃PO₄ = 0.0 ppm) +7 (RhPPh₂); Found: C, 3.38; H, 0.48; N, 0.19 %.

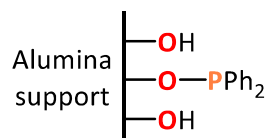
6.4.5 Investigating the reactivity of chlorophosphines with silica and alumina

6.4.5.1 Synthesis of silica-PPh₂



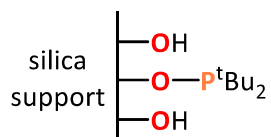
AEROPERL 300/30 silica calcined at 200 or 600 °C (0.25 g) and NEt₃ (0.5 cm³, 3.4 mmol) were added to toluene (10 cm³), and the mixture cooled to -78 °C. Ph₂PCl (0.1 cm³, 0.5 mmol) was then added and the resulting mixture allowed to warm to room temperature and stirred overnight. The suspension was then filtered and washed with chloroform (3 × 5 cm³), then dried *in vacuo* to give a white solid (0.19 g, 55%); ν_{\max} /cm⁻¹ 2964 (C-H), 1061 (Si-O), 787 (Si-O); ²⁹Si CP MAS NMR (79 MHz, versus Si(SiCH₃)₄ = -9.9 ppm) -101 (POSiO₃ + HOSiO₃), -109 (Si-O₄); ³¹P CP MAS NMR (162 MHz, versus 85 % H₃PO₄ = 0.0 ppm) +28 (OP(O)Ph₂), +106 (OPPh₂); ¹³C CP MAS NMR (101 MHz, versus Si(CH₃)₄ = 0.0 ppm): 128.5 (aryl C), 131.6 (aryl C).

6.4.5.2 Synthesis of alumina-PPh₂



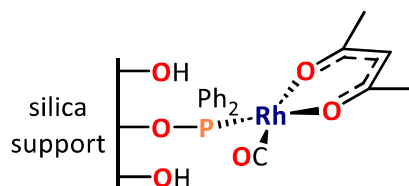
A Schlenk was charged with Alumina calcined at 200 °C (0.49 g, 0.5 mmol of Si-OH), NEt₃ (1.0 cm³, 6.8 mmol) and toluene (20 cm³) and cooled to –78 °C. Ph₂PCl (0.2 cm³, 1.0 mmol) was added dropwise and the mixture allowed to warm up to room temperature and stirred overnight. After subsequent filtration, the remaining solid was washed with CHCl₃ (3 × 5 cm³) and dried *in vacuo* to give a white solid (0.32 g, 50%); ν_{\max} /cm^{–1} 1252 (Al-OH), 500 (Al-O); ³¹P CP MAS NMR (162 MHz, versus 85 % H₃PO₄ = 0.0 ppm) +30 (OP(O)Ph₂), +98 (OPPh₂); ¹³C CP MAS NMR (101 MHz, versus Si(CH₃)₄ = 0.0 ppm): 127.8 (aryl C), 130.0 (aryl C).

6.4.5.3 Attempted synthesis of silica-P^tBu₂



A Schlenk was charged with AEROPERL 300/30 silica calcined at 200 °C (0.25 g, 0.5 mmol of Si-OH), NEt₃ (5.0 cm³, 6.8 mmol) and toluene (15 cm³) and cooled to –78 °C. ^tBu₂PCl (0.1 cm³, 0.5 mmol) was added dropwise and the mixture allowed to warm up to room temperature and stirred overnight. After subsequent filtration, the remaining solid was washed with CHCl₃ (3 × 5 cm³) and dried *in vacuo* to give a white solid (0.23 g, 77%); ν_{\max} /cm^{–1} 1075 (Si-O), 807 (Si-O); ²⁹Si CP MAS NMR (79 MHz, versus Si(SiCH₃)₄ = –9.9 ppm): –101 (Si-OH + Si-O-PPh₂), –109 (Si-O₄); ³¹P CP MAS NMR (162 MHz, versus 85 % H₃PO₄ = 0.0 ppm) +39 (OP(O)^tBu₂).

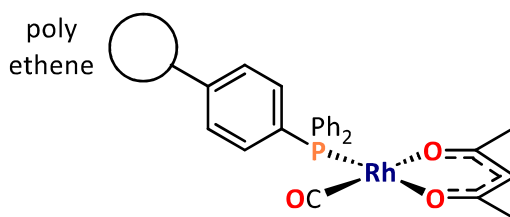
6.4.5.4 Synthesis of silica-immobilised $\text{PPh}_2\text{Rh}(\text{acac})(\text{CO})$



AEROPERL 300/30 silica calcined at 200 °C (1.0 g) and NEt_3 (1.0 cm^3 , 6.8 mmol) were added to toluene (10 cm^3), and the mixture cooled to -78°C . Ph_2PCl (0.5 cm^3 , 2.5 mmol) was then added and the resulting mixture allowed to warm to room temperature and stirred overnight. The suspension was then filtered and washed with chloroform (3 \times 5 cm^3), then dried *in vacuo*. Toluene (10 cm^3) and $\text{Rh}(\text{acac})(\text{CO})_2$ (0.1 g, 0.4 mmol) were then added and the mixture stirred for 2 h. After filtration, the solid was washed with toluene (3 \times 5 cm^3) and dried *in vacuo* to give a yellow solid (0.8 g, 64%); $\nu_{\text{max}}/\text{cm}^{-1}$ 2964 (C-H), 1066 (Si-O), 804 (Si-O); ^{29}Si CP MAS NMR (79 MHz, versus $\text{Si}(\text{SiCH}_3)_4 = -9.9$ ppm) -101 ($\text{POSiO}_3 + \text{HOSiO}_3$), -109 (Si-O_4); ^{31}P CP MAS NMR (162 MHz, versus 85 % $\text{H}_3\text{PO}_4 = 0.0$ ppm) $+22$ ($\text{OP}(\text{O})\text{Ph}_2$), $+82$ (RhPPh_2), $+106$ (OPPh_2); Found: C, 8.26; H, 0.95 %.

6.4.6 Synthesis of a FibrecatTM-supported rhodium hydroformylation catalyst

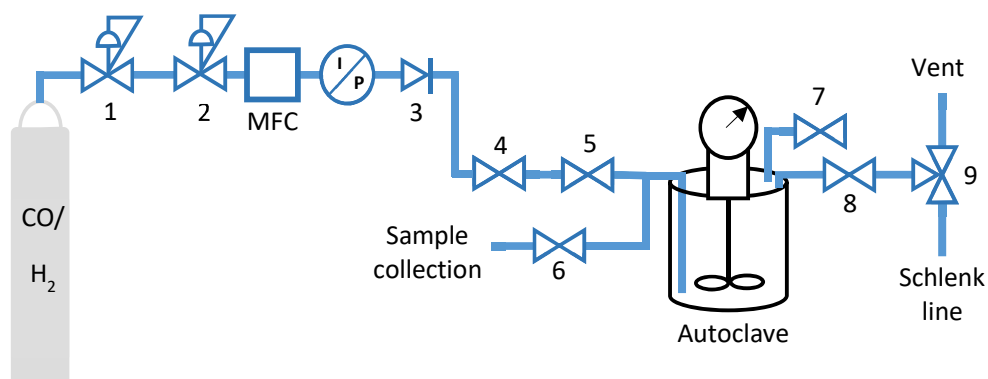
6.4.6.1 Synthesis of FibrecatTM-supported $\text{Rh}(\text{acac})(\text{PPh}_3)(\text{CO})$



A Schlenk was charged with FibrecatTM (2.0 g), toluene (20 cm^3) and $\text{Rh}(\text{acac})(\text{CO})_2$ (0.26 g, 1.0 mmol) and stirred for 3 h. After filtration, the solid was washed with toluene (3 \times 5 cm^3) and dried *in vacuo* to give an orange solid (0.8 g, 64%); $\nu_{\text{max}}/\text{cm}^{-1}$ 3027 (C-H aromatic), 2920 (C-H), 1579 (C=C), 1435 (P-Ph); ^{31}P CP MAS NMR (162 MHz, versus 85 % $\text{H}_3\text{PO}_4 = 0.0$ ppm) -6 (PPh_3), $+30$ ($\text{Rh}(\text{acac})(\text{PPh}_3)_2$), $+42$ ($\text{Rh}(\text{acac})(\text{PPh}_3)(\text{CO})$); Found: C, 80.01; H, 8.06 %. NMR spectroscopic analysis and CHN elemental analysis showed good agreement with reported literature values.¹⁶

6.5 Chapter 5 experimental

6.5.1 Hydroformylation reactor setup



Valves:

5 = autoclave gas inlet

1 = CO/H₂ cylinder pressure regulator 6 = autoclave sampling valve

2 = CO/H₂ pressure regulator in lab 7 = septum inlet

3 = post-MFC one-way valve 8 = autoclave gas outlet

4 = gas inlet isolation 9 = L-three way valve: autoclave vent
/ Schlenk line

Figure 6.4. Hydroformylation reactor schematic, autoclave housed and operated in a fume hood.

6.5.2 Homogeneous hydroformylation catalysis

Catalyst testing is performed in a commercial 316 stainless steel Parr 4566 autoclave with 200 mL maximum specified working volume (300 mL total volume), with Teflon liner, integral pressure gauge and certified Fike Rupture disc (138.00 barg {ambient}).

The autoclave is assembled then evacuated and backfilled with argon *via* a connected Schlenk line. A solution of toluene, 1-octene (5 cm³, 32 mmol), nonane (1000 μ L, internal standard) and catalyst (0.5 mmol) is added and the autoclave then purged with reactant gases (1:1 H₂ and CO) (1 \times 10 barg, 5 \times barg). Finally, the vessel is pressurised to 20 barg, and heated to 90 °C, maintained *via* a thermocouple, pressure transducer, and mass flow controller. The reaction is maintained for 1 h (minimum) with samples collected at 15 min intervals, filtered through a silica plug and analysed by gas chromatography.

6.5.3 Heterogeneous hydroformylation catalysis

Catalyst testing is performed in a commercial 316 stainless steel Parr 4566 autoclave with 200 mL maximum specified working volume (300 mL total volume), with Teflon liner, integral pressure gauge and certified Fike Rupture disc (138.00 barg {ambient}).

The autoclave is assembled and purged with argon for 0.5 h. Solid catalyst (0.5 mmol) is then quickly added under air and the autoclave reassembled and evacuated for 0.5 h. A solution of toluene, 1-octene (5 cm³, 32 mmol), nonane (1000 µL, internal standard) is added and the autoclave then purged with reactant gases (1:1 H₂ and CO) (1 × 10 barg, 5 × barg). Finally, the vessel is pressurised to 20 barg, and heated to 90 °C, maintained *via* a thermocouple, pressure transducer, and mass flow controller. The reaction is maintained for 1 h (minimum) with samples collected at 15 min intervals, filtered through a silica plug and analysed by gas chromatography. Leaching samples were collected after cooling to room temperature following a 1 h reaction.

6.5.4 Autoclave cleaning

In between hydroformylation reactions the Teflon liner was removed from the autoclave and washed in an acid and base bath, rinsed with water and acetone and dried in air. The autoclave was cleaned with acetone, including flushing the internal dip tube. Periodically, blank experiments were performed where no catalyst was added to a hydroformylation reaction to verify that no contamination of the autoclave/Teflon liner had occurred, which would result in hydroformylation activity.

6.6 Chapter 6 references

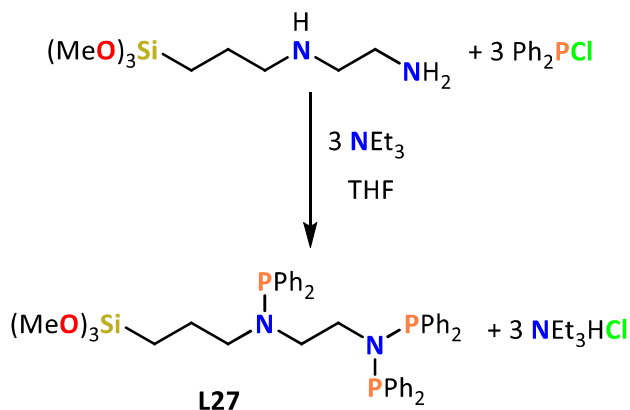
1. S. Komiyama, *Synthesis of Organometallic Compounds – A Practical Guide*, Wiley-Interscience, New York, 1998.
2. G. R. Fulmer, A. J. M. Miller, N. H. Sherden, H. E. Gottlieb, A. Nudelman, B. M. Stoltz, J. E. Bercaw and K. I. Goldberg, *Organometallics*, 2010, **29**, 2176–2179, DOI: 10.1021/om100106e.

3. A. Poater, B. Cosenza, A. Correa, S. Giudice, F. Ragone, V. Scarano and L. Cavallo, *Eur. J. Inorg. Chem.*, 2009, 1759–1766, DOI: 10.1002/ejic.200801160.
4. P. Braunstein, H. Kormann, W. Meyer-Zaika, R. Pugin and G. Schmid, *Chem. Eur. J.*, 2000, **6**, 4637–4646, DOI: 10.1002/1521-3765(20001215)6:24<4637::AID-CHEM4637>3.0.CO;2-A.
5. K. Szpakolski, K. Latham, C. Rix, R. A. Rani and K. Kalantar-Zadeh, *Polyhedron*, 2013, **52**, 719–732, DOI: 10.1016/j.poly.2012.07.078.
6. R. B. King and N. D. Sadanani, *Synth. React. Org. Met.-Org. Chem.*, 1985, **15**, 149–153, DOI: 10.1080/00945718508059375.
7. J. Li, M. Lutz, A. L. Spek, G. P. M. van Klink, G. van Koten, R. J. M. K. Gebbink, *J. Organomet. Chem.*, 2010, **695**, 2618–2628, DOI: 10.1016/j.jorganchem.2010.08.026.
8. H. Gulyás, J. Benet-Buchholz, E. C. Escudero-Adan, Z. Freixa, and P. W. N. M. van Leeuwen, *Chem. Eur. J.*, 2007, **13**, 3424–3430, DOI: 10.1002/chem.200601640.
9. (a) J. Fawcett, P. A. T. Hoye, R. D. W. Kemmitt, D. J. Lawa and D. R. Russel, *J. Chem. Soc., Dalton Trans.*, 1993, 2563–2568, DOI: 10.1039/DT9930002563. b) K. Heuzý, D. Mýry, D. Gauss, J. Blais and D. Astruc, *Chem. Eur. J.*, 2004, **10**, 3936–3944, DOI: 10.1002/chem.200400150
10. R. G. Nuzzo, S. L. Haynie, M. E. Wilson, and G. M. Whitesides, *J. Org. Chem.*, 1981, **46**, 2861–2867, DOI: 10.1021/jo00327a005.
11. F. Bonatti and G. Wilkinson, *J. Chem. Soc.*, 1964, 3156–3160, DOI: 10.1039/JR9640003156.
12. M. Aydemir, N. Meric, C. Kayan, F. Ok and A. Baysal, *Inorganica Chim. Acta*, 2013, **398**, 1–10, DOI: 10.1016/j.ica.2012.12.005.
13. S. Komiya and F. Fukuoka, *Synthesis of Organometallic Compounds*, John Wiley & Sons Ltd, Chichester, 1997.
14. R. Frank, A. Börner, S. Kloss and D. Selent, (Evonik Operations GMBH), US Patent, 20220056059A1, 2021.
15. M. G. Voronkov, V. M. Dyakov, US Patent, 4048206A, 1977.
16. T. A. Zeelie, A. Root and A. O. I. Krause, *Appl. Catal. A: Gen.*, 2005, **285**, 96–109, DOI: 10.1016/j.apcata.2005.02.010.

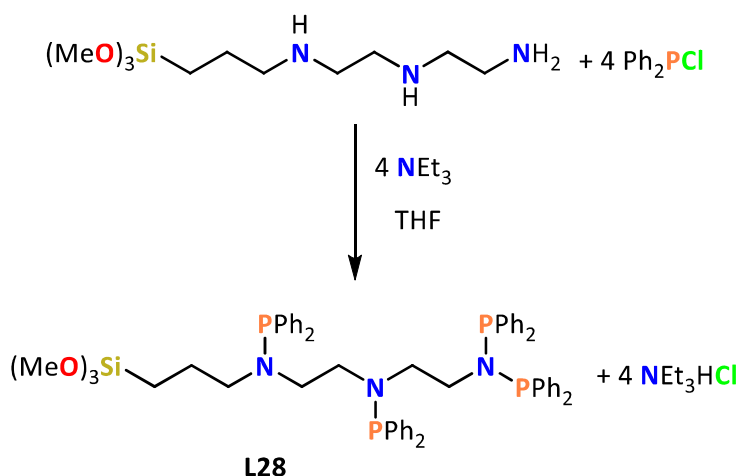
Appendix A: Synthesis of multidentate tetherable phosphine ligands

One aspect of immobilised ligand design that requires further exploration is the length of the alkyl spacer between the point of immobilisation and ligand donor site. Previous studies have shown an increase in hydroformylation catalytic activity with increased tether length.¹ This enhanced performance has been attributed to greater freedom of movement of the ligand backbone.¹ However, to the best of the author's knowledge, no investigation into the tether chain length between the solid support and donor atoms of bidentate ligands has been performed. This is likely due to the difficult synthesis required and the lack of commercially available ligand scaffolds suitable for this work.

In order to vary the alkyl spacer length between the alkoxy silane immobilisation group and PNP phosphine ligand donor moiety, compounds **L27** and **L28** were designed that could be synthesised in one step from commercially available amines (Schemes A1 and A2). These compounds were isolated as sticky solids, which were then analysed by ³¹P, ¹H and ¹³C NMR spectroscopies.

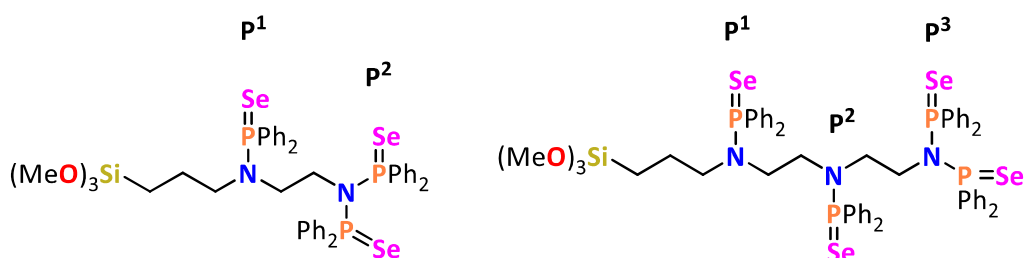


Scheme A1. Synthesis of L27.



*Scheme A2. Synthesis of **L28**.*

To determine whether all the phosphines donor sites of **L27** and **L28** were accessible and reactive, **L27** and **L28** were reacted with an excess of elemental selenium to produce their corresponding phosphorus selenides (Figure A1). The reactions were performed in Young's NMR tubes and the compounds were not isolated. From the $|^1J_{\text{SeP}}|$ coupling constants measured from their ^{31}P NMR spectra, the basicity of the phosphines was estimated, giving an indication of phosphine donor strength (Table A1). The results showed that all the phosphorus atoms were accessible to reaction with elemental selenium and gave similar $|^1J_{\text{SeP}}|$ coupling constants ranging from 751 – 789 Hz, showing good agreement with previously reported (diphenylphosphino)amines.^{2,3}



*Figure A1. Structures of **L27Se₃** and **L28Se₄**.*

Table A1. ^{31}P NMR chemical shifts and $|^1J_{\text{SeP}}|$ coupling constants of **L27Se₃** and **L28Se₄** measured in CD_2Cl_2 at 162 MHz.

Compound	P atom	$ ^1J_{\text{SeP}} $ / Hz	δ_{P} / ppm
L27Se₃	p¹	760	+67
	p²	789	+69
L28Se₄ (in CDCl_3)	p¹	751	+65
	p²	756	+69
	p³	783	+69

Synthesis of L27

(3-(2-Aminoethyl)-3-aminopropyl)trimethoxysilane (2.0 cm^3 , 9 mmol) and NEt_3 (4.0 cm^3 , 28 mmol) were dissolved in THF (50 cm^3). The reaction mixture was cooled to $-78\text{ }^\circ\text{C}$ and Ph_2PCl (5.0 cm^3 , 27 mmol) added dropwise. After warming up to room temperature the solution was stirred overnight, the solution was filtered and the filtrate dried *in vacuo* to give a pale yellow gummy solid (5.3 g, 76 %); ^1H NMR (400 MHz, CD_2Cl_2) δ : 0.18 – 0.28 (2H, m, SiCH_2), 1.01 – 1.14 (2H, m, $\text{CH}_2\text{CH}_2\text{CH}_2$), 2.56 (2H, q, $^3J_{\text{HH}} + J_{\text{HP}} = 8.4\text{ Hz}$, $\text{CH}_2\text{CH}_2\text{CH}_2\text{N}$), 2.65 – 2.75 (2H, m, $\text{CH}_2\text{N}(\text{PPh}_2)$), 3.21 (2H, p, $^3J_{\text{HH}} + J_{\text{HP}} = 9.1\text{ Hz}$, $\text{CH}_2\text{N}(\text{PPh}_2)_2$), 3.42 (9H, s, OCH_3), 7.20 – 7.26 (5H, m, phenyl), 7.27 – 7.36 (25 H, m, phenyl); $^{31}\text{P}\{^1\text{H}\}$ NMR (162 MHz, CD_2Cl_2) δ : + 60 (1P, s, NPPH_2), + 62 (2P, s, $\text{N}(\text{PPh}_2)_2$); $^{13}\text{C}\{^1\text{H}\}$ NMR (101 MHz, CD_2Cl_2) δ : 5.57 (s, SiCH_2), 22.18 (s, $\text{CH}_2\text{CH}_2\text{CH}_2$), 45.76 (s, $\text{CH}_2\text{CH}_2\text{CH}_2\text{N}$), 50.44 (s, OCH_3), 53.77 (s, $\text{CH}_2\text{N}(\text{PPh}_2)$), 53.87 (s, $\text{CH}_2\text{N}(\text{PPh}_2)_2$), 127.55 (s, aryl-C), 127.61 (s, aryl-C), 127.77 (s, aryl-C), 128.25 (s, aryl-C), 131.40 (d, $^2J_{\text{PC}} = 19.4\text{ Hz}$, aryl-C), 132.06 (d, $^2J_{\text{PC}} = 22.2\text{ Hz}$, aryl-C), 138.55 (d, $^1J_{\text{PC}} = 12.6\text{ Hz}$, aryl-C), 139.22 (d, $^1J_{\text{PC}} = 14.2\text{ Hz}$, aryl-C).

Synthesis of L28

Trimethoxysilylpropyldiethylenetriamine (2.1 cm^3 , 8 mmol) and NEt_3 (4.7 cm^3 , 32 mmol) were dissolved in THF (50 cm^3). The reaction mixture was cooled to $-78\text{ }^\circ\text{C}$ and Ph_2PCl (6.0 cm^3 , 32 mmol) added dropwise. After warming up to room temperature the solution

was stirred overnight, the solution was filtered and the filtrate dried *in vacuo* to give sticky oil. The product was dissolved in DCM (5 cm³) and dried *in vacuo* to give a pale yellow solid (3.4 g, 42 %); ¹H NMR (400 MHz, CDCl₃) δ: 0.23 – 0.34 (2H, m, SiCH₂), 1.17 – 1.28 (2H, m, CH₂CH₂CH₂), 2.55 – 2.88 (8H, m, CH₂N(PPh₂)), 3.28 (2H, p, ³J_{HH+HP} = 10.2 Hz, CH₂N(PPh₂)₂), 3.45 (9H, s, OCH₃), 7.12 – 7.19 (4H, m, phenyl), 7.22 – 7.35 (36 H, m, phenyl); ³¹P{¹H} NMR (162 MHz, CDCl₃) δ: + 61 (1P, s, NPh₂), + 61 (1P, s, NPh₂), + 62 (2P, s, N(PPh₂)₂); ¹³C{¹H} NMR (101 MHz, CDCl₃) δ: 6.23 (s, SiCH₂), 22.57 (s, CH₂CH₂CH₂), 47.92 (s, CH₂CH₂CH₂N), 49.93 (s, OCH₃), 50.97 (s, CH₂N(PPh₂)), 52.18 (s, CH₂N(PPh₂)₂), 52.58 (s, CH₂N(PPh₂)₂), 54.64 (d, ²J_{PC} = 12.5 Hz, CH₂N(PPh₂)₂), 128.04 (s, aryl-C), 128.06 (s, aryl-C), 128.09 (s, aryl-C), 128.10 (s, aryl-C), 128.25 (d, ³J_{PC} = 3.7 Hz, aryl-C), 128.72 (s, aryl-C), 131.97 (d, ²J_{PC} = 19.7 Hz, aryl-C), 132.03 (d, ²J_{PC} = 19.9 Hz, aryl-C), 132.70 (d, ²J_{PC} = 22.0 Hz, aryl-C), 139.41 (d, ¹J_{PC} = 13.4 Hz, aryl-C), 139.48 (d, ¹J_{PC} = 15.2 Hz, aryl-C), 140.20 (d, ¹J_{PC} = 14.6 Hz, aryl-C).

References

1. W. Zhou and D. He, *Green Chem.*, 2009, **11**, 1146–1154, DOI: 10.1039/B900591A.
2. N. Biricik, F. Durap, C. Kayan, B. Gümgüm, N. Gürbüz, I. Özdemir, W. H. Ang, Z. Fei and R. Scopelliti, *J. Organomet. Chem.*, 2008, **693**, 2693–2699, DOI: 10.1016/j.jorganchem.2008.05.010.
3. C. Kayan, N. Biricik and M. Aydemir, *Transit. Met. Chem.*, 2011, **36**, 513–520, DOI: 10.1007/s11243-011-9497-8.

Appendix B: Crystallographic data

Complex	L5	Ph ₂ (O)POP(O)Ph ₂	L9
Local identifier code	22srv103	22srv093	21srv129
Empirical formula	C _{33.5} H ₃₉ ClN ₂ O ₃ P ₂ Si	C ₂₄ H ₂₀ O ₃ P ₂	C ₃₀ H ₃₁ NO ₇ P ₂ Si
Formula weight	643.14	418.34	607.59
Temperature / K	120.00	120.00	120
Crystal system	monoclinic	monoclinic	monoclinic
Space group	P2 ₁ /c	P2 ₁ /c	P2 ₁ /c
a / Å	10.2673(3)	7.9347(2)	11.1068(5)
b / Å	16.9015(5)	15.0927(3)	17.2769(7)
c / Å	18.4353(5)	17.0697(4)	15.1206(6)
α / °	90	90	90
β / °	96.9874(11)	99.3217(9)	90.9948(17)
γ / °	90	90	90
Volume / Å ³	3175.37(16)	2017.20(8)	2901.51
Z	4	4	4
ρ _{calc} / g cm ³	1.345	1.377	1.391
μ / mm ⁻¹	0.297	0.239	0.240
F(000)	1356.0	872.0	1272
Crystal size / mm ³	0.21 × 0.16 × 0.05	0.16 × 0.09 × 0.01	0.09 × 0.0112 × 0.478
Radiation	Mo Kα (λ = 0.71073)	Mo Kα (λ = 0.71073)	MoKα (λ = 0.71073)
2θ range for data collection / °	3.996 to 59.994	5.202 to 59.998	4.36 to 67.454
Index ranges	-14 ≤ h ≤ 14, -23 ≤ k ≤ 23, -25 ≤ l ≤ 25	-11 ≤ h ≤ 11, -21 ≤ k ≤ 21, -23 ≤ l ≤ 24	-17 ≤ h ≤ 17, -26 ≤ k ≤ 26, -23 ≤ l ≤ 23
Reflections collected	75603	47981	69693
Independent reflections	9246 [R _{int} = 0.0445, R _{sigma} = 0.0260]	5851 [R _{int} = 0.0523, R _{sigma} = 0.0306]	11568 [R _{int} = 0.0562, R _{sigma} = 0.0424]
Data / restraints / parameters	9246/0/392	5851/0/342	11568 / 73 / 496
Goodness-of-fit on F ²	1.055	1.047	1.028
Final R indexes [I ≥ 2σ(I)]	R ₁ = 0.0475, wR ₂ = 0.1059	R ₁ = 0.0447, wR ₂ = 0.1074	R ₁ = 0.0436, wR ₂ = 0.1012
Final R indexes [all data]	R ₁ = 0.0558, wR ₂ = 0.1102	R ₁ = 0.0539, wR ₂ = 0.1122	R ₁ = 0.0605, wR ₂ = 0.1087
Largest diff. peak/hole / e Å ⁻³	0.82/-0.97	0.64/-0.38	0.47 / -0.59

Complex	L11	L17	[Rh(L5)₂]Cl
Local identifier code	23srv047	mo_23srv212_P1	mo_22srv278
Empirical formula	C ₃₃ H ₃₄ N ₂ O ₇ P ₂ Si	C ₃₅ H ₄₂ N ₂ O ₃ P ₂ Si	C ₇₆ H ₉₉ N ₅ O- 10P ₅ RhSi ₂
Formula weight	660.65	628.73	1556.54
Temperature / K	120.00	120.00(10)	120.00(10)
Crystal system	monoclinic	monoclinic	monoclinic
Space group	P2 ₁ /c	P2 ₁	P21/n
a / Å	18.6233(13)	17.91489(19)	10.0412(4)
b / Å	10.6954(7)	36.3101(3)	21.6100(6)
c / Å	15.4973(10)	20.43051(19)	34.3663(10)
α / °	90	90	90
β / °	95.862(2)	90.0197(9)	97.057(3)
γ / °	90	90	90
Volume / Å ³	3070.7(4)	13289.9(2)	7400.7(4)
Z	4	16	4
ρ _{calc} / g cm ³	1.429	1.257	1.397
μ / mm ⁻¹	0.234	0.204	0.433
F(000)	1384.0	5344.0	3272.0
Crystal size / mm ³	0.191 × 0.171 × 0.046	0.496 × 0.338 × 0.182	0.193 × 0.04 × 0.023
Radiation	Mo Kα (λ = 0.71073)	Mo Kα (λ = 0.71073)	Mo Kα (λ = 0.71073)
2θ range for data collection / °	4.398 to 67.344	3.194 to 67.328	3.042 to 50.052
Index ranges	-28 ≤ h ≤ 28, 0 ≤ k ≤ 16, 0 ≤ l ≤ 24	-27 ≤ h ≤ 25, -56 ≤ k ≤ 55, -30 ≤ l ≤ 31	-11 ≤ h ≤ 11, -25 ≤ k ≤ 25, -40 ≤ l ≤ 40
Reflections collected	11116	284574	120083
Independent reflections	11116 [R _{int} = 0.1424, R _{sigma} = 0.0876]	91242 [R _{int} = 0.0621, R _{sigma} = 0.0824]	13053 [R _{int} = 0.1457, R _{sigma} = 0.0838]
Data / restraints / parameters	11116/0/407	91242/2698/3086	13053/450/906
Goodness-of-fit on F ²	1.031	1.005	1.045
Final R indexes [I > 2σ (I)]	R ₁ = 0.0936, wR ₂ = 0.2475	R ₁ = 0.0561, wR ₂ = 0.1126	R ₁ = 0.0810, wR ₂ = 0.1830
Final R indexes [all data]	R ₁ = 0.1424, wR ₂ = 0.2777	R ₁ = 0.0745, wR ₂ = 0.1212	R ₁ = 0.1193, wR ₂ = 0.2050
Largest diff. peak/hole / e Å ⁻³	1.06/-0.78	0.54/-0.31	1.20/-0.79

Complex	[Rh(L5) ₂] ₂ BF ₄	[Rh(L19)(COD)]BF ₄	[Rh(L5S ₂)(COD)]BF ₄
Local identifier code	23srv153	23srv251	23srv146
Empirical formula	C ₆₉ H ₇₈ BCl _{9.22} F ₄ N ₄ O ₆ P ₄ RhSi ₂	C ₄₉ H ₈₃ BClF ₄ N ₂ O ₃ P ₂ RhSi	C ₄₁ H ₅₀ BF ₄ N ₂ O ₃ P ₂ Rh S ₂ Si
Formula weight	1756.16	1063.37	962.70
Temperature / K	120.00	120.00	120.00
Crystal system	triclinic	monoclinic	monoclinic
Space group	P-1	P2 ₁	P2 ₁ /n
a / Å	11.9734(5)	9.8552(4)	18.3138(7)
b / Å	19.1548(7)	20.2543(7)	12.3281(5)
c / Å	19.2831(7)	13.0267(5)	18.5568(7)
α / °	77.7860(10)	90	90
β / °	74.3220(10)	95.7940(10)	91.374(2)
γ / °	76.7720(10)	90	90
Volume / Å ³	4091.8(3)	2586.98(17)	4188.4(3)
Z	2	2	4
ρ _{calc} / g cm ³	1.425	1.365	1.527
μ / mm ⁻¹	0.676	0.523	0.672
F(000)	1798.0	1124.0	1984.0
Crystal size / mm ³	0.186 × 0.058 × 0.017	0.253 × 0.237 × 0.087	0.293 × 0.104 × 0.094
Radiation	Mo Kα (λ = 0.71073)	Mo Kα (λ = 0.71073)	Mo Kα (λ = 0.71073)
2θ range for data collection / °	3.862 to 52.744	3.73 to 64.994	3.966 to 69.378
Index ranges	-14 ≤ h ≤ 14, -23 ≤ k ≤ 23, -24 ≤ l ≤ 24	-14 ≤ h ≤ 14, -30 ≤ k ≤ 30, -19 ≤ l ≤ 19	-29 ≤ h ≤ 29, -19 ≤ k ≤ 19, -29 ≤ l ≤ 29
Reflections collected	97107	109333	162773
Independent reflections	16717 [R _{int} = 0.0986, R _{sigma} = 0.0752]	18699 [R _{int} = 0.0359, R _{sigma} = 0.0257]	17959 [R _{int} = 0.0627, R _{sigma} = 0.0369]
Data / restraints / parameters	16717/923/1005	18699/529/629	17959/1657/707
Goodness-of-fit on F ²	1.022	1.055	1.052
Final R indexes [I ≥ 2σ (I)]	R ₁ = 0.0516, wR ₂ = 0.1072	R ₁ = 0.0238, wR ₂ = 0.0566	R ₁ = 0.0491, wR ₂ = 0.1262
Final R indexes [all data]	R ₁ = 0.0928, wR ₂ = 0.1238	R ₁ = 0.0247, wR ₂ = 0.0570	R ₁ = 0.0683, wR ₂ = 0.1385
Largest diff. peak/hole / e Å ⁻³	0.68/-0.63	0.55/-0.50	3.00/-0.82

Complex	PdI ₂ (L5)	PdI ₂ (L17)	PdI ₂ (L18)
Local identifier code	22srv197	22srv198	22srv199
Empirical formula	C ₃₃ H ₃₈ I ₂ N ₂ O ₃ P ₂ PdSi	C ₃₅ H ₄₂ I ₂ N ₂ O ₃ P ₂ PdSi	C ₂₉ H ₆₀ Cl ₆ I ₂ N ₂ O ₃ P ₂ PdSi
Formula weight	960.88	988.93	1147.72
Temperature / K	120.00	120.00	120.00
Crystal system	monoclinic	triclinic	triclinic
Space group	P2 ₁ /n	P-1	P-1
a / Å	20.3737(5)	11.1623(3)	10.5793(3)
b / Å	8.6965(2)	11.4460(3)	14.5066(4)
c / Å	21.9728(5)	15.6070(4)	15.2934(4)
α / °	90	107.9952(10)	112.8081(10)
β / °	112.7589(8)	99.4459(11)	99.5805(10)
γ / °	90	100.5930(10)	93.1671(11)
Volume / Å ³	3590.02(15)	1811.35(8)	2114.77(10)
Z	4	2	2
ρ _{calc} / g cm ³	1.778	1.813	1.802
μ / mm ⁻¹	2.394	2.376	2.414
F(000)	1880.0	972.0	1140.0
Crystal size / mm ³	0.12 × 0.11 × 0.06	0.11 × 0.09 × 0.03	0.12 × 0.1 × 0.07
Radiation	Mo Kα (λ = 0.71073)	Mo Kα (λ = 0.71073)	Mo Kα (λ = 0.71073)
2θ range for data collection / °	5.098 to 59.998	3.82 to 60	4.666 to 60
Index ranges	-28 ≤ h ≤ 28, -12 ≤ k ≤ 12, -30 ≤ l ≤ 30	-15 ≤ h ≤ 15, -16 ≤ k ≤ 16, -21 ≤ l ≤ 21	-14 ≤ h ≤ 14, -20 ≤ k ≤ 20, -21 ≤ l ≤ 21
Reflections collected	126837	65841	76626
Independent reflections	10451 [R _{int} = 0.0440, R _{sigma} = 0.0203]	10535 [R _{int} = 0.0373, R _{sigma} = 0.0254]	12291 [R _{int} = 0.0401, R _{sigma} = 0.0276]
Data / restraints / parameters	10451/0/397	10535/60/451	12291/21/439
Goodness-of-fit on F ²	1.059	1.038	1.062
Final R indexes [I ≥ 2σ (I)]	R ₁ = 0.0218, wR ₂ = 0.0444	R ₁ = 0.0296, wR ₂ = 0.0633	R ₁ = 0.0543, wR ₂ = 0.1471
Final R indexes [all data]	R ₁ = 0.0255, wR ₂ = 0.0456	R ₁ = 0.0345, wR ₂ = 0.0655	R ₁ = 0.0617, wR ₂ = 0.1530
Largest diff. peak/hole / e Å ⁻³	0.55/-0.44	2.20/-1.76	1.63/-3.01

Complex	PdI ₂ (L19)	PdI ₂ (L11)	PdI ₂ (L12)
Local identifier code	23srv248	23srv058	23srv067
Empirical formula	C ₃₆ H ₆₈ Cl ₂ I ₂ N ₂ O ₃ P ₂ P dSi	C ₃₆ H ₄₀ Cl ₆ I ₂ N ₂ O ₇ P ₂ P dSi	C ₅₁ H ₄₄ Cl ₆ I ₂ N ₂ O ₇ P ₂ P dSi
Formula weight	1098.05	1275.63	1459.81
Temperature / K	120.00	120.00	120.00(10)
Crystal system	monoclinic	monoclinic	monoclinic
Space group	P2 ₁	P2 ₁ /c	P2 ₁
a / Å	8.2592(7)	11.6131(3)	15.1388(9)
b / Å	26.873(2)	25.5021(7)	10.5416(6)
c / Å	19.7769(17)	16.8413(5)	18.3766(11)
α / °	90	90	90
β / °	92.595(3)	110.0540(10)	108.690(7)
γ / °	90	90	90
Volume / Å ³	4385.0(6)	4685.3(2)	2778.0(3)
Z	4	4	2
ρ _{calc} / g cm ³	1.663	1.808	1.745
μ / mm ⁻¹	2.089	2.196	1.865
F(000)	2208.0	2496.0	1436.0
Crystal size / mm ³	0.183 × 0.155 × 0.061	0.32 × 0.18 × 0.14	0.202 × 0.046 × 0.011
Radiation	MoKα (λ = 0.71073)	Mo Kα (λ = 0.71073)	Mo Kα (λ = 0.71073)
2θ range for data collection / °	4.394 to 72.736	3.734 to 62	4.22 to 52.742
Index ranges	-13 ≤ h ≤ 13, -44 ≤ k ≤ 44, -32 ≤ l ≤ 32	-16 ≤ h ≤ 16, -36 ≤ k ≤ 36, -24 ≤ l ≤ 24	-18 ≤ h ≤ 18, -13 ≤ k ≤ 13, -22 ≤ l ≤ 22
Reflections collected	78117	180317	49314
Independent reflections	78117 [R _{int} = 0.0974, R _{sigma} = 0.1015]	14914 [R _{int} = 0.0396, R _{sigma} = 0.0183]	11300 [R _{int} = 0.0955, R _{sigma} = 0.1014]
Data / restraints / parameters	78117/807/912	14914/40/568	11300/604/649
Goodness-of-fit on F ²	1.053	1.197	1.021
Final R indexes [I ≥ 2σ (I)]	R ₁ = 0.0607, wR ₂ = 0.1058	R ₁ = 0.0408, wR ₂ = 0.0848	R ₁ = 0.0654, wR ₂ = 0.1322
Final R indexes [all data]	R ₁ = 0.0974, wR ₂ = 0.1224	R ₁ = 0.0462, wR ₂ = 0.0873	R ₁ = 0.0927, wR ₂ = 0.1481
Largest diff. peak/hole / e Å ⁻³	1.36/-2.24	1.60/-1.26	1.43/-0.93

Complex	CoBr ₂ (L1)	L16 (BH ₃)	L16 (BH ₃){BH ₃ }
Local identifier code	21srv202	22srv104	22srv125
Empirical formula	C ₁₃₅ H _{152.5} Br ₈ Cl _{2.5} Co ₄ N ₄ O ₁₂ P ₈ Si ₄	C ₃₄ H ₄₃ BCl ₂ N ₂ O ₃ P ₂ Si	C ₃₃ H _{41.6} B _{1.2} N ₂ O _{3.3} P ₂ Si
Formula weight	3346.85	699.44	622.08
Temperature / K	120	120.00	120.00
Crystal system	Triclinic	orthorhombic	triclinic
Space group	P-1	P2 ₁ 2 ₁ 2 ₁	P-1
a / Å	11.6233(4)	9.8896(3)	8.3118(2)
b / Å	15.2191(5)	16.6345(6)	9.4271(2)
c / Å	21.0112(7)	21.6134(8)	21.5976(5)
α / °	92.7541(14)	90	89.0277(8)
β / °	90.8623(13)	90	81.1506(9)
γ / °	104.1430(14)	90	76.5916(8)
Volume / Å ³	3598.6(2)	3555.6(2)	1626.27(6)
Z	1	4	2
ρ _{calc} / g cm ³	1.544	1.307	1.270
μ / mm ⁻¹	2.900	0.343	0.208
F(000)	1693.0	1472.0	660.0
Crystal size / mm ³	0.173 × 0.094 × 0.051	0.31 × 0.25 × 0.21	0.14 × 0.12 × 0.05
Radiation	MoKα (λ = 0.71073)	Mo Kα (λ = 0.71073)	Mo Kα (λ = 0.71073)
2θ range for data collection / °	4.15 to 49.998	3.768 to 59.992	3.818 to 59.988
Index ranges	-13 ≤ h ≤ 13, -18 ≤ k ≤ 18, -24 ≤ l ≤ 24	-13 ≤ h ≤ 13, -23 ≤ k ≤ 23, -30 ≤ l ≤ 30	-11 ≤ h ≤ 11, -13 ≤ k ≤ 13, -30 ≤ l ≤ 30
Reflections collected	62433	85450	39492
Independent reflections	12623 [R _{int} = 0.0384, R _{sigma} = 0.0329]	10318 [R _{int} = 0.0588, R _{sigma} = 0.0332]	9483 [R _{int} = 0.0416, R _{sigma} = 0.0400]
Data / restraints / parameters	12623 / 70 / 846	10318/0/406	9483/42/457
Goodness-of-fit on F ²	1.018	1.060	1.032
Final R indexes [I>=2σ (I)]	R ₁ = 0.0458, wR ₂ = 0.1053	R ₁ = 0.0495, wR ₂ = 0.1362	R ₁ = 0.0423, wR ₂ = 0.0957
Final R indexes [all data]	R ₁ = 0.0639, wR ₂ = 0.1162	R ₁ = 0.0538, wR ₂ = 0.1400	R ₁ = 0.0583, wR ₂ = 0.1042
Largest diff. peak/hole / e Å ⁻³	1.02 / -0.68	1.06/-1.08	0.45/-0.32

Complex	BISBI(Se) ₂	PdCl ₂ (L5)
Local identifier code	mo_23srv310_twin 1_hklf4	22srv089
Empirical formula	C ₃₉ H ₃₄ Cl ₂ P ₂ Se ₂	C ₃₃ H ₃₈ Cl ₂ N ₂ O ₃ P ₂ PdS i
Formula weight	793.42	777.98
Temperature / K	120.00(10)	120.00
Crystal system	triclinic	monoclinic
Space group	P-1	P2 ₁ /c
a / Å	14.4043(7)	23.6306(6)
b / Å	14.7150(4)	17.2635(4)
c / Å	16.5338(6)	17.5394(4)
α / °	89.013(2)	90
β / °	87.899(4)	111.7710(10)
γ / °	87.111(3)	90
Volume / Å ³	3497.3(2)	6644.8(3)
Z	4	8
ρ _{calc} / g cm ³	1.507	1.555
μ / mm ⁻¹	2.387	0.889
F(000)	1600.0	3184.0
Crystal size / mm ³	0.152 × 0.134 × 0.027	0.08 × 0.07 × 0.04
Radiation	Mo Kα (λ = 0.71073)	Mo Kα (λ = 0.71073)
2θ range for data collection / °	3.68 to 54.998	4.326 to 60
Index ranges	-18 ≤ h ≤ 18, -19 ≤ k ≤ 19, -21 ≤ l ≤ 21	-33 ≤ h ≤ 33, -24 ≤ k ≤ 24, -24 ≤ l ≤ 24
Reflections collected	61228	163919
Independent reflections	61228 [R _{int} = 0.1727, R _{sigma} = 0.2708]	19378 [R _{int} = 0.1029, R _{sigma} = 0.0613]
Data / restraints / parameters	61228/1342/868	19378/23/806
Goodness-of-fit on F ²	0.671	1.028
Final R indexes [I ≥ 2σ (I)]	R ₁ = 0.0402, wR ₂ = 0.0591	R ₁ = 0.0528, wR ₂ = 0.0917
Final R indexes [all data]	R ₁ = 0.1126, wR ₂ = 0.0640	R ₁ = 0.0688, wR ₂ = 0.0979
Largest diff. peak/hole / e Å ⁻³	0.90/-0.69	1.02/-1.01

Appendix C: GC calibration curves for 1-octene and nonanal in the hydroformylation of 1-octene

This appendix consists of the GC calibration curves used to identify the number of moles of 1-octene (Figure C1) and nonanal (Figure C2) produced during the hydroformylation of 1-octene. nonane is used as an internal standard. The areas of the peaks in the GC-FID spectrum were used to calculate the datapoints. Figures C1 and C2 were fitted with a linear trendline with the intercept set to zero. 1-Octene and nonanal isomers were assumed to have the same response factors.

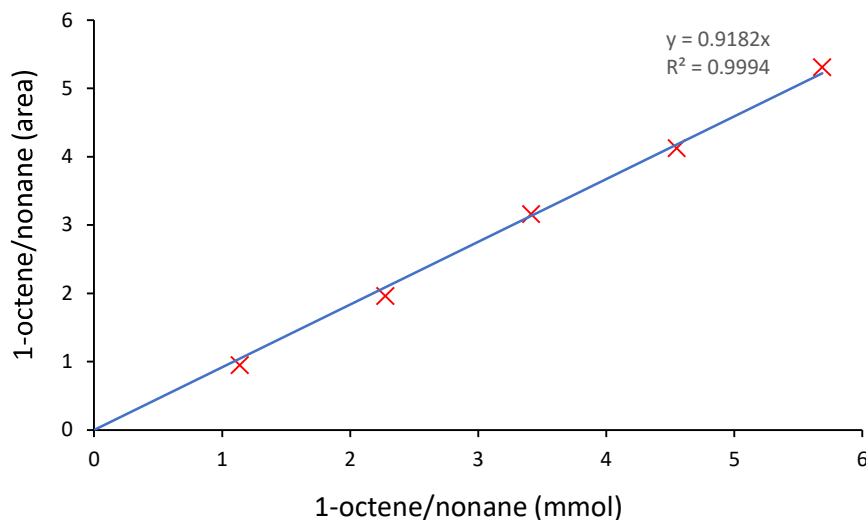


Figure C1. 1-octene vs nonane calibration curve.

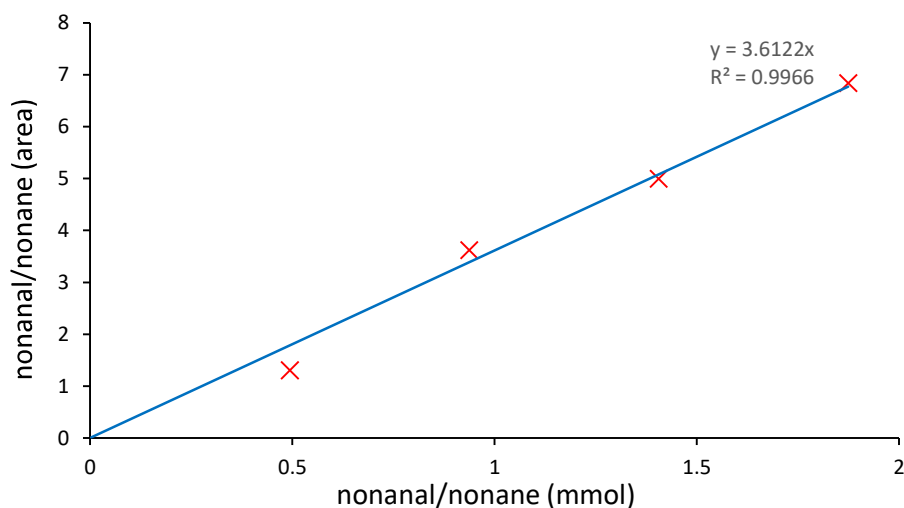


Figure C2. nonanal vs nonane calibration curve.